Parton Shower Matching for Electroweak Corrections

Von der Fakultät für Mathematik, Informatik und
Naturwissenschaften der RWTH Aachen University zur Erlangung
des akademischen Grades eines Doktors der Naturwissenschaften
genehmigte Dissertation

vorgelegt von

Lennart Oymanns, M.Sc.

aus Oberhausen

Berichter: Universitätsprofessor Dr. rer. nat. Michael Krämer
Universitätsprofessor Dr. rer. nat. Robert Harlander

Tag der mündlichen Prüfung: 31. Mai 2017

Abstract

The LHC (Large Hadron Collider) is a proton-proton collider that is used to advance our knowledge of fundamental physical laws. To test predictions of the Standard Model of particle physics, it is crucial to be able to simulate proton-proton collisions as precisely as possible. Hence, fixed-order calculations in perturbation theory have to be matched to parton shower programs. In this thesis, we discuss how parton-shower matching can be performed for QCD and electroweak corrections. In particular, we discuss the dimensionally regularized standard FKS (Frixione-Kunszt-Signer) subtraction scheme in detail, we derive FKS for photon-radiation off fermions within mass regularization, and we discuss the POWHEG method. Moreover, we discuss our C++ implementation of FKS and the POWHEG method.

We use the POWHEG implementation to simulate the Drell-Yan process at NLO QCD and NLO electroweak accuracy and perform parton-shower matching. We find that care has to be taken to avoid large uncontrolled higher-order terms due to the vector-boson resonance if QCD and electroweak radiation is generated. We use a resonance-improved POWHEG method to avoid the uncontrolled higher-order terms. These terms can introduce shifts in the measured W-boson mass of about 10 MeV. Hence, it is crucial to use a resonance-improved POWHEG method to be able to match the W-boson mass measurment with an accuracy of 10 – 20 MeV at the LHC.

Furthermore, we use our FKS implementation to implement a fixed-order NLO calculation for the process $pp \to W + \text{jet}$. This implementation can serve as a first step for a resonance-improved POWHEG implementation for $V + \text{jet}$, where $V = W, Z$-boson.

Zusammenfassung

Der LHC ist ein Proton-Proton-Beschleuniger, der benutzt wird, um unser Verständnis von fundamentalen physikalischen Gesetzen zu verbessern. Um Vorhersagen des Standardmodells der Teilchenphysik zu verbessern, ist es wichtig Proton-Proton-Kollisionen so präzise wie möglich zu simulieren. Daher müssen fixed-order Rechnung in der Störungstheorie mit Parton-Shower-Programmen gematcht werden. In dieser Arbeit diskutieren wir wie Parton-Shower-Matching für QCD und elektroschwache Korrekturen durchgeführt werden kann. Insbesondere diskutieren wir das dimensional regularisierte Standard-FKS-Subtraktionsschema (Frixione-Kunszt-Signer), wir leiten FKS für photonische Abstrahlung von Fermionen in Massenregularisierung her und wir diskutieren die POWHEG-Methode. Des Weiteren diskutieren wir unsere C++-Implementation für FKS und die POWHEG-Methode.
Wir verwenden unsere POWHEG-Implementierung, um den Drell-Yan-Prozess auf NLO-Genauigkeit für QCD und elektroschwache Korrekturen zu simulieren und das Parton-Shower-Matching durchzuführen. Dabei stellen wir fest, dass man darauf achten muss große nicht kontrollierte Terme höherer Ordnung auf Grund der Vektorboson-Resonanz zu vermeiden, wenn QCD und elektroschwache Abstrahlung generiert wird. Wir benutzen eine resonanz-verbesserte POWHEG-Methode, um die Terme höherer Ordnung zu vermeiden. Diese Terme können zu Veränderungen der gemessenen W-Bosonmasse um etwa 10 MeV führen. Deswegen ist es wichtig eine resonanz-verbesserte POWHEG-Methode zu verwenden, um die W-Bosonmasse mit einer Genauigkeit von 10 – 20 MeV am LHC zu messen.

Des Weiteren verwenden wir unsere FKS-Implementation, um eine fixed-order NLO Rechnung für den Prozess $pp \to W + \text{jet}$ zu machen. Diese Implementation kann als erster Schritt für eine Implementierung der resonanz-verbesserten POWHEG-Methode für $V + \text{jet}$ dienen ($V = W, Z$-Boson).

Contents

1. Introduction **11**

2. NLO Calculations **14**

3. FKS Subtraction Scheme **20**
3.1. Initial-State Radiation 20
3.1.1. Collinear Term 22
3.1.2. Soft Term 26
3.1.3. Finite Term and Phase-Space Generation 28
3.2. Final-State Radiation 33
3.2.1. Collinear Limit 34
3.2.2. Soft Limit 37
3.2.3. Finite Term and Phase-Space Generation 38
3.3. Combination of Initial-State and Final-State Singularities 43
3.3.1. Choice of S functions 44
3.3.2. Combining Soft and Virtual Limits 47
3.4. Final Result 49
3.4.1. Subtracted Real Matrix Element 49
3.4.2. Virtual Term 53
3.4.3. PDF Renormalization Term 53
3.5. EW Corrections 54

4. FKS with Mass Regularization **55**
4.1. Initial-State Radiation 59
4.2. Final-State Radiation 64
4.3. Final Result 67

5. Parton Shower Matching with POWHEG **71**
5.1. Parton Shower 71
5.2. Matching a Parton Shower With an NLO Calculation 74
5.3. POWHEG Method 75

5.4. Strong Coupling and Scales . . . 76
5.5. Event Generation . . . 78
5.5.1. Underlying Born Events . . . 78
5.5.2. Negative Weights . . . 80
5.5.3. Generation of Radiation . . . 82
5.5.4. Implementation . . . 92
5.5.5. Matching a Parton Shower to POWHEG Events . . . 93

6. Neutral-Current Drell-Yan 96
6.1. Details of the Calculation . . . 98
6.1.1. Complex-Mass Scheme . . . 98
6.1.2. Massless Fermion Approximation . . . 99
6.1.3. Numerical Integration . . . 101
6.2. Parameters and Setup . . . 103
6.3. NLO Calculation . . . 104
6.4. Phenomenology . . . 105
6.4.1. QCD Corrections . . . 106
6.4.2. Electroweak Corrections . . . 108
6.5. Resonance Improvement . . . 111
6.6. Combining QCD and EW Corrections . . . 114
6.7. Influence of Different Matching Schemes in PYTHIA . . . 117

7. Charged-Current Drell-Yan 120

8. W-Boson Production at Large Transverse Momentum 125
8.1. Subprocesses . . . 126
8.2. Singular Regions . . . 128
8.3. Generation and Analysis Cuts . . . 129
8.4. NLO Calculation . . . 130
8.5. Outlook . . . 132

9. Conclusions 133

Appendices 135

A. Acronyms 136

B. Virtual Corrections for Drell-Yan in Mass Regularization 137

C. Phase Space **145**
C.1. Spherical Coordinates in n Dimensions . . . 145
C.2. Integrating the Momentum in d-1 Dimensions . . . 146
C.3. Phase-Space Identity . . . 147

D. Monte-Carlo Methods **148**
D.1. Rejection Sampling . . . 148
D.2. Monte-Carlo integration . . . 148
D.2.1. Importance Sampling . . . 149
D.3. Sampling Random Variables for POWHEG Radiation . . . 150
D.3.1. Veto Method . . . 153
D.4. Highest-Bid Method . . . 156

E. Plus Distributions **157**
E.1. Removing Non-Singular Parts from the Plus Distribution . . . 158
E.2. Plus Distributions with Theta Functions . . . 159
E.3. Distribution Expansion for the Collinear Singularities . . . 159
E.4. Plus Distribution for Mass Regularization . . . 161

F. Integrating the Eikonal Factor **163**
F.1. Angular Integration . . . 163
F.1.1. Massless Partons . . . 163
F.1.2. Massive Partons . . . 165
F.1.3. Soft Integral for Mass Regularization . . . 165
F.2. Momentum Integral . . . 166

G. Scalar Integrals **169**
G.1. Scalar One Point Function . . . 169
G.2. Scalar Two Point Function . . . 169
G.3. Vectorlike Two Point Function . . . 171
G.4. Three Point Function . . . 171

H. Soft and Collinear Limits **173**
H.1. Soft Limit . . . 173
H.1.1. Color Factor . . . 175
H.2. Collinear Limit . . . 178

I. Implementation **182**
I.1. Adding a Process . . . 182

Bibliography **186**

1. Introduction

The particle collider Large Hadron Collider (LHC) is used to advance our understanding of fundamental physical laws. By discovering the Higgs boson in 2012 [1, 2], the standard model of particle physics [3–9] was verified experimentally. Furthermore, it is possible to search beyond the standard model physics in proton-proton collisions at the LHC. Due to the remarkable performance of the LHC, it is possible to perform precision measurements for a large number of standard model processes. The Drell-Yan process [10] is an important standard candle at the LHC. Furthermore, the pure leptonic final state is very clean. Therefore, the Drell-Yan process can be used to measure standard model parameters like the weak mixing angle [11, 12] or the W-boson mass [13] with very high precision. Since events are generated over the whole rapidity range, the Drell-Yan process can be used to extract parton distribution function (pdf) [14]. It is also an important background in searches for heavy gauge bosons W' and Z' in Beyond the Standard Model (BSM) physics. Recent reviews can be found in references [15, 16].

Since the LHC delivers large statistics for many standard model processes, the statistical error is small and theoretical uncertainties should be always smaller than experimental uncertainties. From a theory point of view, the Drell-Yan process is one of the simplest processes at a hadron collider because only the initial-state partons can be the origin of QCD radiation. To improve the theoretical uncertainties, higher-order corrections in perturbation theory have to be included into the calculation. The next-to leading order (NLO) QCD corrections were calculated in reference [17]. NNLO QCD corrections were calculated in references [18–20] and are available in Monte-Carlo tools [21–26]. A naive comparison of the coupling constants shows that $\alpha_s^2 \approx 0.01$ and $\alpha \approx 0.01$ have the same order of magnitude. Therefore, electroweak (EW) NLO corrections [27–31] can play an important role when we go beyond NLO in QCD. NLO EW corrections are implemented in the tools HORACE [32, 33], WGRAD/ZGRAD [28, 29, 34, 35], WINHAC [36] and SANC [37–41]. Also NNLO QCD corrections were combined additively with NLO EW corrections [42]. A full calculation of $\mathcal{O}(\alpha\alpha_s)$ terms is not available, yet. However, the dominant corrections of $\mathcal{O}(\alpha\alpha_s)$ were calculated in [43, 44]. Fixed-order NNLO results were also combined with resummation results to predict the transverse momentum distribution of the vector-boson in the region with small transverse momentum [45].

At hadron colliders like the LHC events consist of multi-particle final states due to quark and gluon splittings and the subsequent hadronization. Fixed-order calculations in perturbation theory, however, are ordered in the coupling of fundamental particle interactions. It is only possible to calculate cross sections up to a few orders in the coupling. For instance, NLO calculations include only one possibly soft or collinear splitting. Hence, fixed-order calculations can be used to predict inclusive observables. Moreover, large logarithms can arise at each order for more differential observables. To obtain physical predictions, these logarithms have to be resummed to all orders in perturbation theory.

A method to simulate more realistic events and resum the large logarithms is the parton-shower approach. The parton shower starts from a LO process and additional soft and collinear splittings are generated recursively until the hadronization scale is reached. Parton showers use that matrix elements factorize in the limit of soft and collinear radiation. Hence, a sequence of soft and collinear $1 \to 2$ splittings is added to the LO event. However, splittings that are neither soft nor collinear are not included properly in parton showers. Moreover, interference effects are neglected.

Many effort was put into combining parton showers with NLO calculations to obtain realistic event samples with one possibly hard splitting. The main obstacle in combining the two approaches is that parton showers include the first splitting in a soft and collinear approximation. Therefore, double counting is encountered when we combine parton showers and NLO calculations naively.

In the past years, two methods have been established to combine parton showers with NLO calculations. The MC@NLO method [46] subtracts parton-shower contributions from the NLO calculation to avoid double counting. Whereas, the POWHEG method [47] uses the NLO matrix element to perform the hardest splitting in a parton-shower way and uses standard (p_T ordered and vetoed) parton showers for all subsequent splittings. Both methods overcome the double counting problem and have NLO accuracy. Only higher order terms due to the resummation can be different. The NLO QCD corrections for the Drell-Yan process were matched to parton showers within the MC@NLO framework [46] and the POWHEG framework [48]. The combination of EW and QCD corrections matched to parton showers is available in the POWHEGBOX framework [49–51]. Parton-shower matching at NNLO QCD level has also been achieved [52–54].

In the following, we use the POWHEG method to combine NLO calculations with standard parton-shower programs and study the phenomenological effects for the Drell-Yan process.

The standard POWHEG approach is usually used to combine NLO calculations in QCD with parton showers. We also include EW corrections, because they can play an

important role in high-precision measurements at the LHC.

In the following we discuss the outline of this thesis. In chapter 2 we show that the calculation of NLO observables is hindered by technical difficulties. For instance, the real radiation and virtual part of the NLO cross section diverge. Since the structure of the integrals is complicated, we have to integrate them numerically. To obtain a finite result, we have to parametrize (regulate) the divergent structure of the real and virtual part, i.e. we have to isolate the divergent pieces. The divergent pieces cancel analytically between the real radiation and the virtual part. Hence, the rest can be integrated numerically.

Different subtractions schemes like Catani-Seymour [55] and FKS [56] can be used to handle the divergent structures of observables at NLO. Standard subtraction schemes use dimensional regularization because QCD calculations are done in this regularization scheme. However, EW calculations often use mass regularization where fermion masses serve as regulators. Hence, the standard subtraction schemes have to be modified to incorporate mass regularization. In chapter 3 we give a full derivation of the FKS subtraction for massless partons in dimensional regularization and we introduce FKS for mass regularization in chapter 4. The results are also published in reference [57]. The FKS subtraction scheme is well suited for POWHEG because both methods start from an leading order (LO) process and add a splitting to it.

In chapter 5 we discuss parton showers and parton shower matching. In particular, we discuss the POWHEG method and how we implemented it in a C++ code.

When QCD and EW radiation is simultaneously matched to parton showers with POWHEG, care has to be taken. The standard FKS subtraction used in POWHEG splits the phase space in different regions to handle all IR divergences properly. We find that the standard FKS splitting can lead to large unwanted higher-order terms when we use POWHEG to generate QCD and EW radiation simultaneously. To avoid the higher order terms, we use ideas from reference [58] to take the s-channel resonance of the Drell-Yan process properly into account. In chapter 6 we apply our POWHEG implementation to the neutral-current Drell-Yan process and in chapter 7 we apply it to the charged-current Drell-Yan process. The results are also published in reference [57].

In chapter 8 we discuss the process $pp \to W + \text{jet}$ and show that we can use the C++ implementation described in chapter 5 to calculate fixed-order EW and QCD corrections. Therefore, our implementation can be used as a starting point for a resonance improved parton shower matching as discussed in [58].

2. NLO Calculations

The LHC is a particle collider that is used to study proton-proton collisions at $\sqrt{S} = 7, 8$ and, 13 TeV center of mass energy. Hadron-hadron collisions include a large variety of reactions. When there is only a small momentum transfer between the hadrons, the hadrons themselves interact. For large momentum transfer, short distance effects become more important, i.e. the constituents of protons interact with each other. The interaction between the partons from both hadrons is approximately independent of the rest of the proton. Therefore, we can describe the hadronic cross section for a proton-proton collision as a convolution of a partonic cross section $\mathrm{d}\hat{\sigma}_{ij}$ and parton distribution functions (pdfs) $f_i(x)$. This is known as the *factorization theorem*. The hadronic cross section reads

$$\mathrm{d}\sigma = \sum_{i,j} \int_0^1 \mathrm{d}x_1 \int_0^1 \mathrm{d}x_2 \, f_i(x_1) f_j(x_2) \, \mathrm{d}\hat{\sigma}_{ij}. \tag{2.1}$$

The pdf $f_i(x)$ represents the distribution of partons i with proton momentum fraction x in the proton, i.e. $p_i = xP_p$, where p_i denotes the parton momentum and P_p the proton momentum. The pdfs capture the long distance physics and are universal for all scattering processes. The partonic cross section $\mathrm{d}\hat{\sigma}_{ij}$ represents the cross section of the interaction of parton i and j. It is independent of the properties of the proton.

We calculate the partonic cross section in perturbation theory. Calculating processes at NLO in perturbation theory has been fully automatized in the recent years and is now the new standard.

Compared to the LO cross section, the NLO process has two additional types of diagrams:

1. Real radiation diagrams with one additional emission of a quark or a gluon,
2. Virtual 1-loop diagrams.

We write the squared real radiation matrix element multiplied with the flux as

$$\mathcal{R}_{p_1 p_2} = \frac{1}{2s_r} |\mathcal{M}_r|^2, \tag{2.2}$$

where p_1, p_2 denote the initial-state quarks and gluons and $s_r = 2k_1 \cdot k_2$ is the Mandelstam-s of the initial-state momenta of the real process. The virtual diagrams have the same external particles as the born diagrams. Therefore, we have to add them to the born matrix element before squaring. We find at NLO

$$|\mathcal{M}_b + \mathcal{M}_v|^2 = |\mathcal{M}_b|^2 + 2\,\mathrm{Re}(\mathcal{M}_v \mathcal{M}_b^*) + \mathcal{O}(\alpha^2), \tag{2.3}$$

where $\mathcal{M}_b$ is the LO and $\mathcal{M}_v$ is the virtual matrix element. We define a LO function $\mathcal{B}$ and a virtual function $\mathcal{V}$ in the following way

$$\mathcal{B} = \frac{1}{2s_b}|\mathcal{M}_b|^2, \tag{2.4}$$

$$\mathcal{V} = \frac{1}{2s_b} 2\,\mathrm{Re}(\mathcal{M}_v \mathcal{M}_b^*), \tag{2.5}$$

where $s_b = 2\bar{k}_1 \cdot \bar{k}_2$ is the Mandelstam-s of the initial-state momenta of the born process. The functions $\mathcal{B}$ and $\mathcal{V}$ include the flux factor and average over initial-state spins and sum over final state spins. Using the definition (2.1), the NLO cross section can be calculated via

$$\sigma_{NLO} = \sum_{p_1,p_2} \int \mathrm{d}x_1\,\mathrm{d}x_2\,\mathrm{d}\Phi_n f_{p_1}(x_1) f_{p_2}(x_2)(\mathcal{B}+\mathcal{V}) + \\ + \sum_{p_1,p_2} \int \mathrm{d}x_1\,\mathrm{d}x_2\,\mathrm{d}\Phi_{n+1} f_{p_1}(x_1) f_{p_2}(x_2) \mathcal{R}_{p_1 p_2}, \tag{2.6}$$

where f_p is the pdf for parton p and Φ_n is the n particle phase-space.

Virtual matrix elements contain ultra-violet (UV) divergences that have to be regularized and handled by *renormalization*. In the course of this thesis, we assume that all UV divergences are removed by renormalization.

After UV renormalization, infrared (IR) divergences connected to soft and collinear particles remain. These singularities are present in the virtual as well as in the real part. In physical quantities like cross sections, the singularities from the virtual and real part cancel so that a finite result is obtained. At first, we show the origin of the singularities. When a mother particle radiates a massless daughter particle (e.g. gluon) with momentum k the propagator of the mother particle is proportional to

$$\frac{1}{(p+k)^2 - m^2} = \frac{1}{2p \cdot k} = \frac{1}{2E_k E_p (1 - M\cos\theta)}, \tag{2.7}$$

where p is the momentum of the mother particle after the radiation. In the last step, we expressed the momenta in terms of their energies E_k, E_p and the angle θ between the

two daughter particles. The factor M is defined as

$$M = \frac{|\vec{p}|}{E_p} = \sqrt{1 - \frac{m^2}{E_p^2}}. \tag{2.8}$$

When we integrate the squared propagator over the phase space, the gluon integration is proportional to

$$\mathrm{d}E_k \, \mathrm{d}\cos\theta \frac{1}{E_k(1 - M\cos\theta)^2} \tag{2.9}$$

which is singular for soft radiation, i.e. $E_k \to 0$. When the mother particle is also massless ($m = 0$), the angular integration is singular for collinear radiation with $\cos\theta = 1$. In QCD calculations, dimensional regularization [59] (dim. reg.) is commonly used to regularize IR divergences, i.e. matrix elements and integrals are calculated in $d = 4 - 2\varepsilon$ dimensions. In dim. reg., the result for the integrated squared matrix element has $\frac{1}{\varepsilon}$ poles which parametrize the singularities. When we combine virtual and real part, the result is finite, i.e. all $\frac{1}{\varepsilon}$ poles cancel and the limit $\varepsilon \to 0$ can be used. In EW calculations, however, mass regularization is often used. In the course of this section, we focus on dim. reg. and discuss mass regularization in chapter 4.

The pole cancellation is a consequence of the KLN theorem [60, 61]. However, a pole due to collinear parton splittings does not cancel. We discuss this pole and the pdf renormalization later in this section. The NLO cross section reads

$$\sigma = \sigma_{\mathrm{LO}} + \int_{n+1} \mathrm{d}\sigma_{\mathrm{real}} + \int_n \mathrm{d}\sigma_{\mathrm{virt}}, \tag{2.10}$$

where the integrals denote the integration over the n and $n+1$ particle phase-spaces. In general, we cannot integrate the virtual and real matrix elements analytically and we cannot integrate them numerically in $d = 4$ dimensions because they diverge due to IR singularities. The solution is to subtract the divergent parts of the matrix elements in $d = 4 - 2\varepsilon$ dimensions and integrate the remaining finite part numerically, i.e. the cross sections is given by

$$\sigma = \sigma_{\mathrm{LO}} + \int_{n+1} \left[\mathrm{d}\sigma_{\mathrm{real}} - \mathrm{d}\sigma_A\right] + \int_n \left[\mathrm{d}\sigma_{\mathrm{virt}} + \int_1 \mathrm{d}\sigma_A\right]. \tag{2.11}$$

The subtraction term $\mathrm{d}\sigma_A$ has to be chosen such that the divergent part of the real cross section is subtracted. The remaining subtracted $n+1$ particle phase-space integral is then finite and we can use numerical integration in four dimensions. The subtraction term has to be simple enough that we can perform the one-particle phase-space integral and add it to the virtual part. All divergent terms have to cancel between the virtual

part and the integrated subtraction term. Therefore, the remaining integral is also finite and can be done by numerical integration methods. To show how a subtraction actually works, we introduce a simple toy cross section. We assume that the real contribution to the cross section reads

$$\int_{n+1} \mathrm{d}\sigma_{\mathrm{real}} = \int_n \int_0^1 \mathrm{d}E \, \frac{1}{E^{1+\varepsilon}} g(E). \tag{2.12}$$

In our toy calculation, the integration over the momentum of the radiated particle is given by an energy integration only. The matrix element times Jacobian is given by a function $\frac{1}{E}$ which is analogous to the energy in (2.9) and an arbitrary non-singular function $g(E)$. The regulator ε is analogous to the $d = 4 - 2\varepsilon$ dimensions in dim. reg. and is introduced here by hand. The integral is divergent in the limit $\varepsilon \to 0$ if g is not proportional to E. To extract the singularity, we subtract and add $g(0)$. The cross section is then given by

$$\int_{n+1} \mathrm{d}\sigma_{\mathrm{real}} = \int_n \int_0^1 \mathrm{d}E \, \frac{1}{E^{1+\varepsilon}} \left[g(E) - g(0) + g(0) \right]. \tag{2.13}$$

We can define the integrated subtraction term as

$$\mathrm{d}\sigma_A = g(0) \frac{1}{E^{1+\varepsilon}} \tag{2.14}$$

and calculate the one-particle phase-space

$$\int_1 \mathrm{d}\sigma_A = g(0) \int_0^1 \mathrm{d}E \, \frac{1}{E^{1+\varepsilon}} = -g(0) \frac{1}{\varepsilon} \tag{2.15}$$

which has a $\frac{1}{\varepsilon}$ pole. The subtracted real part is finite. Therefore, we can use the limit $\varepsilon \to 0$. In terms of the subtraction term, the subtracted real cross section reads

$$\int_{n+1} \mathrm{d}\sigma_{\mathrm{real}} = \int_{n+1} \left[\mathrm{d}\sigma_{\mathrm{real}} - \mathrm{d}\sigma_A \right] + \int_n \int_1 \mathrm{d}\sigma_A. \tag{2.16}$$

The $\frac{1}{\varepsilon}$ pole in the integrated subtraction term has to cancel the singularity in the virtual part. The most used subtraction schemes are the Catani-Seymour subtraction scheme [55] and the FKS subtraction scheme [56]. We use the FKS subtraction in the following. A derivation of the subtraction terms for the standard FKS subtraction in dimensional regularization is given in chapter 3. All terms that have to be implemented in an NLO calculation are summarized in section 3.4. Since EW calculations are traditionally performed in mass regularization, we have derived the subtraction terms for FKS in mass regularization. Our results are given in chapter 4.

As mentioned earlier not all divergences cancel, when we combine the real and virtual part in the hadronic cross section. The KLN theorem states that all IR divergences cancel if we sum over all soft and collinear degenerate initial- and final-states. Since we do not sum over all degenerate initial-states in the hadronic cross section, a collinear divergence remains. We can absorb the remaining divergence into the pdfs. In dimensional regularization the redefined pdf is given by

$$f_p(x) = f_p(x,\mu_F) - \frac{\alpha_s}{2\pi}\sum_{p'}\int_x^1 \frac{\mathrm{d}z}{z} f_{p'}\left(\frac{x}{z},\mu_F\right)\left\{P_{pp'}(z)\left(\frac{1}{\hat{\varepsilon}} - \ln\frac{\mu_F^2}{\mu^2}\right) + r^F_{pp'}\right\} + \mathcal{O}\left(\alpha_s^2\right), \quad (2.17)$$

where μ_F is the factorization scale, $P_{pp'}$ is the regularized Altarelli-Parisi splitting function in 4 dimensions, and

$$\frac{1}{\hat{\varepsilon}} = \frac{1}{\varepsilon} - \gamma_E + \log(4\pi). \quad (2.18)$$

The factorization scheme dependent r^F piece is set to zero in the $\overline{MS}$ scheme which we will use here. The factorization scale μ_F separates collinear and non-collinear radiation, i.e. regions where the matrix element can be approximated using splitting functions. Below the factorization scale, we assume partons to be part of the hadron, i.e. the factorization scale is the upper bound for the momentum scale of collinear splittings. Large collinear logarithms due to the collinear splittings are resummed by the DGLAP equations [62–64] that link the pdfs at different scales. Above the factorization scale, parton splittings belong to the hard process and are not part of the incoming partons. The scale could be chosen freely since it is an unphysical quantity and the physical quantities at all orders cannot depend on it. At NLO, the dependence on the scale is reduced but still present. Therefore, we choose μ_F to be equal to a scale of the process to avoid large corrections.

The redefinition of the pdfs is similar to renormalization. We combine the infinite bare pdf $f_p(x)$ with a singularity in order to get the finite physical pdf $f_p(x,\mu_F)$. The pdfs have to be extracted from experimental data. If we substitute the redefined pdfs into (2.6), we obtain

$$\sigma_{NLO} = \sigma^{(b+v)} + \sigma^{(r)} + \sigma_+^{(\mathrm{pdf})} + \sigma_-^{(\mathrm{pdf})} + \mathcal{O}\left(\alpha_s^2\right), \quad (2.19)$$

where

$$\sigma^{(b+v)} = \sum_{p_1,p_2} \int \mathrm{d}x_1\, \mathrm{d}x_2\, \mathrm{d}\Phi_n f_{p_1}(x_1,\mu_F) f_{p_2}(x_2,\mu_F)(\mathcal{B}+\mathcal{V}), \tag{2.20}$$

$$\sigma^{(r)} = + \sum_{p_1',p_2'} \int \mathrm{d}x_1\, \mathrm{d}x_2\, \mathrm{d}\Phi_{n+1} f_{p_1'}(x_1,\mu_F) f_{p_2'}(x_2,\mu_F)\mathcal{R}_{p_1'p_2'}, \tag{2.21}$$

$$\sigma_+^{(\mathrm{pdf})} = - \frac{\alpha_s}{2\pi} \sum_{p_1,p_2} \int \mathrm{d}x_1\, \mathrm{d}x_2\, \mathrm{d}\Phi_n F_{p_1}(x_1,\mu_F) f_{p_2}(x_2,\mu_F)\mathcal{B}, \tag{2.22}$$

$$\sigma_-^{(\mathrm{pdf})} = - \frac{\alpha_s}{2\pi} \sum_{p_1,p_2} \int \mathrm{d}x_1\, \mathrm{d}x_2\, \mathrm{d}\Phi_n f_{p_1}(x_1,\mu_F) F_{p_2}(x_2,\mu_F)\mathcal{B}. \tag{2.23}$$

In dimensional regularization, according to (2.17), we have (s. [65, chapter 3.6.4])

$$F_p(x,\mu_F) = \sum_{p'} \left(\frac{1}{\hat{\varepsilon}} - \ln \frac{\mu_F^2}{\mu^2} \right) \int_x^1 \frac{\mathrm{d}z}{z} P_{pp'}(z) f_{p'}\left(\frac{x}{z},\mu_F\right). \tag{2.24}$$

3. FKS Subtraction Scheme

One way to handle the singularities for soft and collinear radiation in the real matrix element is the FKS subtraction scheme [56]. It uses the plus-distribution prescription to extract the singular parts of the matrix element. Its structure is similar to the simple subtraction example in eq. (2.16). However, the plus distribution can only extract one singular structure. Since the radiated parton can be collinear to different particles in a general process, we cannot parametrize the whole phase space such that all singularities are handled at once. It is the main idea of the FKS subtraction scheme to split the full real phase space into regions with only one singularity and parametrize the phase space in each region such that the singularity is at the boundary of the integration region. In each piece we can then use plus distributions to extract the singularities. We will first derive subtraction terms under the assumption that there is only one singular region. We start with radiation from initial-state partons in section 3.1 and we continue with final-state radiation in section section 3.2. We generalize these results by introducing a phase-space splitting in section 3.3. In section 3.4, we summarize the final result, i.e. what has to be implemented in an NLO calculation.

3.1. Initial-State Radiation

Our aim is to extract the singularities from the real part of the NLO cross section (2.21). We start by using the FKS subtraction scheme for the Drell-Yan process $q\bar{q} \to \mu^+\mu^-$. This process is particularly simple because there is only initial-state radiation at NLO in QCD. However, we write our findings in a general form and show later how to generalize our results to more complex processes. In particular, we do not make any assumptions about the explicit expression for the matrix element, i.e. we use a general real-emission matrix element $\mathcal{R}$ and the born matrix element $\mathcal{B}$. Note, that the flux is included in $\mathcal{B}$ and $\mathcal{R}$ (cf. (2.2) and (2.4)). The $d = 4 - 2\varepsilon$ dimensional real phase space reads

$$\mathrm{d}\Phi_{n+1} = (2\pi)^d \, \delta^{(d)} \left(x_1 K_1 + x_2 K_2 - k - \sum_{i=1}^{n} p_i \right) \prod_{i=1}^{n} \frac{\mathrm{d}^{d-1} p_i}{(2\pi)^{d-1} 2p_i^0} \frac{\mathrm{d}^{d-1} k}{(2\pi)^{d-1} 2k^0}, \qquad (3.1)$$

where K_1, K_2 are the momenta of the incoming protons, k is the momentum of the emitted parton and the momenta p_i are all other final-state momenta. The momentum fractions of the interacting partons are denoted by x_1 and x_2. In the Drell-Yan case, the final-state momenta p_i are the muon momenta and k is the gluon momentum. We define

$$\begin{aligned} \mathrm{d}\Pi &= (2\pi)^d \, \delta^{(d)} \left(x_1 K_1 + x_2 K_2 - k - \sum_{i=1}^{n} p_i \right) \mathrm{d}P, \qquad (3.2) \\ \mathrm{d}P &= \prod_{i=1}^{n} \frac{\mathrm{d}^{d-1} p_i}{(2\pi)^{d-1} 2 p_i^0} \qquad (3.3) \end{aligned}$$

to simplify the notation. The real matrix element diverges when the momentum k becomes soft or collinear to the beam axis, i.e. the initial state partons. We can rewrite the momentum integration of the radiated parton k in spherical coordinates

$$\frac{\mathrm{d}^{d-1} k}{(2\pi)^{d-1} 2k^0} = K_0 \xi^{1-2\varepsilon} (1-y^2)^{-\varepsilon} (\sin\phi)^{-2\varepsilon} \, \mathrm{d}\xi \, \mathrm{d}y \, \mathrm{d}\phi, \qquad (3.4)$$

where $y = \cos\theta$ is the angle between the radiated parton and the beam axis, $\xi = \frac{2k^0}{\sqrt{s_r}}$ is the energy fraction (see (C.11)), and

$$K_0 = \frac{2^{-5+4\varepsilon} \pi^{-\frac{5}{2}+\varepsilon} s_r^{1-\varepsilon}}{\Gamma\left(\frac{1}{2} - \varepsilon\right)}. \qquad (3.5)$$

Next, we investigate the real matrix element. The collinear limit is approached for $y \to \pm 1$ and the soft limit for $\xi \to 0$. For massless partons the singular structure from the internal propagator reads $\frac{1}{\xi^2(1-y^2)}$. We can extract this structure from the general real matrix element by defining a regular function

$$g(\xi, y) = \xi^2 (1-y^2) \mathcal{R} \qquad (3.6)$$

that is not singular for $y \to \pm 1$ and $\xi \to 0$. We can use the real phase space (3.1) and the regular function g to rewrite the real cross section. We obtain

$$\mathrm{d}\hat{\sigma} = \mathrm{d}\Phi_{n+1} \mathcal{R} = \mathrm{d}\Pi \, \mathrm{d}\xi \, \mathrm{d}y \, \mathrm{d}\phi K_0 \xi^{-1-2\varepsilon} (1-y^2)^{-1-\varepsilon} g(\xi, y) \qquad (3.7)$$

for the partonic cross section. By using the distribution expansions (see Appendix E)

$$\xi^{-1-2\varepsilon} = -\frac{1}{2\varepsilon}\delta(\xi) + \left(\frac{1}{\xi}\right)_+ - 2\varepsilon\left(\frac{\log\xi}{\xi}\right)_+ + \mathcal{O}\left(\varepsilon^2\right), \tag{3.8}$$

$$(1-y^2)^{-1-\varepsilon} = -\frac{4^{-\varepsilon}}{2\varepsilon}\left[\delta(1-y)+\delta(1+y)\right] + \frac{1}{2}\left[\left(\frac{1}{1+y}\right)_+ + \left(\frac{1}{1-y}\right)_+\right] + \mathcal{O}\left(\varepsilon\right), \tag{3.9}$$

we can split the partonic cross section into a soft part, a collinear part, and a finite part, i.e.

$$\mathrm{d}\hat{\sigma} = [\mathrm{d}\Phi_{n+1}\mathcal{R}]^{(\mathrm{s})} + [\mathrm{d}\Phi_{n+1}\mathcal{R}]^{(\mathrm{coll},1)} + [\mathrm{d}\Phi_{n+1}\mathcal{R}]^{(\mathrm{coll},-1)} + [\mathrm{d}\Phi_{n+1}\mathcal{R}]^{(\mathrm{fin})}. \tag{3.10}$$

The soft term reads

$$[\mathrm{d}\Phi_{n+1}\mathcal{R}]^{(\mathrm{s})} = \mathrm{d}\Phi_n K_0\left(-\frac{1}{2\varepsilon}\right)\mathrm{d}\phi(\sin\phi)^{-2\varepsilon}\,\mathrm{d}y(1-y^2)^{-1-\varepsilon}g(0,y), \tag{3.11}$$

where the real phase space reduces to a born phase space and an integration over the radiation variables. This term includes also the soft-collinear singularity, i.e. a $\frac{1}{\varepsilon^2}$ pole. For the collinear part, we have two terms because the radiated parton can become collinear to both initial-state partons. The collinear term for a radiation in z direction ($y = 1$) is given by

$$[\mathrm{d}\Phi_{n+1}\mathcal{R}]^{(\mathrm{coll},1)} = -\,\mathrm{d}\Pi\Big|_{y\to 1}\,\mathrm{d}\xi\,\mathrm{d}\phi\left[\frac{4^{-\varepsilon}}{2\varepsilon}\left(\frac{1}{\xi}\right)_+ - \left(\frac{\log\xi}{\xi}\right)_+\right]K_0(\sin\phi)^{-2\varepsilon}g(\xi,1). \tag{3.12}$$

The second collinear part $[\mathrm{d}\Phi_{n+1}\mathcal{R}]^{(coll,-1)}$ for $y = -1$ is analogous. The finite part reads

$$[\mathrm{d}\Phi_{n+1}\mathcal{R}]^{(\mathrm{fin})} = \frac{1}{2}\,\mathrm{d}\Pi\,\mathrm{d}\xi\,\mathrm{d}y\,\mathrm{d}\phi\left(\frac{1}{\xi}\right)_+\left[\left(\frac{1}{1+y}\right)_+ + \left(\frac{1}{1-y}\right)_+\right]K_0 g(\xi,y), \tag{3.13}$$

where we can use $\varepsilon = 0$. The soft and collinear poles have to cancel with the poles from the virtual corrections. However, finite pieces are included in $[\mathrm{d}\Phi_{n+1}\mathcal{R}]^{(coll,1)}$, $[\mathrm{d}\Phi_{n+1}\mathcal{R}]^{(coll,-1)}$, and $[\mathrm{d}\Phi_{n+1}\mathcal{R}]^{(s)}$. In the following sections, we will extract those finite terms.

3.1.1. Collinear Term

We start by investigating the collinear term. We focus on (3.12). The virtual correction is integrated over the born phase space. To combine the collinear limit with the virtual

part, we have to rewrite the $n+1$ particle delta function into an n particle delta function. We introduce the integral over the pdf of the initial-state parton which flies in positive z direction. The collinear phase space reads

$$\mathrm{d}\Pi_{y\to 1} = (2\pi)^d \delta^{(d)} \left(x_1(1-\xi)K_1 + x_2 K_2 - \sum_{i=1}^{n} p_i \right) \mathrm{d}P, \tag{3.14}$$

where we combined the radiated momentum $k = \frac{\sqrt{s}}{2}\xi(1,0,0,1)$ in the partonic center of mass frame with the partonic initial-state momentum.

We change the integration variables of the pdf and the real phase space into $\bar{x}_1 = x_1(1-\xi)$ and $\bar{\xi} = \xi$. (In the following, we omit the bar.) Since pdfs are defined only for arguments between 0 and 1, we swap the order of integration and obtain $0 < x_1 < 1$ and $0 < \xi < 1 - x_1$ as integration regions. Therefore, the collinear cross section part reads

$$\begin{aligned} &\mathrm{d}x_1 f(x_1,\mu_F)[\mathrm{d}\Phi_{n+1}\mathcal{R}]^{(\mathrm{coll},1)} = -\,\mathrm{d}\Phi_n\,\mathrm{d}\phi(\sin\phi)^{-2\varepsilon} K_0 \\ &\quad\times \mathrm{d}x_1\,\mathrm{d}\xi\theta(1-x_1-\xi)\left[\frac{4^{-\varepsilon}}{2\varepsilon}\left(\frac{1}{\xi}\right)_+ - \left(\frac{\log\xi}{\xi}\right)_+\right]\frac{1}{1-\xi} f\left(\frac{x_1}{1-\xi},\mu_F\right) g(\xi,1), \end{aligned} \tag{3.15}$$

where $\mathrm{d}\Phi_n = (2\pi)^d\delta^{(d)}\left(x_1K_1 + x_2K_2 - \sum_{i=1}^n p_i\right)\mathrm{d}P$. Note that the plus distribution acts on the theta function (s. section E.2). The next step is to evaluate the function $g(\xi,1)$. As discussed in section H.2, we can use spin-averaged splitting functions to write the collinear matrix element as

$$\mathcal{R} = \frac{4\pi\alpha_s\mu^{2\varepsilon}}{k_1\cdot k}\hat{P}_{p_1p_1'}(z)\,\mathcal{B}\,\frac{s_b}{s_r}, \tag{3.16}$$

where $\hat{P}_{p_1p_1'}$ is the unregularized spin-averaged Altarelli-Parisi splitting function. The splitting particles are denoted by the indices p_1 and p_1'. The factor $\frac{s_b}{s_r}$ converts the flux factor of $\mathcal{R}$ to the flux factor included in $\mathcal{B}$. The denominator reads

$$k_1\cdot k = \xi(1-y)\frac{s_b}{4} \tag{3.17}$$

and z is the momentum fraction of that particle

$$k = (1-z)k_1 \quad\Rightarrow\quad z = 1-\xi. \tag{3.18}$$

Therefore, we can write

$$\begin{aligned} g(\xi,1) &= g_s^2(1+y)\xi\hat{P}_{p_1p_1'}(1-\xi)\mathcal{B}\frac{4}{s_r}\mu^{2\varepsilon}\Big|_{y=1} \\ &= \frac{32\pi\alpha_s\mu^{2\varepsilon}}{s_r}\xi\hat{P}_{p_1p_1'}(1-\xi)\mathcal{B}. \end{aligned} \tag{3.19}$$

When we use this limit in the collinear cross section part (3.15) and integrate ϕ in $[0,\pi]$ (see Appendix C), we obtain

$$\begin{aligned} &\mathrm{d}x_1 f(x_1,\mu_F)[\mathrm{d}\Phi_{n+1}\mathcal{R}]^{(\mathrm{coll},1)} = 16\pi\,\mathrm{d}\Phi_n\mathcal{B} \\ &\times\mathrm{d}x_1\,\mathrm{d}\xi\theta(1-x_1-\xi)\,\frac{\alpha_s\mu^{2\varepsilon}}{s_r}K_0'\left[\frac{4^{-\varepsilon}}{\varepsilon}\left(\frac{1}{\xi}\right)_+ - 2\left(\frac{\log\xi}{\xi}\right)_+\right]\frac{\xi\hat{P}_{p_1p_1'}(1-\xi)}{1-\xi}f\Big(\frac{x_1}{1-\xi},\mu_F\Big), \end{aligned} \tag{3.20}$$

where $K_0' = \frac{2^{-5+4\varepsilon}\pi^{-2+\varepsilon}s_r^{1-\varepsilon}}{\Gamma(1-\varepsilon)}$. The unregularized splitting functions $\hat{P}_{p_1p_1'}$ in $d = 4-2\varepsilon$ dimensions are given by [64]

$$\hat{P}_{qq}(1-\xi) = C_F\left[\frac{1+(1-\xi)^2}{\xi} - \varepsilon\xi\right], \tag{3.21}$$

$$\hat{P}_{qg}(1-\xi) = C_F\left[\frac{1+\xi^2}{1-\xi} - \varepsilon(1-\xi)\right], \tag{3.22}$$

$$\hat{P}_{gq}(1-\xi) = T_F\left[1 - \frac{2\xi(1-\xi)}{1-\varepsilon}\right], \tag{3.23}$$

$$\hat{P}_{gg}(1-\xi) = 2C_A\left[\frac{1-\xi}{\xi} + \frac{\xi}{1-\xi} + \xi(1-\xi)\right]. \tag{3.24}$$

We separate the $\mathcal{O}(\varepsilon)$ terms in the splitting functions and write

$$\hat{P} = \hat{P}^0 + \varepsilon\hat{P}^\varepsilon. \tag{3.25}$$

Since the collinear term has the same structure as the pdf renormalization term (2.24), we can combine them. The origin of the regularized splitting functions in the pdf

renormalization is the DGLAP equation [62–64]. They are defined as

$$P_{qq}(1-\xi) = C_F \left(\frac{1+(1-\xi)^2}{\xi}\right)_+ = C_F \left(1+(1-\xi)^2\right)\left(\frac{1}{\xi}\right)_+ + \frac{3}{2}C_F\delta(\xi) \tag{3.26}$$

$$P_{qg}(1-\xi) = \hat{P}_{qg}(1-\xi) \tag{3.27}$$

$$P_{gq}(1-\xi) = \hat{P}_{qg}(1-\xi) \tag{3.28}$$

$$P_{gg}(1-\xi) = 2C_A\left[(1-\xi)\left(\frac{1}{\xi}\right)_+ + \frac{\xi}{1-\xi} + \xi(1-\xi)\right] + \frac{1}{6}\left(11C_A - 4n_f T_R\right)\delta(\xi) \tag{3.29}$$

Thus, we can write

$$P_{ab}(1-\xi) = \xi\hat{P}^0_{ab}(1-\xi)\left(\frac{1}{\xi}\right)_+ + \delta(\xi)\gamma_{ab} \tag{3.30}$$

where we define $\gamma_{qq} = \frac{3}{2}C_F$, $\gamma_{gg} = \frac{1}{6}(11C_A - 4n_f T_R)$, and $\gamma_{gq} = \gamma_{qg} = 0$. We also define $\gamma_p = \gamma_{pp}$. Using these expressions for the splitting functions, we find

$$\begin{aligned}\mathrm{d}x_1 f_p(x_1,\mu_F)[\mathrm{d}\Phi_{n+1}\mathcal{R}]^{(\mathrm{coll},1)} = \mathrm{d}\Phi_n\mathcal{B}\,\mathrm{d}x_1\Bigg[&-\frac{\alpha_s}{2\pi}f_p(x_1,\mu_F)\gamma_p\left(\frac{1}{\hat{\varepsilon}} - \log\frac{\mu_F^2}{\mu^2}\right)\\ &+ \mathrm{d}\xi\theta(1-x_1-\xi)f_p\left(\frac{x_1}{1-\xi},\mu_F\right)\frac{1}{1-\xi}G(1-\xi)\Bigg],\end{aligned} \tag{3.31}$$

where

$$G(1-\xi) = \frac{\alpha_s}{2\pi}\left\{\xi\hat{P}^0_{pp'}(1-\xi)\left[\left(\frac{1}{\xi}\right)_+\log\frac{\mu_F^2}{s_r} - 2\left(\frac{\log\xi}{\xi}\right)_+\right] + \hat{P}^{\varepsilon}_{pp'}(1-\xi)\right\}. \tag{3.32}$$

The pole in the first line of (3.31) has to cancel with a collinear pole from the virtual corrections. The second line contains finite contributions to the cross section. We can introduce a scale Q to obtain the same normalization as in [47].

$$\begin{aligned}\mathrm{d}x_1 f_p(x_1,\mu_F)[\mathrm{d}\Phi_{n+1}\mathcal{R}]^{(coll,1)} = \mathrm{d}\Phi_n\mathcal{B}\,\mathrm{d}x_1\Bigg[&-\frac{\alpha_s}{2\pi}f_p(x_1,\mu_F)\mathcal{N}\gamma_p\left(\frac{1}{\varepsilon} - \log\frac{\mu_F^2}{Q^2}\right)\\ &+ \mathrm{d}\xi\theta(1-x_1-\xi)\ f_p\left(\frac{x_1}{1-\xi},\mu_F\right)\frac{1}{1-\xi}G(1-\xi)\Bigg],\end{aligned} \tag{3.33}$$

where

$$\mathcal{N} = \frac{(4\pi)^{\varepsilon}}{\Gamma(1-\varepsilon)}\left(\frac{\mu^2}{Q^2}\right)^{\varepsilon}. \tag{3.34}$$

The calculation for the limit $y = -1$ leads to an analogous result.

3.1.2. Soft Term

The next step is to investigate the soft term of the real cross section (3.11). It reads

$$[\mathrm{d}\Phi_{n+1}\mathcal{R}]^{(\mathrm{s})} = -\frac{K_0}{2\varepsilon}\,\mathrm{d}\Phi_n\,\mathrm{d}y(1-y^2)^{-1-\varepsilon}\,\mathrm{d}\phi(\sin\phi)^{-2\varepsilon}g(0,y,\phi). \tag{3.35}$$

We can use the *eikonal approximation* of the real matrix element for massless partons

$$|\mathcal{M}_{\mathrm{soft}}|^2 = 4\pi\alpha\sum_{\substack{ij\\i\neq j}}\frac{k_i\cdot k_j}{(k_i\cdot k)(k_j\cdot k)}\mathcal{B}_{ij}. \tag{3.36}$$

A derivation of this formula can be found in appendix H. The indices i, j run over all particles with momentum k_i that can radiate a gluon with momentum k. The case $i = j$ is not included in the sum because this term is proportional to the parton mass $k_i^2 = 0$. The *color correlated born amplitude* $\mathcal{B}_{ij}$ is the born matrix element with the color structure of the real matrix element. Details are given in (H.22). The momentum of the radiated particle is parametrized by its energy fraction ξ and the unit vector of the 3-momentum, i.e.

$$k = \frac{\sqrt{s_r(\xi)}}{2}\xi(1,\hat{k}). \tag{3.37}$$

We can immediately see that the soft matrix element (3.36) is proportional to ξ^{-2}. When we calculate $g(\xi, y)$ this factor cancels. Therefore, we define

$$\tilde{k} = \frac{\sqrt{s}}{2}\begin{pmatrix}1\\ \sqrt{1-y^2}\cos\phi\\ \sqrt{1-y^2}\sin\phi\\ y\end{pmatrix}, \tag{3.38}$$

where s is the born center-of-mass energy, and obtain

$$g(0,y) = 4\pi\alpha_s(1-y^2)\delta_{kg}\sum_{\substack{ij\\i\neq j}}\frac{k_i\cdot k_j}{(k_i\cdot\tilde{k})(k_j\cdot\tilde{k})}\mathcal{B}_{ij}, \tag{3.39}$$

where δ_{kg} means that this function is only non-zero if the radiated parton is a gluon. Since the born matrix element cannot depend on the variables of the radiated particle, $g(0, y)$ has no soft divergence. However, there can still be a collinear divergence.

We have to integrate the soft cross-section term (3.35) over the angles y and ϕ. The ϕ

and y dependent part is given by

$$I_{ij} = \int_0^\pi \mathrm{d}\phi (\sin\phi)^{-2\varepsilon} \int_{-1}^1 \mathrm{d}y (1-y^2)^{-\varepsilon} \frac{k_i \cdot k_j}{(k_i \cdot k)(k_j \cdot k)}. \tag{3.40}$$

Since, the soft term (3.42) has a $\frac{1}{\varepsilon}$ pole, we need $\mathcal{O}(\varepsilon)$ terms. Furthermore, I_{ij} is singular itself when parton i and j are collinear to the gluon. Hence, I_{ij} has a $\frac{1}{\varepsilon}$ pole and we write

$$I_{ij} = \frac{1}{\varepsilon} I^{ij}_{\mathrm{div}} + I^{ij}_0 + \varepsilon I^{ij}_\varepsilon + \mathcal{O}(\varepsilon^2). \tag{3.41}$$

The terms I_{div} and I_0 contribute to the poles and they have to cancel with the poles of the virtual diagrams. The term I_ε gives a finite contribution to the cross section. The solution of this integral is given in Appendix F.
Plugging the result into (3.42), we find

$$\begin{aligned}
[\mathrm{d}\Phi_{n+1}\mathcal{R}]^{(\mathrm{s})} &= -\,\mathrm{d}\Phi_n \frac{\alpha_s}{2\pi} \frac{(4\pi)^\varepsilon}{\Gamma(1-\varepsilon)} \left(\frac{\mu^2}{Q^2}\right)^\varepsilon \times \\
&\quad \times \frac{s_b}{8\pi} \left\{ -\frac{1}{\varepsilon} - \log\frac{Q^2}{s_b} + \varepsilon \left(\frac{\pi^2}{6} - \frac{1}{2}\log^2\frac{Q^2}{s_b} \right) \right\} \frac{1}{2s_b} \sum_{\substack{ij \\ i\neq j}} I_{ij} \mathcal{B}_{ij} \\
&= -\,\mathrm{d}\Phi_n \frac{\alpha_s}{2\pi} \frac{(4\pi)^\varepsilon}{\Gamma(1-\varepsilon)} \left(\frac{\mu^2}{Q^2}\right)^\varepsilon \sum_{\substack{ij \\ i\neq j}} \Bigg\{ \\
&\qquad + \frac{1}{\varepsilon^2} - \frac{1}{\varepsilon}\left[\log\left(\frac{2k_i\cdot k_j}{Q^2}\right) - \log\left(\frac{4k_i^0 k_j^0}{s_b}\right) \right] + \qquad \textbf{(poles)} \\
&\qquad + \left[\frac{1}{2}\log^2\frac{Q^2}{s_b} - \log\frac{Q^2}{s}\log\frac{k_i\cdot k_j}{2k_i^0 k_j^0} - \frac{\pi^2}{6} - \mathrm{Li}_2\left(\frac{x_{ij}}{x_{ij}-1}\right) \right] \qquad \textbf{(finite)} \\
&\qquad \Bigg\} \frac{1}{2s_b} \mathcal{B}_{ij},
\end{aligned} \tag{3.42}$$

where

$$x_{ij} = 1 - \frac{k_i \cdot k_j}{2k_i^0 k_j^0}. \tag{3.43}$$

This term can be combined with the virtual contribution to the cross section because it is only integrated over the born phase space and the pdfs.

3.1.3. Finite Term and Phase-Space Generation

All poles and finite contributions can now be combined with the virtual part of the NLO cross section. The last step is to investigate the subtracted real cross section of (3.13). Since the subtracted real matrix element is finite by construction, we can use the limit $d = 4$ and obtain

$$[\mathrm{d}\Phi_{n+1}\mathcal{R}]^{(fin)} = \mathrm{d}\Phi_{n+1}\frac{1}{2}\left(\frac{1}{\xi}\right)_+\left[\left(\frac{1}{1-y}\right)_+ + \left(\frac{1}{1+y}\right)_+\right]\frac{1}{\xi}g(\xi, y, \phi). \tag{3.44}$$

However, the function g depends not only on the radiation variables ξ, y, ϕ. It depends on the real phase space Φ_{n+1} because the real matrix element depends on it. Our aim is to construct a real phase space from the radiation variables ξ, y, ϕ and an underlying born phase space, i.e. we have to find a mapping $\Phi_{n+1} = \Phi_{n+1}(\Phi_n, \xi, y, \phi)$.

This section describes how we can construct a real phase space from a born phase space and the radiation variables ξ, y and, ϕ. This phase-space construction will be used when we generate events with the POWHEG method (s. chapter 5) where we generate radiation starting from a born process. The description is based on [47].

The real phase space reads

$$\mathrm{d}\Phi_{n+1} = (2\pi)^4\delta^{(4)}\left(x_1K_1 + x_2K_2 - k_{n+1} - \sum_{i=1}^{n}k_i\right)\prod_{i=1}^{n}\frac{\mathrm{d}^3k_i}{(2\pi)^3 2k_i^0}\frac{\mathrm{d}^3k_{n+1}}{(2\pi)^3 2k_{n+1}^0}, \tag{3.45}$$

where k_{n+1} is the momentum of the radiated parton. Our aim is to write the phase space $\mathrm{d}\Phi_{n+1}$ in terms of a born phase space and radiation variables, i.e. we have to combine the momentum k_{n+1} with the initial-state partons within the delta function. We define the total momentum of the initial-state partons and the radiated parton as

$$k_{\mathrm{tot}} = x_1K_1 + x_2K_2 - k_{n+1}. \tag{3.46}$$

Next, we introduce a boost B that transforms the total momentum into a born like total momentum, i.e.

$$\bar{k}_{\mathrm{tot}} = \bar{x}_1K_1 + \bar{x}_2K_2 = Bk_{\mathrm{tot}}. \tag{3.47}$$

We require that the boost is chosen such that the rapidity is invariant. The new momentum fractions $\bar{x}_1$ and $\bar{x}_2$ that we introduced have to be calculated. We assume

that the initial-state momenta of (3.45) are in their center-of-mass (CM) frame, i.e.

$$k_+ = x_1 K_1 = \frac{\sqrt{s}}{2}\begin{pmatrix}1\\ \vec{0}\\ 1\end{pmatrix}, \quad k_- = x_2 K_2 = \frac{\sqrt{s}}{2}\begin{pmatrix}1\\ \vec{0}\\ -1\end{pmatrix}. \tag{3.48}$$

The radiation momentum in this frame is defined as

$$k_{n+1} = \frac{\sqrt{x_1 x_2 S}}{2}\xi\begin{pmatrix}1\\ \sqrt{1-y^2}\cos\phi\\ \sqrt{1-y^2}\sin\phi\\ y\end{pmatrix}. \tag{3.49}$$

Therefore, we have

$$k_{\text{tot}} = \frac{\sqrt{x_1 x_2 S}}{2}\begin{pmatrix}2-\xi\\ -\xi\sqrt{1-y^2}\cos\phi\\ -\xi\sqrt{1-y^2}\sin\phi\\ -\xi y\end{pmatrix}. \tag{3.50}$$

Using (3.48), we find

$$K_{1,2} = \frac{\sqrt{x_1 x_2 S}}{2}\frac{1}{x_{1,2}}\begin{pmatrix}1\\ 0\\ 0\\ \pm 1\end{pmatrix}. \tag{3.51}$$

Plugging the momenta into (3.47), we obtain

$$B\begin{pmatrix}2-\xi\\ -\xi\sqrt{1-y^2}\cos\phi\\ -\xi\sqrt{1-y^2}\sin\phi\\ -\xi y\end{pmatrix} = \begin{pmatrix}\frac{\bar{x}_1}{x_1}+\frac{\bar{x}_2}{x_2}\\ 0\\ 0\\ \frac{\bar{x}_1}{x_1}-\frac{\bar{x}_2}{x_2}\end{pmatrix}. \tag{3.52}$$

Since B is chosen such that the rapdity of k_{tot} is conserved, we find

$$\frac{\bar{x}_1}{x_1}\frac{x_2}{\bar{x}_2} = \frac{2-\xi(1+y)}{2-\xi(1-y)}. \tag{3.53}$$

Using the invariant mass leads to

$$\frac{\bar{x}_1}{x_1}\frac{\bar{x}_2}{x_2} = 1-\xi. \tag{3.54}$$

Solving both equations for $\bar{x}_1$, $\bar{x}_2$, we obtain

$$\bar{x}_{1/2} = x_{1/2}\sqrt{1-\xi}\sqrt{\frac{2-\xi(1\pm y)}{2-\xi(1\mp y)}}. \tag{3.55}$$

Therefore, we can rewrite the real phase space in terms of a born phase space and radiation variables, i.e.

$$\begin{aligned}\int_0^1 \mathrm{d}x_1 \int_0^1 \mathrm{d}x_2 \; \mathrm{d}\Phi_{n+1} = \int_0^{\bar{x}_1^{\max}} \mathrm{d}\bar{x}_1 \int_0^{\bar{x}_2^{\max}} \mathrm{d}\bar{x}_2 \, (2\pi)^4 \delta^{(4)}\left(\bar{x}_1 K_1 + \bar{x}_2 K_2 - \sum_{i=1}^n \bar{k}_i\right) \prod_{i=1}^n \frac{\mathrm{d}^3\bar{k}_i}{2\bar{k}_i^0 (2\pi)^3} \\ \times \frac{s}{(4\pi)^3}\frac{\xi}{1-\xi}\,\mathrm{d}\xi\,\mathrm{d}y\,\mathrm{d}\phi,\end{aligned} \tag{3.56}$$

where we define

$$\bar{k}_i = B k_i \quad i = 1, \ldots, n, \tag{3.57}$$

and use that the momentum integration is boost invariant. Furthermore, we use

$$\frac{\mathrm{d}^3 k_{n+1}}{(2\pi)^3 2E} = \mathrm{d}\xi\,\mathrm{d}y\,\mathrm{d}\phi \frac{\xi s}{(4\pi)^3}. \tag{3.58}$$

When we transform the integration variables $x_{1,2}$ into $\bar{x}_{1,2}$, the $\bar{x}_{1,2}$ integration is not bound to the interval $[0,1]$ anymore. However, the interpretation of $\bar{x}_{1,2}$ as born momentum fractions requires a restriction to $[0,1]$. Therefore, we use

$$\theta(\bar{x}_1^{\max}(\xi,y) - \bar{x}_1)\theta(\bar{x}_2^{\max}(\xi,y) - \bar{x}_2) = \theta(\xi_{\max}(\bar{x}_1,\bar{x}_2,y) - \xi), \tag{3.59}$$

where

$$\begin{aligned}\xi_{\max} = 1 - \max\Bigg\{ &\frac{2(1+y)\bar{x}_1^2}{\sqrt{(1+\bar{x}_1^2)^2(1-y)^2 + 16y\bar{x}_1^2} + (1-y)(1-\bar{x}_1^2)}, \\ &\frac{2(1-y)\bar{x}_2^2}{\sqrt{(1+\bar{x}_2^2)^2(1+y)^2 - 16y\bar{x}_2^2} + (1+y)(1-\bar{x}_2^2)}\Bigg\}.\end{aligned} \tag{3.60}$$

This means that the maximal radiation energy is limited by the maximal energy of the born initial-state momenta. We can write the phase space (3.56) as

$$\int_0^1 \mathrm{d}x_1 \int_0^1 \mathrm{d}x_2 \; \mathrm{d}\Phi_{n+1} = \int_0^1 \mathrm{d}\bar{x}_1 \int_0^1 \mathrm{d}\bar{x}_2 \; \mathrm{d}\bar{\Phi}_n \, \mathrm{d}\Phi_{\mathrm{rad}} \theta(\xi_{\max}(\bar{x}_1,\bar{x}_2,y) - \xi), \tag{3.61}$$

where the underlying born phase space is given by

$$\mathrm{d}\bar{\Phi}_n = (2\pi)^4 \delta^{(4)} \left(\bar{x}_1 K_1 + \bar{x}_2 K_2 - \sum_{i=1}^{n} \bar{k}_i \right) \prod_{i=1}^{n} \frac{\mathrm{d}^3 \bar{k}_i}{2\bar{k}_i^0 (2\pi)^3} \tag{3.62}$$

and the radiation phase space reads

$$\mathrm{d}\Phi_{\mathrm{rad}} = \frac{s}{(4\pi)^3} \frac{\xi}{1-\xi} \, \mathrm{d}\xi \, \mathrm{d}y \, \mathrm{d}\phi. \tag{3.63}$$

The momenta $\bar{k}_i$ are the final-state moment of the underlying born, i.e.

$$\bar{k}_{\mathrm{tot}} = \sum_{i=1}^{n} \bar{k}_i. \tag{3.64}$$

Since our goal is to construct the real phase space from the underlying born phase space, we use the CM frame of $\bar{x}_1 K_1$ and $\bar{x}_2 K_2$ as reference frame for the construction of the momenta. We can express the real momenta k_+ and k_- in this frame in terms of the momentum fractions, i.e.

$$k_+ = \frac{\sqrt{\bar{x}_1 \bar{x}_2 S}}{2} \frac{x_1}{\bar{x}_1} \begin{pmatrix} 1 \\ 0 \\ 0 \\ 1 \end{pmatrix} \qquad \text{and} \qquad k_- = \frac{\sqrt{\bar{x}_1 \bar{x}_2 S}}{2} \frac{x_2}{\bar{x}_2} \begin{pmatrix} 1 \\ 0 \\ 0 \\ -1 \end{pmatrix}. \tag{3.65}$$

The momentum of the radiated parton (3.49) is defined in the CM frame of k_+ and k_-. Therefore, we have to boost the momentum into the CM system of $\bar{x}_1 K_1$ and $\bar{x}_2 K_2$. To do this, we construct a boost that boosts k_+ and k_- into their CM system, i.e.

$$\Lambda(k_+ + k_-) = \begin{pmatrix} \sqrt{x_1 x_2 S} \\ \vec{0} \end{pmatrix} \tag{3.66}$$

and use the inverse boost to transform k. The boost is given by

$$\Lambda = \frac{1}{2\sqrt{x_1 x_2 \bar{x}_1 \bar{x}_2}} \begin{pmatrix} \bar{x}_1 x_2 + x_1 \bar{x}_2 & 0 & 0 & \bar{x}_1 x_2 - x_1 \bar{x}_2 \\ 0 & 1 & 0 & 0 \\ 0 & 0 & 1 & 0 \\ \bar{x}_1 x_2 - x_1 \bar{x}_2 & 0 & 0 & \bar{x}_1 x_2 + x_1 \bar{x}_2 \end{pmatrix}. \tag{3.67}$$

We can now calculate the initial-state momenta and the momentum of the radiated parton from the underlying born phase space. Concerning the final-state momenta, we

have to find a boost which connects the final-state momenta of Φ_{n+1} with the momenta of $\bar{\Phi}_n$.
Since we choose $\bar{\Phi}_n$ such that it is given in the partonic CM system, the rapidity is zero and its invariant mass is given by $\bar{m}^2 = \bar{x}_1\bar{x}_2 S$. Using the boost Λ, we obtain

$$k^x_{\text{tot}} = -\frac{1}{2}\xi\cos\phi\sqrt{x_1x_2S(1-y^2)} \tag{3.68}$$

$$k^y_{\text{tot}} = -\frac{1}{2}\xi\sin\phi\sqrt{x_1x_2S(1-y^2)}. \tag{3.69}$$

Since the rapidity is invariant under the boost that connects k_{tot} and $\bar{k}_{\text{tot}}$, we obtain $k^z_{\text{tot}} = 0$. Using that the invariant mass is conserved, we find

$$k^0_{\text{tot}} = \frac{1}{2}\sqrt{x_1x_2S\left[\xi^2(1-y^2)+4(1-\xi)\right]}. \tag{3.70}$$

Since the transverse components of $\bar{k}_{\text{tot}}$ are zero in its CM frame, we need a transverse boost that fulfills

$$\Lambda_T k_{\text{tot}} = \bar{k}_{\text{tot}}. \tag{3.71}$$

There is more than one boost with properties. One possible choice is to use

$$\Lambda_T = \begin{pmatrix} \cosh\eta_2 & 0 & -\sinh\eta_2 & 0 \\ 0 & 1 & 0 & 0 \\ -\sinh\eta_2 & 0 & \cosh\eta_2 & 0 \\ 0 & 0 & 0 & 1 \end{pmatrix} \begin{pmatrix} \cosh\eta_1 & -\sinh\eta_1 & 0 & 0 \\ -\sinh\eta_1 & \cosh\eta_1 & 0 & 0 \\ 0 & 0 & 1 & 0 \\ 0 & 0 & 0 & 1 \end{pmatrix}, \tag{3.72}$$

where

$$\sinh\eta_1 = \xi\cos\phi\sqrt{\frac{y^2-1}{\xi^2(y^2-1)\sin^2\phi+4(\xi-1)}}, \tag{3.73}$$

$$\sinh\eta_2 = \frac{1}{2}\xi\sin\phi\sqrt{\frac{1-y^2}{1-\xi}}. \tag{3.74}$$

Using Λ_T we can calculate the final state momenta of Φ_{n+1} with

$$k_i = \Lambda\Lambda_T^{-1}\bar{k}_i \quad \text{for } i = 1,\ldots,n, \tag{3.75}$$

where Λ is used to transform the real phase space into its CM system. We also have to transform k_{tot} with Λ. This completes the construction of the initial-state FKS phase space.

3.2. Final-State Radiation

When a parton is radiated from a final-state parton, the matrix element has soft and collinear singularities as well. In contrast to initial-state radiation, we cannot use the beam axis as natural direction for the phase-space parameterization because the collinear singularity would not occur at $\cos\theta = 1$. Here, we define the spherical coordinate system in terms of the final-state particle momenta. In general, the matrix element has multiple divergences connected to all possible emissions. In the following derivation, we assume, as for initial-state radiation, that there is only one singularity which is connected to the emission of a gluon from a quark. The general case is discussed at the end of this section. We use the gluon as radiated FKS parton k and the momentum p_j of the quark as basis for the coordinate system because there is no soft singularity connected to the quark. In contrast to initial-state radiation, the anti-collinear singularity for $\cos\theta = -1$ is not present in final-state radiation. We parametrize the momenta of the real phase space in the center-of-mass frame of the incoming partons where the partons move along the z direction. We construct another spherical coordinate system where p_j defines the z-direction, i.e.

$$p'_j = \frac{\sqrt{s}}{2}\xi_j \begin{pmatrix} 1 \\ \vec{0} \\ 1 \end{pmatrix}. \tag{3.76}$$

This coordinate system is connected to the original system by a rotation, i.e. $p_j = Rp'_j$. In this system, the radiated parton has the four momentum

$$k' = R^{-1}(\theta_j, \phi_j)k = \frac{\sqrt{s}}{2}\xi \begin{pmatrix} 1 \\ \cos\phi\sqrt{1-y^2} \\ \sin\phi\sqrt{1-y^2} \\ y \end{pmatrix}, \tag{3.77}$$

where $y = \cos\theta$ is the angle between the momenta k and p_j. Therefore, the matrix element has a collinear divergence at $y = 1$. Since the phase space integral is Lorentz invariant, we can write the real phase space as

$$\mathrm{d}\Phi_{n+1} = (2\pi)^d\, \delta^{(d)}\left(q - Rk' - \sum_{i=1}^{n} p_i\right) \prod_{i=1}^{n} \frac{\mathrm{d}^{d-1}p_i}{(2\pi)^{d-1}2p_i^0} \frac{\mathrm{d}^{d-1}k'}{(2\pi)^{d-1}2k'^0}, \tag{3.78}$$

where

$$q = x_1K_1 + x_2K_2. \tag{3.79}$$

We define

$$g(\xi, y, \phi) = (1-y)\xi^2 \mathcal{R} \tag{3.80}$$

to remove the singularities from the real matrix element. We use the distribution expansions (3.9) and

$$(1-y)^{-1-\varepsilon} = -\frac{2^{-\varepsilon}}{\varepsilon}\delta(1-y) + \left(\frac{1}{1-y}\right)_+ + \mathcal{O}(\varepsilon) \tag{3.81}$$

to split the partonic cross section into a soft, a collinear and a finite part, i.e.

$$\mathrm{d}\hat{\sigma} = [\mathrm{d}\Phi_{n+1}\mathcal{R}]^{(\mathrm{s})} + [\mathrm{d}\Phi_{n+1}\mathcal{R}]^{(\mathrm{coll})} + [\mathrm{d}\Phi_{n+1}\mathcal{R}]^{(\mathrm{fin})}. \tag{3.82}$$

This splitting is analogous to the splitting for initial-state radiation in (3.10). The soft term reads

$$[\mathrm{d}\Phi_{n+1}\mathcal{R}]^{(\mathrm{s})} = -\,\mathrm{d}\Phi_n\,\mathrm{d}y\,\mathrm{d}\phi \frac{K_0}{2\varepsilon}\frac{(1-y^2)^{-\varepsilon}}{1-y}\,(\sin\phi)^{-2\varepsilon}\,g(0,y,\phi), \tag{3.83}$$

where K_0 is defined in (3.5). Note that this term contains a soft-collinear $\frac{1}{\varepsilon^2}$-pole. The soft limit and the integrals are the same as in the initial-state case in section 3.1.2. The collinear term is given by

$$[\mathrm{d}\Phi_{n+1}\mathcal{R}]^{(\mathrm{coll})} = -\,\mathrm{d}\Pi\Big|_{y\to 1}\,\mathrm{d}\xi\,\mathrm{d}\phi K_0\left[\frac{2^{-\varepsilon}}{\varepsilon}\left(\frac{1}{\xi}\right)_+ - 2\left(\frac{\log\xi}{\xi}\right)_+\right]2^{-\varepsilon}\,(\sin\phi)^{-2\varepsilon}\,g(\xi,1,\phi). \tag{3.84}$$

The finite term reads

$$[\mathrm{d}\Phi_{n+1}\mathcal{R}]^{(fin)} = \mathrm{d}\Phi_{n+1}\left(\frac{1}{\xi}\right)_+\left(\frac{1}{1-y}\right)_+\frac{1}{\xi}g(\xi,y,\phi). \tag{3.85}$$

In the following sections, we will investigate the soft and collinear terms further.

3.2.1. Collinear Limit

In the collinear limit, the emitted parton flies in the same direction as the emitter, i.e.

$$\frac{\sqrt{s}}{2}\xi R\begin{pmatrix}1\\ \vec{0}\\ 1\end{pmatrix} + p_j = \frac{\sqrt{s}}{2}(\xi+\xi_j)\begin{pmatrix}1\\ \hat{p}_j\end{pmatrix}, \tag{3.86}$$

where j is the emitter, $\hat{p}_j$ is its direction and $\xi_{i,j}$ are the momentum fractions. We define the energy fraction of the mother parton as

$$\hat{\xi} = \xi + \xi_j. \tag{3.87}$$

The collinear phase space reads

$$\mathrm{d}\Pi\Big|_{y\to 1} = (2\pi)^d\,\delta^{(d)}\left(q - \sum_{\substack{i=1\\ l\neq j}}^{n} p_i - \frac{\sqrt{s}}{2}(\xi+\xi_j)\hat{p}_j\right)\prod_{i=1}^{n}\frac{\mathrm{d}^{d-1}p_i}{(2\pi)^{d-1}2p_i^0}. \tag{3.88}$$

Next, we also write the p_j integration in spherical coordinates and obtain

$$\begin{aligned}[\mathrm{d}\Phi_{n+1}\mathcal{R}]^{(\mathrm{coll})} = \prod_{\substack{i=1\\ i\neq j}}^{n}\frac{\mathrm{d}^{d-1}k_i}{(2\pi)^{d-1}2k_i^0}\,\mathrm{d}y_j\,\mathrm{d}\phi_j K_0^2(\sin\phi_j)^{-2\varepsilon}(1-y_j^2)^{-\varepsilon}2^{-\varepsilon}\\ \times\,\mathrm{d}\phi(\sin\phi)^{-2\varepsilon}\,\mathrm{d}\xi\left[\frac{2^{-\varepsilon}}{\varepsilon}\left(\frac{1}{\xi}\right)_+ - 2\left(\frac{\log\xi}{\xi}\right)_+\right]F(\xi),\end{aligned} \tag{3.89}$$

where

$$F(\xi) = \mathrm{d}\xi_j\xi_j^{1-2\varepsilon}(2\pi)^d\,\delta^{(d)}\left(q - \sum_{\substack{i=1\\ i\neq j}}^{n} p_i - \frac{\sqrt{s}}{2}\bar{\xi}\hat{p}_j\right)g(\xi,1,\phi) \tag{3.90}$$

contains the whole ξ dependence. The collinear limit of g is given by the splitting function (3.21) and the born matrix element

$$\begin{aligned} g(\xi,1,\phi) &= \xi^2(1-y)\frac{4\pi\alpha_s\mu^{2\varepsilon}}{k\cdot p_j}\hat{P}_{qq}\left(\frac{\xi_j}{\bar{\xi}}\right)\mathcal{B}(\bar{\xi})\\ &= \alpha_s\mu^{2\varepsilon}\frac{16\pi}{s}\frac{\xi}{\xi_j}\hat{P}_{qq}\left(\frac{\xi_j}{\bar{\xi}}\right)\mathcal{B}(\bar{\xi}),\end{aligned} \tag{3.91}$$

where the born matrix element $\mathcal{B}$ depends on the energy fraction $\bar{\xi}$ of the mother particle. Using $\bar{\xi}$ instead of ξ_j as integration variable, where $\xi_j = \bar{\xi} - \xi$, we obtain

$$F(\xi) = \int_\xi^1 \mathrm{d}\bar{\xi}\,(\bar{\xi}-\xi)^{1-2\varepsilon}(2\pi)^d\,\delta^{(d)}\left(q - \sum_{\substack{i=1\\ i\neq j}}^{n} p_i - \frac{\sqrt{s}}{2}\bar{\xi}\hat{p}_j\right)\frac{16\pi\alpha_s\mu^{2\varepsilon}\xi}{(\bar{\xi}-\xi)s}\hat{P}_{qq}\left(\frac{\xi_j}{\bar{\xi}}\right)\mathcal{B}(\bar{\xi}), \tag{3.92}$$

where we used energy conservation to restrict the integration range. In (3.89), we have to apply the plus distributions. When we apply a plus distribution $[f(\xi)]_+$, we obtain

$$\begin{aligned}\mathrm{d}\xi\,[f(\xi)]_+\,F(\xi) = \frac{16\pi\alpha_s\mu^{2\varepsilon}}{s}\,\mathrm{d}\bar{\xi}\bar{\xi}^{1-2\varepsilon}\mathcal{B}(\bar{\xi})(2\pi)^d\,\delta^{(d)}\left(q-\sum_{\substack{i=1\\i\neq j}}^{n}p_i-\frac{\sqrt{s}}{2}\bar{\xi}\hat{p}_j\right)\\ \times\,\mathrm{d}z\theta(\frac{1}{\bar{\xi}}-z)\bar{\xi}f(\bar{\xi}z)\left\{\theta(\bar{\xi}(1-z))\frac{z(1-z)^{-2\varepsilon}}{1-z}\hat{P}_{qq}(1-z)-\left[\frac{\xi}{\bar{\xi}}\hat{P}_{qq}\left(\frac{\bar{\xi}-\xi}{\bar{\xi}}\right)\right]_{\xi=0}\right\}.\end{aligned} \tag{3.93}$$

We can rewrite the z integral in the following way

$$\int_0^{\frac{1}{\bar{\xi}}}\mathrm{d}z\,\cdots=\int_0^1\mathrm{d}z\,\left[\xi\left[f(\bar{\xi}z)\right]_+(1-z)^{-2\varepsilon}z\hat{P}_{qq}(1-z)\right]+\left[\frac{\xi}{\bar{\xi}}\hat{P}_{qq}\left(\frac{\bar{\xi}-\xi}{\bar{\xi}}\right)\right]_{\xi=0}\int_{\frac{1}{\bar{\xi}}}^1\mathrm{d}z\,\bar{\xi}f(z\bar{\xi}). \tag{3.94}$$

Using (3.93) in (3.89), we obtain

$$\begin{aligned}[\mathrm{d}\Phi_{n+1}\mathcal{R}]^{(\mathrm{coll})} = \frac{\alpha_s}{2\pi}\mathcal{N}\,\mathrm{d}\Phi_n\mathcal{B}\left\{\frac{1}{\varepsilon}\left(\mathcal{I}_1+\left[\frac{\xi}{\bar{\xi}}\hat{P}_{qq}\left(\frac{\bar{\xi}-\xi}{\bar{\xi}}\right)\right]_{\xi=0}\log\bar{\xi}\right)\right.\\ \left.+\log\frac{Q^2}{s}\mathcal{I}_1-2\mathcal{I}_2(\bar{\xi})+\left[\frac{\xi}{\bar{\xi}}\hat{P}_{qq}\left(\frac{\bar{\xi}-\xi}{\bar{\xi}}\right)\right]_{\xi=0}\left(\log\bar{\xi}\log\frac{Q^2}{s}-\log^2\bar{\xi}\right)\right\},\end{aligned} \tag{3.95}$$

where we integrated over the azimuthal angle ϕ, introduced the same normalization (3.34) as in initial-state radiation, and calculated

$$\mathcal{I}_1=\int_0^1\mathrm{d}z\,\left(\frac{1}{z}\right)_+(1-z)^{-2\varepsilon}z\hat{P}_{qq}(1-z)=-\frac{3}{2}C_F+\left(\frac{2}{3}\pi^2-3\right)C_F\varepsilon+\mathcal{O}(\varepsilon^2), \tag{3.96}$$

$$\mathcal{I}_2(\xi)=\int_0^1\mathrm{d}z\,\left(\frac{\log(\xi z)}{z}\right)_+(1-z)^{-2\varepsilon}z\hat{P}_{qq}(1-z)=\left(\frac{7}{4}-\frac{3}{2}\log\xi\right)C_F+\mathcal{O}(\varepsilon). \tag{3.97}$$

In QCD, there are also processes with a gluon in the LO final state. When the gluon splits into two quarks, we get an analogous contribution as for the $q\to qg$ splitting. We use the $\hat{P}_{qg}$ splitting functions in (3.96) and (3.97) and obtain

$$\mathcal{I}_1=\frac{2}{3}T_Fn_f+\frac{10}{9}\varepsilon T_Fn_f+\mathcal{O}(\varepsilon^2), \tag{3.98}$$

$$\mathcal{I}_2(\xi)=\frac{6}{9}T_Fn_f\log\xi-\frac{13}{18}T_Fn_f+\mathcal{O}(\varepsilon), \tag{3.99}$$

where the factor n_f is there because the gluon can split into n_f quark flavors. A gluon can also split into two gluons. However, this term cannot be calculated by substituting $\hat{P}_{gg}$ because both gluons can become soft. In the above calculation we assumed that parton k is soft and subtracted the divergence. When two gluons are in the final state, we have another divergence for $z = 1$ in (3.96) and (3.97). We have to introduce FKS S functions to handle the problem. Therefore, the calculation is postponed to section 3.3.1.

3.2.2. Soft Limit

Evaluating the soft term defined in (3.83) leads to the same result as for initial-state radiation (ISR) in section 3.1.2 because we have to solve the same eikonal integral.

However, evaluating the soft limit of $g(\xi, y, \phi)$ defined in (3.80) is more involved. Hence, we describe how to implement $g(0, y, \phi)$. The soft matrix element in the eikonal limit is given in (3.36). The momenta entering the eikonal factor cannot be parametrized in spherical coordinates with the beam axis as main axis. We have to construct the momentum of the gluon in a frame where the mother particle momentum points in an arbitrary direction. When we take the soft limit, i.e. $\xi \to 0$, the momentum of the radiated parton approaches zero and the real phase space is equal to the born phase space. However, the energy fraction ξ of the momentum k is canceled in the eikonal factor with the ξ^2 factor which is used to regularize the matrix element in g. Therefore, we have to use a momentum $\tilde{k} = \frac{1}{\xi}k$ which is parametrized in the angular FKS variables y and ϕ.

We start in a frame where the mother particle flies in z-direction. Mother particle means here the particle which we have chosen to parametrize the phase space in terms of FKS variables. Note that the particle from the real phase space, which is not soft, flies in the same direction because the soft particle does not affect this particle. The four momentum of the gluon is then given by

$$\tilde{k}' = \frac{\sqrt{s}}{2} \begin{pmatrix} 1 \\ \sqrt{1-y^2}\cos\phi \\ \sqrt{1-y^2}\sin\phi \\ y \end{pmatrix}. \tag{3.100}$$

In a given born phase space Φ_n the final-state particles do not fly in z-direction. Therefore, we have to rotate $\tilde{k}'$ into the frame of the mother particle p_m on born level, i.e. we have to find a rotation which transforms the mother particle from the frame where it flies in z

direction to the frame of Φ_n. The rotation matrix R has to fulfill

$$p_m = R\frac{\sqrt{s}}{2}\begin{pmatrix}1\\ \vec{0}\\ 1\end{pmatrix}, \tag{3.101}$$

where p_m is a given momentum from the born phase space Φ_n. To obtain the rotation matrix R, we calculate the polar angle of p_m with respect to $\vec{p}_m = (\vec{0}, 1)$

$$\cos\theta_m = \frac{p_m^z}{p_m^0}. \tag{3.102}$$

The azimuthal angle can be computed using[1]

$$\tan\phi = \frac{p_m^y}{p_m^x}. \tag{3.103}$$

The rotation matrix is given by

$$R = \begin{pmatrix}1 & 0 & 0 & 0\\ 0 & \cos\phi_m & \sin\phi_m & 0\\ 0 & -\sin\phi_m & \cos\phi_m & 0\\ 0 & 0 & 0 & 1\end{pmatrix}\begin{pmatrix}1 & 0 & 0 & 0\\ 0 & 1 & 0 & 0\\ 0 & 0 & \cos\theta_m & \sin\theta_m\\ 0 & 0 & -\sin\theta_m & \cos\theta_m\end{pmatrix}. \tag{3.104}$$

Now, we can evaluate the eikonal factor and the matrix element using $\tilde{k}$ and the born phase space Φ_n. The FKS g function for gluon radiation is similar to the ISR case in (3.105), i.e.

$$g(0,y) = 4\pi\alpha_s(1-y)\delta_{kg}\sum_{\substack{ij\\ i\neq j}}\frac{k_i\cdot k_j}{(k_i\cdot R\tilde{k})(k_j\cdot R\tilde{k})}\mathcal{B}_{ij}. \tag{3.105}$$

3.2.3. Finite Term and Phase-Space Generation

As for the initial-state subtracted real cross section, we have to construct the real phase space from an underlying born phase space and the FKS radiation variables ξ, y, and ϕ. The finite term in (3.85) is an integral over the real phase space $\mathrm{d}\Phi_{n+1}$, where the FKS parton is parametrized by the angle y and the energy fraction ξ. As for the initial-state case, the phase-space construction is based on [47]. We construct the real phase space in the center-of-mass frame of the initial-state partons, i.e.

$$q = x_1K_1 + x_2K_2 = (q^0, 0, 0, 0), \tag{3.106}$$

[1] In practice, it useful to use the function atan2 defined in C99, POSIX.1-2001 to calculate ϕ.

where $q^0 = \sqrt{s}$. The real phase space is given by

$$\mathrm{d}\Phi_{n+1} = \frac{\mathrm{d}^3 k_{n+1}}{(2\pi)^3 2k_{n+1}^0} \frac{\mathrm{d}^3 k_j}{(2\pi)^3 2k_j^0} \prod_{\substack{i=1 \\ i\neq j}}^{n} \frac{\mathrm{d}^3 k_l}{(2\pi)^3 2k_i^0} (2\pi)^4 \, \delta^{(4)} \left(q - k - \sum_{\substack{i=1 \\ i\neq j}}^{n} k_i \right), \tag{3.107}$$

where we define

$$k = k_{n+1} + k_j \tag{3.108}$$

because we consider that a born parton splits into two partons with momenta k_{n+1} and k_j. Our goal is to write the real phase space in terms of a born phase space $\mathrm{d}\bar{\Phi}_n$ and parametrize the radiated particle with the FKS variables ξ, y, and ϕ, i.e.

$$\mathrm{d}\Phi_{n+1} = J \, \mathrm{d}\xi \, \mathrm{d}y \, \mathrm{d}\phi \, \mathrm{d}\bar{\Phi}_n, \tag{3.109}$$

where J is a Jacobian that we calculate in the following and ϕ is an azimuthal angle. To write the delta-function of the real phase space (3.107) in terms of the born momenta $\bar{k}_i$ in $\mathrm{d}\Phi_n$, we use boost invariance. Furthermore, the initial-state momenta shall not change in the construction of the final-state radiation (FSR) phase space, i.e. $x_{1,2} = \bar{x}_{1,2}$. Therefore, we introduce a boost which fulfills

$$\Lambda \left(q - k - k_{\mathrm{rec}} \right) = q - \bar{k}_j - \sum_{\substack{i=1 \\ i\neq j}}^{n} \bar{k}_i, \tag{3.110}$$

where the recoiling momenta are defined by

$$k_{\mathrm{rec}} = \sum_{\substack{i=1 \\ i\neq j}}^{n} k_i, \tag{3.111}$$

$\bar{k}_i = \Lambda k_i$ for $1 \leq i \leq n, i \neq j$ and,

$$\Lambda(q - k) = q - \bar{k}_j. \tag{3.112}$$

That this boost always exists can be shown by direct construction. Momentum conservation for the underlying born phase space implies

$$q = \sum_{i=1}^{n} \bar{k}_i \;\Rightarrow\; \bar{k}_j = q - \Lambda k_{\mathrm{rec}}. \tag{3.113}$$

Since the mother particle $\bar{k}_j$ is massless, we have the condition

$$0 = \bar{k}_j^2 = (q - \Lambda k_{\text{rec}})^2 \,. \tag{3.114}$$

We use a boost in direction of k_{rec} and after a lengthy calculation, we obtain from (3.114) the boost velocity

$$\beta = \frac{q^2 - (k_{\text{rec}}^0 + |k_{\text{rec}}|)^2}{q^2 + (k_{\text{rec}}^0 + |k_{\text{rec}}|)^2}. \tag{3.115}$$

Using Lorentz invariance of the delta function and the momentum integration, we obtain

$$\mathrm{d}\Phi_{n+1} = \frac{\mathrm{d}^3 k_{n+1}}{(2\pi)^3 2k_{n+1}^0} \frac{\mathrm{d}^3 k_j}{(2\pi)^3 2k_j^0} \prod_{\substack{i=1 \\ i\neq j}}^{n} \frac{\mathrm{d}^3 \bar{k}_i}{(2\pi)^3 2\bar{k}_i^0} (2\pi)^4 \, \delta^{(4)} \left(q - \sum_{i=1}^{n} \bar{k}_i \right). \tag{3.116}$$

We can change the integration from $\mathrm{d}^3 k_j$ to $\mathrm{d}^3 k$ because k_j and k are connected by linear shift. The integration over the emitted parton is most easily parametrized in spherical coordinates

$$\frac{\mathrm{d}^3 k_{n+1}}{(2\pi)^3 2k_{n+1}^0} = \frac{s}{(4\pi)^3} \xi \, \mathrm{d}\xi \, \mathrm{d}\cos\psi \, \mathrm{d}\phi, \tag{3.117}$$

where the angle ψ is the angle between k_{n+1} and k. The azimuthal integration ϕ can be identified with the azimuthal integration in (3.109). The real phase space is then given by

$$\mathrm{d}\Phi_{n+1} = \frac{s}{(4\pi)^3} \xi \, \mathrm{d}\xi \, \mathrm{d}\cos\psi \, \mathrm{d}\phi \frac{|k|^2 \, \mathrm{d}|k| \, \mathrm{d}\Omega}{(2\pi)^3 2k^0} \prod_{\substack{i=1 \\ i\neq j}}^{n} \frac{\mathrm{d}^3 \bar{k}_i}{(2\pi)^3 2\bar{k}_i^0} (2\pi)^4 \, \delta^{(4)} \left(q - \sum_{i=1}^{n} \bar{k}_i \right). \tag{3.118}$$

The momentum of the mother particle has the same direction as the momentum of particle j in the underlying born phase space. Therefore, we can write

$$\mathrm{d}^3 k \quad = |k|^2 \, \mathrm{d}|k| \, \mathrm{d}\Omega \tag{3.119}$$

$$\mathrm{d}^3 \bar{k}_j \quad = |\bar{k}_j|^2 \, \mathrm{d}|\bar{k}_j| \, \mathrm{d}\Omega, \tag{3.120}$$

where the angular integration $\mathrm{d}\Omega$ is the same in both cases. Therefore, we only have to change the radial integration of k to the underlying born momentum in order to write $\mathrm{d}\Phi_{n+1}$ in terms of $\mathrm{d}\Phi_n$. Comparing (3.118) with (3.109), we have to find $y(\psi, k)$, $\bar{k}_j(\psi, k)$ and derive the associated Jacobian J in

$$\frac{s}{(4\pi)^3} \xi \frac{|k|^2}{k_j^0} \, \mathrm{d}\cos\psi \, \mathrm{d}|k| = J |\bar{k}_j|^2 \, \mathrm{d}y \, \mathrm{d}|\bar{k}_j|. \tag{3.121}$$

First, we derive y in terms of $\cos\psi$ and $|k|$. We find that

$$y = \frac{|k|^2 - |k_j|^2 - |k_{n+1}|^2}{2|k_j||k_{n+1}|}. \tag{3.122}$$

The length of the vector $|k_j|$ in terms of the angle ψ and the length $|k|$ is given by

$$|k_j|^2 = |k|^2 + |k_{n+1}|^2 - 2|k||k_{n+1}|\cos\psi. \tag{3.123}$$

Using (3.112) we obtain

$$(q - \bar{k}_j)^2 = (q^0 - k^0)^2 - |k|^2 \tag{3.124}$$

because we work in the center of mass frame with $q = (q^0, 0, 0, 0)$. Hence, the new integration variable is given by

$$|\bar{k}_j| = \frac{q^2 - (q^0 - k^0)^2 + |k|^2}{2q^0}. \tag{3.125}$$

For the Jacobian determinant of the transformation, we find

$$J = \frac{q^2\xi}{(4\pi)^3}\frac{|k_j|^2}{|\bar{k}_j|}\left(|k_j| - \frac{k^2}{2q^0}\right)^{-1}, \tag{3.126}$$

where $k^2 = 2|k_j||k_{n+1}|(1-y)$. The term $|k_j|$ depends on ψ. Therefore, we have to express it in terms of y and ξ.

First, we use that the energy of the emitted parton is given by

$$k^0_{n+1} = \xi\frac{\sqrt{s}}{2}. \tag{3.127}$$

The maximal energy of k_{n+1} is limited by the energy of the mother parton $\bar{k}_j$. Since the mother parton is massless, we find $k^0_{n+1} < |\bar{k}_j|$, i.e.

$$\xi_{\max} = 1 - \frac{M^2}{s}, \tag{3.128}$$

where we defined the invariant mass M^2 as

$$M^2 = k^2_{\text{rec}} = (q^0 - k^0)^2 - |k|^2. \tag{3.129}$$

In a frame, where the mother momentum k points in z direction, we have

$$\vec{k}_{n+1} = k^0_{n+1} \begin{pmatrix} \sin\psi\cos\phi \\ \sin\psi\sin\phi \\ \cos\psi \end{pmatrix} \tag{3.130}$$

and

$$k_j = \begin{pmatrix} |k_j| \\ -k^0_{n+1}\sin\psi\cos\phi \\ -k^0_{n+1}\sin\psi\sin\phi \\ |k| - k^0_{n+1}\cos\psi \end{pmatrix}. \tag{3.131}$$

The absolute value of k is given by

$$|k|^2 = |k_j|^2 + (k^0_{n+1})^2 + 2k^0_{n+1}|k_j|y. \tag{3.132}$$

We use energy conservation to obtain a relation for $|k_j|$, i.e.

$$\sqrt{s} = |k_j| + k^0_{n+1} + \sqrt{M^2 + |k|^2}, \tag{3.133}$$

where M^2 is the invariant mass of the 4 momentum which recoils against k. We can express M^2 also in terms of the underlying born phase space $\mathrm{d}\bar{\Phi}_n$ and obtain

$$M^2 = k^2_{\mathrm{rec}} = \left(\sum_{\substack{l=1 \\ l\neq j}}^{n} \bar{k}_l \right)^2 = (q - \bar{k}_j)^2. \tag{3.134}$$

Solving (3.133) yields

$$|k_j| = \frac{s - M^2 - 2\sqrt{s}k^0_{n+1}}{2(\sqrt{s} - k^0_{n+1}(1-y))}. \tag{3.135}$$

Using this in (3.126), we find

$$\mathrm{d}\Phi_{\mathrm{rad}} = \frac{2s\xi}{(4\pi)^3} \frac{|k_j|}{|\bar{k}_j|} \frac{1}{2 - \xi(1-y)} \,\mathrm{d}\xi\,\mathrm{d}y\,\mathrm{d}\phi, \tag{3.136}$$

where

$$\frac{|k_j|}{|\bar{k}_j|} = \frac{(1-\xi)s - M^2}{s - M^2} \frac{2}{2 - \xi(1-y)}. \tag{3.137}$$

The momenta k_{n+1} and k_j are in a frame where the mother particle momentum points in z-direction. Therefore, we have to rotate them into the frame of the underlying born momenta. We can use the rotation (3.104) to do that. Finally, we have to boost the

recoiling born momenta $\bar{k}_i$ to the frame of k_{n+1}, i.e.

$$k_i = \Lambda^{-1}\bar{k}_i. \tag{3.138}$$

This completes the construction of the real final-state phase space from an underlying born phase space and the FKS radiation variables ξ and y.

3.3. Combination of Initial-State and Final-State Singularities

A general matrix element has more than one singular region. However, the cancellation of divergences with plus distributions as discussed in the previous sections works only if there is only one singular region. Following FKS, we split the phase space into multiple singular regions by introducing functions $S_i(\Phi_{n+1})$ and $S_{ij}(\Phi_{n+1})$ that fulfill

$$\sum_i S_i + \sum_{ij} S_{ij} = 1. \tag{3.139}$$

The function S_i corresponds to a region where parton i is radiated from an initial-state parton and S_{ij} corresponds to the radiation of parton i from the final-state parton j. Introducing the S functions into the real partonic cross section leads to

$$\mathrm{d}\hat{\sigma} = \mathrm{d}\Phi_{n+1}\mathcal{R} = \sum_i \mathrm{d}\Phi_{n+1} S_i \mathcal{R} + \sum_{ij} \mathrm{d}\Phi_{n+1} S_{ij} \mathcal{R}. \tag{3.140}$$

To achieve a phase-space splitting into regions with only one singularity, we require that S_i and S_{ij} fulfill the following properties

- $S_i = 0$ and $S_{ij} = 0$ if m soft and $i \neq m$
- $S_i = 0$ if m is collinear to an initial state parton and $i \neq m$
- $S_{ij} = 0$ if m is collinear to an initial state
- $S_{ij} = 0$ if m and n are collinear and $i \neq m, j \neq l; i \neq l, j \neq m$

If particles i and j do not lead to a singular region in the matrix element, we can define $S_{ij} = 0$. The term $\sum_i \mathrm{d}\Phi_{n+1} S_i \mathcal{R}$ in (3.140) has only a singularity if parton i is soft or collinear to an initial-state parton. Therefore, we substitute

$$g \to S_i g \tag{3.141}$$

in (3.6). For final-state radiation we can perform a similar substitution in (3.80), i.e.

$$g \to S_{ij} g. \tag{3.142}$$

The radiated parton can only be collinear to one final-state parton because otherwise the underlying born matrix element would have singularities. Two collinear regions can overlap only if a final-state particle flies in beam direction. We assume that there are phase-space cuts to prevent this case. Therefore, the S functions are 1 in the collinear limit and we do not have to change our previous calculation. In general, two soft singularities can share one collinear singularity. If parton i is soft and it has also a collinear singularity connected to parton j, this singularity is the same as for a soft parton j and a non-soft parton i. This means that the sum $S_{ij} + S_{ji}$ has to be 1 in the collinear limit. We can simply set $S_{ij} = 0$ for $i = q$ because there is no soft singularity connected to a quark. However, there is the three gluon vertex in QCD where we have to take both soft regions into account. The consequences are discussed in section 3.3.1.

The soft limit is not so simple because a soft parton can be collinear to multiple partons. Hence, a soft singularity has more than one contributing S function. Since the soft limit is the same for ISR and FSR, all soft regions can be treated together and are combined by (3.139). Therefore, the calculation also does not change.

Hence, the S functions only affect the calculation of the finite part. We obtain

$$\begin{aligned}[\mathrm{d}\Phi_{n+1}\mathcal{R}]^{(\mathrm{fin})} = &\sum_i \mathrm{d}\Phi_{n+1} \frac{1}{2} \left(\frac{1}{\xi_i}\right)_+ \left[\left(\frac{1}{1-y_i}\right)_+ + \left(\frac{1}{1+y_i}\right)_+\right] \frac{1}{\xi_i} g(\xi_i, y_i, \phi_i) S_i(\Phi_{n+1}) \\ &+ \sum_{ij} \mathrm{d}\Phi_{n+1} \left(\frac{1}{\xi_i}\right)_+ \left(\frac{1}{1-y_{ij}}\right)_+ \frac{1}{\xi_i} g(\xi_i, y_{ij}, \phi_{ij}) S_{ij}(\Phi_{n+1}),\end{aligned} \tag{3.143}$$

where y_{ij} denotes the angle between parton i and j, y_i denotes the angle between parton i and the beam axis and ξ_i is the energy fraction of parton i.

3.3.1. Choice of S functions

To be able to evaluate (3.143) numerically for each region, we have to specify the S functions. The original FKS approach used θ functions to split the phase space. However, we choose smooth functions that are easier to implement [47, 66]. First, we motivate the form of the S functions by investigating $e^+e^- \to q\bar{q} + g$ which has only final-state singularities. The two regions are S_{53} and S_{54}. The limits of the S functions are 0 and 1.

Therefore, we use the ansatz

$$S_{ij} = \frac{1}{1 + A_{ij}}. \tag{3.144}$$

If the gluon (5) is collinear to the quark (3) (i.e. $y_{53} = 1$), we have $S_{53} = 1$ and consequently $A_{53} \to 0$ and if the gluon is collinear to the anti-quark (4) (i.e. $y_{54} = 1$), we have $S_{53} = 0$ and $A_{53} \to \infty$. We choose

$$A_{53} = \frac{1 - y_{53}}{1 - y_{54}}, \; A_{54} = A_{53}^{-1} \tag{3.145}$$

which fulfills

$$S_{53} + S_{54} = 1. \tag{3.146}$$

If we want to extend this to more than two final-state regions, we choose

$$1 + A_{ij} = (1 - y_{ij}) \sum_l \frac{1}{1 - y_{il}} \tag{3.147}$$

and find

$$\sum_j S_{ij} = \sum_j \frac{1}{(1 - y_{ij}) \sum_l \frac{1}{(1 - y_{il})}} = \sum_j \frac{1}{D(1 - y_{ij})} = 1, \tag{3.148}$$

where $D = \frac{1}{\sum_l \frac{1}{1 - y_{il}}}$.

If we have more than one potentially singular parton i, we have to introduce the energy in S_{ij} to fulfill $S_{ij} = 0$ if m is soft and $i \neq m$, i.e.

$$1 + A_{ij} = E_i E_j (1 - y_{ij}) \sum_{kl} \frac{1}{E_k E_l (1 - y_{kl})}. \tag{3.149}$$

We define

$$d_{ij} = E_i E_j (1 - y_{ij}). \tag{3.150}$$

For initial-state radiation, we write

$$S_i = \frac{1}{D d_i}, \tag{3.151}$$

where

$$d_i = \frac{\sqrt{s}}{2} E_i (1 - y_i^2) \tag{3.152}$$

and we extend D to

$$D = \sum_k \frac{1}{d_k} + \sum_{kl} \frac{1}{d_{kl}}. \tag{3.153}$$

We have

$$(k_1 + k_2) \cdot k_i = \sqrt{s} E_i, \tag{3.154}$$

$$k_i \cdot k_1 = E_i \frac{\sqrt{s}}{2}(1 - y_i), \tag{3.155}$$

$$k_i \cdot k_j = E_i E_j (1 - y_{ij}), \tag{3.156}$$

in the partonic center-of-mass frame which we can use to write $d_{i/ij}$ with invariant quantities. In case of the three gluon vertex, we have a soft singularity connected to both gluons. Therefore, we cannot simply substitute P_{qq} with P_{gg} in (3.95). We introduce a function h in S_{ij} which ensures that only one soft gluon leads to a singularity

$$S_{ij} \to \delta_{jg} S_{ij}\, h\left(\frac{E_i}{E_i + E_j}\right), \tag{3.157}$$

where $h(0) = 1$, $h(1) = 0$ and $h(z) + h(1-z) = 1$. The function h is 1 at the soft endpoint because only one gluon can become soft. If both gluons would be soft, the gluon from the born phase space would be soft and the matrix element would be divergent. When we insert P_{gg} in (3.96), we see that the integral diverges if $z = \frac{\xi_i}{\xi} \to 1$, i.e. if the gluon which is not the FKS parton is soft. Therefore, we need the property $h(z) \to 0$ for $z \to 1$ to get a convergent integral. The property $h(z) + h(1 - z) = 1$ ensures that the sum of all S functions is one. We choose

$$h(z) = 1 - z. \tag{3.158}$$

When we use $h(z)P_{gg}$ in (3.96) and (3.97) we obtain

$$\mathcal{I}_1 = -\frac{11}{6} C_A + \left(\frac{2}{3}\pi^2 - \frac{65}{36}\right) C_A \varepsilon + \mathcal{O}(\varepsilon^2) \tag{3.159}$$

and

$$\mathcal{I}_2(\xi) = \frac{203}{72} C_A - \frac{11}{6} C_A \log \xi + \mathcal{O}(\varepsilon). \tag{3.160}$$

So far we considered only one initial-state region. However, we can also split the initial-state region d_i into a part for an initial-state parton coming from the left $d_i^{(l)}$ and one coming from the right $d_i^{(r)}$. We find

$$\frac{1}{d_i} = \frac{1}{d_i^{(l)}} + \frac{1}{d_i^{(r)}} = \frac{1}{\sqrt{s} E_i (1 - y_i)} + \frac{1}{\sqrt{s} E_i (1 + y_i)}. \tag{3.161}$$

We need this splitting when a real process has different underlying born processes. For

instance, the process $qq \to W^+q'q$ has two underlying born flavor configurations. The final-state quark q can come from an initial-state splitting $q \to gq$ from both initial-state quarks. Therefore, the underlying born processes are $qg \to W^+q'$ and $gq \to W^+q'$. We cannot use one singular region for both born processes because we have to use different born matrix elements in the collinear limits $y = 1$ and $y = -1$.

Other choices

For NLO calculations, the explicit form of the S functions does not matter. However, when FKS is used for parton shower matching, the choice of S function matters because they define the type of radiation, i.e. if ISR or FSR is generated. In the POWHEGBOX the following S functions are used because they are based on k_T [47, 67]:

$$d_i = E_i^2(1 - y_i^2), \tag{3.162}$$

$$d_i^{(l/r)} = 2E_i^2(1 \mp y_i), \tag{3.163}$$

$$d_{ij} = 2k_i \cdot k_j \frac{E_i E_j}{(E_i + E_j)^2}. \tag{3.164}$$

In the following, we use the same S functions as the POWHEGBOX.

3.3.2. Combining Soft and Virtual Limits

In this section, we collect all collinear and soft terms from the previous sections. To simplify the notation, we define

$$\gamma_i = \begin{cases} \frac{3}{2}C_F & \text{if } i = \text{quark} \\ \frac{11}{6}C_A - \frac{2}{3}n_f T_F & \text{if } i = \text{gluon} \end{cases} \qquad \gamma_i^0 = \begin{cases} 2C_F & \text{if } i = \text{quark} \\ 2C_A & \text{if } i = \text{gluon} \end{cases} \tag{3.165}$$

$$\gamma_i' = \begin{cases} \left(\frac{13}{2} - \frac{2}{3}\pi^2\right) C_F & \text{if } i = \text{quark} \\ \left(\frac{67}{9} - \frac{2}{3}\pi^2\right) C_A - \frac{23}{9}T_F n_f & \text{if } i = \text{gluon} \end{cases} \tag{3.166}$$

Furthermore, all γ are zero if i does not denote a QCD parton. We start by collecting all divergent parts. In (3.42), we found the divergent part

$$\mathcal{I}_{ij}^{\text{div}} = \left\{ \frac{1}{\varepsilon^2} - \frac{1}{\varepsilon} \left[\log\left(\frac{2k_i \cdot k_j}{Q^2}\right) - \log\left(\frac{4k_i^0 k_j^0}{s_b}\right) \right] \right\}. \tag{3.167}$$

For collinear radiation, we found in (3.33), (3.95), (3.96), (3.98), and (3.159) the following collinear part

$$\mathcal{Q}^{\text{div}} = \frac{1}{\varepsilon}\left(\gamma_1 + \gamma_2 + \sum_{i=3}^{n}\left[\gamma_i - \gamma_i^0 \log\left(\frac{2E_i}{\sqrt{s}}\right)\right]\right). \tag{3.168}$$

Hence, the divergent part reads

$$\mathcal{V}^{\text{div}} = \mathrm{d}x_1\,\mathrm{d}x_2\,\mathrm{d}\Phi_n f(x_1,\mu_F) f(x_2,\mu_F)\mathcal{N}\frac{\alpha_s}{2\pi}\left[\mathcal{Q}^{\text{div}}\mathcal{B} + \sum_{\substack{i,j\\ i\neq j}}^{n}\mathcal{I}_{ij}^{\text{div}}\mathcal{B}_{ij}\right], \tag{3.169}$$

where the normalization $\mathcal{N}$ is defined in (3.34). Using color conservation and the $i \leftrightarrow j$ symmetry of the color factor, we find

$$\begin{aligned}\mathcal{V}^{\text{div}} = \mathrm{d}x_1\,\mathrm{d}x_2\,\mathrm{d}\Phi_n f(x_1,\mu_F) f(x_2,\mu_F)\mathcal{N}\frac{\alpha_s}{2\pi}\times \\ \times\left[\frac{1}{2}\frac{1}{\varepsilon^2}\mathcal{B}\sum_{i=1}^{n}\gamma_i^0 + \frac{1}{\varepsilon}\left(\mathcal{B}\sum_{i=1}^{n}\gamma_i - \sum_{\substack{i,j\\ i\neq j}}^{n}\log\frac{2k_i\cdot k_j}{Q^2}B_{ij}\right)\right].\end{aligned} \tag{3.170}$$

Now, we state the finite parts of the integrated soft and collinear limits that contribute to the cross section. The finite part of soft and collinear limits is given by

$$\mathcal{V}^{\text{fin}} = \mathrm{d}x_1\,\mathrm{d}x_2\,\mathrm{d}\Phi_n f(x_1,\mu_F) f(x_2,\mu_F)\frac{\alpha_s}{2\pi}\left[\mathcal{Q}_{\text{in}}\mathcal{B} + \mathcal{Q}_{\text{fin}}\mathcal{B} + \sum_{\substack{i,j\\ i\neq j}}\mathcal{I}_{ij}\mathcal{B}_{ij}\right]. \tag{3.171}$$

The finite part of the soft end point in (3.42) is

$$\mathcal{I}_{ij} = \frac{1}{2}\log^2\frac{Q^2}{s_b} - \log\frac{Q^2}{s_b}\log\frac{k_i\cdot k_j}{2k_i^0 k_j^0} - \frac{\pi^2}{6} - \text{Li}_2\left(\frac{x_{ij}}{x_{ij}-1}\right), \tag{3.172}$$

where

$$x_{ij} = 1 - \frac{k_i\cdot k_j}{2k_i^0 k_j^0}. \tag{3.173}$$

The finite part of the collinear end points in (3.33) and (3.95) are given by

$$\mathcal{Q}_{\text{in}} = -\log\frac{\mu_F^2}{Q^2}\left[\gamma_1 + \gamma_2\right] \tag{3.174}$$

for initial-state radiation and

$$\mathcal{Q}_{\text{fin}} = \sum_{i=3}^{n+2} \left\{ \gamma_i' - \log \frac{s}{Q^2} \left(\gamma_i - \gamma_i^0 \log \frac{2E_i}{\sqrt{s}} \right) + \gamma_i^0 \log^2 \frac{2E_i}{\sqrt{s}} - 2\gamma_i \log \frac{2E_i}{\sqrt{s}} \right\} \tag{3.175}$$

for final-state radiation.

3.4. Final Result

In this section, we summarize all terms that have to be calculated in an FKS based NLO calculation. The FKS cross section consists of multiple parts that have to be implemented independently, i.e.

$$\begin{aligned} \mathrm{d}\sigma = {} & \mathrm{d}x_1\, \mathrm{d}x_2\, \mathrm{d}\Phi_n \mathcal{L}(x_1, x_2)(\mathcal{B} + \hat{\mathcal{V}}) + \mathrm{d}x_1\, \mathrm{d}x_2\, \mathrm{d}\Phi_{n+1} \mathcal{L}(x_1, x_2)\hat{\mathcal{R}} \\ & + \mathrm{d}x_1\, \mathrm{d}x_2\, \mathrm{d}\Phi_n \frac{\mathrm{d}z}{z} \mathcal{L}(x_1/z, x_2) G_1 + \mathrm{d}x_1\, \mathrm{d}x_2\, \mathrm{d}\Phi_n \frac{\mathrm{d}z}{z} \mathcal{L}(x_1, x_2/z) G_2, \end{aligned} \tag{3.176}$$

where $\mathrm{d}\Phi_n \mathcal{L}(x_1, x_2)\mathcal{B}$ is the LO part and

$$\mathcal{L} = f_1(x_1, \mu_F) f_2(x_2, \mu_F). \tag{3.177}$$

The subtracted real part $\hat{\mathcal{R}}$ is described in section 3.4.1. The virtual part $\hat{\mathcal{V}}$ is given in section 3.4.2. Finally, the collinear remnant terms G_1, G_2 are described in section 3.4.3.

3.4.1. Subtracted Real Matrix Element

The subtracted real matrix element (3.143) reads

$$\mathrm{d}\Phi_{n+1} \mathcal{L} \hat{\mathcal{R}} = \sum_{ij} \mathrm{d}\Phi_{n+1}^{(ij)} \mathcal{L} \hat{\mathcal{R}}_{ij} + \sum_i \mathrm{d}\Phi_{n+1}^{(i)} \mathcal{L} \hat{\mathcal{R}}_i, \tag{3.178}$$

where

$$\hat{\mathcal{R}}_i = \frac{1}{\xi_i} \frac{1}{2} \left(\frac{1}{\xi_i} \right)_+ \left[\left(\frac{1}{1 - y_i} \right)_+ + \left(\frac{1}{1 + y_i} \right)_+ \right] S_i(\Phi_{n+1}^{(i)}) \xi_i^2 (1 - y_i^2) \mathcal{R}. \tag{3.179}$$

and

$$\hat{\mathcal{R}}_{ij} = \frac{1}{\xi_i} \left(\frac{1}{\xi_i} \right)_+ \left(\frac{1}{1 - y_{ij}} \right)_+ S_{ij}(\Phi_{n+1}^{(ij)}) \xi_i^2 (1 - y_{ij}) \mathcal{R}. \tag{3.180}$$

The functions S_i and S_{ij} are defined in section 3.3 and

$$\mathcal{R} = \frac{1}{2s}|\mathcal{M}_{n+1}|^2. \tag{3.181}$$

We have to implement the plus distributions in $\hat{\mathcal{R}}_i$ and $\hat{\mathcal{R}}_{ij}$ in a numerical code.

We start by investigating $\mathrm{d}\Phi_{n+1}^{(i)}\hat{\mathcal{R}}_i$. The real phase-space element is given by

$$\mathrm{d}\Phi_{n+1}^{(i)} = \mathrm{d}\bar{\Phi}_n \, \mathrm{d}\Phi_{\mathrm{rad}}^{(i)}, \tag{3.182}$$

where $\mathrm{d}\bar{\Phi}_n$ is an underlying born phase space and $\mathrm{d}\Phi_{\mathrm{rad}}^{(i)}$ is defined in (3.63). Therefore, we obtain

$$\begin{aligned}
&\mathrm{d}x_1 \, \mathrm{d}x_2 \, \mathrm{d}\Phi_{n+1}^{(i)} \mathcal{L}\hat{\mathcal{R}}_i = \\
&\quad \frac{1}{2(4\pi)^3} \int_0^1 \mathrm{d}\bar{x}_1 \int_0^1 \mathrm{d}\bar{x}_2 \int \mathrm{d}\bar{\Phi}_n \int_{-1}^1 \mathrm{d}y \int_0^{2\pi} \mathrm{d}\phi \int_0^1 \mathrm{d}\xi \Bigg\{ \\
&\qquad \frac{1}{1-y}\frac{1}{\xi}\Big[G_i(\bar{x}_1, \bar{x}_2, \bar{\Phi}_n, \xi_{\max}[\bar{x}_1, \bar{x}_1, y]\xi, y, \phi) && \textbf{(real)} \\
&\qquad\quad - G_i(\bar{x}_1, \bar{x}_2, \bar{\Phi}_n, 0, y, \phi) && \textbf{(soft)} \\
&\qquad\quad - G_i(\bar{x}_1, \bar{x}_2, \bar{\Phi}_n, \xi_{\max}[\bar{x}_1, \bar{x}_1, 1]\xi, 1, \phi) && \textbf{(collinear)} \\
&\qquad\quad + G_i(\bar{x}_1, \bar{x}_2, \bar{\Phi}_n, 0, 1, \phi)\Big] && \textbf{(soft collinear)} \\
&\qquad + \frac{1}{1-y}\Big[\log\left(\xi_{\max}[\bar{x}_1, \bar{x}_1, y]\right) G_i(\bar{x}_1, \bar{x}_2, \bar{\Phi}_n, 0, y, \phi) && \textbf{(endpoint)} \\
&\qquad\quad - \log\left(\xi_{\max}[\bar{x}_1, \bar{x}_1, 1]\right) G_i(\bar{x}_1, \bar{x}_2, \bar{\Phi}_n, 0, 1, \phi)\Big] \Bigg\} \\
&\qquad + \text{term for } (y = -1),
\end{aligned} \tag{3.183}$$

where $\xi_{\max}$ is defined in (3.60). The function G_i is given by

$$G_i(\bar{x}_1, \bar{x}_2, \bar{\Phi}_n, \xi, y, \phi) = \frac{s_r}{1-\xi} f_1(x_1, \mu_F) f_2(x_2, \mu_F) \, S_i(\Phi_{n+1}) \, g(\xi, y), \tag{3.184}$$

where $s_r = x_1 x_2 S$, $x_{1,2}(\bar{x}_{1,2}, y, \xi)$ are defined in (3.55), and g is defined in (3.6). Note that we omitted the indices for the radiation variables because the radiation variables are integration variables. The endpoint term arise from the region $\xi > \xi_{\max}$ of the subtracted soft end point which can be analytically integrated. The soft limit of g is given in (3.39) and the collinear limit for splittings with a quark as born particle is given in (3.19). For a gluon as born particle, we have to use the spin-correlated matrix element limit (H.25)

in (3.19). The construction of the real phase space from an underlying born phase space is described in section 3.1.3. Here, we give it in an algorithmic form:

function GeneratePhasespaceISR($\bar{\Phi}_n(\bar{x}_{1,2}, \bar{k}_\pm, \bar{k}_i, J_{\Phi_n}), \xi, y, \phi$)
  $x_1, x_2 =$ (3.55)
  $k_\pm =$ (3.65)
  $k_{n+1} =$ (3.49)
  $\Lambda =$ (3.67)
  $\Lambda_T =$ (3.72)
  $k_{n+1} = \Lambda^{-1} k_{n+1}$
  for $i = 1, \ldots, n$ **do**
    $k_i = \Lambda_T^{-1} \bar{k}_i$
  end for
  $k_\pm = \Lambda k_\pm$
  for $i = 1, \ldots, n+1$ **do**
    $k_i = \Lambda k_i$
  end for
  $J = J_{\Phi_n} \frac{s}{(4\pi)^3} \frac{\xi}{1-\xi}$
  return $\Phi_{n+1}(x_{1,2}, k_\pm, k_i, k_{n+1}, J)$
end function

Next, we investigate $\mathrm{d}\Phi_{n+1}^{(ij)} \hat{\mathcal{R}}_{ij}$. The final-state real phase-space reads

$$\mathrm{d}\Phi_{n+1}^{(ij)} = \mathrm{d}\bar{\Phi}_n \, \mathrm{d}\Phi_{\mathrm{rad}}^{(ij)}, \tag{3.185}$$

where $\mathrm{d}\bar{\Phi}_n$ is the underlying born phase space as before and $\mathrm{d}\Phi_{\mathrm{rad}}^{(ij)}$ is defined in (3.136).

Using the real phase space, we find

$$\begin{aligned}
\mathrm{d}x_1\,\mathrm{d}x_2\,\mathrm{d}\Phi_{n+1}^{(ij)}\mathcal{L}\hat{\mathcal{R}}_{ij} = \int_0^1\mathrm{d}x_1\int_0^1\mathrm{d}x_2\;\mathrm{d}\bar{\Phi}_n\int_{-1}^1\mathrm{d}y\int_0^{2\pi}\mathrm{d}\phi\int_0^1\mathrm{d}\xi\Bigg\{ \\
\frac{1}{1-y}\frac{1}{\xi}\Big[G_{ij}(x_1,x_2,\bar{\Phi}_n,\xi_{\max}\xi,y,\phi) && \textbf{(real)} \\
- G_{ij}(x_1,x_2,\bar{\Phi}_n,0,y,\phi) && \textbf{(soft)} \\
- G_{ij}(x_1,x_2,\bar{\Phi}_n,\xi_{\max}\xi,1,\phi) && \textbf{(collinear)} \\
+ G_{ij}(x_1,x_2,\bar{\Phi}_n,0,1,\phi)\Big] && \textbf{(soft-collinear)} \\
+\frac{1}{1-y}\Big[\log(\xi_{\max})\,G_{ij}(x_1,x_2,\bar{\Phi}_n,0,y,\phi) && \textbf{(endpoint)} \\
-\log(\xi_{\max})\,G_{ij}(x_1,x_2,\bar{\Phi}_n,0,1,\phi)\Big]\Bigg\},
\end{aligned} \tag{3.186}$$

where $\xi_{\max}$ is defined in (3.128). The function G_{ij} is given by

$$G_{ij}(\bar{\Phi}_n,\xi,y,\phi) = \frac{1}{\xi}Jf_1(x_1,\mu_F)f_2(x_2,\mu_F)S_{ij}g(\xi,y,\phi), \tag{3.187}$$

where J is defined by (3.126) and (3.136) and g is defined in (3.80). The limits of g are defined in (3.105) and (3.91). The real phase-space generation is described in section 3.2.3 and can be constructed with the following algorithm:

function GeneratePhasespaceFSR($\bar{\Phi}_n(\bar{x}_{1,2},\bar{k}_\pm,\bar{k}_i,J_{\Phi_n}),\xi,y,\phi$)
- $M^2 =$ (3.134)
- $k_{n+1}^0 =$ (3.127)
- $|k_j| =$ (3.135)
- $|k| =$ (3.132)
- $\cos\psi =$ (3.123), (3.132)
- $k_{n+1} =$(3.130)
- $k_j =$(3.131)
- $R =$ (3.104)
- $k_{n+1} = Rk_{n+1}$
- $k_j = Rk_j$
- $k_{\mathrm{rec}} = q - k_{n+1} - k_j$
- $\beta =$(3.115)
- $\Lambda = \mathrm{Boost}(k_{\mathrm{rec}},\beta)$

for $i = 1, \ldots, n; i \neq j$ **do**
$k_i = \Lambda^{-1} \bar{k}_i$
end for
$J = J_{\Phi_n} \times (3.136)$
return $\Phi_{n+1}(\bar{x}_{1,2}, \bar{k}_{\pm}, k_i, k_{n+1}, J)$
end function

3.4.2. Virtual Term

In section 3.3.2, we found the contribution

$$\mathcal{V}_{\text{FKS}} = \mathcal{V}^{\text{div}} + \mathcal{V}^{\text{fin}}, \tag{3.188}$$

where $\mathcal{V}^{\text{div}}$ is divergent and defined in (3.170) and $\mathcal{V}_{\text{fin}}$ is finite and defined in (3.171). We combine this part with the 1-loop contribution

$$\mathcal{V}^{\text{1-loop}} = \mathrm{d}x_1 \, \mathrm{d}x_2 \mathcal{L} \, \mathrm{d}\Phi_n \mathcal{V} \tag{3.189}$$

and obtain

$$\mathrm{d}x_1 \, \mathrm{d}x_2 \, \mathrm{d}\Phi_n \mathcal{L} \hat{\mathcal{V}} = \mathcal{V}_{\text{FKS}} + \mathcal{V}^{\text{1-loop}}. \tag{3.190}$$

Due to the KLN theorem, all poles in $\mathcal{V}_{\text{FKS}}$ have to cancel with poles in $\mathcal{V}^{\text{1-loop}}$.

3.4.3. PDF Renormalization Term

In (3.33), we found a finite contribution to the cross section that is a remnant of the pdf renormalization. This contribution is given by

$$\begin{aligned}
&\mathrm{d}x_1 \, \mathrm{d}x_2 \, \mathrm{d}\Phi_n \frac{\mathrm{d}z}{z} \mathcal{L}\left(\frac{x_1}{z}, x_2\right) G_1 = \\
&\qquad \sum_{q_1'} \int_0^1 \mathrm{d}x_1 \int_0^1 \mathrm{d}x_2 \, \mathrm{d}\Phi_n \mathcal{B}_{q_1'} \int_{x_1}^1 \mathrm{d}z \, \frac{1}{z} f_{q_1}\left(\frac{x_1}{z}, \mu_F\right) f_{q_2}(x_2, \mu_F) \\
&\times \left\{ (1-z) \hat{P}^0_{q_1' q_1}(z) \left[\left(\frac{1}{1-z} \right)_+ \log \frac{s}{z \mu_F^2} + 2 \left(\frac{\log(1-z)}{1-z} \right)_+ \right] - \hat{P}^{\varepsilon}_{q_1' q_1}(z) - r^F_{q_1 q_1'} \right\},
\end{aligned} \tag{3.191}$$

where $\hat{P}^0(z)$ is the unregularized Altarelli-Parisi splitting function in four dimensions and $\hat{P}^{\varepsilon}$ is its $\mathcal{O}(\varepsilon)$ term in $d = 4 - 2\varepsilon$ dimensions (s. (3.21)-(3.24)). We introduced the factorization scheme depend term $r^F_{q_1 q_1'}$ from (2.17). We have to sum over all possible born initial-state partons q_1' in the splitting $q_1 \to q_1'$ and choose the appropriate born

matrix element $\mathcal{B}_{q_1'}$. Note that s is the Mandelstam variable of the born phase space Φ_n. The contribution G_2 is similar to the term above. The only difference is that q_1 and q_2 change their role.

3.5. EW Corrections

When we calculate EW processes with a radiated photon, we can use the FKS subtraction scheme with some minor changes. We have to change the splitting functions in the previous calculation to the QED ones, i.e. $C_F \to Q_f^2$, $C_A \to 0$ and $T_F \to Q_f^2$, where Q_f is the charge of the fermions. We have to change (3.166) accordingly, where we replace $n_f T_F$ with $\sum_i Q_i^2$. In summary, we find

$$\gamma_i = \begin{cases} \frac{3}{2} Q_i^2 & \text{if } i = \text{fermion} \\ -\frac{2}{3} \sum_l Q_l^2 & \text{if } i = \gamma \end{cases} \qquad \gamma_i^0 = \begin{cases} 2Q_i^2 & \text{if } i = \text{fermion} \\ 0 & \text{if } i = \gamma \end{cases} \tag{3.192}$$

$$\gamma_i' = \begin{cases} \left(\frac{13}{2} - \frac{2}{3}\pi^2\right) Q_i^2 & \text{if } i = \text{fermion} \\ -\frac{23}{9} \sum_l Q_l^2 & \text{if } i = \gamma \end{cases} \tag{3.193}$$

The analogon to the color factor in $\mathcal{B}_{ij}$ is the charge. Therefore, we use $\mathcal{B}_{ij} = -Q_i \sigma_i Q_j \sigma_j \mathcal{B}$ where $\sigma_f = +1$ for incoming fermions and outgoing anti-fermions and $\sigma_f = -1$ for outgoing fermions and incoming anti-fermions [68]. The color conservation is replace by the charge conservation $\sum_i \sigma_i Q_i = 0$. The form of $\mathcal{V}_{\text{FKS}}$ remain unchanged with these substitutions. We use the DIS scheme for EW pdf renormalization as suggested in [69]. Hence, we have to use

$$r_{ff}^{\text{DIS}} = \left(P_{ff}(z) \left(\log \frac{1-z}{z} - \frac{3}{4} \right) + \frac{9+5z}{4} \right)_+ \tag{3.194}$$

in (3.191).

4. FKS with Mass Regularization

The usual FKS subtraction, as derived in the previous chapter, uses dim. reg. to regulate soft and collinear singularities. Since QCD calculations are usually performed in dim. reg., the FKS subtraction scheme can widely be used for NLO QCD calculations. However, EW corrections are often calculated in mass regularization, where a fictitious photon mass m_γ and the fermion masses are used as regulators. Only terms that are singular in the massless limit are kept and they have to cancel between virtual and real corrections. Hence, these terms play the same role as the $\frac{1}{\varepsilon}$ poles in dim. reg..

Our aim is to use the FKS subtractions scheme for mass regulated EW corrections. In the following sections we derive the FKS terms for mass regularization in a similar way as in the previous chapter for dim. reg.. We restrict the derivation to photon radiation off fermions because we will apply FKS to the Drell-Yan process in chapter 6 and to $pp \to Wj$ in chapter 8. In section 4.3, we summarize what has to be implemented for an NLO calculation. We also published the results of this chapter in [57].

We start with the partonic part of the real cross section (2.21), i.e. without pdfs,

$$\hat{\sigma}_{n+1} = \mathrm{d}\Phi_{n+1}\mathcal{R} = (2\pi)^4\delta^{(4)}\left(k_1 + k_2 - k - \sum_{i=1}^{n} p_i\right)\prod_{i=1}^{n}\frac{\mathrm{d}^3 p_i}{(2\pi)^3 2E_i}\frac{\mathrm{d}^3 k}{(2\pi)^3 2E}\mathcal{R}, \tag{4.1}$$

where k is an additionally emitted photon with mass m_γ, $k_{1,2}$ are the initial-state momenta, p_i are the final-state momenta, and

$$\mathcal{R} = \frac{1}{2s}|\mathcal{M}_{n+1}|^2 \tag{4.2}$$

is the massive real matrix element. The massless squared matrix element contains singularities which are connected to soft radiation. We introduce a fictitious photon mass m_γ in order to regulate those singularities. The massless matrix element is also divergent for collinear radiation but those singularities are regulated by the fermion masses in the massive matrix element. Since we are interested in the massless case, we expand the cross section in the masses and keep only divergent and finite terms. To handle the soft

singularities, we split the energy integration into a soft and a hard part, i.e.,

$$\hat{\sigma}_{n+1} = \hat{\sigma}^s_{n+1} + \hat{\sigma}^h_{n+1}. \tag{4.3}$$

The soft part is given by

$$\hat{\sigma}^s_{n+1} = \pi\delta^{(4)}\left(k_1 + k_2 - \sum_{i=1}^{n} p_i\right) \mathrm{d}P \int_{|\vec{k}|\leq\Delta E} \frac{\mathrm{d}^3k}{E} \frac{|\mathcal{M}_{n+1}|^2}{2s} \tag{4.4}$$

and the hard part by

$$\hat{\sigma}^h_{n+1} = \int_{|\vec{k}|>\Delta E} \mathrm{d}\Phi_{n+1}\mathcal{R}, \tag{4.5}$$

where $\mathrm{d}P = \prod_{i=1}^{n} \frac{\mathrm{d}^3p_i}{(2\pi)^3 2E_i}$ and ΔE is an intermediate soft energy scale that fulfills $m_\gamma \ll \Delta E$.

We can use the eikonal (soft) approximation for the matrix element

$$|\mathcal{M}^{(\mathrm{soft})}_{n+1}|^2 = g^2 \sum_{i,j} \mathcal{M}_{ij} \frac{k_i \cdot k_j}{(k_i \cdot k)(k_j \cdot k)} |\mathcal{M}_n|^2, \tag{4.6}$$

in the soft part (s. section H.1), where (s. section 3.5)

$$\mathcal{M}_{ij} = Q_i\sigma_i Q_j\sigma_j. \tag{4.7}$$

We obtain

$$\hat{\sigma}^s_{n+1} = 4\pi^2\alpha\delta^{(4)}\left(k_1 + k_2 - \sum_{i=1}^{n} p_i\right) \mathrm{d}P\mathcal{B} \sum_{i,j} \mathcal{M}_{ij} \int_{|\vec{k}|\leq\Delta E} \frac{\mathrm{d}^3k}{E} \frac{p_i \cdot p_j}{(p_i \cdot k)(p_j \cdot k)}. \tag{4.8}$$

The solution to the integral over the eikonal factor is given in section F.2. We obtain

$$\hat{\sigma}^s_{n+1} = \frac{\alpha}{4\pi^2} \mathrm{d}\Phi_n\mathcal{B} \sum_{\substack{i,j \\ i\neq j}} \mathcal{M}_{ij} I_{ij} - \frac{\alpha}{4\pi^2} \mathrm{d}\Phi_n\mathcal{B} \sum_i Q_i^2 I_i, \tag{4.9}$$

where

$$I_{ij} = 2\pi \left\{ \frac{1}{2} \log \frac{4(p_i \cdot p_j)^2}{m_i^2 m_j^2} \log \frac{\Delta E^2}{m_\gamma^2} - \frac{1}{4} \log^2 \frac{m_i^2}{E_i^2} - \frac{1}{4} \log^2 \frac{m_j^2}{E_j^2} + 2 \log 2 \log \frac{p_i \cdot p_j}{2E_i E_j} \right.$$
$$- \mathrm{Li}_2 \left(\frac{p_i \cdot p_j}{2E_i E_j} \right) - \log \left(\frac{p_i \cdot p_j}{2E_i E_j} \right) \log \left(1 - \frac{p_i \cdot p_j}{2E_i E_j} \right) + \frac{1}{2} \log^2 \left(\frac{p_i \cdot p_j}{2E_i E_j} \right)$$
$$\left. + 2 \log^2 2 - \frac{\pi^2}{6} \right\} \quad (4.10)$$

and

$$I_i = 2\pi \left(\log \frac{4\Delta E^2}{m_\gamma^2} + \log \frac{m_i^2}{4E_i^2} \right). \quad (4.11)$$

(Note $I_i \neq I_{ii}$). We can use charge conservation $\sum_i \sigma_i Q_i = 0$ to simplify the soft part further and arrive at

$$\hat{\sigma}^s_{n+1} = -\frac{\alpha}{2\pi} \mathrm{d}\Phi_n \mathcal{B} \left\{ \sum_{\substack{ij \\ i \neq j}} \sigma_i \sigma_j Q_i Q_j \mathcal{I}_{ij} + \frac{1}{2} \sum_i Q_i^2 \log^2 \frac{m_i^2}{E_i^2} - \left(2 \log^2 2 - \frac{\pi^2}{6} \right) \sum_i Q_i^2 \right.$$
$$\left. + \sum_i Q_i^2 \left(\log \frac{4\Delta E^2}{m_\gamma^2} + \log \frac{m_i^2}{4E_i^2} \right) \right\}, \quad (4.12)$$

where

$$\mathcal{I}_{ij}(\Delta E) = \frac{1}{2} \log \frac{4(p_i \cdot p_j)^2}{m_i^2 m_j^2} \log \frac{\Delta E^2}{m_\gamma^2} + 2 \log 2 \log \frac{p_i \cdot p_j}{2E_i E_j} - \mathrm{Li}_2 \left(\frac{p_i \cdot p_j}{2E_i E_j} \right)$$
$$- \log \left(\frac{p_i \cdot p_j}{2E_i E_j} \right) \log \left(1 - \frac{p_i \cdot p_j}{2E_i E_j} \right) + \frac{1}{2} \log^2 \left(\frac{p_i \cdot p_j}{2E_i E_j} \right). \quad (4.13)$$

In the following, we investigate the divergence structure of the hard cross section $\hat{\sigma}^h_{n+1}$. The squared matrix element includes matrix elements with singularities connected to the emission from different charged particles. Therefore, the hard cross section is divergent in different phase-space regions. We want to split the real phase space in multiple regions such that each region contains only one soft and collinear divergence. Therefore, we use the FKS S functions introduced in section 3.3. After introducing the S functions in the hard cross section, we use the invariance of the phase space integral under rotations to choose different parametrization in every region r, i.e.

$$\hat{\sigma}^h_{n+1} = \sum_{r=0}^{n} \int_{|\vec{k}| > \Delta E} \mathrm{d}\Phi^r_{n+1} S_r(\Phi^r_{n+1}) \mathcal{R}. \quad (4.14)$$

We assume that the radiated photon is always particle $n+1$, i.e. r labels the regions and $S_r = S_{n+1,r}$ for $r > 0$.

First, we express the integration over the momentum of the radiated particle in terms of its energy and angles and we obtain

$$\begin{aligned}\frac{\mathrm{d}^3 k}{(2\pi)^3 2k^0} &= \frac{1}{2(2\pi)^3}\int_{m_\gamma}^{\frac{\sqrt{s}}{2}} \mathrm{d}E \int_{-1}^{1}\mathrm{d}y \int_0^{2\pi}\mathrm{d}\phi \sqrt{E^2 - m_\gamma^2} \\ &= \frac{1}{2(2\pi)^3}\int_a^1 \mathrm{d}\xi \int_{-1}^{1}\mathrm{d}y \int_0^{2\pi}\mathrm{d}\phi \sqrt{1-\frac{a^2}{\xi^2}}\xi\frac{s}{4},\end{aligned} \tag{4.15}$$

where we introduced $\xi = \frac{2}{\sqrt{s}}E$ and $a = \frac{2m_\gamma}{\sqrt{s}}$. We obtain

$$\begin{aligned}\hat{\sigma}^h_{n+1} = \pi \sum_r \mathrm{d}P^r \int_{\xi_{\min}}^1 \mathrm{d}\xi^r \int_{-1}^1 \mathrm{d}y^r \int_0^{2\pi}\mathrm{d}\phi^r\, \delta^{(4)}\left(k_1^r + k_2^r - k^r - \sum_{i=1}^n p_i^r\right) \times \\ \times \sqrt{1-\frac{a^2}{(\xi^r)^2}}\frac{\xi^r s}{4} S_r \frac{|\mathcal{M}_{n+1}|^2}{2s},\end{aligned} \tag{4.16}$$

where $\xi_{\min} = \frac{2\Delta E}{\sqrt{s}}$. In the following we drop the superscript r for the phase space and implicitly assume that the phase space is parametrized such that k is collinear to p_r respectively k_1 for $y = 1$. In section E.4, it is shown how to write the ξ integration in terms of a plus distribution:

$$\begin{aligned}\hat{\sigma}^h_{n+1} = \pi \sum_r \mathrm{d}P \Bigg\{ &\delta^{(4)}\left(k_1 + k_2 - k - \sum_{i=1}^n p_i\right)\int_0^1 \mathrm{d}\xi \int_{-1}^1 \mathrm{d}y \int_0^{2\pi}\mathrm{d}\phi \left(\frac{1}{\xi}\right)_+ S_r \frac{\xi^2}{8}|\mathcal{M}_{n+1}|^2 \\ &-\delta^{(4)}\left(k_1 + k_2 - \sum_{i=1}^n p_i\right)\log\xi_{\min}\int_{-1}^1 \mathrm{d}y \int_0^{2\pi}\mathrm{d}\phi\, S_r \left[\frac{\xi^2}{8}|\mathcal{M}_{n+1}|^2\right]_{\xi\to 0}\Bigg\}.\end{aligned} \tag{4.17}$$

We can use the eikonal approximation (4.6) for the matrix element in the second line. Therefore, we have to solve the integral

$$I = 4\pi\alpha \sum_r \sum_{ij} \int_{-1}^1 \mathrm{d}y \int_0^{2\pi}\mathrm{d}\phi\, S_r \frac{\xi^2}{8}\mathcal{M}_{ij}\frac{k_i\cdot k_j}{(k_i\cdot k)(k_j\cdot k)}|\mathcal{M}_n|^2. \tag{4.18}$$

The integrand does not depend on ξ because the factor ξ^2 cancels the denominator of the eikonal approximation. Furthermore, the denominator is invariant under Lorentz transformations and we can evaluate the integrand in one reference frame. Therefore, we can use that the sum of S functions equals to one. When we use the angular integral

over the eikonal factor from section F.2, we obtain

$$I = -8\pi^2\alpha\mathcal{B}\left(\sum_{\substack{ij\\i\neq j}}\mathcal{M}_{ij}\log\frac{m_i^2m_j^2}{(2k_i\cdot k_j)^2}+2\sum_i Q_i^2\right). \tag{4.19}$$

We can use this result in (4.17) and obtain

$$\begin{aligned}\hat{\sigma}_{n+1}^h = \pi\,\mathrm{d}P\sum_r\delta^{(4)}\left(k_1+k_2-k-\sum_{i=1}^n p_i\right)\int_0^1\mathrm{d}\xi\int_{-1}^1\mathrm{d}y\int_0^{2\pi}\mathrm{d}\phi\left(\frac{1}{\xi}\right)_+ S_r\frac{\xi^2}{8}|\mathcal{M}_{n+1}|^2\\ +\frac{1}{2}\frac{\alpha}{2\pi}\,\mathrm{d}\Phi_n\mathcal{B}\log\frac{4\Delta E^2}{s}\left(\sum_{\substack{ij\\i\neq j}}\mathcal{M}_{ij}\log\frac{m_i^2m_j^2}{(2k_i\cdot k_j)^2}+2\sum_i Q_i^2\right).\end{aligned} \tag{4.20}$$

We investigate the term in the first line for initial-state radiation and final-state radiation in the next sections.

4.1. Initial-State Radiation

The initial-state term in (4.20) is given by

$$\hat{\sigma}_0 = \pi\,\mathrm{d}P\delta^{(4)}\left(k_1+k_2-k-\sum_{i=1}^n p_i\right)\int_0^1\mathrm{d}\xi\int_{-1}^1\mathrm{d}y\int_0^{2\pi}\mathrm{d}\phi\left(\frac{1}{\xi}\right)_+ S_0\frac{\xi^2}{8}|\mathcal{M}_{n+1}|^2. \tag{4.21}$$

This term has only divergences for $y\to\pm1$. Therefore, we split the y integration into three parts

1. $y\in[-1,-1+\varepsilon]$
2. $y\in[-1+\varepsilon,1-\varepsilon]$
3. $y\in[1-\varepsilon,1]$

where $\varepsilon>0$ is a small number. We write

$$\hat{\sigma}_0 = \hat{\sigma}_{0,1}+\hat{\sigma}_{0,2}+\hat{\sigma}_{0,3}, \tag{4.22}$$

where the subscript labels the y region. The matrix element times S_0 function is only divergent in region 1 and 3. We start with evaluating the non divergent region 2 by subtracting and adding the collinear limits of the matrix element, i.e.

$$\hat{\sigma}_{0,2} = \hat{\sigma}_{0,2+}+\hat{\sigma}_{0,2}^{y\to1}+\hat{\sigma}_{0,2}^{y\to-1}, \tag{4.23}$$

where $\hat{\sigma}_{0,2+} = \hat{\sigma}_{0,2} - \hat{\sigma}_{0,2}^{y\to 1} - \hat{\sigma}_{0,2}^{y\to -1}$ is the subtracted cross section and

$$\hat{\sigma}_{0,2}^{y\to\pm 1} = \pi \,\mathrm{d}P \int_0^1 \mathrm{d}\xi \int_{-1+\varepsilon}^{1-\varepsilon} \mathrm{d}y \int_0^{2\pi} \mathrm{d}\phi \left(\frac{1}{\xi}\right)_+ \left[\delta^{(4)}\left(k_1 + k_2 - k - \sum_{i=1}^{n} p_i\right) S_0 \frac{\xi^2}{8} |\mathcal{M}_{n+1}|^2\right]_{y\to\pm 1}. \tag{4.24}$$

The matrix element in its collinear limit is given by [70]

$$|\mathcal{M}_{n+1}^{(\mathrm{coll})}|^2 = \frac{Q_i^2 g^2}{z(p_i \cdot k)} \left[P_{ff}(z) - \frac{z m_i^2}{(p_i \cdot k)}\right] |\mathcal{M}_n(z p_i)|^2 \tag{4.25}$$

for initial-state radiation, i.e. the collinear limit is given by the born matrix element times a splitting function $P_{ff}(x) = \frac{1+x^2}{1-x}$. The argument of the splitting function is the ratio of energy that the emitting particle has after the emission $z = 1 - \frac{k^0}{p_i^0} = 1 - \xi$. The subtracted cross section is given by

$$\begin{aligned}
\hat{\sigma}_{0,2+} &= \hat{\sigma}_{0,2} - \hat{\sigma}_{0,2}^{y\to 1} - \hat{\sigma}_{0,2}^{y\to -1} \\
&= \pi \,\mathrm{d}P \int_{-1+\varepsilon}^{1-\varepsilon} \mathrm{d}y \int_0^1 \mathrm{d}\xi \int_0^{2\pi} \mathrm{d}\phi \, \delta^{(4)}\left(k_1 + k_2 - k - \sum_{i=1}^{n} p_i\right) \left(\frac{1}{\xi}\right)_+ \times \\
&\quad \times \frac{1}{1-y^2} \left\{ g_0(\xi, y, \phi) - \frac{1}{2}(1+y) g_0(\xi, 1, \phi) - \frac{1}{2}(1-y) g_0(\xi, -1, \phi) \right\},
\end{aligned} \tag{4.26}$$

where we defined

$$g_0(\xi, y, \phi) = \frac{1}{2s} \frac{(k_1 \cdot k)(k_2 \cdot k)}{E_1 E_2} S_0 |\mathcal{M}_{n+1}^0|^2. \tag{4.27}$$

Since we do not evaluate the matrix element in its collinear divergences at $y \to \pm 1$, we can use the massless matrix element $|\mathcal{M}_{n+1}^0|^2$. When we perform a partial fraction decomposition for the term $\frac{1}{1-y^2}$, we find that we can write the subtracted cross section as

$$\begin{aligned}
\hat{\sigma}_{0,2+} = \pi \,\mathrm{d}P \int_{-1}^{1} \mathrm{d}y \int_0^1 \mathrm{d}\xi \int_0^{2\pi} \mathrm{d}\phi \, \delta^{(4)}\left(k_1 + k_2 - k - \sum_{i=1}^{n} p_i\right) \times \\
\times \left(\frac{1}{\xi}\right)_+ \frac{1}{2} \left[\left(\frac{1}{1-y}\right)_+ + \left(\frac{1}{1+y}\right)_+\right] g_0(\xi, y, \phi),
\end{aligned} \tag{4.28}$$

where we used the limit $\varepsilon \to 0$. We can combine the integral of the third integration region $y \in [1-\varepsilon, 1]$ with the subtraction term $\hat{\sigma}_{0,2}^{y\to 1}$

$$\hat{\sigma}_{0,3} + \hat{\sigma}_{0,2}^{y\to 1} = \pi \, \mathrm{d}P \int_0^1 \mathrm{d}\xi \int_{-1+\varepsilon}^1 \mathrm{d}y \int_0^{2\pi} \mathrm{d}\phi \left(\frac{1}{\xi}\right)_+ \delta^{(4)}\left(x_1(1-\xi)K_1 + x_2 K_2 - \sum_{i=1}^n p_i\right) \times \\ \times \frac{\xi^2}{8} \frac{Q_1^2 g^2}{z(p_1\cdot k)} \left[P_{ff}(z) - \frac{z m_1^2}{(p_1\cdot k)}\right] |\mathcal{M}_n(z p_1)|^2, \quad (4.29)$$

where $z = 1-\xi$. The integrand is only singular at $y \to 1$ and not for $y \to -1$. Therefore, we can set $\varepsilon \to 0$ for the lower bound of the y integration. The only y dependent terms are the $p_1 \cdot k$ terms and we can use the integral identities

$$\int_{-1}^1 \mathrm{d}y \, \frac{1}{p_1\cdot k} = -\frac{4}{\xi s} \log \frac{m_1^2}{4E_1^2} + \mathcal{O}(m_1^2), \quad (4.30)$$

$$\int_{-1}^1 \mathrm{d}y \, \frac{1}{(p_1\cdot k)^2} = \frac{8}{\xi^2 s} \frac{1}{m_1^2} + \mathcal{O}(m_1^2). \quad (4.31)$$

We obtain

$$\hat{\sigma}_{0,3} + \hat{\sigma}_{0,2}^{y\to 1} = -\frac{\pi}{2} \, \mathrm{d}P \int_0^1 \mathrm{d}\xi \int_0^{2\pi} \mathrm{d}\phi \left(\frac{1}{\xi}\right)_+ \delta^{(4)}\left(x_1(1-\xi)K_1 + x_2 K_2 - \sum_{i=1}^n p_i\right) \times \\ \times \left[g_0(\xi, 1, \phi) \log \frac{m_1^2}{4E_1^2} + \frac{2}{s} Q_1^2 g^2 |\mathcal{M}_n((1-\xi)x_1 K_1)|^2\right], \quad (4.32)$$

where we used that

$$g_0(\xi, 1, \phi) = \frac{Q_1^2 g^2}{(1-\xi)s} \xi P_{ff}(1-\xi) |\mathcal{M}_n((1-\xi)x_1 K_1)|^2. \quad (4.33)$$

When we calculate the hadronic cross section

$$\sigma = \int_0^1 \mathrm{d}x_1 \int_0^1 \mathrm{d}x_2 \, f(x_1, \mu_F) f(x_2, \mu_F) \hat{\sigma}, \quad (4.34)$$

we can use the integral transformation $\bar{x}_1 = (1-\xi)x_1$ to reduce the delta function and the born matrix element to the born case. For an arbitrary function $h(\xi, x_1)$, we find

$$\int_0^1 \mathrm{d}x_1 \int_0^1 \mathrm{d}\xi \left(\frac{1}{\xi}\right)_+ \delta^{(4)}\left(x_1(1-\xi)K_1 + x_2K_2 - \sum_{i=1}^n p_i\right) h(\xi, x_1)|\mathcal{M}_n((1-\xi)x_1K_1)|^2 = \int_0^1 \mathrm{d}x_1 \int_0^{1-x_1} \mathrm{d}\xi \left(\frac{1}{\xi}\right)_+ \frac{1}{1-\xi}\delta^{(4)}\left(x_1K_1 + x_2K_2 - \sum_{i=1}^n p_i\right) h\left(\xi, \frac{x_1}{1-\xi}\right)|\mathcal{M}_n(x_1K_1)|^2. \tag{4.35}$$

The upper bound of the ξ integration has to be understood as a theta function under the plus distribution. We can split the integration into two parts and obtain

$$\int_0^{1-x} \mathrm{d}\xi \left(\frac{1}{\xi}\right)_+ f(\xi) = \int_0^{1-x} \mathrm{d}\xi \frac{1}{\xi}\left[f(\xi) - f(0)\right] - f(0)\int_{1-x}^1 \mathrm{d}\xi \frac{1}{\xi}, \tag{4.36}$$

where the second integral can be integrated analytically (s. section E.2). Using (4.35) in (4.34), we find

$$\int_0^1 \mathrm{d}x_1\, f(x_1, \mu_F)\left(\hat{\sigma}_{0,3} + \hat{\sigma}_{0,2}^{y\to 1}\right) = -\frac{\alpha}{2\pi}Q_1^2\,\mathrm{d}\Phi_n\mathcal{B}\int_0^1 \mathrm{d}x_1 \int_0^{1-x_1} \mathrm{d}\xi \left(\frac{1}{\xi}\right)_+ \left[\frac{\xi P_{ff}(1-\xi)}{1-\xi}\log\frac{m_1^2(1-\xi)}{s} + 2\right] f\left(\frac{x_1}{1-\xi}, \mu_F\right), \tag{4.37}$$

where we used $s = x_1x_2S$, $E_1 = \frac{\sqrt{s}}{2}$ and, we omitted the $f(x_2, \mu_F)$ part because it remains unchanged. We obtain a similar result for the first region combined with the other subtracted term, i.e.

$$\int_0^1 \mathrm{d}x_2\, f(x_2, \mu_F)\left(\hat{\sigma}_{0,1} + \hat{\sigma}_{0,2}^{y\to -1}\right) = -\frac{\alpha}{2\pi}Q_2^2\,\mathrm{d}\Phi_n\mathcal{B}\int_0^1 \mathrm{d}x_2 \int_0^{1-x_2} \mathrm{d}\xi \left(\frac{1}{\xi}\right)_+ \left[\frac{\xi P_{ff}(1-\xi)}{1-\xi}\log\frac{m_2^2(1-\xi)}{s} + 2\right] f\left(\frac{x_2}{1-\xi}, \mu_F\right). \tag{4.38}$$

The terms with the integral over ξ have the same form as the pdf part of (2.19). Therefore, we can combine them. However, we have to use different pdf renormalization terms for mass regularization. The explicit form can be obtained from a comparision of the calculation in dim. reg. and mass regularization because the cross section cannot depend on the regularization procedure. One finds the following renormalized pdfs [30, eq

(3.19)-(3.20)] [69, eq (5.1)]

$$f_q(x) = f_q(x,\mu_F) - \frac{3\alpha Q^2}{2\pi}\int_x^1 \mathrm{d}z\,\frac{1}{z} f_\gamma\left(\frac{x}{z},\mu_F\right)\left\{\log\frac{\mu_F^2}{m^2}P_{f\gamma}(z) + r_{f\gamma}(z)\right\}$$
$$- \frac{\alpha Q^2}{2\pi}\int_x^1 \mathrm{d}z\,\frac{1}{z} f_q\left(\frac{x}{z},\mu_F\right)\left\{\log\frac{\mu_F^2}{m^2}\left(P_{ff}(z)\right)_+ - \left(P_{ff}(z)(2\log(1-z)+1)\right)_+ + r_{ff}(z)\right\} \tag{4.39}$$

and

$$f_\gamma(x) = f_\gamma(x,\mu_F) - \frac{\alpha Q^2}{2\pi}\sum_{a=q,\bar{q}}\int_x^1 \mathrm{d}z\,\frac{1}{z} f_a\left(\frac{x}{z},\mu_F\right)\times$$
$$\times\left\{\log\frac{\mu_F^2}{m^2}P_{\gamma f}(z) - P_{\gamma f}(z)(2\log(z)+1) + r_{\gamma f}(z)\right\}, \tag{4.40}$$

where

$$P_{ff}(z) = \frac{1+z^2}{1-z}, \quad P_{f\gamma}(z) = z^2 + (1-z)^2, \quad P_{\gamma f}(z) = \frac{1+(1-z)^2}{z}. \tag{4.41}$$

Therefore, we find

$$F_q(x_1,\mu_F) = 3\int_{x_1}^1 \mathrm{d}z\,\frac{1}{z} f_\gamma\left(\frac{x_1}{z},\mu_F\right)\left\{\log\frac{\mu_F^2}{m^2}P_{f\gamma}(z) + r_{f\gamma}(z)\right\}$$
$$+\int_{x_1}^1 \mathrm{d}z\,\frac{1}{z} f_q\left(\frac{x_1}{z},\mu_F\right)\left\{\log\frac{\mu_F^2}{m^2}\left(P_{ff}(z)\right)_+ - \left(P_{ff}(z)(2\log(1-z)+1)\right)_+ + r_{ff}(z)\right\} \tag{4.42}$$

as pdf renormalization term in (2.22) and (2.23). If we neglect the photon pdf in (4.39) (as we will do in chapter 6) we obtain

$$\begin{aligned}\sigma_+^{(\mathrm{pdf})} + \int_0^1 \mathrm{d}x_1 \int_0^1 \mathrm{d}x_2\, f(x_1,\mu_F) f(x_2,\mu_F) \left(\hat{\sigma}_{0,3} + \hat{\sigma}_{0,2}^{y\to 1}\right) \\ = -\frac{\alpha}{2\pi} Q_1^2 \int_0^1 \mathrm{d}x_1 \int_0^1 \mathrm{d}x_2\, \mathrm{d}\Phi_n f(x_2,\mu_F) \mathcal{B} \left[\int_{x_1}^1 \mathrm{d}z\, \frac{1}{z} f\left(\frac{x_1}{z},\mu_F\right) \times \right. \\ \times \left\{ \left[\left(\log\frac{z\mu_F^2}{s} - 1 \right) \left(\frac{1}{1-z}\right)_+ - 2\left(\frac{\log(1-z)}{1-z}\right)_+ \right] (1-z)\hat{P}_{ff}(z) + r_{ff}(z) \right\} \\ \left. + f(x_1,\mu_F) \left(\frac{3}{2}\log\frac{\mu_F^2}{s} + 2 \right) - \frac{3}{2}\log\frac{m_1^2}{s} f(x_1,\mu_F) \right], \end{aligned} \tag{4.43}$$

after expanding the plus distribution according to (4.36), transforming $\xi \to 1-z$ and moving non-singular parts from the plus distribution to the test function. We get the same collinear remnant for the pdf renormalization of second pdf $f(x_2,\mu_F)$. We only have to swap the indices x_1 and x_2.

4.2. Final-State Radiation

The final-state radiation part of (4.20) is given by

$$\hat{\sigma}_r = \pi\, \mathrm{d}P \delta^{(4)} \left(k_1 + k_2 - k - \sum_{i=1}^n p_i \right) \int_0^1 \mathrm{d}\xi \int_{-1}^1 \mathrm{d}y \int_0^{2\pi} \mathrm{d}\phi \left(\frac{1}{\xi}\right)_+ S_r \frac{\xi^2}{8} |\mathcal{M}_{n+1}|^2 \tag{4.44}$$

and it is only divergent for $y \to 1$. Therefore, we split the y integration region into two parts

1. $y \in [-1, 1-\varepsilon)$
2. $y \in [1-\varepsilon, 1]$,

where ε is a small technical parameter. We write

$$\hat{\sigma}_r = \hat{\sigma}_{r,1} + \hat{\sigma}_{r,2}, \tag{4.45}$$

where the last subscript labels the region. We add a zero to the cross section in region two

$$\hat{\sigma}_{r,2} = \hat{\sigma}_{r+} + \hat{\sigma}_{r,2}^{y\to 1} \tag{4.46}$$

and define the subtracted cross section $\hat{\sigma}_{r+} = \hat{\sigma}_{r,2} - \hat{\sigma}_{r,2}^{y\to 1}$, where

$$\hat{\sigma}_{r,2}^{y\to 1} = \pi \,\mathrm{d}P \int_0^1 \mathrm{d}\xi \int_{-1}^{1-\varepsilon} \mathrm{d}y \int_0^{2\pi} \mathrm{d}\phi \left(\frac{1}{\xi}\right)_+ \left[\delta^{(4)}\left(k_1 + k_2 - k - \sum_{i=1}^{n} p_i\right) S_r \frac{\xi^2}{8} |\mathcal{M}_{n+1}|^2\right]_{y\to 1}. \tag{4.47}$$

The matrix element for final-state radiation in its collinear limit is given by [70]

$$|\mathcal{M}_{n+1}^{(\mathrm{coll})}|^2 = \frac{Q_r^2 g^2}{(p_r \cdot k)} \left[P_{ff}(z) - \frac{m_r^2}{(p_r \cdot k)}\right] |\mathcal{M}_n(p_r + k)|^2, \tag{4.48}$$

i.e. the collinear limit is given by the born matrix element times a splitting function $P_{ff}(x) = \frac{1+x^2}{1-x}$. The argument of the splitting function is given by $z = \frac{p_r^0}{p_r^0 + k^0}$, i.e. the ratio of the energy of the emitting particle before and after the emission. The phase-space parametrization is chosen such that the radiated particle k is collinear with p_r for $y = 1$, i.e. we can combine both momenta. When we evaluate the subtracted cross section, we can neglect the masses in the collinear limit of the matrix element because y is always smaller than one. We arrive at

$$\hat{\sigma}_{r+} = \pi \,\mathrm{d}P \int_0^1 \mathrm{d}\xi \int_{-1}^{1-\varepsilon} \mathrm{d}y \int_0^{2\pi} \mathrm{d}\phi \left(\frac{1}{\xi}\right)_+ \left(\frac{1}{1-y}\right)_+ \delta^{(4)}\left(k_1 + k_2 - k - \sum_{i=1}^{n} p_i\right) g_r(\xi, y, \phi), \tag{4.49}$$

where

$$g_r(\xi, y, \phi) = \frac{1}{2s} \frac{E(p_r \cdot k)}{E_r} S_r |\mathcal{M}_{n+1}^0|^2. \tag{4.50}$$

When we combine the subtraction term with the first region, we obtain

$$\hat{\sigma}_{r,1} + \hat{\sigma}_{r,2}^{y\to 1} = \pi \,\mathrm{d}P \int_0^1 \mathrm{d}\xi \int_{-1}^{1} \mathrm{d}y \int_0^{2\pi} \mathrm{d}\phi \left(\frac{1}{\xi}\right)_+ \times \\ \times \left[\delta^{(4)}\left(k_1 + k_2 - k - \sum_{i=1}^{n} p_i\right) S_r \frac{\xi^2}{8} |\mathcal{M}_{n+1}|^2\right]_{y\to 1}. \tag{4.51}$$

Since the emitted particle k flies in the same direction as particle p_r in the collinear limit, we can use that

$$k + p_r = (E + E_r) \begin{pmatrix} 1 \\ \hat{p}_r \end{pmatrix}, \tag{4.52}$$

where $\hat{p}_r$ is the direction of the emitting particle. Using this and the collinear limit of the matrix element (4.48), we arrive at

$$\hat{\sigma}_{r,1} + \hat{\sigma}_{r,2}^{y\to 1} = \pi \,\mathrm{d}P \int_0^1 \mathrm{d}\xi \int_{-1}^1 \mathrm{d}y \int_0^{2\pi} \mathrm{d}\phi \left(\frac{1}{\xi}\right)_+ \delta^{(4)} \left(k_1 + k_2 - \frac{\sqrt{s}}{2}(\xi + \xi_r) \begin{pmatrix} 1 \\ \hat{p}_r \end{pmatrix} - \sum_{\substack{i=1 \\ i\neq r}}^n p_i \right) \times$$
$$\times \frac{\xi^2}{8} \frac{Q_r^2 g^2}{(p_r \cdot k)} \left[P_{ff}\left(\frac{\xi_r}{\xi_r + \xi}\right) - \frac{m_r^2}{(p_r \cdot k)} \right] \left| \mathcal{M}_n \left(\frac{\sqrt{s}}{2}(\xi + \xi_r) \begin{pmatrix} 1 \\ \hat{p}_r \end{pmatrix} \right) \right|^2 . \quad (4.53)$$

We can use the integrals (4.30) and (4.31) to obtain

$$\hat{\sigma}_{r,1} + \hat{\sigma}_{r,2}^{y\to 1} = -8\pi^3 Q_r^2 \alpha \,\mathrm{d}P \int_0^1 \mathrm{d}\xi \left(\frac{1}{\xi}\right)_+ \delta^{(4)} \left(k_1 + k_2 - \frac{\sqrt{s}}{2}(\xi + \xi_r) \begin{pmatrix} 1 \\ \hat{p}_r \end{pmatrix} - \sum_{\substack{i=1 \\ i\neq r}}^n p_i \right) \times$$
$$\times \frac{1}{2s} \left[\frac{\xi}{\xi_r} P_{ff}\left(\frac{\xi_r}{\xi_r + \xi}\right) \log \frac{m_r^2}{4E_r^2} + 2 \right] \left| \mathcal{M}_n \left(\frac{\sqrt{s}}{2}(\xi + \xi_r) \begin{pmatrix} 1 \\ \hat{p}_r \end{pmatrix} \right) \right|^2 . \quad (4.54)$$

Since there is an integration over E_r in $\mathrm{d}P$, we can write

$$\mathrm{d}P \propto \int_0^1 \mathrm{d}\xi_r \, \frac{\xi_r s}{4}, \quad (4.55)$$

where $E_r = \xi_r \frac{\sqrt{s}}{2}$. We transform this integral according to $\bar{\xi}_r = \xi + \xi_r$ and obtain

$$\hat{\sigma}_{r,1} + \hat{\sigma}_{r,2}^{y\to 1} = Q_r^2 \frac{\alpha}{2\pi} \,\mathrm{d}\Phi_n \mathcal{B} \Bigg\{ \left(\log \frac{m_r^2}{s\xi_r^2} - 1 \right) \int_{\xi_r}^1 \mathrm{d}\xi \, \frac{2}{\xi}$$
$$- \int_0^{\xi_r} \mathrm{d}\xi \, \frac{1}{\xi} \left[\frac{\xi}{\xi_r} P_{ff}\left(1 - \frac{\xi}{\xi_r}\right) \log \frac{m_r^2}{s(\xi_r - \xi)^2} - \frac{2\xi}{\xi_r} - 2 \log \frac{m_r^2}{s\xi_r^2} \right] \Bigg\}, \quad (4.56)$$

where we used energy conservation. Solving the integrals leads to

$$\hat{\sigma}_{r,1} + \hat{\sigma}_{r,2}^{y\to 1} = -Q_r^2 \frac{2\alpha}{\pi} \,\mathrm{d}\Phi_n \mathcal{B} \left\{ -\frac{3}{2} \log \frac{m_r^2}{\xi_r^2 s} + \frac{2}{3}\pi^2 - \frac{9}{2} + 2 \left(\log \frac{m_r^2}{\xi_r^2 s} - 1 \right) \log \xi_r \right\}. \quad (4.57)$$

In total, we obtain

$$\hat{\sigma}_r = \mathrm{d}\Phi_{n+1} \left(\frac{1}{\xi}\right)_+ \left(\frac{1}{1-y}\right)_+ \frac{4}{\xi s} g_r(\xi, y, \phi) \\ - \frac{\alpha}{2\pi} Q_r^2 \, \mathrm{d}\Phi_n \mathcal{B} \left\{ -\frac{3}{2} \log \frac{m_r^2}{\xi_r^2 s} + \frac{2}{3}\pi^2 - \frac{9}{2} + 2 \left(\log \frac{m_r^2}{\xi_r^2 s} - 1 \right) \log \xi_r \right\}, \quad (4.58)$$

where we used (4.15) to construct a real phase space.

4.3. Final Result

As for the standard FKS subtraction in chapter 3, we collect all terms that contribute to the NLO cross section.

Real Part We get the same subtracted real cross section (3.178) as for dim. reg..

$$\sigma_r = \int_0^1 \mathrm{d}x_1 \int_0^1 \mathrm{d}x_2 \, f(x_1, \mu_F) f(x_2, \mu_F) \times \\ \times \left\{ \sum_i \frac{1}{2} \, \mathrm{d}\Phi_{n+1}^{(i)} \left(\frac{1}{\xi_i}\right)_+ \frac{1}{\xi_i} \left[\left(\frac{1}{1-y_i}\right)_+ + \left(\frac{1}{1+y_i}\right)_+ \right] \xi_i^2 (1-y_i^2) S_i \mathcal{R}^{(0)} \right. \\ \left. + \sum_{ij} \mathrm{d}\Phi_{n+1}^{ij} \left(\frac{1}{\xi_i}\right)_+ \left(\frac{1}{1-y_i}\right)_+ \xi_i^2 (1-y_i) S_{ij} \mathcal{R}^{(0)} \right\}, \quad (4.59)$$

where $\mathcal{R}^{(0)}$ denotes the massless real matrix element (s. (4.2)). All divergences are subtracted by the plus distributions and S functions in this term. Therefore, the integral is finite.

Collinear Remnant Also the collinear remnant for a fermion-fermion splitting is the same as in dimensional regularization, i.e.

$$\begin{aligned}\sigma_{\text{coll},1} = &-\frac{\alpha Q^2}{2\pi}\int_0^1 \mathrm{d}x_1 \int_0^1 \mathrm{d}x_2 \; \mathrm{d}\Phi_n \mathcal{B} f(x_2,\mu_F)\times \\ &\times \int_{x_1}^1 \mathrm{d}z \, f\left(\frac{x_1}{z},\mu_F\right)\left\{\frac{1-z}{z}P_{ff}(z)\left[\left(\log\frac{z\mu_F^2}{s}-1\right)\left(\frac{1}{1-z}\right)_+ - 2\left(\frac{\log(1-z)}{1-z}\right)_+\right]\right. \\ &\left. +2\left(\frac{1}{1-z}\right)_+ + \frac{1}{z}r_{ff}(z)\right\} \\ = &-\frac{\alpha Q^2}{2\pi}\int_0^1 \mathrm{d}x_1 \int_0^1 \mathrm{d}x_2 \; \mathrm{d}\Phi_n \mathcal{B} f(x_2,\mu_F)\times \\ &\times \int_{x_1}^1 \mathrm{d}z \, \frac{1}{z} f\left(\frac{x_1}{z},\mu_F\right)\left\{(1-z)P_{ff}(z)\left[\log\frac{z\mu_F^2}{s}\left(\frac{1}{1-z}\right)_+ - 2\left(\frac{\log(1-z)}{1-z}\right)_+\right]\right. \\ &\left. -(1-z)+\frac{1}{z}r_{ff}(z)\right\}, \end{aligned} \tag{4.60}$$

where r_{ff} specifies the pdf renormalization scheme. It is zero in the $\overline{MS}$ scheme and it is specified in (3.194) for the DIS scheme. The term $\sigma_{\text{coll},2}$ is analogous to $\sigma_{\text{coll},1}$. We only have to swap x_1 and x_2.

Soft-Collinear Endpoint Only the integrated soft and collinear terms are different. Therefore, the conversion of a standard FKS implementation into an implementation with mass regularization is simple because we only have to modify the endpoint and not the plus distributions. The numerical value of the subtracted virtual part $\hat{\mathcal{V}}$ is the same as for dim. reg.. Only the composition of this term changes. It is given by

$$\hat{\mathcal{V}} = \frac{\alpha}{2\pi}\mathcal{B}Q + \frac{\alpha}{2\pi}\sum_{\substack{ij \\ i\neq j}} \mathcal{B}_{ij}\mathcal{I}_{ij} + \mathcal{V}_m^{\text{1-loop}}, \tag{4.61}$$

where $\mathcal{B}$ is the born matrix element divided by the flux, α is the fine-structure constant, and $\mathcal{V}_m^{\text{1-loop}}$ is the mass regulated virtual cross section. The charge correlated born matrix element reads

$$\mathcal{B}_{ij} = -Q_i Q_j \sigma_i \sigma_j \mathcal{B}, \tag{4.62}$$

where Q_i is the charge of fermion i and $\sigma_i = 1$ for incoming fermions and outgoing anti-fermions and $\sigma_i = -1$ for outgoing fermions and incoming anti-fermions. Furthermore,

we introduce

$$\mathcal{I}_{ij} = \frac{1}{2}\log\frac{4(p_i\cdot p_j)^2}{m_i^2 m_j^2}\log\frac{s}{4m_\gamma^2} + 2\log 2\log\frac{p_i\cdot p_j}{2E_iE_j} - \mathrm{Li}_2\left(\frac{p_i\cdot p_j}{2E_iE_j}\right) - \log\left(\frac{p_i\cdot p_j}{2E_iE_j}\right)\log\left(1-\frac{p_i\cdot p_j}{2E_iE_j}\right) + \frac{1}{2}\log^2\left(\frac{p_i\cdot p_j}{2E_iE_j}\right) \quad (4.63)$$

and

$$Q = Q_{\text{soft}} + Q_{\text{initial}} + Q_{\text{final}}\,, \quad (4.64)$$

where

$$Q_{\text{soft}} = \sum_{i=\text{all}} Q_i^2\left(-\frac{1}{2}\log^2\frac{m_i^2}{E_i^2} + 2\log^2 2 - \frac{\pi^2}{6} - \log\frac{s}{4m_\gamma^2} - \log\frac{m_i^2}{4E_i^2}\right), \quad (4.65)$$

$$Q_{\text{final}} = \sum_{k=\text{final}} Q_k^2\left(\frac{3}{2}\log\frac{m_k^2}{4E_k^2} - \frac{2}{3}\pi^2 + \frac{9}{2} + \left(\log\frac{m_k^2}{2E_k^2\delta_{\text{O}}} + 1\right)\log\frac{s}{4E_k^2}\right), \quad (4.66)$$

$$Q_{\text{initial}} = \sum_{l=\text{initial}} Q_l^2\left(\frac{3}{2}\log\frac{m_l^2}{\mu_F^2} - 2\right). \quad (4.67)$$

These terms contain logarithms of fermion masses instead of $\frac{1}{\varepsilon}$ poles. The same type of logarithms exists in the virtual matrix element $\mathcal{V}_m^{\text{1-loop}}$. Overall, all mass logarithms have to cancel due to the KLN theorem and the remaining finite term has to be equal to the dim. reg. result.

To check our results, we calculated the virtual parts of the Drell-Yan process explicitly (s. Appendix B) and found the same logarithmic structure.

Since the standard FKS subtraction scheme uses dim. reg., it can be useful to calculate the difference

$$\Delta = \Big(\mathcal{B}\,\mathcal{Q} + \sum_{\substack{i,j\\ i\neq j}}\mathcal{B}_{ij}\,\mathcal{I}_{ij}\Big)_{\text{dim. reg.}} - \Big(\mathcal{B}\,\mathcal{Q} + \sum_{\substack{i,j\\ i\neq j}}\mathcal{B}_{ij}\,\mathcal{I}_{ij}\Big)_{\text{mass reg.}} \quad (4.68)$$

between dim. reg. and mass regularization. We find

$$\Delta = \sum_{i=\text{all}} q_i^2\mathcal{B}\left(-\log\frac{m_\gamma^2}{Q^2} - \frac{1}{2}\log\frac{m_i^2}{Q^2} + \frac{1}{2}\log^2\frac{m_i^2}{Q^2} + 2 + \frac{\pi^2}{6}\right) - \frac{1}{2}\sum_{\substack{i,j\\ i\neq j}}\mathcal{B}_{ij}\log\frac{m_i^2 m_j^2}{4(p_i\cdot p_j)^2}\log\frac{m_\gamma^2}{Q^2}\,. \quad (4.69)$$

Since only the soft-collinear endpoint changes, this result can be interpreted as conversion rule between the finite part of the dim. reg. $\mathcal{V}_{1-\text{loop}}$ result and $\mathcal{V}_m^{1-\text{loop}}$ in mass regularization. We checked this explicitly for the W + jet case. The same result was also calculated in Appendix A of [71].

5. Parton Shower Matching with POWHEG

A typical event at a particle collider consists of many final-state particles. To predict probabilities for inclusive observables, we calculate cross sections in fixed-order perturbation theory. The perturbation theory is ordered in the coupling of fundamental particle interactions. It is only feasible to calculate the cross section for a few final-state particles and up to a few orders in the coupling. Furthermore, large logarithms can arise at each order of the calculation for more differential observables. These logarithms have to be resummed to all orders in order to obtain physical predictions. We call the process which we calculate in perturbation theory *hard process*. To obtain a more realistic event from the hard process, we have to add radiation and particle splittings. We have to add radiation until the radiation is so collinear or soft that it is not resolvable anymore. For QCD radiation, also hadronization comes into play for very soft and collinear particles because the running strong coupling is not in the asymptotically free regime anymore.

In the previous chapters, we described how to calculate the hard process at NLO. In the following, we illustrate how *parton showers* are used to obtain more realistic event samples for LO hard processes. Furthermore, we discuss how NLO hard processes can be combined to *parton showers* with the POWHEG method.

5.1. Parton Shower

The *parton shower* is used to add radiation to the hard process. It starts from the hard process and adds a sequence of $1 \to 2$ branchings. The kinematics of each splitting is defined by the energy fraction z of one daughter and a scale t, for example the p_T^2 or the splitting angle θ. We call t the *evolution scale* of the shower. In the following, we choose $t = p_T^2$. It is sometimes convenient to think of t as the *shower time* although it is not connected to time. The parton shower generates radiation ordered in t, i.e. it generates first a splitting at t_1 and then a second splitting at t_2 with $t_1 > t_2$. It continues until t reaches a scale where the radiation cannot be resolved anymore. To specify the shower algorithm we define the *Sudakov form factor* $\Delta(t_i, t_e)$ which is the

non-splitting probability between the initial scale t_i and the end scale t_e. We can obtain the non-splitting probability between t_i and an intermediate scale t by splitting the *Sudakov* into two pieces

$$\Delta(t_i, t) = \frac{\Delta(t_i, t_e)}{\Delta(t, t_e)}. \tag{5.1}$$

Since $\Delta(t_i, t)$ is a survival probability, we can define a cumulative probability distribution for a splitting in $[t_i, t]$ as

$$\mathcal{S}(t_i, t) = 1 - \Delta(t_i, t) \tag{5.2}$$

and, therefore, the splitting density $s(t)$ for a splitting at t is given by

$$s(t) = -\frac{\mathrm{d}}{\mathrm{d}t}\Delta(t_i, t). \tag{5.3}$$

A recursive parton shower algorithm can be defined as follows

1. start at t_i
2. draw a random number t according to $s(t) = -\frac{\mathrm{d}}{\mathrm{d}t}\Delta(t_i, t)$
3. use t for a splitting
4. if $t > t_e$, go to 1 with $t_i = t$

To specify the *Sudakov form factor* we use

$$\Delta(t_i, t_e) + \mathcal{S}(t_i, t_e) = 1, \tag{5.4}$$

i.e. there is either one splitting in $[t_i, t_e]$ or there is no splitting. We can rewrite the splitting probability $\mathcal{S}$ in terms of the *Sudakov form factor*. We use that the cumulative probability for a splitting at t is given by the probability $\Delta(t_i, t)$ for no splitting up to scale t times the actual splitting probability $p(t)$. Since the splitting can happen at any intermediate scale t in $[t_i, t_e]$, we have to integrate over all possible values for t, i.e.

$$\mathcal{S}(t_i, t_e) = \int_{t_e}^{t_i} \mathrm{d}t\, \Delta(t_i, t) p(t). \tag{5.5}$$

The integral equation (5.4) is solved by

$$\Delta(t_i, t) = \exp\left\{ -\int_{t}^{t_i} \mathrm{d}t'\, p(t') \right\}. \tag{5.6}$$

To obtain the splitting probability $p(t)$ we use that the cross section for one splitting is given by

$$\mathrm{d}\sigma_{n+1} = \mathrm{d}\sigma_n p(t)\,\mathrm{d}t \quad \Rightarrow \quad \mathrm{d}\Phi_{n+1}|\mathcal{M}_{n+1}|^2 = \mathrm{d}\Phi_n|\mathcal{M}_n|^2 p(t)\,\mathrm{d}t, \tag{5.7}$$

where p includes the integration over the energy fraction z and the azimuthal angle ϕ. The matrix element factorizes for collinear radiation in the following way

$$\int \mathrm{d}\Phi_{n+1}|\mathcal{M}_{n+1}|^2 = \int \mathrm{d}\Phi_n|\mathcal{M}_n|^2 \frac{\alpha}{2\pi} P(z)\,\mathrm{d}z \frac{\mathrm{d}t}{t}, \tag{5.8}$$

where $P(z)$ is an Altarelli-Parisi splitting function and α is the coupling (s. Appendix H). The splitting probability is given by

$$p(t) = \int_{z_-(t)}^{z_+(t)} \mathrm{d}z \frac{\alpha}{2\pi} P(z) \frac{1}{t}, \tag{5.9}$$

where $z_\pm(t)$ are the kinematically allowed limits. So far we considered only one splitting type. In reality, multiple splitting types are possible, e.g. $g \to q\bar{q}$, $q \to qg$ etc. Therefore, we have to extend the *Sudakov* to

$$\Delta_a(t_i, t) = \exp\left\{ -\sum_b \int_t^{t_i} \mathrm{d}t' \int_{z_-}^{z_+} \mathrm{d}z \, \frac{\alpha}{2\pi} \frac{1}{t'} P_{ab}(z) \right\}, \tag{5.10}$$

where particle a splits into b. We can use a recursive algorithm to generate a value for the evolution scale t. Once we have determined a value for t from Δ, we can also draw an energy fraction z from the exponent of Δ. The kinematics for FSR are fully specified by t, z, and an azimuthal angle that is uniformly distributed. We can use a similar *Sudakov* for ISR. However, we have to take the parton distribution functions into account because their arguments change. Therefore, we have

$$p(t) = \int_{z_-}^{z_+} \mathrm{d}z \, \frac{\alpha}{2\pi} \frac{1}{t} P_{ab}(z) \frac{f_a(x/z)}{f_b(z)}. \tag{5.11}$$

The Sudakov form factor in (5.10) resums the leading large logs from the integral over the parton splitting. Well known and widely used standard parton-shower programs are Pythia [72, 73], Herwig [74, 75] and Sherpa [76].

5.2. Matching a Parton Shower With an NLO Calculation

Since the parton shower relies on the factorization of the matrix element in the collinear limit, non-collinear radiation is not described properly. We have to use higher-order corrections for the hard process to describe the non-collinear radiation more accurately. However, we cannot naively combine a NLO calculation with a standard parton shower because the parton shower as well as the NLO matrix element contain the first radiation. Therefore, we would count this radiation twice. Methods like MC@NLO [46] and POWHEG [47] have been devised to combine an NLO calculation with parton showers without double counting. In MC@NLO the hardest radiation from the parton shower is subtracted from the NLO calculation to overcome the double counting problem. A disadvantage of this method is that it depends on the parton shower program. The POWHEG method avoids double counting by using the NLO matrix element for a first shower like radiation. The scale of the radiation is then given to the parton shower as starting scale. Therefore, POWHEG can be used with any p_T-ordered vetoed parton shower program. (Subtleties are discussed in section 5.5.5.) Both methods provide NLO accuracy but they differ at higher-orders.

In the following we describe the combination of parton showers and NLO calculations in more detail. This description is based on [77]. The fully differential cross section for the hardest parton-shower radiation includes unresolved emissions and one resolved shower emission, i.e.

$$\mathrm{d}\sigma_{PS} = \mathrm{d}\sigma_n \Delta(t_i, t_e) + \mathrm{d}\sigma_{NLO}^{(PS)}, \tag{5.12}$$

where the leading order cross section is given by $\mathrm{d}\sigma_n = B\,\mathrm{d}\Phi_n$ and the emission cross section $\mathrm{d}\sigma_{NLO}^{(PS)} = \mathrm{d}\Phi_n\,\mathrm{d}\Phi_{\mathrm{rad}} R^{(PS)}$. The factor $R^{(PS)} = B\mathcal{S}(t_i, t)$ depends on the parton shower program (cf. (5.5)). We go from LO to NLO by adding subtracted real corrections $\hat{R}$ and virtual corrections plus the soft-collinear endpoint $\hat{V}$ to the hard process, i.e.

$$\mathrm{d}\sigma_{NLO} = \mathrm{d}\Phi_n(B + \hat{V}) + \mathrm{d}\Phi_n\,\mathrm{d}\Phi_{\mathrm{rad}}\hat{R}. \tag{5.13}$$

By naively using the NLO cross section as $\mathrm{d}\sigma_n$ in (5.12), we obtain

$$\mathrm{d}\sigma_{PS}^{\mathrm{naive}} = \mathrm{d}\Phi_n \left[B + \hat{V} + \mathrm{d}\Phi_{\mathrm{rad}}\hat{R}\right] \Delta(t_i, t_e) + \mathrm{d}\Phi_n\,\mathrm{d}\Phi_{\mathrm{rad}} R^{(PS)}. \tag{5.14}$$

When we expand the Sudakov, we find at NLO

$$\mathrm{d}\sigma_{PS}^{\mathrm{naive}} = \mathrm{d}\Phi_n \left[B + \hat{V} + \mathrm{d}\Phi_{\mathrm{rad}}\hat{R}\right] - \mathrm{d}\Phi_n \int \mathrm{d}\Phi_{\mathrm{rad}} R^{(PS)} + \mathrm{d}\Phi_n\,\mathrm{d}\Phi_{\mathrm{rad}} R^{(PS)}, \tag{5.15}$$

where $\int \mathrm{d}\Phi_{\mathrm{rad}} R^{(PS)}$ is a non-resolved term from the expansion of the Sudakov and we find two terms for the resolvable emission. This equation includes the NLO real radiation as well as the parton shower radiation. Hence, the hardest radiation is counted twice. One way to avoid the double counting is to subtract $R^{(PS)}$ terms from the real emission, i.e.

$$\mathrm{d}\sigma_{NLO}^{\mathrm{mod}} = \mathrm{d}\Phi_n \left(B + \hat{V} + \int \mathrm{d}\Phi_{\mathrm{rad}} R^{(PS)} \right) + \mathrm{d}\Phi_n \, \mathrm{d}\Phi_{\mathrm{rad}} \left[\hat{R} - R^{(PS)} \right]. \tag{5.16}$$

The terms $R^{(PS)}$ in $\mathrm{d}\sigma_{NLO}^{\mathrm{mod}}$ have the same structure as subtraction terms. Since $\mathrm{d}\sigma_{NLO}^{\mathrm{mod}}$ is not a physical differential cross section, a parton shower has be applied to obtain physical distributions. Using $\mathrm{d}\sigma_{NLO}^{\mathrm{mod}}$ as $\mathrm{d}\sigma_n$ in (5.12), we find at NLO that

$$\mathrm{d}\sigma_{\mathrm{PS@NLO}} = \mathrm{d}\Phi_n \, \mathrm{d}\Phi_{\mathrm{rad}} (B + \hat{V}) + \mathrm{d}\Phi_n \, \mathrm{d}\Phi_{\mathrm{rad}} \hat{R}. \tag{5.17}$$

This procedure is called MC@NLO [46]. One disadvantage of MC@NLO is that the terms $R^{(PS)}$ depend on the parton shower program. Therefore, one has to calculate $\mathrm{d}\sigma_{NLO}^{\mathrm{mod}}$ for a specific parton shower program.

The POWHEG method is another approach to parton shower matching. It is described in detail in the following section.

5.3. POWHEG Method

It is the main idea of the POWHEG method to use a local NLO weight for a born phase-space point and generate NLO accurate radiation with parton-shower methods. To handle IR singularities in the NLO weight, we use the FKS subtraction scheme described in chapter 3. It is convenient to use FKS because it starts, as the parton shower, from a born phase-space. Therefore, it is naturally to write the NLO phase-space as a born phase-space times the radiation phase-space, i.e.

$$\mathrm{d}\Phi_{n+1} = \mathrm{d}\Phi_n \, \mathrm{d}\Phi_{\mathrm{rad}}. \tag{5.18}$$

Using (3.176), we can define the NLO weight by

$$\begin{aligned} \bar{B} = {} & f(x_1, \mu_F) f(x_2, \mu_F) (\mathcal{B} + \hat{\mathcal{V}}) + \sum_\alpha \int \mathrm{d}\Phi_{\mathrm{rad}}^{(\alpha)} f(x_1^{(\alpha)}, \mu_F) f(x_2^{(\alpha)}, \mu_F) \hat{\mathcal{R}}_\alpha \\ & + \int_{x_1}^1 \mathrm{d}z \, f\left(\frac{x_1}{z}, \mu_F\right) f(x_2, \mu_F) \frac{1}{z} G_1(z) + \int_{x_2}^1 \mathrm{d}z \, f(x_1, \mu_F) f\left(\frac{x_2}{z}, \mu_F\right) \frac{1}{z} G_2(z), \end{aligned} \tag{5.19}$$

where α denotes all possible singular regions i and ij and $x_{1/2}^{(\alpha)}$ depend on the radiation phase space. Using the NLO weight $\bar{B}$, we write the NLO cross section as

$$\mathrm{d}\sigma_{NLO} = \mathrm{d}\Phi_n \bar{B}. \tag{5.20}$$

We use the real matrix element and the FKS S functions to define the POWHEG Sudakov as

$$\Delta(p_T) = \exp\left\{ -\sum_\alpha \int \mathrm{d}\Phi_{\mathrm{rad}}^{(\alpha)} \frac{f(x_1^{(\alpha)},\mu_F) f(x_2^{(\alpha)},\mu_F) S_\alpha R}{f(x_1,\mu_F) f(x_2,\mu_F) B} \theta(k_T^\alpha - p_T) \right\}, \tag{5.21}$$

where k_T should be equal to the transverse momentum of the radiated particle in the collinear limit. This Sudakov is used to generate the first and hardest radiation. All subsequent radiation can be generated by a p_T ordered parton-shower program. Truncated angular ordered showers can be used if a p_T veto is introduced to the shower [78]. Using (5.3) and (5.12), we can write the cross section for the hardest radiation as

$$\mathrm{d}\sigma_{POW} = \mathrm{d}\Phi_n \bar{B} \left[\Delta(p_T^{\min}) + \sum_\alpha \frac{\mathrm{d}\Phi_{\mathrm{rad}}^{(\alpha)} f(x_1^{(\alpha)},\mu_F) f(x_2^{(\alpha)},\mu_F) S_\alpha R}{f(x_1,\mu_F) f(x_2,\mu_F) B} \Delta(k_T^{(\alpha)}) \right]. \tag{5.22}$$

Using [47]

$$\begin{aligned}
&\sum_\alpha \frac{\int \mathrm{d}\Phi_{\mathrm{rad}}^{(\alpha)} f(x_1^{(\alpha)},\mu_F) f(x_2^{(\alpha)},\mu_F) S_\alpha R}{f(x_1,\mu_F) f(x_2,\mu_F) B} \Delta(k_T^{(\alpha)}) = \\
&\quad = \int_{p_T^{\min}}^{\infty} \mathrm{d}p_T \sum_\alpha \delta(p_T - k_T^{(\alpha)}) \frac{\int \mathrm{d}\Phi_{\mathrm{rad}}^{(\alpha)} f(x_1^{(\alpha)},\mu_F) f(x_2^{(\alpha)},\mu_F) S_\alpha R}{f(x_1,\mu_F) f(x_2,\mu_F) B} \Delta(p_T) \\
&\quad = \int_{p_T^{\min}}^{\infty} \mathrm{d}p_T \frac{\mathrm{d}}{\mathrm{d}p_T} \Delta(p_T) \\
&\quad = 1 - \Delta(p_T^{\min}),
\end{aligned} \tag{5.23}$$

we see that (5.22) has NLO accuracy because $\mathrm{d}\sigma_{POW} = \mathrm{d}\sigma_{NLO}$.

5.4. Strong Coupling and Scales

It was shown in last section that the POWHEG method has NLO accuracy for infrared safe observables. Furthermore, POWHEG resums large logarithms in leading logarithmic accuracy (LL). Hence, it has the same LL accuracy as the parton shower that is used for the POWHEG events. In order to achieve LL accuracy, we have to use k_T^2 as scale for the strong coupling constant α_s and the pdfs in the radiation Sudakov [47]. If there are no

more than three colored particles in a born process, POWHEG can achieve NLL accuracy if the strong coupling constant

$$\alpha_s^{\mathrm{NLL}}(k_T^2) = \alpha_s(k_T^2)\left(1 + \frac{\alpha_s(k_T^2)}{2\pi}\left[\left(\frac{67}{18} - \frac{\pi^2}{6}\right)C_A - \frac{5}{9}n_f\right]\right), \tag{5.24}$$

and 2-loop α_s running is used [79]. The 2-loop running is given by

$$\alpha_s^{\text{2-loop}}(\mu^2, n_f) = \alpha_s^{\text{1-loop}}(\mu^2, n_f)\left[1 - \frac{\alpha_s^{\text{1-loop}}(\mu^2, n_f)}{2\pi}\frac{17C_A^2 - (5C_A + 3C_F)n_f}{11C_A - 2n_f}\log\left(\log\frac{\mu^2}{\Lambda^2}\right)\right] \tag{5.25}$$

and

$$\alpha_s^{\text{1-loop}}(\mu^2, n_f) = \frac{12\pi}{(11C_A - 2n_f)\log\frac{\mu^2}{\Lambda^2}}. \tag{5.26}$$

The scale Λ is defined such that the strong coupling constant is equal to the strong coupling constant from the pdfs at m_Z, i.e.

$$\alpha_s^{\text{2-loop}}(m_Z^2, 5) = \alpha_s^{\mathrm{pdf}}(m_Z^2). \tag{5.27}$$

Newton's method is used to find the solution Λ for the above equation. The scale Λ from 1-loop running is used as starting scale.

The POWHEGBOX uses a dynamic number of flavors in the running of α_s. For scales larger than the bottom mass, five-flavor running is used, i.e. $\Lambda = \Lambda_5$. In the range from m_c to m_b, four-flavor running is used and, for $\mu < m_c$, three-flavor running is used. To get a continuous α_s at the threshold masses, we use the matching conditions $\alpha_s(m_b^2, 5) = \alpha_s(m_b^2, 4)$ and $\alpha_s(m_c^2, 4) = \alpha_s(m_c^2, 3)$, i.e. we need different scales Λ_{n_f} for the low renormalization scale regions. Using the matching condition in the 1-loop running, we obtain

$$\alpha_s(\mu^2, 4) = \frac{b_4}{\log\frac{\mu^2}{\Lambda_4^2}}, \tag{5.28}$$

with $b_4 = \frac{12\pi}{25}$. We rewrite it in terms of the five flavor scale Λ_5, i.e.

$$\frac{1}{\alpha_s(\mu^2, 4)} = \frac{1}{b_4}\log\frac{\mu^2}{\Lambda_5^2} - \frac{1}{b_4}\log\frac{m_b^2}{\Lambda_5^2} + \frac{1}{b_5}\log\frac{m_b^2}{\Lambda_5^2}, \tag{5.29}$$

where $b_5 = \frac{12\pi}{23}$. We can express this equation in terms of the coupling and find

$$\frac{1}{\alpha_s(\mu^2, 4)} = \frac{1}{\alpha_s(\mu^2, 4, \Lambda_5^2)} - \frac{1}{\alpha_s(m_b^2, 4, \Lambda_5^2)} + \frac{1}{\alpha_s(m_b^2, 5)}, \tag{5.30}$$

where the couplings on the right hand side are evaluated with the five flavor scale Λ_5. We can find an analogous relation for $\mu = m_c$, i.e.

$$\frac{1}{\alpha_s(\mu^2, 3)} = \frac{1}{\alpha_s(\mu^2, 4, \Lambda_5^2)} - \frac{1}{\alpha_s(m_c^2, 3, \Lambda_5^2)} + \frac{1}{\alpha_s(m_c^2, 4)}. \tag{5.31}$$

Following the PowhegBox, we use the matching at 1-loop although the running is at 2-loop because the strong coupling α_s is almost continuous with the 1-loop matching.

5.5. Event Generation

Generating events with the Powheg method consists of two parts. First, we have to generate an underlying born phase space and a born flavor configuration. Second, the hardest radiation has to be generated from the underlying born configuration. These two steps are described in the following sections.

5.5.1. Underlying Born Events

First, we have to generate an underlying born phase-space. This phase-space point Φ_n is used as the basis for the radiation. It is conceptual equivalent to the LO process to which we attach the standard parton shower programs. Here, we use the real matrix element in order to generate the hardest (Powheg) radiation from the underlying born event. The born phase-space points are distributed according to the local NLO weight $\bar{B}(\Phi_n)$. To generate born phase-space points, we use rejection sampling. At first we have to find the maximum $\bar{B}^{\max}$ of $\bar{B}$. This can be done by sampling $\bar{B}$ randomly, for example, while we do a Monte Carlo integration to obtain the NLO cross section. We then draw a random phase-space point Φ_n and an uniformly distributed random number u in $[0, \bar{B}^{\max}]$. We accept this point only if $u < \bar{B}(\Phi_n)$ and reject it otherwise. The set of all accepted phase-space points are then distributed according to $\bar{B}$. Since it is not feasible to do the integration over the radiation phase space in $\bar{B}$ for every underlying born event, we rewrite the integrals in $\bar{B}$ as integrals over the unit cube, i.e.

$$\int \mathrm{d}\Phi_{\mathrm{rad}}^{(\alpha)} f(\Phi_{\mathrm{rad}}^{(\alpha)}) = \int_0^1 \mathrm{d}y_1 \int_0^1 \mathrm{d}y_2 \int_0^1 \mathrm{d}y_3 \, J_\alpha f(\Phi_{\mathrm{rad}}^{(\alpha)}(y_1, y_2, y_3)), \tag{5.32}$$

$$\int_{x_{1/2}}^1 \mathrm{d}z \, f(z) = \int_0^1 \mathrm{d}y_1 \int_0^1 \mathrm{d}y_2 \int_0^1 \mathrm{d}y_2 \, J_z f(z(y_1)), \tag{5.33}$$

where $J_{\alpha/z}$ are the Jacobian determinants of the integral transformations. Using the above equations, we can write

$$\bar{B} = \int_0^1 \mathrm{d}y_1 \int_0^1 \mathrm{d}y_2 \int_0^1 \mathrm{d}y_3 \, \tilde{B}, \tag{5.34}$$

where

$$\begin{aligned}\tilde{B} = {} & f(x_1,\mu_F) f(x_2,\mu_F)(\mathcal{B}+\hat{\mathcal{V}}) + \sum_\alpha J_\alpha f(x_1^{(\alpha)},\mu_F) f(x_2^{(\alpha)},\mu_F)\hat{\mathcal{R}}_\alpha \\ & + J_z f\left(\frac{x_1}{z},\mu_F\right) f(x_2,\mu_F)\frac{1}{z}G_1(z) + J_z f(x_1,\mu_F) f\left(\frac{x_2}{z},\mu_F\right)\frac{1}{z}G_2(z).\end{aligned} \tag{5.35}$$

The new NLO weight $\tilde{B}$ does not contain an integration anymore and is therefore better suited for event generation. In the following, we argue that we can use $\tilde{B}$ to draw born phase-space points according to $\bar{B}$. We use rejection sampling to generate a born phase space Φ_n and three radiation variables $\vec{y}$ according to $\tilde{B}$. However, we only use the born phase space and discard $\vec{y}$. After repeating this procedure very often, the born phase-space points are distributed according to $\bar{B}$. In order to justify this, we first look at generating one phase-space point Φ_n according to $\bar{B}$. After Φ_n is fixed we have to perform a Monte Carlo integration over the radiation phase space in $\bar{B}$, i.e. we draw many random points for the radiation phase space. Then we proceed with the next born phase-space point. When we use $\tilde{B}$, we draw a random born phase-space point and a set of random radiation variables $\vec{y}$. Therefore, the difference is only the ordering of the random variables. In the $\bar{B}$ case, the random radiation variables are ordered in Φ_n while in the $\tilde{B}$ case they are not ordered. When we draw enough points, we could in principle reorder the points to obtain the same result.

A further improvement is to implement a lazy evaluation of the virtual part of $\tilde{B}$. It can be computationally expensive to evaluate the virtual corrections, therefore, we want to avoid to evaluate them. We expect the virtual correction to be stable compared to the born. Therefore, we try to estimate the virtual part by

$$\hat{\mathcal{V}}_{\text{est}} = F\mathcal{B}. \tag{5.36}$$

The constant F is the maximal ratio of $\hat{\mathcal{V}}$ and $\mathcal{B}$. It can be determined when the maximum for $\tilde{B}$ is determined. We define

$$\tilde{B}_{\text{est}} = \tilde{B} \text{ with } \hat{\mathcal{V}} \to \hat{\mathcal{V}}_{\text{est}}. \tag{5.37}$$

Since $\tilde{B}_{\text{est}} \geq \tilde{B}$, we can use it to reject a point without evaluating the virtual corrections.

Every accepted point is then unweighted with $\tilde{B}$ after calculating the virtual corrections. To summarize, we state the unweighting procedure in an algorithmic form:

function UNWEIGHTING(Φ_n,$\vec{x}$, $\tilde{B}^{\max}$)
  $u = \text{random}(0,1)$
  $b' = \tilde{B}_{\text{est}}(\Phi_n, \vec{x})$
  if $u \geq \frac{b'}{\tilde{B}^{\max}}$ **then**
    return rejected
  end if
  $b = \tilde{B}(\Phi_n, \vec{x})$
  if $u \geq \frac{b}{\tilde{B}^{\max}}$ **then**
    return rejected
  end if
  return accepted
end function

So far, we considered only one born flavor configuration for the underlying born process. However, we usually have multiple born flavor configurations for a process at the LHC. The Drell-Yan process, for instance, has the born flavor configuration $u\bar{u} \to \mu^+\mu^-$, $d\bar{d} \to \mu^+\mu^-$ etc. We define $\tilde{B} = \sum_{f_b} \tilde{B}^{f_b}$, where f_b labels the different born flavor configurations. We generate underlying born events by generating a phase-space point with $\tilde{B}$ and picking a born flavor configuration with probability

$$p_{f_b} = \frac{\tilde{B}^{f_b}}{\tilde{B}}. \tag{5.38}$$

In practice, we divide the interval $[0,1]$ in f_b pieces with length p_{f_b}, draw a uniform random number in $[0,1]$, and pick f_b according to the piece where the random number lies.

Using these methods, we generate a born phase-space point Φ_n and a born flavor configuration f_b.

5.5.2. Negative Weights

Although the $\bar{B}$ function is positive in a perturbative regime, it is possible that the integrand $\tilde{B}$ can be negative in some regions of the radiation phase space. Consider for example the Drell-Yan process $q\bar{q} \to l^+l^-$. There is a collinear remnant for the splitting of a gluon to a quark. The collinear remnant contains a term

$$G \supset \frac{\log\xi}{\xi}\left[f_g\left(\frac{x}{1-\xi}, \mu_F\right)\xi P_{gq}(1-\xi) - f_g\left(x, \mu_F\right)\xi P_{gq}(1-\xi)|_{\xi=0}\right], \tag{5.39}$$

where x is the momentum fraction and ξ the energy fraction of the radiated quark. Since the splitting function P_{gq} has no $\frac{1}{\xi}$ pole, the subtraction term is zero, i.e. no subtraction is needed, and the splitting function in the first term is just a number in the interval $[\frac{1}{4}, \frac{1}{2}]$. The ξ integration has an upper bound $\xi_{\max} = 1 - x$. We, hence, define $\xi = \xi_{\max}\tilde{x}$, where $\tilde{x}$ is a number between 0 and 1. Therefore, equation (5.39) reads

$$G \propto \log(\tilde{x}(1-x)) f_g\left(\frac{x}{1-(1-x)\tilde{x}}\right). \tag{5.40}$$

When the argument of the pdf is small, (i.e. $x \sim 0$ and $\tilde{x} \sim 0$), we obtain a large value and multiply it by a negative logarithm. Therefore, the large negative value for the collinear remnant can overcome the positive born matrix element. In total, we obtain a negative integrand and therefore a negative weight of the event. However, when we integrate over the radiation phase-space we obtain a positive weight.

Since one of the main features of the POWHEG idea is to obtain only positive weights, we have to find a way to deal with those negative weights. The negative weights originate from rewriting $\bar{B}$ as an integral over $\tilde{B}$ to avoid a numerical integration over the radiation phase space. If the contribution of events with negative weights to the total cross section is small, we can ignore them. This is for example done in the Drell-Yan case. However, events with negative weights can give substantial contribution to the total cross section in other processes, e.g. $pp \to W + \text{jet}$. One way to reduce the number of negative weights is to at least mimic the integration over the radiation phase space by using a few sampling points. If one weight is negative, other sampled weights can be positive and compensate the negative weight. To do this consistently in a Monte-Carlo integration, we use the method described in [80]. We write

$$\int_0^1 \mathrm{d}x\, f(x) = \int_0^{\frac{1}{2}} \mathrm{d}x\, f(x) + \int_{\frac{1}{2}}^1 \mathrm{d}x\, f(x) = \int_0^{\frac{1}{2}} \mathrm{d}x\, \left[f(x) + f\left(x + \frac{1}{2}\right)\right]. \tag{5.41}$$

We sample two values for x in the Monte Carlo integration belonging to two separate regions. However, it is not clear if two points are enough to significantly reduce the ratio of negative weights. The generalization to more than one integration dimension is obvious, i.e.

$$\int_0^1 \mathrm{d}x\, f(x) = \int_0^1 \mathrm{d}x\, \frac{1}{n} \sum_{i=1}^{n} f\left(\frac{x+i-1}{n}\right). \tag{5.42}$$

It is not a priory clear how many points are needed to reduce the number of negative weights to an acceptable level. Hence, one has to try different values to find the best compromise between performance and accuracy.

The integrand $\tilde{B}$ consists of a part which depends only on the born kinematics and a real radiation part. Therefore, it is possible to calculate the born and virtual part once and then use the described technique for the radiation part.

5.5.3. Generation of Radiation

Having generated the underlying born process, we have to generate the hardest radiation using the POWHEG Sudakov (5.21). As before, we introduce the region label α which is an element of the set of all possible i and ij regions in the Sudakov. We pick a region α and generate radiation variables $\vec{x}$ for the hardest radiation. The radiation phase space is a function of $\vec{x}$, i.e.

$$\Phi_{\text{rad}} = \Phi_{\text{rad}}(\vec{x}). \tag{5.43}$$

Using (5.3), we see that we have to sample a transverse momentum of the radiated parton p_T from the probability density

$$s(p_T) = \sum_\alpha \int \mathrm{d}\Phi^\alpha_{\text{rad}}(\vec{x}) F_\alpha \delta\left[k_T^\alpha(\Phi^\alpha_{\text{rad}}(\vec{x})) - p_T\right] \Delta(p_T), \tag{5.44}$$

where

$$F_\alpha = \frac{f(x_1^{(\alpha)}, \mu_F) f(x_2^{(\alpha)}, \mu_F) S_\alpha R}{f(x_1, \mu_F) f(x_2, \mu_F) B}. \tag{5.45}$$

According to the highest-bid method that is described in section D.4, we find a p_T for every region α with

$$s_\alpha(p_T) = \int \mathrm{d}\Phi^\alpha_{\text{rad}}(\vec{x}) F_\alpha \delta\left[k_T^\alpha(\Phi^\alpha_{\text{rad}}(\vec{x})) - p_T\right] \Delta_\alpha(p_T), \tag{5.46}$$

where

$$\Delta_\alpha(p_T) = \exp\left\{ - \int \mathrm{d}\Phi^\alpha_{\text{rad}}(\vec{x}) F_\alpha \theta\left[k_T^\alpha(\Phi^\alpha_{\text{rad}}(\vec{x})) - p_T\right] \right\} \tag{5.47}$$

and choose the region with highest p_T to generate the radiation. To generate radiation variables $\vec{x}$ that result in a given p_T, we can use the techniques described in section D.3. If p_T is smaller than a minimal resolvable scale $p_T^{\min}$, we do not generate radiation with the POWHEG method. To sample p_T according to (5.46) is not straight-forward, since we cannot solve the integral in the Sudakov analytically. We introduce an upper bounding function U^α with

$$F^\alpha \leq U^\alpha \tag{5.48}$$

for the integrand. We solve the integral for U^α and use the veto method that is described in section D.3.1 to generate a p_T. In the following we describe the generation for

the different radiation regions. Note, that the next sections contain an application of the methods described in section D.3 and section D.3.1. Hence, we only state the region specific equations and calculations. Parts of the calculation can also be found in [47, chapter 7] and [67, appendix C and D]. At the end of each section, we give explicit algorithms that have been implemented in our computer code.

QCD Final-State Radiation

In case of final-state radiation we use an upper bounding function proportional to the singular structure $\frac{1}{\xi^2(1-y)}$ of the real matrix element. The Jacobian in (3.109) is proportional to ξ. Therefore, we choose

$$U(\xi, y) = N \frac{\alpha_s(k_T^2)}{\xi(1-y)} \tag{5.49}$$

as upper bounding function (cf. [67, appendix C]) where N is a constant. The result is independent of the actual upper bounding function. However, the performance of the algorithms depends on the upper bounding function. In practice, we obtain N by sampling $\{\Phi_n, \xi, y, \phi\}$ to find minimum N with $U > F$.

The transverse momentum of the radiated parton in the soft-collinear limit is given by

$$k_T^2 = \frac{s}{2}(1-y)\left(\xi^2 + \mathcal{O}(\xi^3)\right). \tag{5.50}$$

For the Sudakov form factor based on U, we find

$$\begin{aligned} -\log \Delta_U(p_T^2) &= N \int_0^{\xi_{\max}} \mathrm{d}\xi \int_{-1}^{1} \mathrm{d}y \int_0^{2\pi} \mathrm{d}\phi \, \frac{\alpha_s(k_T^2)}{\xi(1-y)} \theta(k_T^2 - p_T^2) \\ &= 2\pi N \int_0^{\xi_{\max}} \mathrm{d}\xi \, \theta(\xi - \sqrt{p_T^2/s}) \int_{p_T^2}^{s\xi^2} \mathrm{d}k_T^2 \, \frac{\alpha_s(k_T^2)}{\xi k_T^2} \\ &= 2\pi N \int_{p_T^2}^{s\xi_{\max}^2} \mathrm{d}k_T^2 \frac{\alpha_s(k_T^2)}{k_T^2} \log\left(\frac{\xi_{\max}\sqrt{s}}{\sqrt{k_T^2}}\right), \end{aligned} \tag{5.51}$$

where $\xi_{\max} = 1 - \frac{M_{\text{rec}}^2}{s}$ (s. (3.128)). Using the one-loop expression for the strong coupling constant

$$\alpha_s(\mu^2) = \frac{1}{b_0 \log\left(\frac{\mu^2}{\Lambda^2}\right)}, \quad b_0 = \frac{11C_A - 4n_f T_R}{12\pi}, \tag{5.52}$$

the analytical solution of the integral in (5.51) is given by

$$-\log\Delta_U(p_T^2) = \frac{\pi N}{b_0}\theta\left(\xi_{\max}-\frac{p_T^2}{s}\right)\left[\log\frac{\xi_{\max}^2 s}{\Lambda^2}\log\left(\frac{\log\frac{\xi_{\max}^2 s}{\Lambda^2}}{\log\frac{p_T^2}{\Lambda^2}}\right)-\log\frac{\xi_{\max}^2 s}{p_T^2}\right], \quad (5.53)$$

where the θ-function reflects an upper bound for p_T and we have to introduce a lower bound $p_T^{\min} > \Lambda$. We use this Sudakov form factor in the veto method to generate a value for p_T. For a given p_T, we generate the variables ξ, y, ϕ according to a distribution

$$p(\xi, y, \phi) = \frac{1}{A}N\frac{\alpha_s(k_T^2)}{\xi(1-y)}\delta(k_T^2 - p_T^2), \quad (5.54)$$

where A is a normalization factor. We start by generating a value for ξ. Therefore, we integrate over the angular variables and obtain

$$\begin{aligned} p_\xi(\xi) &= \frac{N}{A}\frac{1}{\xi}\int_0^{2\pi}\mathrm{d}\phi\int_0^{s\xi^2}\mathrm{d}k_T^2\,\frac{\alpha_s(k_T^2)}{k_T^2}\delta(k_T^2-p_T^2) \\ &= \frac{2\pi N}{Ab_0}\frac{1}{\log\frac{p_T^2}{\Lambda^2}}\frac{1}{\xi}\theta(s\xi^2-p_T^2). \end{aligned} \quad (5.55)$$

To generate a random ξ according to $p_\xi(\xi)$, we use an inverse transform sampling (s. e.g. [81]). Using $P_\xi(\xi_{\max}) = 1$ for the cumulative distribution function, we find

$$P_\xi(\xi) = \int_0^\xi \mathrm{d}\xi'\, p_\xi(\xi') = \frac{\log\left(\xi\sqrt{\frac{s}{p_T^2}}\right)}{\log\left(\xi_{\max}\sqrt{\frac{s}{p_T^2}}\right)}. \quad (5.56)$$

Therefore, we use $\xi = P_\xi^{-1}(u)$ and find

$$\log\xi = u\left(\log\xi_{\max}-\frac{1}{2}\log\frac{p_T^2}{s}\right)+\frac{1}{2}\log\frac{p_T^2}{s}, \quad (5.57)$$

where u is a uniformly distributed random number in $[0,1]$. We can use

$$p_T^2 = \frac{s}{2}\xi^2(1-y) \quad (5.58)$$

to obtain a value for y and generate ϕ uniformly in $[0, 2\pi]$ because the Sudakov does not depend on ϕ. To summarize the radiation generation, we write down pseudo code for the algorithm:

function GENERATERADIATIONFSR

$p^2 = \xi_{\max}^2 s$
while true **do**
$u = \text{random}(\text{distribution} = \text{uniform in } [0,1])$
$p_T^2 = \text{solve}(\Delta_U(p_T^2) = \Delta_U(p^2)u)$
if $p_T^2 < (p_T^{\min})^2$ **or** no solution for p_T^2 **then**
return generate born like event
end if
$\xi = (5.57)$
$y = (5.58)$
$\phi = \text{random}(\text{distribution} = \text{uniform in } [0, 2\pi])$
$v = \text{random}(\text{distribution} = \text{uniform in } [0,1])$
if $v < \frac{F}{U(\xi,y)}$ **then**
return ξ, y, ϕ
end if
$p^2 = p_T^2$
end while
end function

EW Final-State Radiation

EW final-state radiation is similar to the QCD case described in section 5.5.3. However, we do not use a running coupling constant. Therefore, we have

$$-\log \Delta_U(p_T^2) = \frac{\pi N \alpha}{2} \log^2 \frac{\xi_{\max}^2 s}{p_T^2}. \tag{5.59}$$

We find

$$\Delta_U(p_T^2) = \Delta_U(p^2)u \Leftrightarrow p_T^2 = \xi_{\max}^2 s \exp\left(-\sqrt{\log^2\left(\frac{p^2}{\xi_{\max}^2 s}\right) - \frac{2}{\pi\alpha N}\log u}\right). \tag{5.60}$$

In (5.55) only the normalization constant A changes. Therefore, we can use (5.57) to generate a value for ξ and (5.58) for y. The azimuthal angle ϕ is again distributed uniformly in $[0, 2\pi)$.

Alternative Forms of the Upper Bounding Function

If the angle y between emitter and emitted particle is larger than $\frac{\pi}{2}$, the Jacobian determinant J of $\mathrm{d}\Phi_{\mathrm{rad}}$ (3.109) in the ratio $\frac{SJR}{B}$ in (5.21) can become large because

$$J \propto \left(\frac{1}{2-\xi(1-y)}\right)^2 \tag{5.61}$$

which is singular for $\xi = 1$ and $y = -1$. In the singular case the FKS S function is zero and, therefore, suppresses this limit. However, due to the region $y < 0$, the normalization N for the upper bounding function $U(\xi, y)$ is driven to large values. If we find such a phase-space point while sampling the phase space to obtain a value for the norm N, the event generation will be inefficient because most of the events will be vetoed because $\frac{SJR}{B} \ll U(\xi, y)$. On the other hand, if we find such an event only during event generation we can not apply the veto because $\frac{SJR}{B} > U(\xi, y)$. If these events are rare, we can ignore them because the contribution to the cross section is small. Alternatively, we can include the large part of J into the upper bounding function, i.e.

$$U(\xi, y) = N\frac{\alpha_s(k_T^2)}{\xi(1-y)}\left(\frac{1}{1-\frac{\xi}{2}(1-y)}\right)^2. \tag{5.62}$$

Since we cannot solve the integral in (5.51) analytically, we use another upper bounding function U' with

$$U'(\xi, y) = \frac{N}{\xi^2(1-y)}\left(\frac{1}{1-\frac{\xi}{2}(1-y)}\right)^2 \geq U(\xi, y). \tag{5.63}$$

We can use U' to obtain values for p_T according to the veto algorithm. Once we have a value for p_T, we can go from U' to U by drawing a uniformly distributed random number between 0 and 1 and accepting the event with a probability of

$$p(\xi, y) = \frac{U(\xi, y)}{U'(\xi, y)} = \alpha_s(k_T^2)\xi. \tag{5.64}$$

The Sudakov form factor using U' is given by

$$
\begin{aligned}
-\log \Delta_{U'}(p_T^2) &= \int_{p_T^2}^{s\xi_{\max}^2} \mathrm{d}k_T^2 \int_{\underline{\xi}(k_T^2)}^{\xi_{\max}} \mathrm{d}\xi \, \frac{1}{k_T^2} \left(\frac{1}{\xi - \frac{k_T^2}{s}} \right)^2 && (5.65)\\
&= -\frac{2}{\xi_{\max}} + \frac{2}{p} + 2\log\frac{\xi_{\max}}{1-\xi_{\max}} + 2\log\frac{1-p}{p} && (5.66)\\
&\quad - \frac{1}{\xi_{\max}} \left[\log\frac{\xi_{\max}}{1-\xi_{\max}} + \log\left(\frac{\xi_{\max}}{p^2} - 1 \right) \right], && (5.67)
\end{aligned}
$$

where $\underline{\xi}(k_T^2) = \sqrt{\frac{k_T^2}{s}}$ and $p = \sqrt{\frac{p_T^2}{s}}$ (compare to [67, (C.10)]).

QCD Initial-State Radiation

We use a similar upper bounding function as in the final-state radiation case. We choose

$$
U(\xi, y) = N \frac{\alpha_s(k_T^2)}{\xi(1-y^2)} \tag{5.68}
$$

as upper bounding function and

$$
k_T^2 = \frac{s}{4}\xi^2(1-y^2) = \frac{s_b}{4(1-\xi)}\xi^2(1-y^2). \tag{5.69}
$$

The POWHEG Sudakov (5.51) contains pdf ratios for ISR. In [82] it is shown that we can nevertheless use (5.68) as upper bounding function. As mentioned in [47, section 7.4], it is possible that U is not a bounding function for extreme values of x_1 or x_2. If those phase-space regions give only a tiny contributions to the total cross section, we can introduce a technical cut-off. From (3.55), we know that

$$
\frac{s_b}{s} = 1 - \xi, \;\; s < S, \tag{5.70}
$$

where S is the center-of-mass energy of the proton system. This condition defines an upper bound for ξ, i.e.

$$
\xi < \xi_{\max} = 1 - \frac{s_b}{S} < 1. \tag{5.71}
$$

We, therefore, have

$$
\begin{aligned}
-\log \Delta_U(p_T^2) &= \int_0^{\xi_{\max}} \mathrm{d}\xi \int_{-1}^{1} \mathrm{d}y \int_0^{2\pi} \mathrm{d}\phi \, N \frac{\alpha_s(k_T^2)}{\xi(1-y^2)} \theta(k_T^2 - p_T^2) \\
&= 2 \int_0^{\xi_{\max}} \mathrm{d}\xi \int_0^{1} \mathrm{d}y \int_0^{2\pi} \mathrm{d}\phi \, N \frac{\alpha_s(k_T^2)}{\xi(1-y^2)} \theta(k_T^2 - p_T^2),
\end{aligned} \tag{5.72}
$$

where we used that the integrand is even with respect to y. Since $y > 0$, we can change the integration variable to k_T^2 using

$$y = \sqrt{1 - 4\frac{1-\xi}{\xi^2}\frac{k_T^2}{s_b}}. \tag{5.73}$$

The Sudakov form factor is then given by

$$-\log \Delta_U(p_T^2) = 2\pi N \int_0^{\xi_{\max}} \mathrm{d}\xi \int_{p_T^2}^{\bar{k}_T^2} \mathrm{d}k_T^2 \, \frac{1}{\xi} \frac{\alpha_s(k_T^2)}{k_T^2} \left(1 - 4\frac{1-\xi}{\xi^2}\frac{k_T^2}{s_b}\right)^{-\frac{1}{2}}, \tag{5.74}$$

where

$$\bar{k}_T^2 = \frac{s_b}{4}\frac{\xi^2}{1-\xi}. \tag{5.75}$$

We swap the order of integration and perform the ξ integration

$$\begin{aligned} -\log \Delta_U(p_T^2) &= 2\pi N \int_{p_T^2}^{\tilde{k}_T^2} \mathrm{d}k_T^2 \, \frac{\alpha_s(k_T^2)}{k_T^2} \int_{\xi_1}^{\xi_{\max}} \mathrm{d}\xi \, \frac{1}{\sqrt{(\xi-\xi_1)(\xi-\xi_2)}} \\ &= 2\pi N \int_{p_T^2}^{\tilde{k}_T^2} \mathrm{d}k_T^2 \, \frac{\alpha_s(k_T^2)}{k_T^2} I(k_T^2), \end{aligned} \tag{5.76}$$

where

$$\xi_{1/2} = -\frac{2k_T^2}{s_b} \pm \frac{2k_T}{\sqrt{s_b}}\sqrt{1 + \frac{k_T^2}{s_b}}, \tag{5.77}$$

$$\tilde{k}_T^2 = \frac{s_b}{4}\frac{\xi_{\max}^2}{1-\xi_{\max}}. \tag{5.78}$$

The integral $I(k_T^2)$ is given by

$$I(k_T^2) = 2\log\left(\sqrt{\xi_{\max}-\xi_1} + \sqrt{\xi_{\max}-\xi_2}\right) - \log\left(\xi_1 - \xi_2\right). \tag{5.79}$$

Using

$$\begin{aligned} \log\left(\xi_1 - \xi_2\right) &= \log\left(\xi_{\max} - \xi_2 - \xi_{\max} + \xi_1\right) \\ &= \log\left[\left(\sqrt{\xi_{\max}-\xi_2} + \sqrt{\xi_{\max}-\xi_1}\right)\left(\sqrt{\xi_{\max}-\xi_2} - \sqrt{\xi_{\max}-\xi_1}\right)\right] \end{aligned} \tag{5.80}$$

we can write

$$I(k_T^2) = \log\frac{\sqrt{\xi_{\max}-\xi_2} + \sqrt{\xi_{\max}-\xi_1}}{\sqrt{\xi_{\max}-\xi_2} - \sqrt{\xi_{\max}-\xi_1}}. \tag{5.81}$$

The integral in (5.76) has a complicated form. However, Δ_U has the form of a Sudakov form factor with one integration. Therefore, we can find an upper bounding function for the integrand and use the veto method again. We notice that

$$\begin{aligned}\log(\xi_1 - \xi_2) &= \log\left[(1-\xi_2) - (1-\xi_1)\right] \\ &= \log\left(\sqrt{1-\xi_2} - \sqrt{1-\xi_1}\right) + \log\left(\sqrt{1-\xi_2} + \sqrt{1-\xi_1}\right)\end{aligned} \tag{5.82}$$

and

$$\log\left(\sqrt{\xi_{\max} - \xi_1} + \sqrt{\xi_{\max} - \xi_2}\right) \leq \log\left(\sqrt{1-\xi_1} + \sqrt{1-\xi_2}\right). \tag{5.83}$$

Hence, we find an upper bounding function

$$I(k_T^2) \leq \log \frac{\sqrt{1-\xi_2} + \sqrt{1-\xi_1}}{\sqrt{1-\xi_2} - \sqrt{1-\xi_1}} = \frac{1}{2}\log\frac{k_T^2 + s_b}{k_T^2} \leq \frac{1}{2}\log\frac{\tilde{k}_T^2 + s_b}{k_T^2} = \bar{I}(k_T^2). \tag{5.84}$$

The Sudakov form factor for the upper bounding function $\bar{I}(k_T^2)$ is then given by

$$\begin{aligned}-\log\overline{\Delta}_U(p_T^2) &= 2\pi N \int_{p_T^2}^{\tilde{k}_T^2} \mathrm{d}k_T^2 \, \frac{\alpha_s(k_T^2)}{k_T^2}\bar{I}(k_T^2) \\ &= -\frac{\pi N}{b_0}\left[\log\left(\log\frac{\Lambda^2}{k_T^2}\right)\log\frac{\Lambda^2}{\tilde{k}_T^2 + s_b} - \log k_T^2\right]\Bigg|_{k_T^2 = p_T^2}^{\tilde{k}_T^2} \\ &= \frac{\pi N}{b_0}\left[\log\frac{\tilde{k}_T^2 + s_b}{\Lambda^2}\log\frac{\log\frac{\tilde{k}_T^2}{\Lambda^2}}{\log\frac{p_T^2}{\Lambda^2}} - \log\frac{\tilde{k}_T^2}{p_T^2}\right].\end{aligned} \tag{5.85}$$

Again, we have to introduce a lower limit $p_{T,\min}^2 > \Lambda^2$ to ensure that the Sudakov form factor is well defined. We use the veto algorithm to generate a value for p_T.

function GENERATEPT2($p_{T,\max}^2$)
  $p^2 = p_{T,\max}^2$
  while true **do**
    u = random(distribution = uniform in $[0,1]$)
    p_T^2 = solve($\overline{\Delta}_U(p_T^2) = \overline{\Delta}_U(p^2)u$)
    if $p_T^2 < p_{T,\min}^2$ **or** no solution exists **then**
      return
    end if
    v = random(distribution = uniform in $[0,1]$)
    if $v < \frac{I(p_T^2)}{\bar{I}(p_T^2)}$ **then**
      return p_T^2
    end if

$p^2 = p_T^2$
end while
end function

The log of logs in (5.85) can become large when p_T^2 is small because $\tilde{k}_T^2$ is usually a large number. This can lead to numerical problems when we use (5.85) as argument of the exponential function because we obtain numbers which are so small that they cannot be represented as floating point numbers. To circumvent this problem, we have to transform the equation which we have to solve in such a way that we do not need to evaluate an exponential function. This leads to

$$\overline{\Delta}_U(p_T^2) = \overline{\Delta}_U(p^2)u \Leftrightarrow \frac{\pi N}{b_0}\left[\log\frac{\tilde{k}_T^2 + s_b}{\Lambda^2}\log\frac{\log\frac{p_T^2}{\Lambda^2}}{\log\frac{p^2}{\Lambda^2}} + \log\frac{p^2}{p_T^2}\right] = \log u \tag{5.86}$$

Since $p_T^2 \in [p_{T,\min}^2, p^2]$, we do not get numerical problems as long as

$$\frac{p_{T,\min}^2}{\Lambda^2} \gtrsim 2. \tag{5.87}$$

For a given p_T, we generate ξ, y, ϕ which are distributed according to

$$p(\xi, y, \phi) = \frac{N}{A}\frac{\alpha_s(k_T^2)}{\xi(1-y^2)}\delta(k_T^2 - p_T^2), \tag{5.88}$$

where A is a normalization constant. We use the inversion method [81] to generate a value for ξ. The cumulative distribution function with respect to ξ is given by

$$P_\xi(\xi) = \frac{\log f(\xi) - \log f(\xi_{\min})}{\log f(\xi_{\max}) - \log f(\xi_{\min})}, \tag{5.89}$$

where

$$f(\xi) = \sqrt{\frac{4p_T^2}{s_b}(\xi - 1) + \xi^2} + \frac{2p_T^2}{s_b} + \xi \tag{5.90}$$

and

$$\xi_{\min} = \xi_1 = -\frac{2p_T^2}{s_b} + \sqrt{\frac{4p_T^2}{s_b}\left(1 + \frac{p_T^2}{s_b}\right)} \leq \xi_{\max}, \tag{5.91}$$

$$f(\xi_{\min}) = 2\sqrt{\frac{p_T^2}{s_b}\left(1 + \frac{p_T^2}{s_b}\right)}. \tag{5.92}$$

Solving $P_\xi(\xi) = u$, where u is uniformly distributed random number in $[0, 1]$, we obtain

$$\xi = \frac{\frac{4p_T^2}{s_b} + \left(F - \frac{2p_T^2}{s_b}\right)^2}{2F}, \tag{5.93}$$

where

$$F = \exp\left(u \log \frac{f(\xi_{\max})}{f(\xi_{\min})}\right) f(\xi_{\min}). \tag{5.94}$$

Using p_T^2 and ξ we find

$$|y| = \sqrt{1 - 4\frac{1-\xi}{\xi^2}\frac{p_T^2}{s_b}} \tag{5.95}$$

and ϕ is distributed uniformly in $[0, 2\pi)$. The algorithm to generate the radiation variables is

function GENERATERADIATIONISR
  $p^2 = \tilde{k}_T^2$
  while true **do**
    $p_T^2 =$ GENERATEPT2(p^2)
    if no p_T^2 **then**
      return generate born like event
    end if
    $\xi =$ (5.93)
    $y =$ (5.95)
    $\phi =$ random(distribution = uniform in $[0, 2\pi]$)
    $u =$ random(distribution = uniform in $[0, 1]$)
    if $u < \frac{1}{2}$ **then**
      $y = -y$
    end if
    $v =$ random(distribution = uniform in $[0, 1]$)
    if $v \leq \frac{F}{U(\xi,y)}$ **then**
      return ξ, y, ϕ
    end if
    $p^2 = p_T^2$
  end while
end function

EW Initial-State Radiation

The difference to the QCD case described in section 5.5.3 is the coupling constant. The Sudakov is given by (cf. (5.85))

$$\begin{aligned} -\log \overline{\Delta}_U(p_T^2) &= 2\pi N \int_{p_T^2}^{\tilde{k}_T^2} \mathrm{d}k_T^2 \, \frac{\alpha}{k_T^2} \bar{I}(k_T^2) \\ &= \frac{\pi \alpha N}{2} \left(\log^2 \frac{p_T^2}{\tilde{k}_T^2 + s_b} - \log^2 \frac{\tilde{k}_T^2}{\tilde{k}_T^2 + s_b} \right). \end{aligned} \tag{5.96}$$

We find,

$$\overline{\Delta}_U(p_T^2) = \overline{\Delta}_U(p^2)u \Leftrightarrow p_T^2 = (\tilde{k}_T^2 + s_b) \exp\left(-\sqrt{\log^2 \frac{p^2}{\tilde{k}_T^2 + s_b} - \frac{2}{\pi \alpha N} \log u} \right). \tag{5.97}$$

5.5.4. Implementation

We implemented the POWHEG method in a C++ library. This library is similar to the POWHEGBOX [67] framework but completely independent. Therefore, it can be used to do a thorough check of the POWHEGBOX. The source code of the library is available at `https://github.com/lmcoy/mypowheg`.

To use the library for a specific process, the user has to specify a list of all born processes. For each born flavor configuration, the user has to attach all possible real flavor configurations and their singular regions. Note, that a real process can be connected to more than one underlying born process. An example is the W + jet process described in chapter 8. For each born and real flavor configuration, the user has to implement the matrix elements in four dimensions. Also the virtual part in dim. reg. or mass regularization has to be implemented. Furthermore, a born phase-space generator is needed. For born matrix elements that are divergent in certain limits, one also has to implement cuts on the born phase space that render the LO cross section finite. An example is the neutral current Drell-Yan process that is divergent at $Q^2 = 0$ due to the photon exchange (s. chapter 6). In summary, the user has to implement:

- matrix elements (born, color correlated born, real, virtual),
- a born phase space generator and cuts,
- a list of all subprocesses and their singular regions.

An overview of the user interface is given in Appendix I.

When a process is implemented, the resulting program starts by integrating $\tilde{B}$ over the full phase space. The result is the NLO cross section of the process if no cuts are

applied. We use VEGAS to perform the integration and store the grid to use it in the event generation (s. Appendix D). This integration is also used to obtain values for $\tilde{B}^{\max}$ and V_{est}. With these values at hand, we can start the actual event generation. All unweighted events are written to an LHE event file [83, 84].

In the following, we describe how LHE event files are generated with our implementation. The particle flavors and momenta are directly available from the POWHEG method. The parent-child structure of an event is determined by the FKS radiation region. However, we have to include information about the color flow and resonances in the event file. It is necessary to give the resonance structure to the parton shower because it should preserve the resonance mass. Since the resonance structure is not available in POWHEG, the user has to supply which leading order particles originate from a resonance decay. At NLO a particle can be radiated from a decay product of a resonance. This particle has to be included in the decay products of the resonance. Whether a particle was radiated from a resonance daughter, is determined by the radiation region.

Furthermore, the color flow has to be included. We use that the LO color flow is unique for Drell-Yan and W + jet. Therefore, the user can specify the LO color flow. However, the NLO color flow is not unique for W + jet but we can generate it by starting from the LO color flow and using the singular FKS regions. The radiation region determines the mother particle and its color flow configuration is given by the LO color flow. Therefore, we can extend the color flow by the color flow of the splitting. However, this procedure has ambiguities. First, the FKS initial-state regions S_i do not specify which initial-state particle is the emitter. We use the radiation variable y to choose an emitter, i.e. we use the particle which is more collinear to the radiated particle as mother particle. Second, the color flow of the FSR splitting $g \to gg$ is not unique. Hence, we choose the color flow randomly in this case.

All particles are now fully specified and can be written into an LHE event file. However, we have to notify the parton shower that the first radiation is already included in the POWHEG events, i.e. the parton shower has to start its evolution at the POWHEG radiation scale. The starting scale for the parton shower is specified event by event in the `SCALUP` variable of the LHE format. Therefore, we have to store the radiation k_T for every event in this variable.

5.5.5. Matching a Parton Shower to POWHEG Events

Since the POWHEG method is independent of the parton shower, we can use any p_T-ordered parton-shower program. To study phenomenological effects, we use PYTHIA 8 [73] as an example for a parton shower. PYTHIA 8 can use LHE event files as input and

it generates QCD and QED radiation. Results for Drell-Yan are shown in the following sections. In the following, we comment on important flags for parton shower matching with PYTHIA 8.

POWHEG and PYTHIA 8 use p_T related evolution scales. However, the exact definition of the evolution scales differs. The simplest matching solution

```
TimeShower:pTmaxMatch   =  1
SpaceShower:pTmaxMatch  =  1
```

assumes that the evolution scales are the same and starts the shower evolution at the POWHEG scale. Therefore, some phase-space regions can be double counted and some other regions are maybe not counted at all. Furthermore, it is important to use the flag

```
Beams:strictLHEFscale  =  on
```

because PYTHIA 8 would ignore the POWHEG `SCALUP` scale in resonance decays and use the kinematic limit if this flag is not set. Setting this flag is equivalent to implementing the PYTHIA function `UserHooks::scaleResonance` as recommended in [85].

To overcome the issue with different evolution scales, a PYTHIA 8 plug-in `PowHegHook` [86] exists that starts the shower evolution at the kinematic limit and vetoes all emissions with a POWHEG evolution scale above the scale of the hardest POWHEG emission. This is possible because the POWHEG and PYTHIA 8 evolution scales are similar. Otherwise, a truncated shower would be necessary [78].

In order to use the `PowHegHook` plug-in in presence of resonance decays, we have to modify the code. The default `PowHegHook` does not apply any veto in resonance decays. Hence, we have to modify the code such that vetoing is done in resonance decays. Furthermore, `PowHegHook` has to calculate the POWHEG evolution scale after each radiation and veto the radiation if the scale is larger than the POWHEG radiation scale `SCALUP`. For ISR the POWHEG evolution scale is simply the transverse momentum of the emitted particle. For FSR the POWHEG evolution scale is based on the transverse momentum in the soft-collinear limit (5.50). Therefore, the POWHEG evolution scale for FSR is given by

$$k_T^2 = (p_i + p_j)^2 \frac{E_i}{E_j}, \tag{5.98}$$

where the index i denotes the radiated particle and j the emitter after radiation. The explicit changes in the code can be found in the POWHEGBOX implementation of the neutral-current Drell-Yan process [51].

We use the following settings for the `PowHegHook`:

```
POWHEG:nFinal           =  1
POWHEG:pTdef            =  1
POWHEG:QEDveto          =  1
POWHEG:veto             =  1
POWHEG:vetoCount        =  10
TimeShower:pTmaxMatch   =  2
SpaceShower:pTmaxMatch  =  2
Beams:strictLHEFscale   =  off
```

Furthermore, we use

```
HadronLevel:all  =  off
PartonLevel:MPI  =  off
```

to disable hadronization and multi-parton interactions because we are only interested in parton shower matching effects. To be consistent with our POWHEG implementation for EW corrections, we disable the running of the electromagnetic coupling, i.e.

```
TimeShower:alphaEMorder   =  0
SpaceShower:alphaEMorder  =  0.
```

6. Neutral-Current Drell-Yan

The neutral-current Drell-Yan process $pp \to Z/\gamma \to \mu^+\mu^-$ is a standard candle at the LHC. It can be used to extract pdf information and for precision measurements of the weak mixing angle. It can also play an important role in searches for BSM physics because new heavy gauge bosons Z' could show up as peaks in the invariant mass distribution of the leptons.

For all experimental analyses, it is crucial to have precise theoretical predictions. The Drell-Yan process is one of the simplest processes at a hadron collider because of the clean leptonic final state and QCD radiation can only originate from the initial-state partons. Hence, the Drell-Yan process is known up to NNLO for QCD and NLO for EW radiation. References are given in chapter 1.

In this chapter we apply the POWHEG method described in the previous chapter to the neutral-current Drell-Yan process. In particular, we use the POWHEG method to combine QCD and EW corrections. We published the results of this chapter also in reference [57].

The born matrix element consists of two Feynman diagrams, corresponding to photon and Z-boson exchange. The virtual part of the partonic cross section for QCD [17] results in the virtual 1-loop contribution (3.189), i.e.

$$\mathcal{V} = \frac{\alpha_s}{2\pi}\mathcal{N}C_F\left[-\frac{2}{\varepsilon^2} - \frac{3}{\varepsilon} - 2\log\frac{Q^2}{s}\frac{1}{\varepsilon} - 3\log\frac{Q^2}{s} - \log^2\frac{Q^2}{s} - 8 + \pi^2\right]\mathcal{B}, \tag{6.1}$$

where we used the same normalization $\mathcal{N} = \left(\frac{4\pi\mu^2}{Q^2}\right)^{\varepsilon}\frac{1}{\Gamma(1-\varepsilon)}$ as in (3.169). The finite part is also calculated in Appendix B. Note that Q is an arbitrary scale that we will identify with the renormalization scale.

Feynman diagrams for real radiation are shown in Figure 6.1. The real process contains gluon radiation from the initial-state quarks and also an initial-state gluon splitting into a quark-antiquark pair. In an FKS implementation, we need the color correlated born amplitude to calculate the soft limit in (3.39) and (3.105). The color correlated born matrix element is particularly simple for Drell-Yan because only the initial-state partons have color charge. We find a global color factor $C_F N_C$ for all real processes, i.e. the

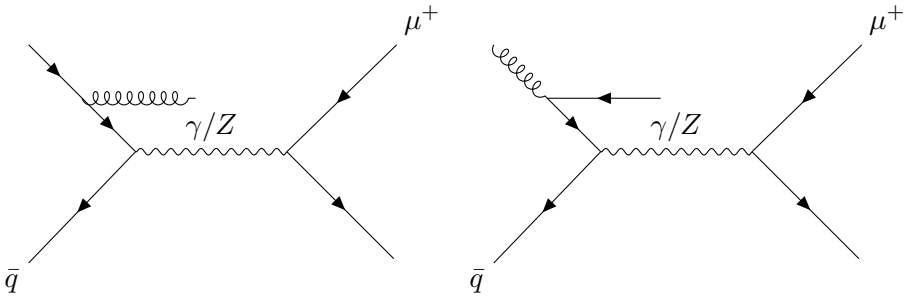

Figure 6.1.: Feynman diagrams that contribute to the real matrix elements of the neutral current Drell-Yan process.

non-zero color correlated born matrix elements read

$$\mathcal{B}_{12} = \mathcal{B}_{21} = C_F \mathcal{B}. \tag{6.2}$$

Using (6.2), we can show that the poles in (6.1) cancel with the real poles in the FKS calculation (3.170).

The structure of the FKS subtraction scheme for QCD is particularly simple because the QCD radiation can only be emitted from the initial-state partons. If the radiated parton is a gluon (left in Figure 6.1), the gluon can arise from the initial-state quark or the antiquark. If an initial-state gluon splits into a quark-antiquark pair (right in Figure 6.1), the quark/antiquark enters into the Z/γ vertex and the antiquark/quark is the radiated real parton. The underlying born process of all real matrix elements is unique. Therefore, there is only one singular region for the initial-state radiation. The corresponding S function is equal to 1 by construction.

We used the implementation of the POWHEG method described in section 5.5.4 to implement the Drell-Yan process. The real matrix elements are generated by the C++ output interface of MadGraph [87, 88]. When the flavor configurations are passed to our library, one always starts with a born process. We consider here the $\bar{u}u \to \mu^+\mu^-$ Drell-Yan sub process as an example. We have to connect the real process $\bar{u}u \to \mu^+\mu^- g$ to the born process and associate the singular region S_5 to it (s. chapter 3). The code automatically detects that the gluon can originate from both initial-state quarks and adds the collinear remnants. Moreover, we have to add the real processes $gu \to \mu^+\mu^- u$ and $\bar{u}g \to \mu^+\mu^-\bar{u}$. Both have the same singular region S_5. The interface of our POWHEG implementation is discussed in Appendix I.

The structure of the EW corrections is more complicated because also the final-state leptons can radiate photons. In fact, the final-state radiation is dominant. Due to the

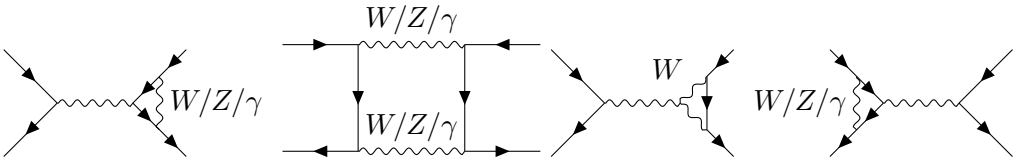

Figure 6.2.: Example Feynman diagrams for EW virtual corrections.

more complex singularity structure, we have to introduce three FKS S functions to separate the singular regions. As for QCD we have one singular region S_5 for initial-state radiation and additionally the regions S_{54} and S_{53} for final-state radiation. Also the matrix elements are more complex. The real radiation matrix elements are generated with MadGraph and the virtual corrections are checked against reference [89]. The virtual corrections contain loops with gauge bosons that become singular for on-shell gauge bosons. A few example Feynman diagrams are shown in Figure 6.2. The treatment of these singularities is described in section 6.1. EW corrections are usually calculated with mass regularization. Using the results from chapter 4, we checked that we get the same result for the FKS endpoint plus virtual part in dim. reg. and mass regularization. Furthermore, we used implementations for the virtual amplitudes within dim. reg. and mass regularization [90].

6.1. Details of the Calculation

In this section we comment on technical aspects of the the matrix element calculations and the implementation of the process.

6.1.1. Complex-Mass Scheme

The propagator of a Z-boson is singular at $q^2 = M^2$, where q is the momentum of the Z-boson and M is its mass. One way to include the Z-boson resonance and capture its physics is to do a Dyson resummation of the self-energy, i.e. we use a geometric series to sum self-energy contributions to all orders, i.e.

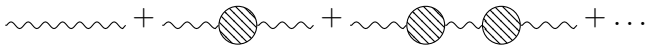

$$= \frac{i}{q^2 - M_0^2 + i\varepsilon} \sum_{n=0}^{\infty} \left(\frac{L}{q^2 - M_0^2 + i\varepsilon} \right) = \frac{i}{q^2 - M_0^2 + i\varepsilon - L}, \quad (6.3)$$

where L denotes the 1PI (1 particle irreducible, s. e.g. [91]) contribution and M_0 is the bare mass. We can use the real part of L to define the renormalized particle mass by the

condition $M^2 - M_0^2 - \mathrm{Re}\, L^2 = 0$. However, the imaginary part cannot be absorbed into the definition of the real particle mass. We find

$$\frac{iZ}{q^2 - M^2 + i\varepsilon - iZ\,\mathrm{Im}\, L}, \tag{6.4}$$

where Z is the wave-function renormalization constant (s. [91, chapter 7]). The squared propagator is proportional to

$$\frac{1}{(q^2 - M^2)^2 + (Z\,\mathrm{Im}\, L(q^2))^2}, \tag{6.5}$$

i.e. the squared matrix element is not divergent at $q^2 = M^2$ anymore. The optical theorem (see e.g. [91]) implies for the Z-boson self-energy that $M\Gamma = -Z\,\mathrm{Im}\, L(M^2)$, where Γ is the total width. Hence, the squared matrix element is proportional to a Breit-Wigner propagator

$$\frac{1}{(q^2 - M^2)^2 + M^2\Gamma^2} \tag{6.6}$$

that is not singular at $q^2 = M^2$ but enhanced. However, we mix different orders in perturbation theory by resumming the loops and this possibly spoils gauge invariance [92, 93]. The *complex-mass scheme* [94–96] is a consistent and universal scheme to handle the finite width effects. It introduces complex gauge-boson masses at the level of the Lagrangian, i.e.

$$\mu_V^2 = M_V^2 - iM_V\Gamma_V. \tag{6.7}$$

This also leads to a complex Weinberg-angle

$$\cos^2\theta_w = \frac{\mu_W^2}{\mu_V^2}. \tag{6.8}$$

The complex-mass scheme is used in the calculation of all matrix elements. The complex-mass scheme preserves the Ward-Identities.

6.1.2. Massless Fermion Approximation

The matrix elements are calculated in the massless limit because the masses are negligible compared to typical energies at the LHC. In particular, the real matrix element and the real phase space are generated under the assumption that quarks and leptons are massless. Using massless leptons introduces artificial collinear singularities that would be cut off by the physical lepton masses. The collinear singularities lead to an unphysical enhancement of collinear photon radiation. These contributions are canceled due to the

KLN theorem [60, 61] if collinear photons are treated fully inclusively. When we perform a fixed-order NLO calculation, the requirements of the KLN theorem are not fully met due to phase-space cuts on the lepton momenta. We would obtain corrections of the order $\alpha \log(m_f)$, where m_f is the fermion mass in a massive calculation [97]. To obtain an IR safe fixed-order NLO cross section, we introduce a *recombination* of collinear photons with leptons. We introduce the quantity

$$\Delta R^2 = \Delta\eta^2 + \Delta\phi^2, \tag{6.9}$$

where $\Delta\eta$ is the rapidity difference between a lepton and a photon and $\Delta\phi$ is the difference of their azimuthal angles. If ΔR for a photon-lepton pair is smaller than a given threshold (e.g. $\Delta R < 0.1$), the photon and the lepton will be combined. The smaller ΔR the more collinear a resolved photon can become. In this way all unphysical collinear photons are *recombined* with leptons.

When we generate POWHEG events, we do not encounter very collinear photon radiation because we use an inclusive NLO weight $\bar{B}$ and the radiation generation for QCD has a lower cut off $k_T^{\min}$ due to the scale Λ_{QCD} and the running coupling constant. In principle, we do not need a cut-off for photon radiation because the Thompson limit of the coupling $\alpha(0)$ is well defined. However, we do not have to generate photon radiation at small k_T because this radiation is in the soft/collinear regime and we do not expect any improvement by the POWHEG method compared to a parton shower. Therefore, it is sensible to use a $k_T^{\min}$ cut-off scale also for EW POWHEG radiation. Furthermore, the hardest QCD radiation has typically k_T values much larger than our default cut-off scale $(k_T^{\min})^2 = 0.8$ GeV^2. We show in section 6.4 the independence of our results of this technical cut off scale. When we combine QCD and EW POWHEG radiation, the hardest radiation is typically of QCD type because the coupling constant is much larger. Therefore, it is unlikely to reach the $k_T^{\min}$ cut-off scale.

The parton shower, however, needs massive particles as input in order to correctly generate the missing soft and collinear radiation. Hence, we use an on-shell projection to introduce the particle masses on the POWHEG event level. In the rest frame of the resonance decay into two muons the four-momentum of the resonance is given by

$$p_m = \begin{pmatrix} 2E \\ \vec{0} \end{pmatrix}, \tag{6.10}$$

where E is the energy of the two massless muons with momentum $\pm\vec{p}$. To obtain massive four-momenta for the muons, we rescale their momenta by a factor λ and find from

energy conservation that

$$\sqrt{m_1^2 + \lambda^2 \vec{p}^2} + \sqrt{m_2^2 + \lambda^2 \vec{p}^2} = 2E. \tag{6.11}$$

Solving this equation for λ^2, we find

$$\lambda^2 = 1 - \frac{m_1^2 + m_2^2}{2E^2} + \frac{(m_1^2 - m_2^2)^2}{16E^4}. \tag{6.12}$$

Therefore, the rescaled four-momenta of the muons read

$$p_{1/2} = \begin{pmatrix} \sqrt{m_{1/2}^2 + \lambda^2 \vec{p}_{1/2}^2} \\ \lambda \vec{p}_{1/2} \end{pmatrix}. \tag{6.13}$$

We use the same rescaling for a resonance decay into two muons and a photon but we solve the energy conservation equation for three particles numerically for λ.

6.1.3. Numerical Integration

We use Monte-Carlo methods to integrate the cross section numerically. A brief overview of Monte-Carlo integration and references are given in Appendix D. We used OpenMPI to adapt the standard VEGAS algorithm such that it can run in parallel. Our implementation can use several CPU cores and can run on multiple computers in a high performance cluster. Since Monte-Carlo integration performs best when the integrand is flat, we transform the integral such that the integrand is nearly flat. The Drell-Yan cross section is proportional to a Breit-Wigner propagator defined in (6.6). We define the quantity

$$\Lambda(s) = \frac{M\Gamma S}{(s - M^2)^2 + M^2\Gamma^2}, \tag{6.14}$$

where M is the Z-boson mass and Γ is its width. The numerator is chosen such that it is convenient in the explicit calculation. The cross section integration can be written as

$$\sigma = \int_0^1 \mathrm{d}x_1 \int_0^1 \mathrm{d}x_2 \int \mathrm{d}\hat{\sigma}(x_1, x_2) = \int_0^1 \mathrm{d}x_1 \int_0^1 \mathrm{d}x_2 \int \mathrm{d}^n y \Lambda(x_1 x_2 S) f(x_1, x_2, \vec{y}), \tag{6.15}$$

where x_1, x_2 are the momentum fractions of the partons, the n particle phase space is defined by the parameters $\vec{y}$ and f is a function containing the rest of the matrix element and the pdfs. We transform the x_1 integral such that the Breit-Wigner is in the direction of an integration variable $\tau = x_1 x_2$. Furthermore, we swap the τ and x_2 integration and use a second transformation to restrict the integration ranges from zero to one. We

obtain,

$$\sigma = \int_0^1 \mathrm{d}\tau \int_0^1 \mathrm{d}z \int \mathrm{d}^n y \frac{1-\tau}{\tau+(1-\tau)z} \Lambda(\tau S) f\left((1-\tau)z+\tau, \frac{\tau}{(1-\tau)z+\tau}, \vec{y}\right). \tag{6.16}$$

Our aim is to find an integral transformation that fulfills the differential equation

$$\frac{\mathrm{d}\tau}{\mathrm{d}t} = \frac{1}{\Lambda(\tau S)} \tag{6.17}$$

because this transformation cancels the Breit-Wigner peak in the integrand. We find

$$\tau(t) = \frac{M\Gamma}{S}\tan(t) + \frac{M^2}{S} \quad \Leftrightarrow \quad t = \arctan\frac{\tau S - M^2}{M\Gamma}. \tag{6.18}$$

Using this integral transformation and rescaling the integration to the unit cube, we obtain

$$\sigma = \int_0^1 \mathrm{d}z \int_0^1 \mathrm{d}u \int \mathrm{d}^n y \frac{1-\tau(t_u)}{x_1(t_u,z)} \Delta f\left(x_1(t_u,z), \frac{\tau(t_u)}{x_1(t_u,z)}, \vec{y}\right), \tag{6.19}$$

where

$$\Delta = \arctan\frac{S-M^2}{M\Gamma} + \arctan\frac{M}{\Gamma}, \tag{6.20}$$

$$t_u = \Delta u - \arctan\frac{M}{\Gamma}, \tag{6.21}$$

$$x_1(t_u,z) = \tau(t_u) + (1-\tau(t_u))z. \tag{6.22}$$

The Breit-Wigner in (6.15) is canceled by the Breit-Wigner in (6.19). Therefore, the new integrand is flat compared to the original integrand and the Monte-Carlo integration converges faster. In practice, we have to cancel the Breit-Wigner numerically because we cannot split the matrix element in our calculation into f and Λ. Hence, we use

$$\mathrm{d}^n y f = \mathrm{d}^n y \frac{1}{\Lambda}(\Lambda f) = \mathrm{d}\hat{\sigma}\frac{1}{\Lambda(\tau(t_u)S)} \tag{6.23}$$

in (6.19). If this method is used, most of the random points are sampled close to the resonance. Therefore, one should be aware of this, if the integrand has other features that are not close to the resonance.

6.2. Parameters and Setup

The gauge boson masses and widths are [98]

$$m_Z = 91.1876 \text{ GeV}, \qquad \Gamma_Z = 2.495 \text{ GeV}, \tag{6.24}$$

$$m_W = 80.385 \text{ GeV}, \qquad \Gamma_W = 2.085 \text{ GeV}. \tag{6.25}$$

We use the Fermi constant, measured in the muon decay,

$$G_F = 1.16637 \times 10^{-5} \text{ GeV}^{-2} \tag{6.26}$$

and the gauge boson masses to define the electromagnetic coupling constant. The coupling, consequently, is defined by the effective coupling of the muon decay. It reads

$$\alpha = \frac{\sqrt{2} G_F M_W^2}{\pi} \left(1 - \frac{M_W^2}{M_Z^2}\right). \tag{6.27}$$

Radiative corrections of the muon decay are already included in the coupling constant. Large universal electroweak corrections (from the running of the coupling etc.) are already incorporated into the LO results when we use the above definition. Hence, the remaining electroweak corrections are minimized. This scheme is called G_μ-scheme. When we transform the usual on-shell renormalization scheme with $\alpha(0)$ in the Thompson limit into the G_μ-scheme at NLO EW, we have to subtract the radiative corrections Δr to muon decay from the vertex counterterm [99, 100], i.e.

$$\delta^{\text{ct}}_{ffV}\Big|_{G_\mu} = \delta^{\text{ct}}_{ffV}\Big|_{\alpha(0)} - \frac{1}{2}\Delta r. \tag{6.28}$$

The coupling constant in the Thompson limit and in the G_μ scheme are connected by

$$\alpha = \alpha(0)(1 + \Delta r) + \mathcal{O}(\alpha^3). \tag{6.29}$$

The quantity Δr contains contributions from the change of $\alpha(0)$ to $\alpha(M_Z)$. These contributions are proportional to logarithms of the light fermion masses ($\alpha(0) \log m_f^2$) that cancel the logarithms from charge renormalization in the $\alpha(0)$-scheme. Contributions from the W-boson self energy with a top-bottom loop are also included in Δr.

We use the following fermion masses as regulator masses in mass regularization, in the on-shell projection of the momenta, and in the running of the strong coupling α_s (s.

section 5.4):

$m_u = 6.983 \times 10^{-2}$ GeV	$m_c = 1.2$ GeV	$m_t = 173.07$ GeV
$m_d = 6.983 \times 10^{-2}$ GeV	$m_s = 0.15$ GeV	$m_b = 4.6$ GeV
$m_e = 0.510998928 \times 10^{-3}$ GeV	$m_\mu = 0.1056583715$ GeV	$m_\tau = 1.77682$ GeV

As pdfs we use the NNPDF 2.3 pdf set. In particular, we use the NLO QCD + LO QED PDF set with $\alpha_s(M_Z) = 0.118$ (ID: 244600) [101–103] interfaced with LHAPDF 6.1.6 [104]. We assume the DIS pdf renormalization scheme for EW corrections (s. (3.194)). The POWHEG events are showered by PYTHIA 8.215 [73] without hadronization and multi-parton interactions because we are interested in the details of the parton-shower matching. We comment on the validity of this assumption in section 6.6. Concerning the PYTHIA parton-shower matching, we use the `PowHegHook` plug-in described in section 5.5.5. Furthermore, we use the PYTHIA internal NNPDF 2.3 QCD+QED NLO pdf set by using

```
PDF:pSet = 15
```

The event selection is done with Rivet 2.4.0 [105].

6.3. NLO Calculation

To validate our implementation, we compare the cross sections for different setups to a fixed-order NLO calculation that uses the Catani-Seymour subtraction scheme [90]. Both implementations use the same virtual matrix elements. When we calculate NLO distributions, we have to use recombination (s. section 6.1.2) and we cut on the real radiation phase space. First, we apply only an invariant mass cut of $m_{ll} > 50$ GeV to render the cross section finite. For EW corrections we set the recombination parameter to $\Delta R = 0.1$. Furthermore, we use a setup (setup2) with the same invariant mass cut and the LHC acceptance cuts $p_T > 20$ GeV and $|\eta| < 2.5$. Since the EW corrections are rather small, we define a third setup (setup3) to enhance corrections. We use the same acceptance cuts as before and increase the invariant mass cut to $m_{ll} > 85$ GeV. The recombination parameter is set to $\Delta R = 0.01$. The EW corrections are larger because we remove all events that are shifted from the Z peak to lower values of m_{ll} by FSR. The lower recombination parameter ΔR leads to more unrecombined photon FSR and enhances the correction at the peak. The results for all setups are shown in Table 6.1. At LO, we find good agreement for all setups. The NLO results agree at the level of 1 per mill but show deviations which are larger than the integration error. The source of these deviations is not resolved so far. There can be many reasons for the deviations, e.g. numerical inaccuracies, underestimated Monte-Carlo errors, technical cut-offs etc.

		setup1	setup2	setup3
		[pb]		
σ_{LO}	POW	1662.49 ± 0.02	759.15 ± 0.02	693.57 ± 0.02
	FO	1662.66 ± 0.07	759.21 ± 0.03	693.59 ± 0.03
$\Delta^{\text{QCD}}_{\text{NLO}}$	POW	227.21 ± 0.02	63.21 ± 0.03	65.34 ± 0.02
	FO	226.56 ± 0.15	62.50 ± 0.10	64.82 ± 0.08
$\Delta^{\text{EW}}_{\text{NLO}}$	POW	-13.35 ± 0.01	-13.73 ± 0.01	-58.19 ± 0.01
	FO	-13.11 ± 0.05	-13.61 ± 0.03	-58.02 ± 0.04
	setup1	$m_{ll} > 50$ GeV, $\Delta R = 0.1$		
	setup2	$m_{ll} > 50$ GeV, $p_T(l) > 20$ GeV, $\lvert\eta\rvert < 2.5$, $\Delta R = 0.1$		
	setup3	$m_{ll} > 85$ GeV, $p_T(l) > 20$ GeV, $\lvert\eta\rvert < 2.5$, $\Delta R = 0.01$		
	$\sqrt{s} = 13$ GeV, NNPDF 2.3 (ID: 244600)			

Table 6.1.: Comparison of the LO cross section and NLO corrections. We compare results from our FKS implementation (POW) with results from a fixed-order NLO calculation (FO) that uses the Catani-Seymour subtraction scheme. Both implementations use the same virtual matrix elements.

It is hard to determine the reason because we cannot compare subsets of the cross sections (e.g. subtracted real emission, virtual plus endpoint) because the calculation in Catani-Seymour and FKS are organized differently. Anyway, the deviations are so small that they are not important for phenomenological studies at the LHC.

6.4. Phenomenology

In this section we investigate the phenomenology of the Drell-Yan process with a muonic final state at the LHC with $\sqrt{s} = 13$ TeV. To render the cross section finite, we have to introduce the cut

$$m_{ll} > 50 \text{ GeV} \tag{6.30}$$

in the generation of POWHEG events, i.e. in $\bar{B}$ (s. section 5.3). This cut is necessary because the photonic Drell-Yan LO cross section is proportional to $1/s$ at small s, where s is the partonic center-of-mass energy. In general, the cuts should be as inclusive as possible because a born event that fails the cuts could pass the cuts after real radiation. Such a case is described in chapter 8 for W + jet production. However, the invariant mass cut does not lead to these problems because ISR does not change the invariant mass of the lepton pair and FSR only reduces it.

	PowhegBox V1	PowhegBox V2	Powheg
	[pb]		
σ_{QCD}	1891.2 ± 1.0	1891.5 ± 0.8	1890.8 ± 0.7
σ_{EW}	–	1661.0 ± 0.4	1663.5 ± 0.6
σ_{QCDxEW}	–	1888.9 ± 0.9	1890.1 ± 0.8
	setup: $m_{ll} > 50$ GeV		

Table 6.2.: NLO cross sections for $\sqrt{s} = 13$ TeV and $m_{ll} > 50$ GeV. These values are obtained from Powheg event generation.

The pure QCD Powheg corrections are implemented in version 1 (V1) [48] and version 2 (V2) [51] of the PowhegBox. EW corrections are only implemented in V2. A comparison of PowhegBox cross sections with cross section obtained with our Powheg implementation in Table 6.2 shows good agreement.

We apply the phase-space cuts

$$p_T > 20 \text{ GeV}, \tag{6.31}$$

$$|\eta| < 2.5 \tag{6.32}$$

to the muon momenta after showering with Pythia. These cuts are supposed to mimic the acceptance cuts of ATLAS and CMS. We use the Pythia settings from section 5.5.5. In the following, we compare distributions obtained with our implementation with results from the PowhegBox.

The main feature of the m_{ll} distribution is the resonance peak at M_Z due to the s-channel Z boson. In the following sections, we describe how the peak is changed due to NLO corrections.

6.4.1. QCD Corrections

Since only initial-state radiation is present at NLO QCD, the real radiation does not change the shape of the m_{ll} distribution. We use a fixed scale $\mu = \mu_F = M_Z$. Since we are interested in QCD corrections only in this section, we switch off the Pythia QED shower by using the following flags:

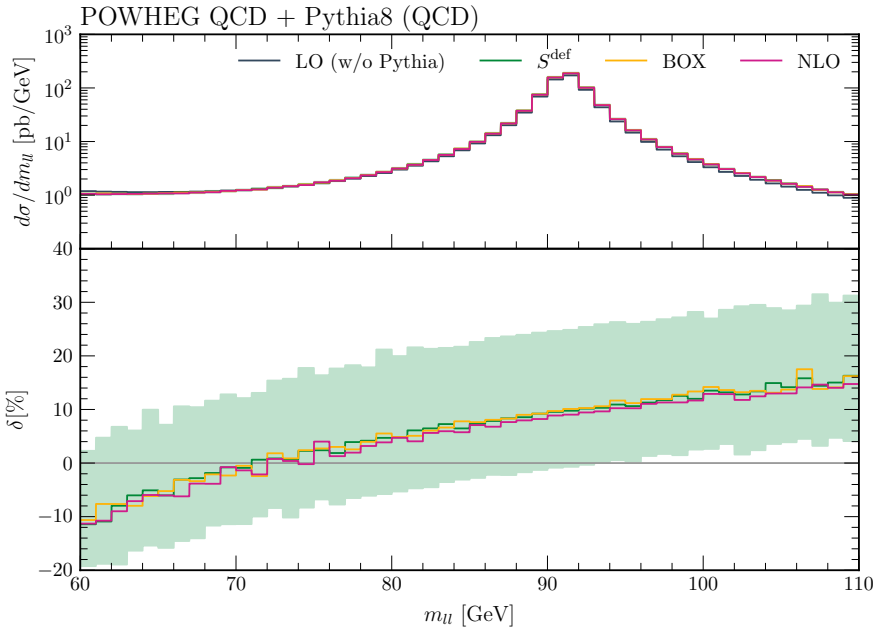

Figure 6.3.: Invariant mass spectrum of the muons. The results obtained with our implementation (labeled by S^{def}) are compared to PowhegBox events (labeled by BOX) and fixed-order NLO results. Concerning Pythia, we only apply the QCD parton shower. The lower panel shows the relative corrections with respect to LO in percent. The shaded band shows the scale variation for 2μ and $\mu/2$.

```
SpaceShower:QEDshowerByL      =  off
SpaceShower:QEDshowerByQ      =  off
TimeShower:QEDshowerByGamma   =  off
TimeShower:QEDshowerByL       =  off
TimeShower:QEDshowerByQ       =  off
```

The distribution m_{ll} is shown in Figure 6.3. We find good agreement between our Powheg implementation (labeled by S^{def}), the PowhegBox (version 2) and the fixed-order NLO calculation [90] in the whole range of the m_{ll} distribution. The shaded band in Figure 6.3 corresponds to a scale variation in the range $M_Z/2 < \mu = \mu_F < 2M_Z$, i.e. the scale variation leads to a constant shift in the resonance region. In particular, there is no feature in the distributions.

In contrast to the invariant mass, the additional radiation has a large effect on the muon transverse momentum $p_T(\mu)$ because the muon system recoils against the additional jet. In fact, the Z-boson and the muons can be highly boosted when a hard jet is radiated from the initial-state partons. Figure 6.4 shows that the muon transverse momentum

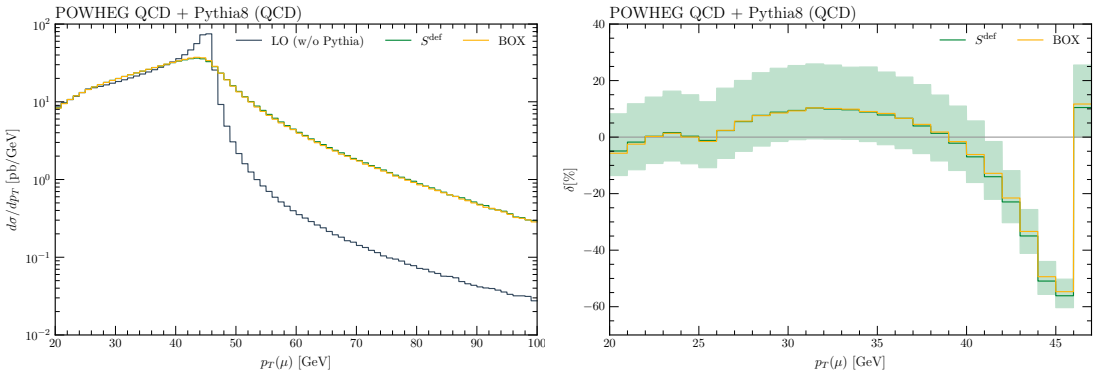

(a) Transverse momentum distribution of the muon.

(b) Relative corrections with respect to the LO (w/o Pythia) result. The shaded area corresponds to scale variation in the range $M_Z/2 < \mu = \mu_F < 2M_Z$.

Figure 6.4.: Muon p_T for the leading order process without Pythia and the matched Powheg NLO process. The results obtained with our Powheg implementation are labeled by S^{def}. For comparison we also show PowhegBox results labeled by BOX. Concerning Pythia, we only consider the QCD parton shower.

$p_T(\mu)$ is washed out due to the additional gluon radiation, i.e. the Jacobian peak is washed out. At LO the muon system has no transverse momentum because the muons recoil against each other. At NLO the muon system recoils against the radiated parton and, therefore, its transverse momentum $p_T(Z)$ is equivalent to the radiation p_T. Large values of $p_T(Z)$ are best described by the NLO matrix element. At small $p_T(Z)$ the distribution is not described by the matrix element because the real matrix element is divergent in this region. The leading soft and collinear logarithms, that make the NLO matrix element divergent, are resummed to all orders by the parton shower. Therefore, we obtain finite cross section results in the region of small $p_T(Z)$ when we use a parton shower. Figure 6.5 shows that the cross section is finite in the small $p_T(Z)$ region if we use a parton shower or Powheg. For large $p_T(Z)$ the parton shower underestimates the cross section because it is based on soft and collinear radiation only.

6.4.2. Electroweak Corrections

The electroweak corrections induce larger corrections to the m_{ll} shape than the QCD corrections although the electromagnetic coupling is much smaller than the strong coupling α_s. Photon radiation leads to larger effects because photons can also be radiated

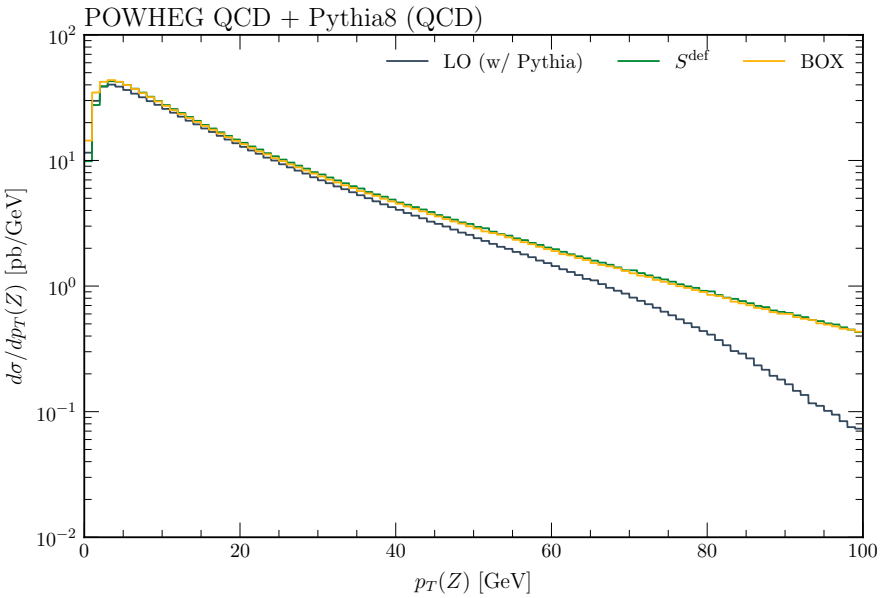

Figure 6.5.: Transverse momentum of the $Z \to \mu^+\mu^-$ system recoiling against the radiated jet for the leading order process with parton shower and the matched POWHEG NLO process. The results obtained with our POWHEG implementation are labeled by S^{def}. For comparison we also show POWHEGBOX results labeled by BOX. Concerning PYTHIA, we only consider the QCD parton shower.

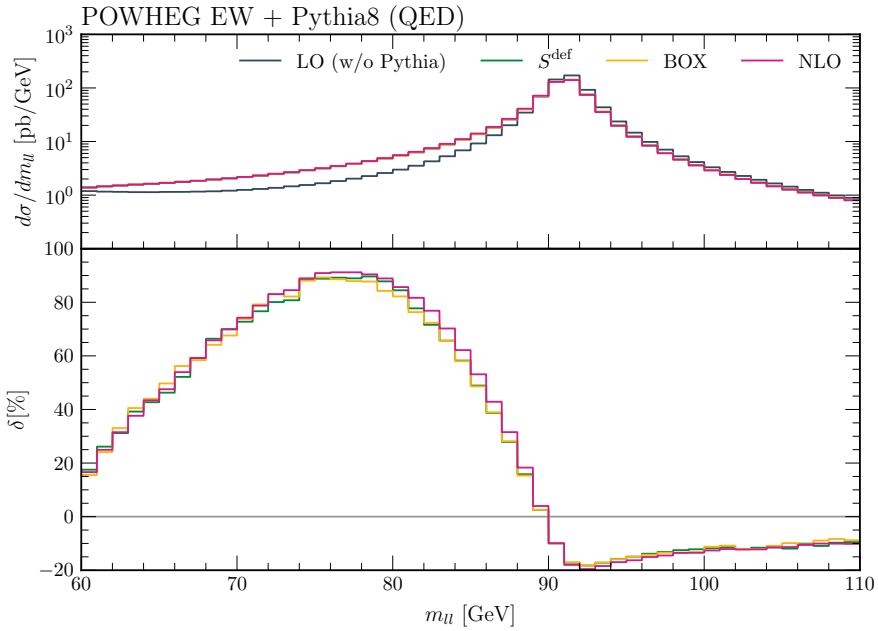

Figure 6.6.: Invariant mass spectrum of the $Z \to \mu^+\mu^-$ system for the leading order process without PYTHIA and the matched POWHEG NLO process. The results obtained with our implementation (labeled by S^{def}) are compared to POWHEGBOX events (labeled by BOX) and fixed-order NLO results. Concerning PYTHIA, we only apply the QED parton shower. The lower panel shows the relative corrections NLO/LO corrections in percent.

from the final-state muons. In fact, the final-state radiation is dominant. Since we are interested in EW corrections only in this section, we disable the QCD parton shower in PYTHIA by using the settings:

```
Checks:event            =  off
PartonLevel:Remnants    =  off
SpaceShower:QCDshower   =  off
TimeShower:QCDshower    =  off
```

Figure 6.6 shows the m_{ll} distribution for EW corrections matched to a QED shower. We find good agreement between our implementation and the POWHEGBOX over a large range of m_{ll}. The reason for the large corrections below the resonance peak is that photonic final-state radiation reduces the invariant mass of the lepton system m_{ll}. Therefore, the events are moved to lower values of m_{ll}. Since the majority of all events is at the peak, we see large relative corrections when events from the peak are moved to smaller m_{ll}. Events with $m_{ll} > M_Z$ before radiation cannot compensate the loss at the peak because their cross section is too small. The scale dependence of the NLO

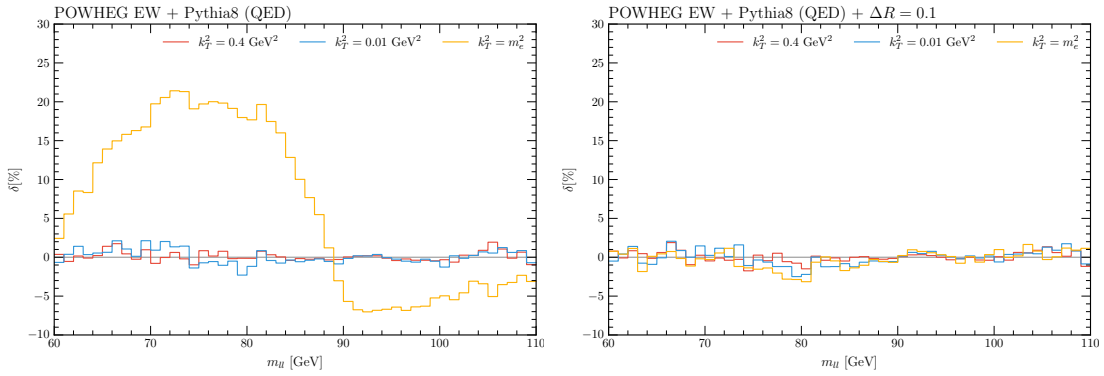

(a) No recombination

(b) Recombination

Figure 6.7.: Invariant mass of the $Z \to \mu^+\mu^-$ system for different POWHEG cut-off scales compared to the default cut-off scale $k_T^2 = 0.8$ GeV^2.

distribution is almost the same as the LO scale dependence. Hence, the scale dependence cancels in the relative corrections in Figure 6.6 and is not shown.

To validate the usage of massless leptons in the POWHEG event generation, we investigate the effects of a small radiation cut-off scale (see section 6.1.2). Using a very small cut-off scale, collinear radiation is enhanced and we find large unphysical corrections. Figure 6.7a shows these unphysical corrections for several cut-off scales compared to our standard value of $k_T^2 = 0.8$ GeV^2. Large unphysical corrections are only present when we set the cut-off scale as small as the electron mass. This shows that the massless lepton approximation is valid for our standard cut-off scale. In Figure 6.7b, we see that the unphysical corrections disappear once we use recombination.

6.5. Resonance Improvement

The FKS phase-space splitting used in POWHEG is not unique because the S functions can be defined in different ways (see section 3.3.1). Only their collinear limit is uniquely defined. The standard S functions do not reflect the resonance structure of the Drell-Yan process. Therefore, large higher-order effects can come about. To illustrate the resulting effects, we consider a phase-space configuration with hard photon radiation. The radiation is also considered not to be collinear to one of the muons or the beam axis. The squared amplitude contains Feynman diagrams for initial-state radiation and for final-state radiation. Therefore, the squared matrix element can be on-shell if the momentum transfer $Q_3^2 = (l_+ + l_- + k)^2 = M_Z^2$ or if the momentum transfer $Q_2^2 = (l_+ + l_-)^2 = M_Z^2$.

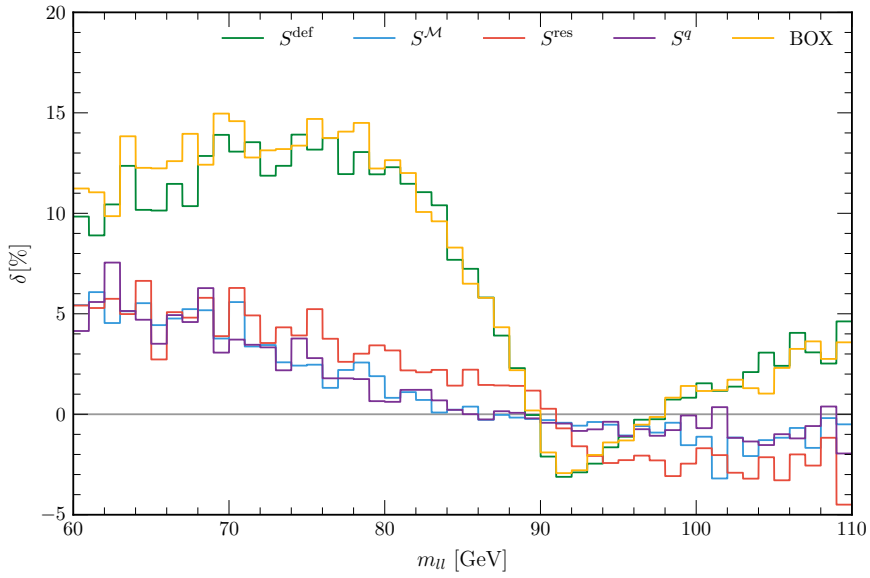

Figure 6.8.: Relative EW corrections in $\bar{B}$ for the invariant mass of the lepton pair. We show results for different choices of the S functions, i.e. S^{def}, $S^{\mathcal{M}}$, and S^{q}. Furthermore, the POWHEGBOX result is shown which agrees well with S^{def}.

The muon momenta are denoted by $l_{\pm}$ and k is the momentum of the real photon. Considering a phase-space configuration with on-shell FSR diagrams ($Q_3^2 = M_Z^2$), the ISR diagrams are suppressed because $Q_2^2 < M_Z^2$. In total, FSR dominates in this phase-space configuration. However, the FKS S functions do not reflect the structure of the matrix element. Depending on the specific choice of S functions, the ISR region can give significant contributions to the NLO weight $\bar{B}$. As shown in Figure 6.8, we find large corrections for the standard FKS splitting S^{def} (described in section 3.3) in the tails of the invariant mass spectrum. Figure 12 in [30] shows that the purely weak corrections close to the peak are small. Below the peak, photonic Drell-Yan contributions are important but the coupling structure is not similar to the muon decay. Therefore, the G_μ scheme that is defined by muon decay (s. section 6.2) is not the best choice anymore. This leads to corrections up to 5 % below the peak.

To minimize the effects of wrongly assigned phase-space regions, we split the squared Drell-Yan amplitude in a gauge invariant way into a pure FSR term $|\mathcal{M}_{FSR}|^2$, a pure ISR part $|\mathcal{M}_{ISR}|^2$, and an interference term, i.e.

$$|\mathcal{M}|^2 = |\mathcal{M}_{FSR}|^2 + |\mathcal{M}_{ISR}|^2 + 2\,\mathrm{Re}\,\mathcal{M}_{ISR}\mathcal{M}_{FSR}^*. \tag{6.33}$$

The FKS subtraction can be applied to all terms separately. The ISR term has only one singular region and the corresponding S function is by construction one. The FSR term has two singular regions, one for each muon. The interference term has the same singular regions as the full process but either the ISR or FSR propagator can be on-shell. Hence, there is no enhancement for ISR or FSR. Figure 6.8 shows that the physical decomposition of the matrix element (labeled by $S^{\mathcal{M}}$ in the following) reproduces qualitatively the results shown in Figure 12 of [30]. This is expected because $\bar{B}$ (s. section 5.3) is an inclusive quantity and, therefore, the large kinematic effects described in section 6.4.2 do not contribute. Furthermore, Figure 6.8 shows a good agreement of our implementation using S^{def} and the POWHEGBOX when no radiation is generated.

We can also improve the FKS S functions such that they respect the resonance structure. The general procedure is discussed in [58]. For Drell-Yan, the standard S functions (labeled by S^{def}) are given by

$$S_0^{\text{def}} = \frac{1}{1 + \frac{d_0}{d_+} + \frac{d_0}{d_-}} \tag{6.34}$$

for initial-state radiation and

$$S_\pm^{\text{def}} = \frac{1}{1 + \frac{d_\pm}{d_0} + \frac{d_\pm}{d_\mp}} \tag{6.35}$$

for final-state radiation (s. section 3.3.1). We use $d_+ = d_{53}$ and $d_- = d_{54}$ and the definitions from section 3.3.1 for all d's. We introduce Breit-Wigner propagators to reflect the resonances within the S functions, i.e.

$$P_{2,3} = \frac{M_Z^4}{(Q_{2,3}^2 - M_Z^2)^2 + \Gamma_Z^2 M_Z^2}. \tag{6.36}$$

As before $Q_3 = l_+ + l_- + k$ is the FSR momentum transfer and $Q_2 = l_+ + l_-$ is the ISR momentum transfer. If we define the resonance improved S functions including the Breit-Wigner factors as

$$S_0^{\text{res}} = \frac{1}{1 + \frac{P_3}{P_2}\left(\frac{d_0}{d_+} + \frac{d_0}{d_-}\right)} \tag{6.37}$$

and

$$S_\pm^{\text{res}} = \frac{1}{1 + \frac{P_2}{P_3}\frac{d_\pm}{d_0} + \frac{d_\pm}{d_\mp}}, \tag{6.38}$$

the unique collinear limits are not changed because the ratios of d functions are either zero or infinity for collinear radiation. Only non-collinear phase-space configurations are

changed because the ratios of the d functions are of order $\mathcal{O}(1)$ in these regions. Consider for example a phase-space configuration, that is equally split into ISR and FSR regions with the standard S functions. The ISR region is given by

$$S_0^{\text{res}} = \frac{P_2}{P_2 + P_3}. \tag{6.39}$$

The separation between ISR and FSR, therefore, is determined by the on-shellness of the Breit-Wigner propagators. The ISR S function is close to one if the ISR propagator is on-shell and the FSR diagrams are highly off-shell. On the other hand it is zero if it is the other way around.

In case of photon radiation, we can add the fermion charges to the Breit-Wigner propagator to improve the FKS region separation further. That is, $P_2 \to Q_q^2 P_2$ and $P_3 \to Q_l^2 P_3$ where Q_q is the quark charge and Q_l is the lepton charge. The corresponding S functions are denoted by S^q in the following.

Figure 6.8 shows that introducing Breit-Wigners to the S functions reduces the large corrections we found with the standard FKS splitting. When we use also the fermion charges, we find very good agreement with the splitting at the matrix-element level into FSR and ISR parts.

The large corrections we found for standard FKS are also present in the Sudakov. Since the POWHEG method has NLO accuracy, these contributions have to cancel the large corrections once we also generate radiation with the POWHEG method. The FKS splitting, therefore, does not matter at $\mathcal{O}(\alpha)$ when we generate POWHEG event samples with pure EW corrections. Only higher-order terms can be induced because the POWHEG method has NLO accuracy.

When we combine QCD and EW corrections, we always use the NLO weight $\bar{B}$ for both types of corrections. But only the hardest radiation is generated with POWHEG, i.e. QCD radiations win the highest-bid method most of the time. Hence, the cancellation between the EW Sudakov and the large corrections in $\bar{B}$ is reduced.

6.6. Combining QCD and EW Corrections

To combine corrections from QCD and EW, we use an NLO weight $\bar{B}$ that includes real and virtual corrections for QCD and EW radiation. In particular, we have to add the finite terms of the 1-loop expressions and all subtracted real matrix elements for QCD and photon radiation. Also pdf renormalization remnants for QCD and EW radiation have to be taken into account. Furthermore, all radiation regions for QCD and EW have to be taken into account.

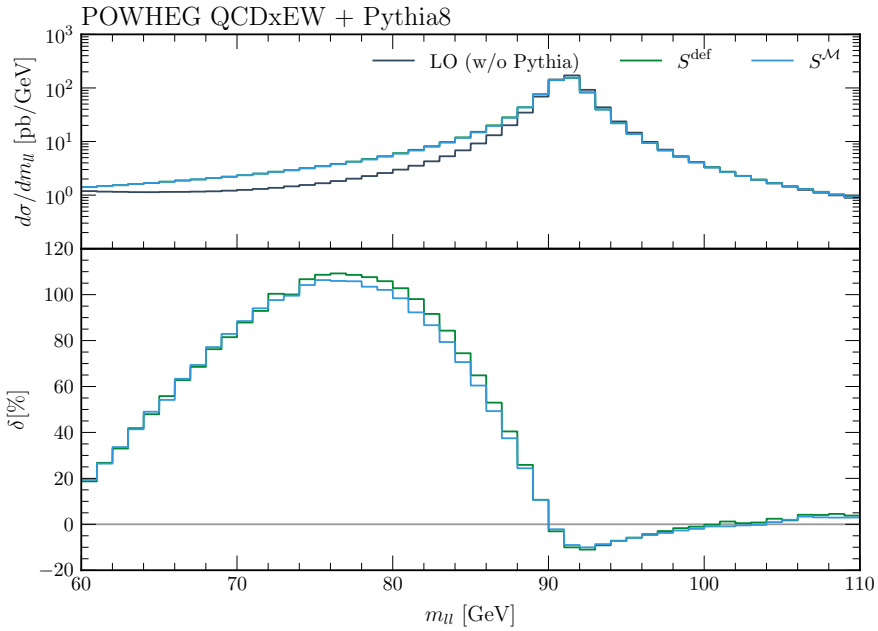

Figure 6.9.: Invariant mass spectrum for combined QCDxEW corrections with different S functions. This plot shows results for LO (without parton shower) and NLO results for S^{def} and $S^{\mathcal{M}}$. The lower panel shows relative corrections with respect to LO.

Figure 6.9 quantifies the effect of different S functions. Since POWHEG generates only the hardest radiation and the QCD coupling α_s is much larger than the fine-structure constant α, the hardest radiation is most likely of QCD type. Hence, contributions from the EW Sudakov are small. These contributions, however, cancel the large corrections we found for the standard FKS splitting in $\bar{B}$ for EW only. This cannot be the case for the combined QCDxEW corrections. Figure 6.10 shows relative corrections for different S functions with respect to the default S^{def} functions. The differences due to the different S functions are reduced compared to the $\bar{B}$ result because the POWHEG emission of real photons compensates part of the deviation. However, a percent-level distortion of the resonance peak remains. Note an alternative solution [106] is described in chapter 7.

So far, we also switched off hadronization and multi-parton interactions (MPI) in PYTHIA for performance reasons. Running PYTHIA with hadronization and MPI takes 16 CPU hours for 10^6 POWHEG events on the RWTH Compute Cluster. Figure 6.11 shows the same plot as Figure 6.10 but hadronization and MPI is enabled and we only show results for $S^{\mathcal{M}}$ in comparison with S^{def}. The total runtime to produce this plot with hadronization and MPI is approximately 2000 CPU hours on the RWTH Compute

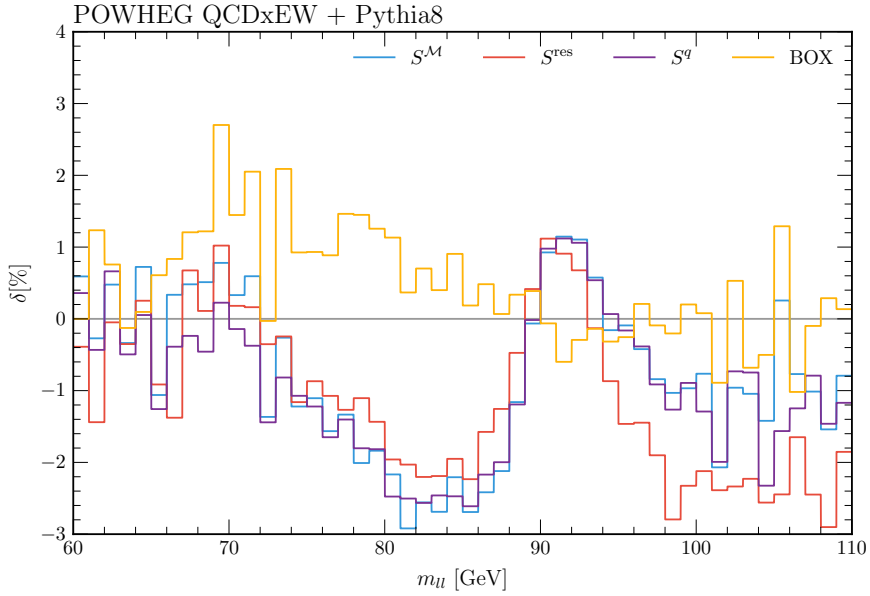

Figure 6.10.: Invariant mass spectrum for combined QCDxEW corrections with different S functions. This plot shows relative corrections with respect to S^{def} for S^{res}, $S^{\mathcal{M}}$, S^{q}, and the PowhegBox.

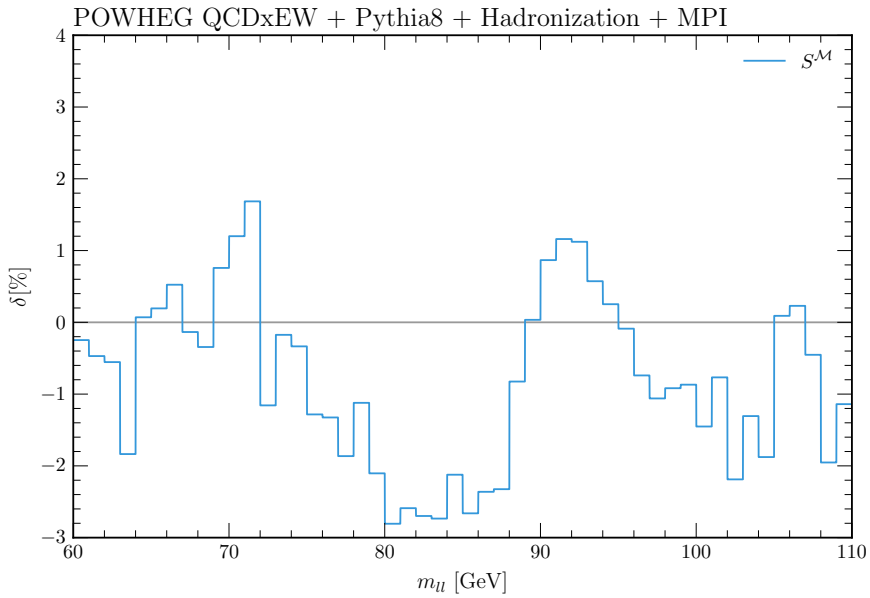

Figure 6.11.: Invariant mass spectrum for combined QCDxEW corrections. This plot shows relative corrections for $S^{\mathcal{M}}$ with respect to S^{def}. Hadronization and MPI is enabled in Pythia.

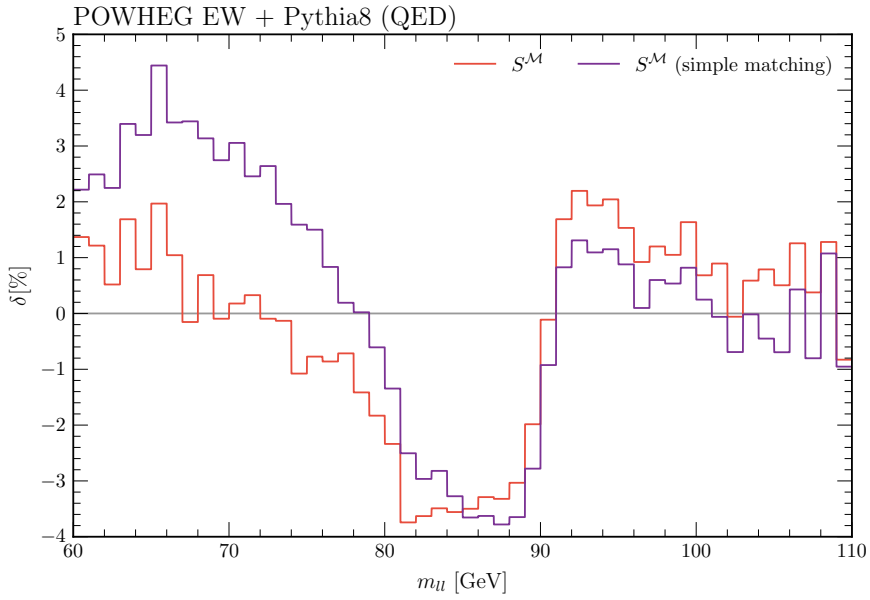

Figure 6.12.: Relative difference of EW corrections matched to a QED parton shower and a fixed-order NLO calculation.

Cluster. If hadronization and MPI is switched off, the runtime reduces to about 30 minutes for 10^6 POWHEG events. Figure 6.11 shows that we obtain the same results when we enable hadronization and MPI. Since all other curves in Figure 6.10 are similar to S^{def} and $S^{\mathcal{M}}$, we do not expect changes in our results. Hence, using the PYTHIA settings in section 5.5.5 is justified.

6.7. Influence of Different Matching Schemes in PYTHIA

In this section we investigate the differences between our default parton-shower matching in PYTHIA (denoted by `PowHegHook` improved parton-shower matching) and the matching without `PowHegHook` described in section 5.5.5 (denoted by *simple matching* in the following).

Figure 6.12 shows the effects due to multi-photon radiation from the parton shower. Our implementation agrees qualitatively with the results in Figure 12 in [30]. Especially for large m_{ll}, we find small corrections. Furthermore, Figure 6.12 shows the effect of the `PowHegHook` improved parton-shower matching compared to the simple parton-shower matching.

The difference between simple matching and the `PowHegHook` improved parton-shower

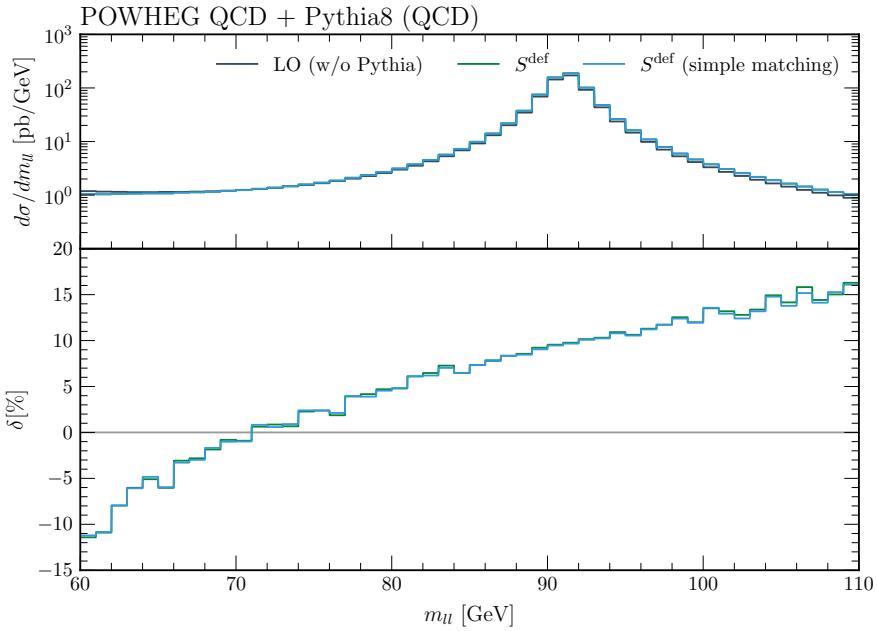

Figure 6.13.: Comparison of `PowHegHook` improved parton-shower matching and simple parton-shower matching.

matching for QCD radiation is shown in Figure 6.13. Since initial-state radiation does not change the invariant mass distribution, we do not find differences between the simple matching and the `PowHegHook` improved partons-shower matching.

The effects of the mismatch of evolution scales for combined QCD and EW corrections is shown in Figure 6.14. We find that the resonance peak is not changed. Only in the low invariant mass tail, we find a difference of up to 2 %.

Since the evolution scale mismatch applies also to the resonance improved POWHEG method, the ratio plot Figure 6.10 does not change for simple parton shower matching.

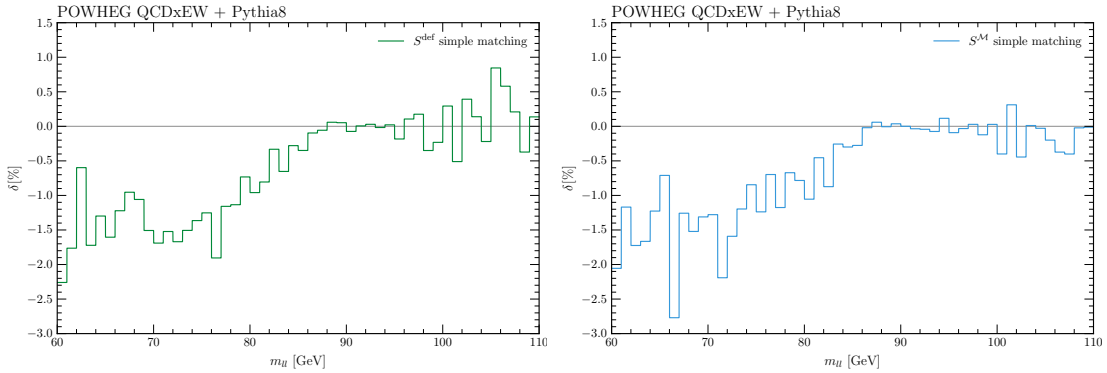

(a) S^{def} (b) $S^{\mathcal{M}}$

Figure 6.14.: Relative difference of `PowHegHook` improved parton-shower matching and simple parton-shower matching for combined QCD and EW corrections.

7. Charged-Current Drell-Yan

The charged current Drell-Yan process $pp \to W^{\pm} \to l^{+}\nu(l^{-}\bar{\nu})$ is important at the LHC due to its large cross section. It can be used to measure the W-boson mass with an accuracy of 10 – 20 MeV [13, 107–109].

The parameters of the standard model of particle physics (SM) are connected by overconstrained relations. Hence, we can use measured parameters to test the validity of the SM. Using a global fit, the W-boson mass can be determined with a better precision than the direct measurement [110, 111]. Therefore, it is important to measure m_W as precisely as possible to test the validity of the SM.

Recently, the first measurement of the W-boson mass at the LHC was published in reference [13, 109]. The measured mass is given by

$$m_W = 80370 \pm 7(\text{stat.}) \pm 11(\text{exp. syst.}) \pm 14(\text{mod. syst.}) \text{ MeV}, \tag{7.1}$$

where the first uncertainty is statistical, the second uncertainty is the experimental systematic uncertainty, and the third corresponds to the physics-modeling systematic uncertainty. To obtain the W-boson mass, the PowhegBox (V1/svn rev. 1556) matched to Pythia 8 was used. Since the modeling uncertainty dominates, better predictions for QCD and EW corrections for the Drell-Yan process in Powheg are necessary to improve the W-boson mass measurement.

Furthermore, it is possible to determine pdfs [112] and measure the luminosity of the LHC [113]. The charged-current Drell-Yan process is also a background in searches for a heavy gauge boson W'.

Technically, the charged-current Drell-Yan process is similar to the neutral-current Drell-Yan process. Therefore, it is known to the same order in QCD and EW perturbation theory. References for the calculations can be found in chapter 1. The charged-current Drell-Yan process including EW corrections is implemented in the PowhegBox framework [49, 50]. In this chapter we apply the resonance improved parton-shower matching described in the previous chapter to the charged-current Drell-Yan process. We published the results of this chapter also in reference [57].

In our Powheg implementation, we use the virtual matrix elements from [114] and

	PowhegBox V2	PowhegBox V2 cmplx	Powheg	NLO
	[pb]			
σ_{LO}	9562 ± 1	9572 ± 1	9559 ± 1	9554 ± 1
σ_{QCD}	10986 ± 1	10998 ± 1	10987 ± 2	10974 ± 3
σ_{EW}	9628 ± 6	9545 ± 1	9511 ± 1	9507 ± 1
σ_{QCDxEW}	–	10972 ± 1	10941 ± 2	10926 ± 3
	setup: $m_{l\nu} > 1$ GeV			

Table 7.1.: NLO cross sections for $\sqrt{s} = 13$ TeV and $m_{l\nu} > 1$ GeV. These values are obtained from Powheg event generation.

the real matrix elements were generated with MadGraph [87, 88]. The elements of the CKM matrix are used as global factors for the born process and the CKM matrix is set to 1 in the calculation of the virtual correction. We use the following block diagonal CKM matrix parametrization

$$V_{\text{ud}} = 0.975, \quad V_{\text{us}} = 0.222, \quad V_{\text{ub}} = 0,$$
$$V_{\text{cd}} = 0.222, \quad V_{\text{cs}} = 0.975, \quad V_{\text{cb}} = 0,$$

i.e. we neglect mixing with third-generation quarks. All other parameters are the same as for the neutral-current Drell-Yan (s. section 6.2).

The singular regions are similar to the neutral-current Drell-Yan case. The only difference is that the final-state neutrino does not radiate photons and no soft/collinear region has to be associated to the neutrino. Hence, we have only one ISR and one FSR singular EW region. In Table 7.1, we list the inclusive cross sections obtained with the PowhegBox implementation, our implementation and a Catani-Seymour subtracted fixed-order NLO calculation [90]. We find a good agreement at the 1‰ level for the LO and QCD NLO cross sections between our Powheg implementation and the PowhegBox V2. The EW corrections show a large deviation due to a bug in the virtual amplitudes in PowhegBox V2 (svn/r3175).[1] If we use the complex-mass scheme implementation in the PowhegBox V2 (svn/r3175) (labeled PowhegBox V2 cmplx), the cross sections agree at the per mill level.[2] Hence, we use PowhegBox V2 cmplx to validate our implementation in the following.

As for neutral-current Drell-Yan, we use

$$p_T^l > 20\text{GeV} \quad \text{and} \quad |\eta^l| < 2.5 \tag{7.2}$$

[1] After private communication with the authors of the PowhegBox, the bug was fixed in PowhegBox V2 (svn/r3344) and the complex-mass scheme is enabled by default.

[2] The complex-mass scheme is enabled by setting `complexmasses=.true.` in `init_couplings.f`.

as LHC acceptance cuts. Furthermore, we use

$$p_T^{\text{miss}} > 20\text{GeV} \tag{7.3}$$

which is implemented as a cut on the neutrino. We use $\mu_F = \mu = M_W$ as factorization and renormalization scales in the event generation.

A relevant observable for the determination of the W-boson mass is the transverse mass m_T. It is defined as

$$m_T^2 = \left(E_T^{(1)} + E_T^{(2)}\right)^2 - \left(\vec{p}_T^{(1)} + \vec{p}_T^{(2)}\right)^2, \tag{7.4}$$

where $\left(E_T^{(i)}\right)^2 = m_i^2 + \left(\vec{p}_T^{(i)}\right)^2$ and i denotes the neutrino and the muon.

The W-boson mass can be determined by comparing measured m_T distributions to template distributions, where template distributions are obtained by simulating events with different values for m_W.

We show the transverse-mass distribution for S^{def} and S^{res} (s. section 6.5) in Figure 7.1. We also compare our results to the POWHEGBOX V2. Figure 7.1 shows the POWHEGBOX curve rescaled to the cross section we found with our implementation. We find a deviation up to 3 per mill at the Jacobian peak when we compare the results for S^{def} and for S^{res}. A similar difference was found in Figure 34 of [115], where POWHEGBOX results for QCD and QCD+EW (both matched to Photos [116]) are compared. In [115], the difference is attributed to missing $\mathcal{O}(\alpha_s\alpha)$ contributions in the POWHEGBOX QCD results. However, the difference can at least partly be attributed to missing resonance improvements. In the transverse-mass distributions, we do not find any differences if we use the simple parton-shower matching described in section 6.7.

We cannot split the matrix element into gauge invariant subsets for ISR and FSR. Furthermore, we cannot define S^q unambiguously due to the W-boson charge. Therefore, we study the m_T distribution for the neutral-current Drell-Yan process where S^q and $S^{\mathcal{M}}$ can be defined (s. section 6.5). Figure 7.2 shows that we find qualitatively the same deviation for S^{res} as for the charged-current case. At the Jacobian peak, the deviation is larger than for the charged-current because there are two radiating final-state particles. The results for S^{def} and $S^{\mathcal{M}}$ are similar at the peak, i.e. S^{def} can be used to resolve the issue found in Figure 34 of [115].

During the completion of this thesis an alternative solution to using S^{res} was published in reference [106]. Most of the radiation in standard POWHEG is ISR QCD radiation due to the large coupling. The POWHEGBOX is modified to generate initial-state radiation and final-state radiation separately. Therefore, the POWHEGBOX can generate up to two

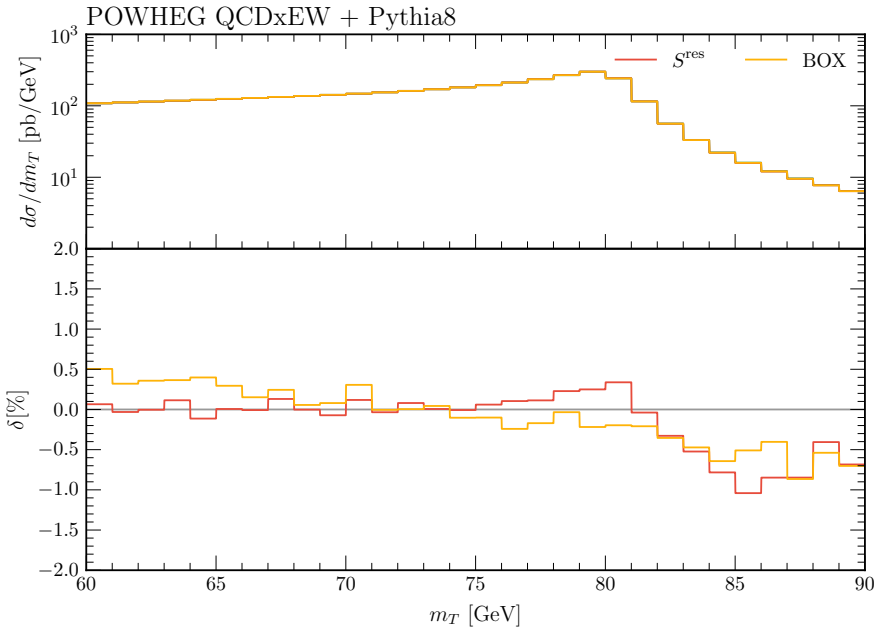

Figure 7.1.: Transverse-mass distribution for the charged-current Drell-Yan process. The upper panel shows the differential cross section and the lower panel shows the relative correction with respect to S^{def} for S^{res} and the PowhegBox.

radiated particles, i.e. an ISR parton or photon and an FSR photon. Furthermore, it gives two radiation scales (ISR/FSR) to the parton shower. Figure 3 in [106] shows also a 5 per mill distortion at $m_T = m_W$. In the future, it would be interesting to compare both approaches in detail.

The authors of [106] also determined M_W by fitting templates to the m_T distribution. They found that the distortion in Figure 7.1 leads to a shift in m_W of about 10 MeV. They also show that the m_W masses obtained with different QED parton showers do not agree on a level of about 10 MeV if no resonance improvement is used (i.e. S^{def}). This discrepancy would contribute to the theory error. However, the m_W masses agree if they use the PowhegBox with up to two radiations.

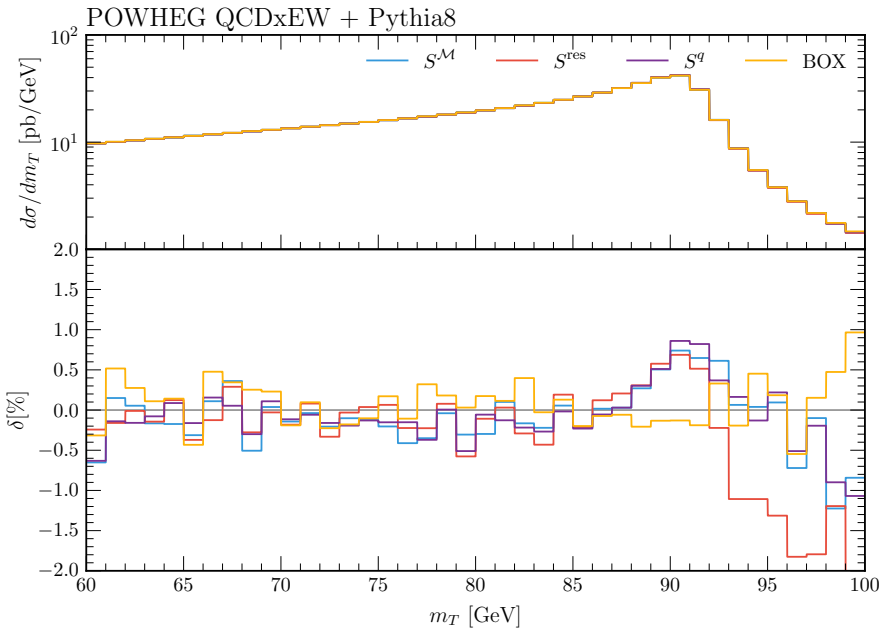

Figure 7.2.: Transverse-mass distribution for the neutral-current Drell-Yan process. The upper panel shows the differential cross section and the lower panel shows the relative correction with respect to S^{def} for S^{res}, $S^{\mathcal{M}}$, S^{q}, and the POWHEG-BOX.

8. W-Boson Production at Large Transverse Momentum

Gauge bosons like the W-boson are created frequently at the LHC. At hadron colliders events are often associated with jets. As the cross section for $pp \to Wj$ production with a hard jet is still large, it is an important process at the LHC. The W-boson recoils against a jet from initial-state radiation. Therefore, the W-boson is highly boosted and can lead to highly boosted charged leptons and neutrinos. Due to its large cross section, $pp \to Wj$ production gives a large contribution to phenomenologically important signatures of missing energy and charged leptons. Thus, it is an important background for BSM searches.

Several experimental analyses from ATLAS and CMS investigate this process in detail [117–120]. It is crucial to have theoretical predictions with high accuracy. The NLO QCD corrections are available in [121–124]. Recently, the full NNLO QCD corrections became available [125] and were compared to experimental data [126]. Furthermore, EW NLO corrections are available in [127–130]. In [131], QCD and EW NLO corrections are combined with the multijet merging approach at NLO [132–135]. Since the $pp \to Zj$ process is similar, it is also known at the same order of perturbation theory as $pp \to Wj$ [136–140]. The parton-shower matching within the PowhegBox framework for QCD radiation is published in [141].

Compared to the Drell-Yan process, new technical difficulties arise for the process $pp \to Wj$. The first step in a Powheg implementation is to implement the NLO corrections. We can use our library described in section 5.5.4 to implement FKS subtracted NLO corrections. For $pp \to Wj$, the FKS method contains ingridients that are not needed for Drell-Yan. For instance, $W +$ jet includes born processes with external gluons and real radiation processes can have multiple underlying born processes. In the following sections, we describe the process specific parts that have to be implemented in order to use the library described in section 5.5.4. Moreover, we discuss the aspects of the FKS implementation that are not needed for the Drell-Yan process.

In section 8.4, we show NLO results obtained with the library described in section 5.5.4. In section 8.5, we give an outlook for the Powheg event generation.

8.1. Subprocesses

The production of a leptonically decaying charged vector boson W^+ in association with a jet has the following LO subprocesses:

$$u_i\,\bar{d}_j \to W^+\,g \to l^+\,\nu_l\,g \tag{8.1}$$
$$g\,u_i \to W^+\,d_j \to l^+\,\nu_l\,d_j \tag{8.2}$$
$$g\,\bar{d}_j \to W^+\,\bar{u}_i \to l^+\,\nu_l\,\bar{u}_i \tag{8.3}$$

where u_i is an up-type quark of generation i, d_j is a down-type quark of generation j, and l is a lepton. At NLO QCD we have to include real radiation diagrams with additional gluon radiation and gluon splittings into quark-antiquark pairs. We find

$$g\,\bar{d}_j \to W^+\,g\,\bar{u} \tag{8.4}$$
$$g\,u_i \to W^+\,g\,d_j \tag{8.5}$$
$$g\,g \to W^+\,d_j\bar{u}_i \tag{8.6}$$
$$u_i\,\bar{d}_j \to W^+\,g\,g \tag{8.7}$$
$$\bar{q}_k\,\bar{d}_j \to W^+\,\bar{u}_i\,\bar{q}_k \tag{8.8}$$
$$q_k\,\bar{d}_j \to W^+\,\bar{u}_i q_k \tag{8.9}$$
$$q_k\,u_i \to W^+\,d_j\,q_k \tag{8.10}$$
$$\bar{q}_k\,u_i \to W^+\,d_j\,\bar{q}_k \tag{8.11}$$
$$u_i\,\bar{d}_j \to W^+\,\bar{q}_k\,q_k \tag{8.12}$$
$$q_k\,\bar{q}_k \to W^+\,\bar{u}_i\,d_j \quad (q_k \neq u_i, d_j) \tag{8.13}$$

where q_k is an up- or down-type quark of generation k and u_i, d_j are defined as for leading order. The leptonic W-boson decay is implied. Note that the list of real processes is not minimal, i.e. some processes are included in more than one of the above equations. For example, the process $u_i\,\bar{d}_j \to W^+\,\bar{u}_i\,u_i$ is included in (8.9) and (8.12). Process (8.13) is special because it does not originate from one of the LO processes by a splitting. These processes correspond to $q_k\,\bar{q}_k \to q'\,\bar{q}'$ with W^+ radiation, e.g. $c\,\bar{c} \to W^+\,d\,\bar{u}$. The contributions of these processes are finite and can be generated with standard Monte-Carlo methods. Since the matrix elements differ for $q_k \neq u_i, d_j$ and $q_k = u_i, d_j$, we have 18 different squared matrix elements for real QCD radiation.

Since there are processes that involve splittings of gluons at born level, we have to use the spin-correlated born matrix elements when we calculate the collinear limits of the real matrix elements. The implementation of the spin-correlated born matrix elements is

more involved than the normal splitting functions. How the collinear limits are calculated is detailed in section H.2.

For photon radiation, we find the following processes with real radiation

$$u_i\,\bar{d}_j \to W^+\,g\,\gamma \tag{8.14}$$
$$g\,u_i \to W^+\,d_j\,\gamma \tag{8.15}$$
$$g\,\bar{d}_j \to W^+\,\bar{u}_i\,\gamma \tag{8.16}$$

We use MadGraph [87] to generate C++ code for the real matrix elements. The virtual QCD and EW 1-loop contributions are taken from [130]. Concerning the parameters, we use the same setup as for the Drell-Yan process (see section 6.2). In particular, the G_μ scheme is used to define the couplings and the complex-mass scheme is used to introduce the width of the W-boson in its propagator.

In an implementation of the FKS subtraction scheme, we need the color-correlated born amplitudes in the soft-collinear endpoint (3.171) and the eikonal limits. In order to find the color-correlated born amplitudes, we have to calculate the color factors of NLO interference terms. Since only three colored partons are present at born level, the color-correlated born amplitude is proportional to the born matrix element and a global color factor. When a gluon is radiated from quarks, we find the color factor $C_F N_C \left(C_F - \frac{1}{2}C_A\right)$, where N_C is the dimension of the $SU(N_C)$, i.e. $N_C = 3$, $C_A = N_C$, and $C_F = \frac{N_C^2-1}{2N_C}$. When a gluon is radiated from a gluon in one of the interfering diagrams and from a quark in the other diagram, we obtain $\frac{1}{2}C_F C_A N_C$. The color correlated born is defined as the born matrix element with the color factor of the real matrix element. Therefore, we have to divide the born matrix element B by its color factor, i.e. $C_F N_C$, and multiply by the color factor of the NLO process. The color correlated born matrix elements read

$$B_{12} = \left(C_F - \frac{1}{2}C_A\right) B \tag{8.17}$$
$$B_{15} = B_{25} = \frac{C_A}{2} B \tag{8.18}$$

for $q\bar{q}' \to \mu^+\nu g$ and

$$B_{25} = \left(C_F - \frac{1}{2}C_A\right) B \tag{8.19}$$
$$B_{12} = B_{15} = \frac{C_A}{2} B \tag{8.20}$$

for $gq \to \mu^+\nu q'$ and $g\bar{q} \to \mu^+\nu\bar{q}'$. Note that $B_{ij} = B_{ji}$ and we do not need the diagonal

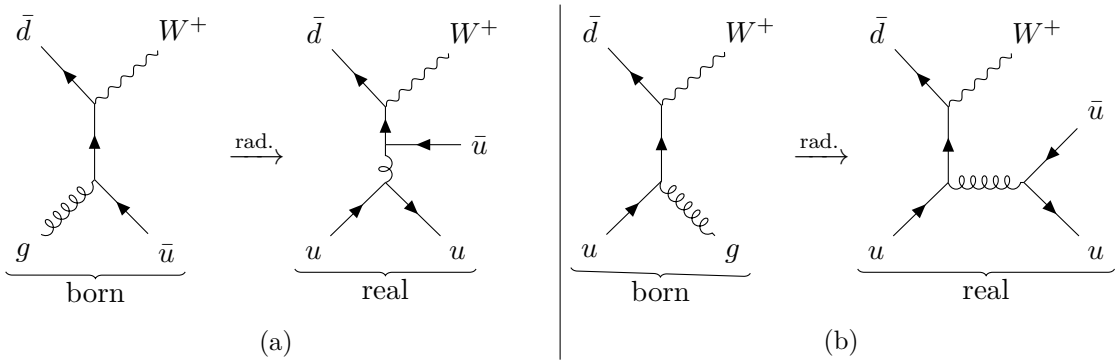

Figure 8.1.: Two diagrams of the real process $\bar{d}\,u \to W^+\,u\,\bar{u}$ and their underlying born matrix elements.

elements for massless particles. Components connected to particles which are not charged under the $SU(N_C)$ are zero, i.e. all elements except the ones above are zero.

8.2. Singular Regions

Since POWHEG event generation starts with a born process, we have to categorize the real processes by their underlying born process. However, a process does not necessarily have a unique underlying born process. For example the process $\bar{d}\,u \to W^+\,u\,\bar{u}$ has two underlying born configurations: $\bar{d}\,g \to W^+\bar{u}$ and $\bar{d}\,u \to W^+\,g$. The Feynman diagrams are shown in Figure 8.1. The squared real matrix element has a singular region for two collinear final-state quarks and a region for quark u close to the beam. Therefore, we assign the S-functions S_{50} and S_{54} to the real process. When we start from a born process, e.g. $\bar{d}\,u \to W^+\,g$ only the splitting $g \to u\bar{u}$ leads to the real process. Therefore, only this splitting is considered in event generation but we have to keep track of both singular regions to be able to calculate the S functions and obtain a finite result. In summary, we have to include all singular regions for possible splittings of born partons when we add a real process to an underlying born process. Furthermore, we have to keep track of all singular regions of a real process in order to calculate the S functions. This was not an issue in the Drell-Yan case because all real radiation processes were associated with a unique underlying born process.

Another difference to Drell-Yan is that we have to split the initial-state region into two regions according to (3.161). This is necessary because a real process can have more than one underlying born process. Since the matrix-element limits are proportional to the born, we have to use the correct born that is determined by the singular region. For example, consider the process $g\,g \to W^+\,\bar{u}\,d$. The singular region for a collinear d

quark from ISR, i.e. $y = 1$, is connected to the underlying born $\bar{d}\,g \to W^+\,\bar{u}$ while the anti-collinear case, i.e. $y = -1$, has the underlying born $g\,\bar{d} \to W^+\,\bar{u}$.

8.3. Generation and Analysis Cuts

In contrast to Drell-Yan, W + jet contains a final-state parton that can become soft or collinear to the initial-state partons already at LO. Therefore, the totally inclusive LO cross section is divergent. To avoid the singular regions, we have to apply cuts that make the cross section finite. How we cut depends whether we generate inclusive POWHEG events or if we calculate well defined NLO quantities. First, we discuss the POWHEG cuts and second, we discuss the NLO cuts.

When we generate POWHEG events, our aim is to generate inclusive event samples and apply cuts in an analysis after showering, i.e. we cut only on the born phase-space during event generation. To render the cross section finite, we nevertheless have to apply a generation cut on the transverse momentum $p_T(j)$ of the jet. We also apply an analysis cut on $p_T(j)$ of events after showering. Since the NLO radiation can increase $p_T(j)$ of the underlying born phase space, it is possible that an event does not pass the generation cut but would pass the analysis cut, if we use the same cut. Therefore, we have to choose a generation cut that is much smaller than the analysis cut, to ensure that we do not cut events that would pass the analysis cut. To justify the choice of a generation cut, we can vary the cut and check if the results stay the same.

When we generate POWHEG events for W + jet at NLO EW accuracy, we also have to include the process $W\gamma$ because $q\bar{q}' \to W^+\gamma$ is an underlying born process of the NLO process $qg \to W^+q'\gamma$. Since, due to the coupling, the cross section of the electroweak process $W\gamma$ is much smaller than the cross section of the QCD process W + jet, we neglect this underlying born process, i.e. we set its NLO weight $\bar{B}$ to zero. However, we have to add an ISR region to the process $qg \to W^+q'\gamma$ to render the cross section finite.

When we calculate NLO cross sections, we also cut on the real phase space. For QCD radiation, we have to introduce a p_T cut for the jets. We have to require at least one hard jet to avoid soft-collinear divergences. Furthermore, the process is divergent if both final-state partons are treated exclusively in the collinear regime. Therefore, we have to use an infrared-safe jet algorithm (e.g. anti-k_t [142]) to combine collinear final-state partons into one jet. Since only two partons are present, the jet algorithm simplifies to a simple ΔR recombination cone, i.e. we recombine two partons if their ΔR distance is smaller than a given threshold.

The NLO cuts for EW corrections are more involved than the QCD cuts. As for the POWHEG event generation, we would have to include the $W\gamma$ process. However, we can

define cuts that remove those contributions. To guarantee the cancellation of infrared singularities, we can use an infrared-safe jet algorithm for the QCD partons and the photon [143–145]. If we apply the jet algorithm to partons and photons, the cancellation of collinear singularities is ensured because the recombination is inclusive for a collinear splitting. However, if a photon is recombined with a gluon, the gluon can be arbitrarily soft and the matrix element would be divergent. We follow the pragmatic approach described in [146] to ensure the consistent cancellation of singularities:

1. recombine a quark and a photon with $\Delta R < 0.1$ and treat the recombined object as QCD jet.

2. recombine partons (quarks, gluons) and photons with $\Delta R < 0.4$. Treat recombined object with photons as QCD jets if $E_\gamma / E_{\text{jet}} < z_{\text{thr}} = 0.8$.

Using this method, we can require at least one hard QCD jet to define a finite cross section.

8.4. NLO Calculation

We use our FKS implementation to generate NLO distributions for the p_T of the leading jet. For simplicity we use a fixed scale $\mu = \mu_F = M_W$ and a p_T cut on the jets

$$p_T(j) > 10 \text{ GeV}. \tag{8.21}$$

Partons are recombined into a single jet if they are closer than $\Delta R < 0.4$. The EW cuts are implemented as described in section 8.3.

Figure 8.2 shows the transverse-momentum distribution of the leading jet for QCD NLO corrections. Since we investigate the transverse-momentum distribution of the leading jet, the results are similar to the results in Figure 9 of reference [130]. The NLO QCD corrections become large at large transverse momentum. This effect is known as giant K factor. The origin is a configuration where two hard jets are recoiling against each other and the W-boson is soft, i.e. one can describe this configuration as dijet production with soft W-boson radiation. The K factor is, therefore, enhanced by a term of order $\alpha_s \log^2(p_T^2/M_W^2)$ from integrating over the W-boson [147].

The EW corrections shown in Figure 8.3 are dominated by Sudakov logarithms of the form $\alpha \log^2(s/M_W^2)$(see [148] and references therein). We find corrections of the order of 10 – 20 % for large transverse momenta of the leading jet. As for the QCD corrections, we find good agreement between our results and the results in Figure 9 of [130].

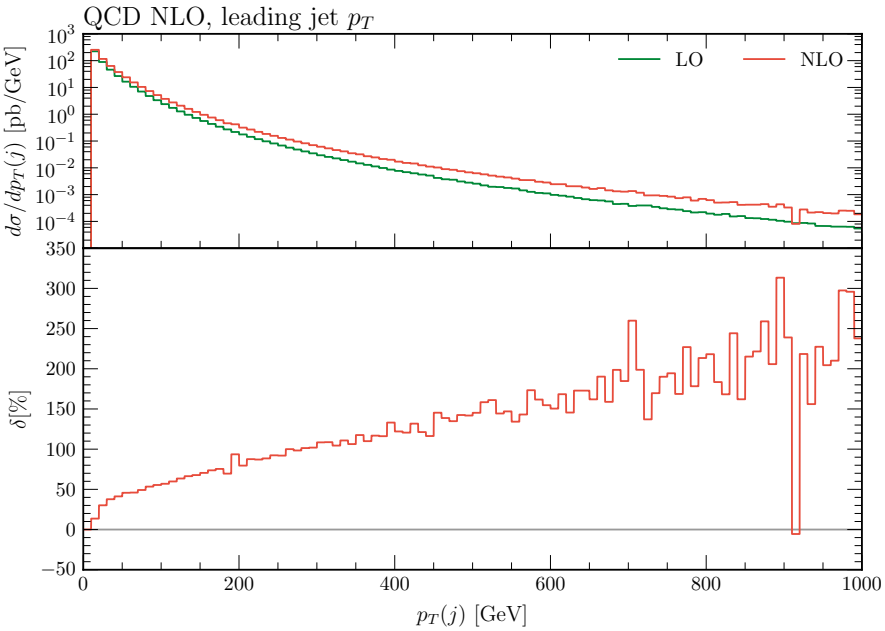

Figure 8.2.: Fixed-order QCD NLO distribution for the leading jet. The lower panel shows the relative corrections with respect to LO in percent.

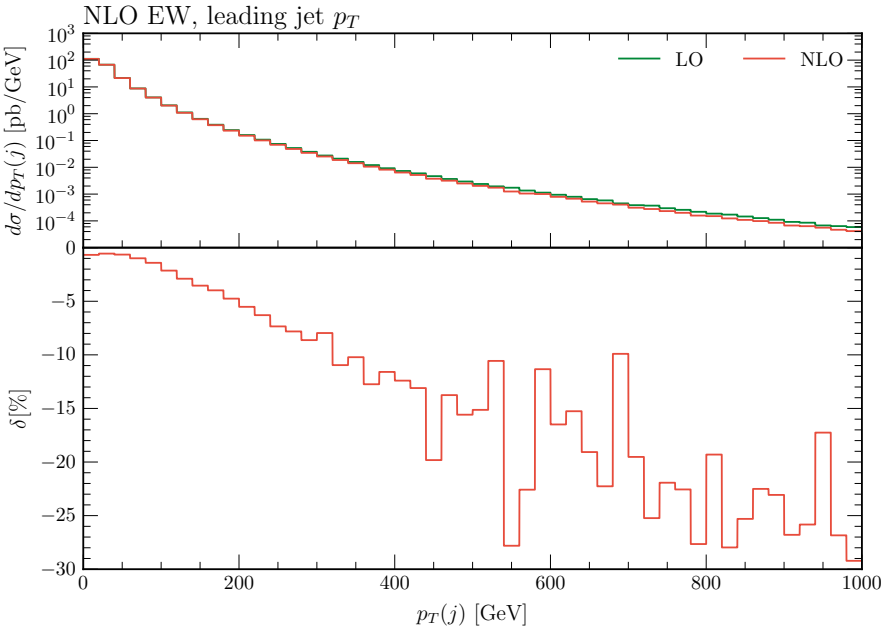

Figure 8.3.: Fixed-order EW NLO distribution for the leading jet. The lower panel shows the relative corrections with respect to LO in percent.

8.5. Outlook

The next step is to use our POWHEG implementation to match W + jet events to a parton shower and examine the phenomenological impact of the matching. The QCD matching is already implemented in the POWHEGBOX framework [141] and can be used to validate the implementation. Furthermore, we expect that the QCD corrections coincide with the fixed-order NLO distribution in Figure 8.2 for large p_T. EW corrections are not matched to a parton shower yet. Combining QCD and EW corrections for W + jet events is more complicated than for Drell-Yan because the resonance structure is more involved. To match the parton shower properly including resonance effects, we have to implement the method described in [58] for the W + jet case. Once the W + jet implementation is finished, it should be straightforward to implement Z + jet due to the structural similarity of the two processes. The final goal would be to implement resonance improved QCD+EW corrections for V + jet in the resonance-improved POWHEGBOX framework because a well tested and maintained POWHEG event generator would be publicly available and experimental collaborations could use it in their analyses. Our independent implementation could be used to validate every part of the POWHEGBOX implementation in detail.

9. Conclusions

In this thesis, parton-shower matching including electroweak corrections is addressed. On the technical side, the FKS subtraction scheme is reviewed in chapter 3 and the parts that have to be implemented in an NLO calculation are given explicitly. Starting from the default FKS subtraction scheme, we derive FKS subtraction terms for mass regularization in chapter 4. We find that only the soft-collinear endpoint changes with respect to default FKS in dimensional regularization. Hence, the actual subtraction does not have to be changed in an existing FKS implementation. Only the endpoint function that is combined with the 1-loop corrections has to be changed. Therefore, we derived a conversion rule for 1-loop amplitudes calculated in mass regularization into the commonly used dimensional regularization scheme. A similar result was found in reference [71].

In chapter 5 we review parton shower matching with the POWHEG method. We give explicit algorithms for QCD and EW matching. Furthermore, we discuss the C++ POWHEG library that was developed during the course of this thesis. The library is used to implement POWHEG for the Drell-Yan process but is extensible to more complicated processes. The library serves the same purpose as the POWHEGBOX which is the standard POWHEG implementation. Hence, the library can be used to validate the POWHEGBOX. In particular, the EW implementation can be validated.

In chapter 6 and 7, we apply our POWHEG library to the Drell-Yan process and study its phenomenology in the resonance region. In particular, we study QCD and EW effects and combined QCD and EW corrections. We find that the standard POWHEG method suffers from large uncontrolled higher-order terms for combined QCD + EW corrections. The origin of the higher-order terms is the W/Z-boson resonance in the Drell-Yan process. We show how the resonance can be taken into account properly and we quantify the effect to be of the order of a few percent in the resonance region. This difference can affect the determination of standard model parameters. For instance, the higher-order terms can lead to a shift of a few MeV in the measured W-boson mass.

These effects were also found in [115] and an independent solution was published in [106] during the completion of this thesis. It would be interesting to compare both solutions in detail.

Furthermore, our POWHEG library can be extended to other processes. The natural

next step is to implement the $W+\text{jet}$ and $Z+\text{jet}$ processes. In chapter 8 we show that our library can be used to make fixed-order NLO QCD + EW predictions for $W+\text{jet}$. This implementation could serve as a starting point for a future project in which the phenomenology of $W/Z+\text{jet}$ could be studied. Using the results one could validate the QCD implementation in the PowhegBox and one would be able to implement and validate EW corrections for $W/Z+$jet in the resonance-improved PowhegBox framework. A QCD+EW implementation in the resonance-improved PowhegBox framework would make them publicly available and they could be used by the experimental collaborations.

Appendices

A. Acronyms

BSM Beyond the Standard Model

dim. reg. dimensional regularization [59]

EW electroweak

FSR final-state radiation

IR infrared

ISR initial-state radiation

LHC Large Hadron Collider

LO leading order

NLO next-to leading order

NNLO next-to-next-to leading order

pdf parton distribution function

QFT quantum field theory

SM standard model of particle physics

UV ultra-violet

B. Virtual Corrections for Drell-Yan in Mass Regularization

In this appendix, we calculate the virtual 1-loop contribution to the photonic Drell-Yan process $q\bar{q} \to \gamma \to \mu^+\mu^-$. We start by evaluating the Born cross section. The Feynman diagram is shown in Figure B.1.

We can write the partonic matrix element as

$$|\mathcal{M}|^2 = \frac{1}{4N_c^2} H_{\mu\nu} L^{\mu\nu}, \tag{B.1}$$

where we average over initial-state and sum over final-state color and spin. The hadronic tensor $H^{\mu\nu}$ includes the contribution from the initial-state quarks, i.e.

$$H^{\mu\nu} = 4\pi\alpha N_c \,\mathrm{tr}\left\{\not{k}_2 \gamma^\mu \not{k}_1 \gamma^\nu\right\}. \tag{B.2}$$

The leptonic tensor contains the photon momentum and the leptonic part of the Feynman diagram, i.e.

$$L^{\mu\nu} = 4\pi\alpha \frac{1}{q^4} \,\mathrm{tr}\left\{\not{p}_2 \gamma^\mu \not{p}_1 \gamma^\nu\right\}. \tag{B.3}$$

The cross section reads

$$\mathrm{d}\sigma = \frac{1}{8sN_C^2} \,\mathrm{d}\Phi_2 H_{\mu\nu} L^{\mu\nu}, \tag{B.4}$$

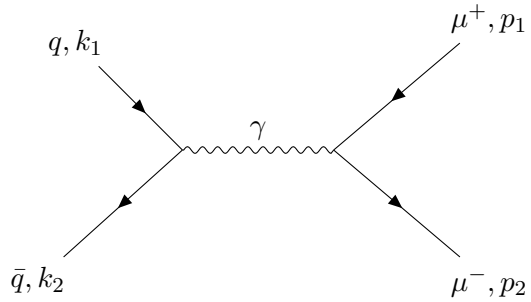

Figure B.1.: Born diagram for $q\bar{q} \to \gamma \to l\bar{l}$

where $\mathrm{d}\Phi_2$ is the two-particle phase-space element and we inserted the flux. We can split the phase space into a hadronic and a leptonic part by inserting

$$\frac{\mathrm{d}Q^2}{2\pi}\frac{\mathrm{d}^{d-1}q}{(2\pi)^{d-1}2q^0}\delta(q-p_1-p_2)=1, \tag{B.5}$$

where $Q^2=(p_1+p_2)^2$. We obtain

$$\mathrm{d}\Phi_2=\frac{\mathrm{d}Q^2}{2\pi}\,\mathrm{d}\Phi_1^h\,\mathrm{d}\Phi_2^l \tag{B.6}$$

The hadronic one particle phase space is defined by

$$\mathrm{d}\Phi_1^h=\frac{\mathrm{d}^{d-1}q}{(2\pi)^{d-1}2q^0}(2\pi)^d\delta^{(d)}(k_1+k_2-q) \tag{B.7}$$

and the leptonic two particle phase space reads

$$\mathrm{d}\Phi_2^l=\frac{\mathrm{d}^{d-1}p_1}{(2\pi)^{d-1}2p_1^0}\frac{\mathrm{d}^{d-1}p_2}{(2\pi)^{d-1}2p_2^0}(2\pi)^d\delta^{(d)}(q-p_1-p_2). \tag{B.8}$$

Hence, the cross section reads

$$\mathrm{d}\sigma=\frac{1}{8sN_C^2}\frac{\mathrm{d}Q^2}{2\pi}\,\mathrm{d}\Phi_1^h\,\mathrm{d}\Phi_2^l H_{\mu\nu}L^{\mu\nu}. \tag{B.9}$$

Both tensors obey the relation

$$q_\mu H^{\mu\nu}=q_\mu L^{\mu\nu}=0. \tag{B.10}$$

Since the leptonic part $\mathrm{d}\Phi_2^l L^{\mu\nu}$ can only depend on the four-vector q, we can deduce its Lorentz structure to be

$$\mathrm{d}\Phi_2^l L^{\mu\nu}=(q^2g^{\mu\nu}-q^\mu q^\nu)L(q^2). \tag{B.11}$$

Note that we can use this relation only for inclusive observables because we integrated over the lepton phase space. Hence, the cross section reads

$$\mathrm{d}\sigma=\frac{1}{8sN_C^2}\frac{\mathrm{d}Q^2}{2\pi}\,\mathrm{d}\Phi_1^h H_{\mu\nu}g^{\mu\nu}q^2L(q^2). \tag{B.12}$$

From (B.11), we find

$$q^2L(q^2)=\frac{1}{d-1}\,\mathrm{d}\Phi_2^l L^{\mu\nu}g_{\mu\nu}. \tag{B.13}$$

Using (C.11) and (C.13), we obtain

$$g_{\mu\nu}L^{\mu\nu}\,\mathrm{d}\Phi_2^l = -\frac{2\alpha}{Q^2}\left(\frac{4\pi}{Q^2}\right)^{\varepsilon}\frac{(1-\varepsilon)\Gamma(1-\varepsilon)}{(1-2\varepsilon)\Gamma(1-2\varepsilon)}. \tag{B.14}$$

Therefore, the cross section in 4 dimensions reads

$$\mathrm{d}\sigma = \frac{1\alpha}{12sN_C^2}\frac{\mathrm{d}Q^2}{2\pi}\frac{1}{Q^2}\,\mathrm{d}\Phi_1^h H_{\mu\nu}g^{\mu\nu}. \tag{B.15}$$

Using the identity (s. section C.3)

$$\int_{-\infty}^{\infty}\mathrm{d}q^0\,\delta(q^2-Q^2)\theta(q^0) = \frac{1}{2q^0}, \tag{B.16}$$

we can write

$$\mathrm{d}\Phi_1^h = 2\pi\delta(s-Q^2),\ s=q^2=(k_1+k_2)^2. \tag{B.17}$$

The hadronic part is given by

$$g^{\mu\nu}H_{\mu\nu} = -16\pi\alpha N_C s. \tag{B.18}$$

In total, we find

$$\frac{\mathrm{d}\sigma}{\mathrm{d}Q^2} = \frac{4\pi\alpha^2}{3N_CQ^2}\delta(s-Q^2). \tag{B.19}$$

The only virtual QCD correction is the vertex correction in Figure B.2a and the counter-term contribution in Figure B.2b. Hence only the hadronic tensor changes. In the following, we use mass regularization to regulate infrared divergences and dimensional regularization for the UV renormalization.

Vertex Correction The matrix element for the 1-loop vertex in Figure B.2a is given by

$$\mathcal{M}_v^{\nu} = -gg_s^2\mu^{\frac{3}{2}(4-d)}\int\frac{\mathrm{d}^dk}{(2\pi)^d}\frac{\bar{u}(k1)\gamma^{\mu}\not{k}'\gamma^{\nu}\not{k}\gamma_{\mu}u(k_2)}{[(k_2-k)^2-\lambda^2]\,[k'^2-m_1^2]\,[k^2-m_2^2]}, \tag{B.20}$$

where we neglected masses in the numerator because we only want to use them as regulators, i.e. $m \ll \not{p}$. We also introduced the fictitious gluon mass λ as regulator. This is possible because we could also replace the gluon by a photon. In general, this is not possible for non-abelian gauge theories. Note that we ignore the color factor at this point.

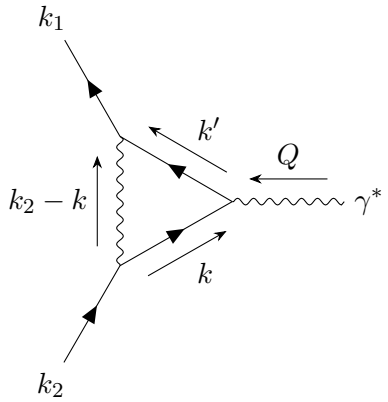

(a) vertex correction

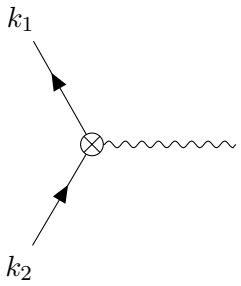

(b) vertex counter term

Figure B.2.: virtual contribution to the NLO matrix element

The order α_s part of the hadronic tensor is given by

$$g_{\mu\nu}H_1^{\mu\nu} = g_{\mu\nu}\mathcal{M}_v^{\nu}\mathcal{M}_b^{*,\mu} = -ig^2 g_s^2 \mu^{2(4-d)} \int \frac{\mathrm{d}^d k}{(2\pi)^d} \frac{\mathrm{tr}\left\{\not{k}_2\gamma^\mu \not{k}_1 \gamma^\alpha \not{k}'\gamma_\mu \not{k}\gamma_\alpha\right\}}{[(k_2-k)^2-\lambda^2]\,[k'^2-m_1^2]\,[k^2-m_2^2]}. \tag{B.21}$$

We evaluate the trace in the numerator in d dimensions and find

$$\begin{aligned}\mathrm{tr}\{\dots\} = -16(\varepsilon-1)(k_1\cdot l(\varepsilon k_2^2 + (\varepsilon+2)\frac{s}{2} - 2k_2\cdot l) \\ + \frac{s}{2}(-\varepsilon l\cdot k_1 + \varepsilon l^2 - 2k_2\cdot l + s) - \varepsilon k_1^2(k_2\cdot l + k_2^2)),\end{aligned} \tag{B.22}$$

where we used $s = 2k_1\cdot k_2$, $q = -k_1 - k_2$ and $k = l + k_2$. The next step is to reduce the integral to scalar integrals in a Passarino-Veltman [149] like way. To do this, we write the denominator of the integral as

$$D = d_1 d_2 d_3 = \left[l^2-\lambda^2\right]\left[(k_1-l)^2 - m_1^2\right]\left[(k_2+k)^2-m_2^2\right]. \tag{B.23}$$

We use now fact that we can rewrite the numerator in terms of d_i. We find,

$$\begin{aligned}-2(k_1\cdot l)(k_2\cdot l) &= \frac{1}{2}\left(d_2 d_3 - d_1 d_2 + (m_2^2 - k_2^2 - \lambda^2)d_2\right) \\ &\quad - (k_2\cdot l)d_1 + (m_2^2 - k_2^2 - \lambda^2), &\text{(B.24)}\\ -2k_1\cdot l &= d_2 - k_1^2 - d_1 - \lambda^2 + m_1^2, &\text{(B.25)}\\ 2k_2\cdot l &= d_3 - k_2^2 - d_1 - \lambda^2 + m_2^2, &\text{(B.26)}\\ l^2 &= d_1 + \lambda^2. &\text{(B.27)}\end{aligned}$$

We do not replace the $k_1 \cdot l$ term in (B.24) with (B.26) because it would lead to a term which does not cancel with the denominator. Since we use the masses only as regulators, we can neglect them in the numerator and set the external momenta k_1^2 and k_2^2 to zero. We will see later that this is justified. We obtain

$$\begin{aligned} g_{\mu\nu} H_1^{\mu\nu} = &- ig^2 g_s^2 \mu^{2(4-d)} \int \frac{\mathrm{d}^d l}{(2\pi)^d} \left[\frac{8s^2(1-\varepsilon)}{d_1 d_2 d_3} + \right. \\ &+ \frac{8s(\varepsilon-1)}{d_1 d_2} + \frac{8s(\varepsilon-1)}{d_1 d_3} + \frac{16s - 8s\varepsilon(\varepsilon+1) + 16(\varepsilon-1)(k_2 \cdot l)}{d_2 d_3} + \\ &\left. + \frac{8(1+\varepsilon)}{d_1} + \frac{8(\varepsilon-1)}{d_3} \right]. \end{aligned} \tag{B.28}$$

Introducing the basic scalar integrals A_0, B_0, C_0 from Appendix G, we obtain

$$\begin{aligned} g_{\mu\nu} H_1^{\mu\nu} = &g^2 g_s^2 \frac{\mu^{4-d}}{16\pi^2} \Bigg[8s^2(1-\varepsilon) C_0(k_1, k_2, \lambda, m_1, m_2) + 8s(\varepsilon-1) B_0(-k_1, \lambda, m_1) \\ &+ 8s(\varepsilon-1) B_0(k_2, \lambda, m_2) + (16s - 8s\varepsilon(\varepsilon+1)) B_0(-k_1-k_2, m_1, m_2) \\ &+ 8(1+\varepsilon) A_0(\lambda) + 8(\varepsilon-1) A_0(m_2) + 16(\varepsilon-1) \frac{(2\pi\mu)^{4-d}}{i\pi^2} \int \mathrm{d}^d l \frac{k_2 \cdot l}{d_2 d_3} \Bigg]. \end{aligned} \tag{B.29}$$

To express the last remaining integral in terms of A_0 and B_0 we write

$$\begin{aligned} \frac{(2\pi\mu)^{4-d}}{i\pi^2} \int \mathrm{d}^d l \frac{k_2 \cdot l}{d_2 d_3} &= \frac{(2\pi\mu)^{4-d}}{i\pi^2} \int \mathrm{d}^d k \frac{k_2^2 - k_2 \cdot k}{(k^2 - m_2^2)\left[(k_1 + k_2 - k)^2 - m_1^2\right]} \\ &= k_2^2 B_0(-k_1-k_2, m_1, m_2) - k_{2,\mu} B^\mu(-k_1-k_2, m_1, m_2), \end{aligned} \tag{B.30}$$

where we introduced the vector-like two point function B^μ defined in (G.16). Neglecting mass terms we find

$$\frac{(2\pi\mu)^{4-d}}{i\pi^2} \int \mathrm{d}^d l \frac{k_2 \cdot l}{d_2 d_3} = \frac{1}{4} \left[A_0(m_2) - A_0(m_1) + s B_0(-k_1-k_2, m_2, m_1) \right]. \tag{B.31}$$

The hadronic tensor in terms of scalar integrals is given by

$$\begin{aligned} g_{\mu\nu} H_1^{\mu\nu} = g^2 g_s^2 \frac{\mu^{2\varepsilon}}{16\pi^2} 4(1-\varepsilon) \Big[&2s^2 C_0(k_1, k_2, \lambda, m_1, m_2) + 2A_0(\lambda) - A_0(m_1) - A_0(m_2)) \\ &+ (2\varepsilon+3) s B_0(-k_1-k_2, m_1, m_2) - 2s B_0(-k_1, \lambda, m_1) - 2s B_0(k_2, \lambda, m_2) \Big], \end{aligned} \tag{B.32}$$

where we used $B_0(q, m_1, m_2) = B_0(q, m_2, m_1)$. Finally, we find

$$g_{\mu\nu}H_1^{\mu\nu} = g^2 g_s^2 \frac{\mu^{2\varepsilon}}{16\pi^2} 4(1-\varepsilon)s \times \\ \times \left(\Delta_\varepsilon - 2sC_0(k_1, k_2, \lambda, m_1, m_2) + 3\log\frac{s}{\mu^2} - 2\log\frac{m_1^2}{\mu^2} - 2\log\frac{m_2^2}{\mu^2} \right) \tag{B.33}$$

Counter Term The contribution from the vertex counter term is given by

$$\begin{aligned} g_{\mu\nu}H_2^{\mu\nu} &= g^2\mu^{2\varepsilon}\delta_1 \operatorname{tr}\{\not{k}_1\gamma^\mu\not{k}_2\gamma_\mu\} \\ &= 4s(1-\varepsilon)\delta_1 g^2\mu^{2\varepsilon}. \end{aligned} \tag{B.34}$$

We have to determine the renormalization coefficient δ_1 from the (on-shell) renormalization conditions. It follows from the Ward identities that $\delta_1 = \delta_2$ (s. e.g. [91]). Therefore, we can use the renormalization conditions

$$\left[-i\Sigma_2(p) + i(\not{p} - m)\delta_2 - i\delta_m\right]_{\not{p}=m} = 0, \tag{B.35}$$

$$\frac{\mathrm{d}}{\mathrm{d}\not{p}}\left[-i\Sigma_2(p) + i(\not{p} - m)\delta_2 - i\delta_m\right]_{\not{p}=m} = 0 \tag{B.36}$$

to calculate δ_1, i.e.

$$\delta_1 = \delta_2 = \left.\frac{\mathrm{d}}{\mathrm{d}\not{p}}\Sigma_2(p)\right|_{\not{p}=m}. \tag{B.37}$$

The fermion self energy is given by

$$\Sigma_2 = ig^2\mu^{4-d}\int\frac{\mathrm{d}^d q}{(2\pi)^d}\frac{\gamma^\mu(\not{q}+m)\gamma_\mu}{(q^2-m^2)[(q-p)^2-\lambda^2]}. \tag{B.38}$$

We use the Clifford algebra to rewrite the numerator and express the integrals as two point functions

$$\begin{aligned} \Sigma_2 &= ig^2\mu^{4-d}\int\frac{\mathrm{d}^d q}{(2\pi)^d}\frac{-(2-d)\not{q}+dm}{(q^2-m^2)[(q-p)^2-\lambda^2]} \\ &= -\frac{g^2}{16\pi^2}\left[(2-d)\gamma^\mu B_\mu(-p, m, \lambda) - dmB_0(-p, m, \lambda)\right]. \end{aligned} \tag{B.39}$$

When we use (G.15) and (G.21), we find

$$\delta_1 = \frac{\alpha}{4\pi}\left[-\Delta_\varepsilon + \frac{1}{2}\log\frac{m_1^2}{\mu^2} + \frac{1}{2}\log\frac{m_2^2}{\mu^2} - 2\log\frac{\lambda}{m_1} - 2\log\frac{\lambda}{m_2} - 4\right], \tag{B.40}$$

where $\Delta_\varepsilon = \frac{1}{\varepsilon} - \gamma_E + \log 4\pi$ and we split the fermion mass logarithms symmetrically.

Combining the counter term contribution with the vertex correction, we find

$$\begin{aligned}\mathrm{Re}(g_{\mu\nu}H_v^{\mu\nu}) = 4s\alpha\alpha_s N_C C_F \Bigg[&-\frac{3}{2}\log\frac{m_1^2}{\mu^2} - \frac{3}{2}\log\frac{m_2^2}{\mu^2} - 2\log\frac{\lambda}{m_1} - 2\log\frac{\lambda}{m_2} \\ &- \left(\log\frac{m_1^2}{s} + \log\frac{m_2^2}{s}\right)\log\frac{\lambda^2}{s} \\ &+ \frac{1}{2}\log^2\frac{m_1^2}{s} + \frac{1}{2}\log^2\frac{m_2^2}{s} + 3\log\frac{s}{\mu^2} - 4 + \frac{4}{3}\pi^2\Bigg], \end{aligned} \tag{B.41}$$

where we added the color factor and $H_v^{\mu\nu} = H_1^{\mu\nu} + H_2^{\mu\nu}$. Since the UV pole cancels due to renormalization, we state the result in four dimensions. Only logarithmic IR divergences for $\lambda, m \to 0$ are left. These divergent logarithms have to cancel with logarithms from real radiation. In total, we obtain

$$\begin{aligned}\frac{\mathrm{d}\sigma}{\mathrm{d}Q^2} = \frac{4\pi\alpha^2}{3N_C Q^2}\delta(s-Q^2)\Bigg\{1 + \frac{\alpha_s}{2\pi}C_F\Bigg[&-\frac{3}{2}\log\frac{m_1^2}{\mu^2} - \frac{3}{2}\log\frac{m_2^2}{\mu^2} - 2\log\frac{\lambda}{m_1} - 2\log\frac{\lambda}{m_2} \\ &- \left(\log\frac{m_1^2}{s} + \log\frac{m_2^2}{s}\right)\log\frac{\lambda^2}{s} \\ &+ \frac{1}{2}\log^2\frac{m_1^2}{s} + \frac{1}{2}\log^2\frac{m_2^2}{s} + 3\log\frac{s}{\mu^2} - 4 + \frac{4}{3}\pi^2\Bigg]\Bigg\} \end{aligned} \tag{B.42}$$

as cross-section contribution from born and virtual diagrams.

We can also interpret the hadronic tensor as production of a massive photon. The squared born matrix element is given by

$$|\mathcal{M}_b|^2 = -\frac{1}{4N_C^2} g_{\mu\nu}H^{\mu\nu} = \frac{4\pi\alpha s}{N_C} \tag{B.43}$$

and the virtual matrix element in mass regularization reads

$$\begin{aligned}\mathcal{V}_m = 2\,\mathrm{Re}\,(\mathcal{M}_v\mathcal{M}_b^*) &= -\frac{1}{2N_C^2}\,\mathrm{Re}(g_{\mu\nu}H_v^{\mu\nu}) \\ &= \frac{\alpha_s}{2\pi}C_F|\mathcal{M}_b|^2\bigg[-\frac{3}{2}\log\frac{m_1^2}{\mu^2}-\frac{3}{2}\log\frac{m_2^2}{\mu^2}-2\log\frac{\lambda}{m_1}-2\log\frac{\lambda}{m_2} \\ &\qquad -\left(\log\frac{m_1^2}{s}+\log\frac{m_2^2}{s}\right)\log\frac{\lambda^2}{s} \\ &\qquad +\frac{1}{2}\log^2\frac{m_1^2}{s}+\frac{1}{2}\log^2\frac{m_2^2}{s}+3\log\frac{s}{\mu^2}-4+\frac{4}{3}\pi^2\bigg] \qquad \text{(B.44)}\end{aligned}$$

In section 4.3, we define a conversion rule for virtual matrix elements from mass regularization to dim. reg.. The conversion part for Drell-Yan reads

$$\begin{aligned}\Delta = C_F|\mathcal{M}_b|^2\bigg[&-2\log\frac{\lambda^2}{\mu^2}-\frac{1}{2}\log\frac{m_1^2}{\mu^2}-\frac{1}{2}\log\frac{m_2^2}{\mu^2}+\frac{1}{2}\log^2\frac{m_1^2}{\mu^2}+\frac{1}{2}\log^2\frac{m_2^2}{\mu^2} \\ &-\log\frac{m_1^2m_2^2}{s^2}\log\frac{\lambda^2}{\mu^2}+4+\frac{\pi^2}{3}\bigg], \qquad \text{(B.45)}\end{aligned}$$

where we replaced the charge by the color factor. The finite part of the virtual matrix element contribution in dim. reg. reads

$$\mathcal{V}_{dr} = \mathcal{V}_m - \frac{\alpha_s}{2\pi}\Delta = \frac{\alpha_s}{2\pi}C_F|\mathcal{M}_b|^2\left[-\log^2\frac{\mu^2}{s}+3\log\frac{s}{\mu^2}-8+\pi^2\right] \qquad \text{(B.46)}$$

which is the same result as in (6.1).

C. Phase Space

C.1. Spherical Coordinates in n Dimensions

We define n dimensional spherical coordinates

$$\begin{aligned} x_1 &= r\sin\phi_0\sin\phi_1\sin\phi_2\cdots\sin\phi_{n-2}, \\ x_2 &= r\cos\phi_0\sin\phi_1\sin\phi_2\cdots\sin\phi_{n-2}, \\ x_3 &= r\cos\phi_1\sin\phi_2\cdots\sin\phi_{n-2}, \\ &\vdots \\ x_{n-2} &= r\cos\phi_{n-4}\sin\phi_{n-3}\sin\phi_{n-2}. \\ x_{n-1} &= r\cos\phi_{n-3}\sin\phi_{n-2}, \\ x_n &= r\cos\phi_{n-2}, \end{aligned} \tag{C.1}$$

where $\phi_0 \in [0, 2\pi)$ is an azimuthal and all other angles ϕ_n are in the range $[0, \pi]$. The determinant of the Jacobian is given by

$$|J(r, \phi_0, \{\phi_i\})| = r^{n-1} \prod_{i=1}^{n-2} (\sin\phi_i)^i \,. \tag{C.2}$$

We define

$$\phi = \phi_{n-3}, \tag{C.3}$$

$$\theta = \phi_{n-2}. \tag{C.4}$$

The physical quantities in 4 dimensions can only depend on two angles. Therefore, we can set all angles but two to zero. We choose the angles ϕ and θ to be non-zero because then vectors are similar to three dimensional vectors, i.e.

$$\vec{x} = \begin{pmatrix} \vec{0}_{n-3} \\ r\sin\theta\sin\phi \\ r\sin\theta\cos\phi \\ r\cos\theta \end{pmatrix}. \tag{C.5}$$

Since the physical quantities cannot depend on any angle except ϕ and θ, we can perform almost all integrations in the volume element. Using

$$\int_0^\pi \mathrm{d}\phi \, \sin^n \phi = \sqrt{\pi} \frac{\Gamma\left(\frac{n+1}{2}\right)}{\Gamma\left(\frac{n+2}{2}\right)}, \tag{C.6}$$

we obtain

$$\begin{aligned} \int_0^{2\pi} \mathrm{d}\phi_0 \int_0^\pi \mathrm{d}\phi_i \prod_{i=1}^{n-4} (\sin\phi_i)^i &= 2\pi\sqrt{\pi}^{n-2} \frac{\Gamma(1)}{\Gamma\left(\frac{3}{2}\right)} \frac{\Gamma\left(\frac{3}{2}\right)}{\Gamma(2)} \cdots \frac{\Gamma\left(\frac{n-3}{2}\right)}{\Gamma\left(\frac{n-2}{2}\right)} \\ &= 2\pi \frac{\sqrt{\pi}^{n-4}}{\Gamma\left(\frac{n-2}{2}\right)}. \end{aligned} \tag{C.7}$$

The volume element for spherical coordinates in n dimension reads

$$\int \mathrm{d}^n x f(r,\theta,\phi) = 2\pi \frac{\sqrt{\pi}^{n-4}}{\Gamma\left(\frac{n-2}{2}\right)} \int_0^\infty \mathrm{d}r \int_0^\pi \mathrm{d}\phi \int_0^\pi \mathrm{d}\theta \, r^{n-1} \sin^{n-3}\phi \sin^{n-2}\theta f(r,\theta,\phi), \tag{C.8}$$

where f is an arbitrary function.

C.2. Integrating the Momentum in d-1 Dimensions

Using spherical coordinates and $|\vec{k}| = E$, we find

$$\frac{\mathrm{d}^{d-1}\vec{k}}{(2\pi)^{d-1}2E} = \frac{1}{(2\pi)^{d-1}2E} E^{d-2} \, \mathrm{d}E \, \mathrm{d}\Omega_{d-2}, \tag{C.9}$$

where

$$\mathrm{d}\Omega_{d-2} = 2\pi \frac{\sqrt{\pi}^{d-5}}{\Gamma\left(\frac{d-3}{2}\right)} \sin^{d-4}\phi \sin^{d-3}\theta \, \mathrm{d}r \, \mathrm{d}\phi \, \mathrm{d}\theta. \tag{C.10}$$

Next, we can rewrite (C.9) as

$$\frac{\mathrm{d}^{d-1}\vec{k}}{(2\pi)^{d-1}2E} = \mathrm{d}\xi \, \mathrm{d}y \, \mathrm{d}\phi \frac{s^{1-\varepsilon} 2^{-5+4\varepsilon} \pi^{-\frac{5}{2}+\varepsilon}}{\Gamma\left(\frac{1}{2}-\varepsilon\right)} (1-y^2)^{-\varepsilon} \xi^{1-2\varepsilon} \sin^{-2\varepsilon}\phi, \tag{C.11}$$

where we defined $y = \cos\theta_{d-3}$, $\xi = \frac{2E}{\sqrt{s}}$ with $\xi \in [0,1]$, $y \in [-1,1]$ and $\phi \in [0,\pi]$. After performing the ϕ integration, we obtain

$$\frac{\mathrm{d}^{d-1}\vec{k}}{(2\pi)^{d-1}2E} = \mathrm{d}\xi\,\mathrm{d}y \frac{s^{1-\varepsilon}2^{-5+4\varepsilon}\pi^{-2+\varepsilon}}{\Gamma(1-\varepsilon)}(1-y^2)^{-\varepsilon}\xi^{1-2\varepsilon}. \tag{C.12}$$

C.3. Phase-Space Identity

In this section we show that

$$\int_{-\infty}^{\infty}\mathrm{d}p^0\,\delta\left(p^2-M^2\right)\theta(p^0) = \frac{1}{2p^0}. \tag{C.13}$$

To prove (C.13), we rewrite the delta distribution using $p^2 = E^2 - \vec{p}^2$

$$I = \int_{-\infty}^{\infty}\mathrm{d}E\,\delta\left(p^2-M^2\right)\theta(E) = \int_{-\infty}^{\infty}\mathrm{d}E\,\delta\left(E^2-\vec{p}^2-M^2\right)\theta(E). \tag{C.14}$$

Next, we rewrite the delta distribution such that the argument depends on the integration variable E only linearly. Hence, we obtain

$$I = \int_{-\infty}^{\infty}\mathrm{d}E\,\frac{\delta\left(E-\sqrt{\vec{p}^2+M^2}\right)}{2\sqrt{\vec{p}^2+M^2}}\theta(E) + \int_{-\infty}^{\infty}\mathrm{d}E\,\frac{\delta\left(E+\sqrt{\vec{p}^2+M^2}\right)}{2\sqrt{\vec{p}^2+M^2}}\theta(E). \tag{C.15}$$

Only the first integral is not zero, therefore, we obtain

$$I = \frac{1}{2E} \tag{C.16}$$

and (C.13) is proven.

D. Monte-Carlo Methods

In this appendix we describe Monte-Carlo methods that are used to generate Monte-Carlo events and are relevant for this work. A more detailed description of standard Monte-Carlo techniques can be found in [81].

D.1. Rejection Sampling

Rejection sampling is a Monte-Carlo method to generate events according to a density p. The algorithm for *rejection sampling* reads as follows

1. Sample a random point x from a uniform distribution.
2. Sample a random point y between 0 and the absolute maximum of p.
3. Accept the point x if $y < p(x)$ otherwise reject x and return to step 1.

The points x are then distributed according to the density $p(x)$.

This method is useful for event unweighting. The differential cross section $\mathrm{d}\sigma$ parametrizes the probability for a specific phase-space configuration Φ. The cross section value $\mathrm{d}\sigma(\Phi)$ is the *weight* for the phase-space point Φ. We only accept a phase-space point Φ if $y < \mathrm{d}\sigma$, where y is uniformly distributed random number between zero and $\mathrm{d}\sigma_{\mathrm{max}}$. The accepted events are called *unweighted events* and correspond to physical events. We can improve the unweighting performance when we use a density g that approximates $\mathrm{d}\sigma$ closely to sample phase-space points Φ. The advantage is that the number of rejected phase-space points is minimized. The rejection criterion is then $cg(\Phi)y < \mathrm{d}\sigma(\Phi)$ where y is uniformly distributed random number in $[0, 1]$ and c is a constant that ensures $cg(\Phi) \geq \mathrm{d}\sigma(\Phi)$ for all Φ.

D.2. Monte-Carlo integration

To calculate cross sections we have to integrate higher-dimensional functions numerically. The best way to perform the integration is to use *Monte Carlo integration. Monte Carlo*

integration uses the fact that an integral can be approximated by

$$I = \int_0^1 \mathrm{d}x\, f(x) \approx \frac{1}{N} \sum_{i=1}^{N} f(x_i), \tag{D.1}$$

where N is large and x_i are uniformly distributed random numbers between zero and one.

D.2.1. Importance Sampling

In order to improve a Monte-Carlo integration we can attempt to transform the integral such that the integrand is flat

$$I = \int_a^b \mathrm{d}x\, f(x) \to I = \int_0^1 \mathrm{d}y\, J(y) f(x(y)), \tag{D.2}$$

where $J = \frac{\mathrm{d}x}{\mathrm{d}y}$ is the Jacobian determinant of the transformation. If $J(y)f(x(y))$ is flat (i.e. $J(y) \propto f(x(y))$) the error of the Monte-Carlo integration is zero. Unfortunately, we can only perform the transformation if we can solve the integral analytically. However, it can be possible to find a transformation which makes the integrand flatter if we have at least some knowledge about the function f. This procedure is equivalent to use random numbers which are not distributed uniformly in $[0, 1]$ because we transform the uniformly distributed random numbers before using them in f. Since $\mathrm{d}x f(x) \propto \mathrm{d}y$ regions where x is large become large regions in y. Therefore, it is more likely to draw random numbers in regions where $f(x)$ is large. Since these regions are most important for the value of the integral, this technique is called *importance sampling*.

VEGAS Algorithm

To find a good probability distribution for importance sampling, we would have to know the structure of the integrand. The VEGAS algorithm [150, 151] can be used to determine a distribution without a-priori knowledge about the integrand. VEGAS uses a setup phase, where integrand values are histogrammed and the resulting histograms are used to refine the probability function. In order to be space efficient the algorithm assumes that the optimal distribution is separable, i.e. $p(\vec{x}) = p_1(x_1)p_2(x_2)\dots p_d(x_d)$. Hence, the space efficiency is $\mathcal{O}(d)$ instead of $\mathcal{O}(2^d)$, where d is the dimension of the integral. The efficiency of the VEGAS algorithm depends on the validity of the assumption of a separable integrand.

Monte Carlo integration can be parallelized efficiently because the sum in (D.1) can

be split into multiple sums, i.e.

$$\sum_{i=1}^{N} f(x_i) = \sum_{i=1}^{\tilde{N}_1} f(x_i) + \sum_{i=\tilde{N}_1+1}^{\tilde{N}_2} f(x_i) + \cdots + \sum_{i=\tilde{N}_{n-1}+1}^{\tilde{N}_n} f(x_i), \tag{D.3}$$

where $\tilde{N}_k = \sum_{i=1}^{k} N_i$ and $\tilde{N}_n = N$. Each sum in (D.3) can be evaluated in a separate computing thread independently from all other sums. Once all sums are evaluated, a (master) thread has to collect all results from the other threads and combine them. We improved the standard VEGAS algorithm such that it uses the *Message Passing Interface* (MPI) [152, 153] to distribute the evaluation of the integrand to n processes. Once all evaluations completed, the master thread is responsible for refining the probability function and calculating the integral value. Using MPI allows us to distribute the evaluation to multiple machines. Hence, we could run our program on the RWTH compute cluster by the IT Center of RWTH Aachen university.

D.3. Sampling Random Variables for Powheg Radiation

This section follows the discussion in [47] appendix A and [82] appendix C. A special case of the veto algorithm can be found in [72] section 4.2.

We want to to sample random variables according to

$$f(\mathbf{x})\Delta(h(\mathbf{x})), \tag{D.4}$$

where $h(\mathbf{x}), f(\mathbf{x}) \geq 0$ and

$$\Delta(h) = \exp\left\{-\int \mathrm{d}^d\mathbf{x}' f(\mathbf{x}')\theta(h(\mathbf{x}') - h)\right\}. \tag{D.5}$$

The integral in the exponential function makes it difficult to generate random numbers according to this distribution because we would have to evaluate this integral for every random number we generate. If this integral is not analytically solvable, we would have to perform a numerical integration which is time consuming. Therefore, we have to find a way to sample random variables without evaluating this integral explicitly.

We notice that we can write

$$p(h) = \frac{\mathrm{d}\Delta(h)}{\mathrm{d}h} = \int \mathrm{d}^d\mathbf{x} f(\mathbf{x})\Delta(h(\mathbf{x}))\delta(h(\mathbf{x}) - h) \tag{D.6}$$

and use this as probability density. The cumulative distribution function is given by

$$P(h) = \int_0^h \mathrm{d}h'\, p(h) = \Delta(h) - \Delta(0). \tag{D.7}$$

If we assume that the integral in the exponential function in Δ is divergent, we have

$$\Delta(0) = \exp\left\{ - \int \mathrm{d}^d\mathbf{x}' f(\mathbf{x}') \right\} = 0 \tag{D.8}$$

and due to the exponential form of Δ, we have

$$\lim_{h\to\infty} \Delta(h) = 1. \tag{D.9}$$

We are now able to sample random numbers H according to the distribution $p(h)$ when we use the inversion method, i.e. we have to pick a uniformly distributed random number u in the interval $[0, 1]$ and solve

$$\Delta(H) = u \tag{D.10}$$

for H. The number H is distributed according to $p(h)$. When we have generated a value H, we have restricted $\mathbf{x}$ to a surface in the $\mathbf{x}$ space where $h(\mathbf{x}) = H$. The probability to sample H is given by

$$p(H) = \left.\frac{\mathrm{d}\Delta(h)}{\mathrm{d}h}\right|_{h=H} = \int \mathrm{d}^d x f(\mathbf{x}) \Delta(H) \delta(h(\mathbf{x}) - H). \tag{D.11}$$

This is the sum (integral) of all probabilities on the surface $h(\mathbf{x}) = H$. Therefore, the contribution of one particular point $\mathbf{x}$ is given by a probability density proportional to

$$f(\mathbf{x})\delta(h(\mathbf{x}) - H), \tag{D.12}$$

where the factor $\Delta(H)$ is omitted because it does not depend on $\mathbf{x}$. Therefore, we have to sample $\mathbf{x}$ according to this distribution.

Example We use the function

$$f(x, y) = \frac{1}{xy}, \tag{D.13}$$

where $x, y \in [0, 1]$. These functions are singular for $x \to 0$ and $y \to 0$. We choose

$$h(x, y) = xy \tag{D.14}$$

to have a lower bound on x and y. We can solve the integrals in Δ analytically

$$\begin{aligned}\Delta(h) &= \exp\left\{-\int_0^1 \mathrm{d}x \int_0^1 \mathrm{d}y \, \frac{1}{xy}\theta(xy-h)\right\} \\ &= \exp\left\{-\int_h^1 \mathrm{d}x \int_{\frac{h}{x}}^1 \mathrm{d}y \, \frac{1}{xy}\right\} \\ &= \exp\left\{-\frac{1}{2}\log^2 h\right\}.\end{aligned} \tag{D.15}$$

When we solve (D.10) for H, we obtain

$$H = \exp\left\{-\sqrt{-2\log u}\right\}, \tag{D.16}$$

where u is an uniformly distributed random number in $[0,1]$ as solution for $H \leq 1$. Now we want to generate x, y according to

$$p(x,y) = \frac{1}{N}\frac{1}{xy}\delta(xy-H), \tag{D.17}$$

where N is normalization constant. We can sample random numbers x from the density

$$p_x(x) = \frac{1}{xN}\int_0^1 \mathrm{d}y \, \frac{1}{y}\delta(xy-H) = \frac{1}{NHx}\theta\left(1-\frac{H}{x}\right). \tag{D.18}$$

The cumulative distribution function is

$$P_x(x) = \frac{1}{NH}\log\frac{x}{H} \tag{D.19}$$

From this we can obtain the normalization factor

$$\frac{1}{N} = -\frac{H}{\log H} \tag{D.20}$$

Using the inversion method, we obtain a random number x by solving

$$P_x(x) = u_2 \Leftrightarrow x = H^{1-u_2}, \tag{D.21}$$

where u_2 is a uniformly distributed random number in $[0,1]$. The delta function in (D.18) gives

$$y = H^{u_2} \tag{D.22}$$

D.3.1. Veto Method

When we want to apply the method from the previous section, we have to solve (D.10) for H. In order to do that we have to calculate the integral in (D.5) analytically. However, this is often not possible. We describe in this section the veto method which we can use to sample random numbers even if we cannot solve the integral analytically.

We have to find a function $F(x)$ for which we can solve the integral analytically. The function F has to be an upper bounding function of f, i.e.

$$f(x) \leq F(x). \tag{D.23}$$

First, we sample random numbers according to the density

$$p_F(\mathbf{x}) = F(\mathbf{x})\Delta_F(h(\mathbf{x})), \tag{D.24}$$

where

$$\Delta_F(h) = \exp\left\{-\int \mathrm{d}^d\mathbf{x}' F(\mathbf{x}')\theta(h(\mathbf{x}') - h)\right\}. \tag{D.25}$$

We use the sampled random numbers $\mathbf{x}$ only with a probability of $\frac{f(\mathbf{x})}{F(\mathbf{x})}$. Therefore, the probability for an accepted $\mathbf{x}$ is given by

$$p_0(\mathbf{x}) = f(\mathbf{x})\Delta_F(h(\mathbf{x})) = \int_0^{h_{\max}} \mathrm{d}h\, \Delta_F(h)\delta(h(\mathbf{x}) - h)f(\mathbf{x}). \tag{D.26}$$

If $\mathbf{x}$ is rejected, we sample a new $\mathbf{x}'$ with the constraint that the new $h' = h(\mathbf{x}')$ is smaller than $h(\mathbf{x})$ from the rejected step. The probability for accepting the new $\mathbf{x}$ is

$$\begin{aligned} p_1(\mathbf{x}) = &\int \mathrm{d}^d x_0 \int_0^{h_{\max}} \mathrm{d}h\, \Delta_F(h)\delta(h(\mathbf{x}_0) - h)(F(\mathbf{x}_0) - f(\mathbf{x}_0)) \\ &\times \int_0^h \mathrm{d}h' \frac{\Delta_F(h')}{\Delta_F(h)}\delta(h(\mathbf{x}) - h')f(\mathbf{x}). \end{aligned} \tag{D.27}$$

The first line is the rejection probability integrated over all possible values $\mathbf{x}_0$ which may have been chosen in the rejected step. The ratio

$$\frac{\Delta_F(h')}{\Delta_F(h)} = \exp\left\{-\int \mathrm{d}^d x' F(\mathbf{x}') \left[\theta(h(\mathbf{x}') - h') - \theta(h(\mathbf{x}') - h)\right]\right\} \tag{D.28}$$

makes sure that the constraint $h(\mathbf{x}') < h$ is fulfilled in the exponential in Δ_F. We can

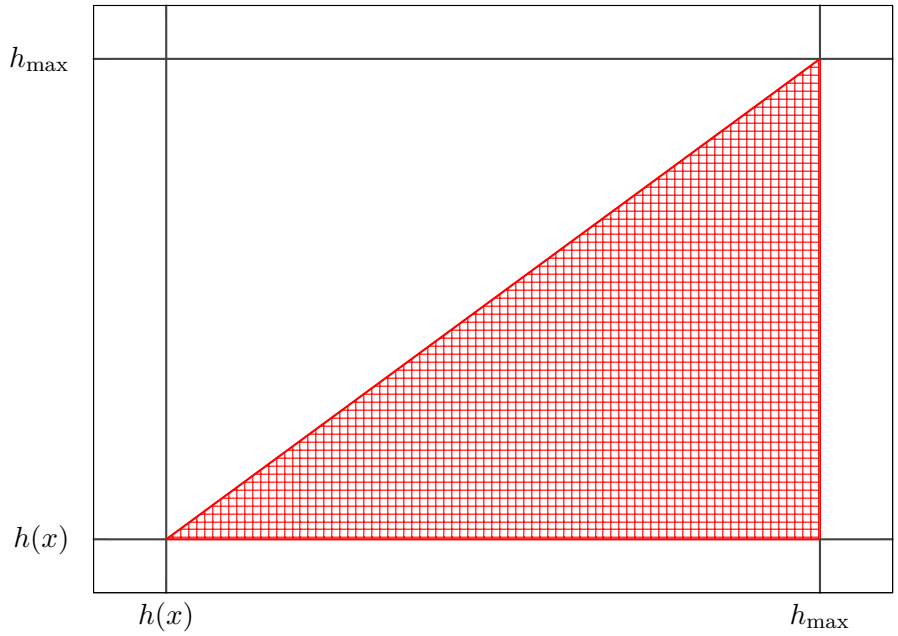

Figure D.1.: Integration area of the h, h' integration in (D.31)

simplify the probability so that

$$\begin{aligned} p_1(\mathbf{x}) &= \int_0^\infty \mathrm{d}h'\, \delta(h(\mathbf{x}) - h') f(\mathbf{x}) \Delta_F(h') \times \\ &\quad \times \int \mathrm{d}^d x_0 \int_0^\infty \mathrm{d}h\, (F(\mathbf{x}_0) - f(\mathbf{x}_0)) \delta(h(\mathbf{x}_0) - h) \theta(h' - h) \theta(h - h_{\max}) \\ &= p_0(\mathbf{x}) \int_{h(\mathbf{x})}^{h_{\max}} \mathrm{d}h\, g(h), \end{aligned} \tag{D.29}$$

where

$$g(h) = \int \mathrm{d}^d x (F(\mathbf{x}) - f(\mathbf{x})) \delta(h(\mathbf{x}) - h). \tag{D.30}$$

When we write down the probability for two rejections in the same way, we obtain

$$\begin{aligned} p_2(\mathbf{x}) = p_0(\mathbf{x}) \int \mathrm{d}^d x_0 \int \mathrm{d}^d x_1 \int_0^\infty \mathrm{d}h \int_0^\infty \mathrm{d}h'\, \delta(h(\mathbf{x}_0) - h)(F(\mathbf{x}_0) - f(\mathbf{x}_0)) \\ \times \delta(h(\mathbf{x}_1) - h')(F(\mathbf{x}_1) - f(\mathbf{x}_1)) \theta(h' - h(\mathbf{x})) \theta(h - h') \theta(h - h_{\max}). \end{aligned} \tag{D.31}$$

The integration area for the h, h' integration is shown in Figure D.1. Since the integrand is symmetric in $h \leftrightarrow h'$, the integral over the upper triangle has the same value as the integral in the lower triangle. Therefore, we can integrate in (D.31) over the square and multiply it with $\frac{1}{2}$ to correct for the integration over the upper triangle. We obtain

$$p_2(\mathbf{x}) = p_0(\mathbf{x})\frac{1}{2}\left[\int_{h(\mathbf{x})}^{h_{\max}} \mathrm{d}h\, g(h)\right]^2 \tag{D.32}$$

When we have more than two rejections, the probability has the same form as p_2. Therefore, we have

$$p_n(\mathbf{x}) = p_0(\mathbf{x})\frac{1}{n!}\left[\int_{h(\mathbf{x})}^{h_{\max}} \mathrm{d}h\, g(h)\right]^n \tag{D.33}$$

When we sum all contributions, we obtain

$$\begin{aligned} p(\mathbf{x}) &= \sum_{n=0}^{\infty} p_n(\mathbf{x}) = f(\mathbf{x})\Delta_F(h(\mathbf{x}))\exp\left\{\int_{h(\mathbf{x})}^{h_{\max}} \mathrm{d}h\, g(h)\right\} \\ &= f(\mathbf{x})\Delta_F(h(\mathbf{x}))\exp\left\{\int \mathrm{d}^d x'\theta(h(\mathbf{x}) - h(\mathbf{x}'))[F(\mathbf{x}') - f(\mathbf{x}'))]\right\} \\ &= f(\mathbf{x})\exp\left\{-\int \mathrm{d}^d x'\theta(h(\mathbf{x}) - h(\mathbf{x}'))f(\mathbf{x}')\right\}. \end{aligned} \tag{D.34}$$

This shows that we sample variables $\mathbf{x}$ according to distribution (D.5), when we use the described procedure.

To summarize, we present the algorithm which we can use to sample random numbers $\mathbf{x}$ according to (D.5).

function VETOMETHOD
  $x = 0$
  $h_{\max} = \sup\{h|\Delta_F(h) = 1\}$
  $h = h_{\max}$
  while true **do**
    $u =$ random(distribution = uniform in $[0, 1]$)
    $H =$ solve($\Delta_F(H) = \Delta_F(h)u$)
    $x =$ random(distribution = $F(x)\delta(H - h(x))$)
    $v =$ random(distribution = uniform in $[0, 1]$)
    if $v < \frac{f(x)}{F(x)}$ **then**
      return x
    end if
    $h = H$
  end while
end function

The efficiency of this algorithm depends on the upper bounding function $F(x)$. For $F(x) = f(x)$, the efficiency would be the best. Hence, the upper bound function F should be chosen as close to the function f as possible.

D.4. Highest-Bid Method

The highest-bid method is described in [154, Appendix A.2] and [47, Appendix B]. It is usually the case that we have multiple competing real flavor configurations for the hardest radiation. If we consider NLO QCD radiation from $q\bar{q} \to Z$, a gluon can be emitted by one of the quarks or a gluon from the proton can split into one of the initial-state quarks. The probability for the hardest radiation is then given by

$$p(x) = \sum_k f_k(x) \prod_i \Delta_i(k_T^k(x)), \tag{D.35}$$

where i and k label the possible regions (i.e. $q\bar{q} \to Zg$, $g\bar{q} \to Z\bar{q}$ and $qg \to Zq$). Hence, the Sudakov $\Delta_i(k)$ is the probability that no parton with $k_T > k$ was emitted by subprocess i. To generate events we have to pick a subprocess i and a value for x.

We generate values x_k according to the probability distribution

$$\Delta_k(k_T^k(x_k)) f_k(x_k) \tag{D.36}$$

and choose for x the x_k with the largest $k_T^k(x_k)$. This procedure works because the probability that x came from a subprocess i is given by the product of (D.36) and the no-splitting probability for all other subprocesses, i.e.,

$$p_i(x) = f_i(x)\Delta_i(k_T^i(x)) \times \prod_{n \neq i} \Delta_n(k_T^i(x)) = f_i(z) \prod_n \Delta_n(k_T^i(x)). \tag{D.37}$$

To obtain the total probability, we have to sum over the probabilities of the subprocesses

$$\sum_k p_k(x) = \sum_k f_k(x) \prod_i \Delta_i(k_T^k(x)) \tag{D.38}$$

which reproduces the probability for the hardest radiation (D.35).

E. Plus Distributions

The plus distributions $(\cdot)_+$ are used to split an integration with singularities into a finite and a divergent part. When we investigate, for example, the integral

$$I(\varepsilon) = \int_0^1 \mathrm{d}x \, \frac{f(x)}{x^{1+\varepsilon}}, \tag{E.1}$$

where f is a test function. We notice that the integral is divergent for $\varepsilon \to 0$ (if f is not proportional to x in the limit $x \to 0$). If we assume that we can express f as a power series, we can rewrite the integral as

$$\begin{aligned} I(\varepsilon) = \int_0^1 \mathrm{d}x \, \frac{f(x)}{x^{1+\varepsilon}} &= \int_0^1 \mathrm{d}x \, \frac{\sum_{n=0}^{\infty} a_n x^n}{x^{1+\varepsilon}} \\ &= \underbrace{\int_0^1 \mathrm{d}x \, \sum_{n=1}^{\infty} a_n x^{n-1} x^{-\varepsilon}}_{\text{finite}} + \underbrace{\int_0^1 \mathrm{d}x \, \frac{a_0}{x^{1+\varepsilon}}}_{\text{singular}}. \end{aligned} \tag{E.2}$$

Since the first term is finite, we can expand it in $\varepsilon = 0$. The coefficient a_0 of the power series is equal to $f(0)$. If we express the power series as $f(x)$ and $x^{-\varepsilon}$ as series around $\varepsilon = 0$, we obtain

$$\begin{aligned} I(\varepsilon) = \int_0^1 \mathrm{d}x \, \frac{f(x)}{x^{1+\varepsilon}} &= \int_0^1 \mathrm{d}x \, \sum_{n=0}^{\infty} \frac{(-\varepsilon \log x)^n}{n!} \frac{1}{x} [f(x) - f(0)] + f(0) \int_0^1 \mathrm{d}x \, x^{-1-\varepsilon} \\ &= \underbrace{\sum_{n=0}^{\infty} \frac{(-1)^n}{n!} \varepsilon^n \int_0^1 \mathrm{d}x \, \left(\frac{\log^n x}{x} \right)_+ f(x)}_{\text{finite}} - \frac{1}{\varepsilon} f(0), \end{aligned} \tag{E.3}$$

where we integrated the singular part and defined

$$\int_0^1 \mathrm{d}x \, (g(x))_+ \, f(x) = \int_0^1 \mathrm{d}x \, g(x) [f(x) - f(0)]. \tag{E.4}$$

We rewrite $f(0)$ using the δ-function and we obtain

$$\int_0^1 \mathrm{d}x \, x^{-1-\varepsilon} f(x) = \int_0^1 \mathrm{d}x \, \left[\sum_{n=0}^{\infty} \frac{(-1)^n}{n!} \varepsilon^n \left(\frac{\log^n x}{x} \right)_+ - \frac{1}{\varepsilon} \delta(x) \right] f(x). \tag{E.5}$$

Therefore, the integral is split into two parts, a singular part that is proportional to $\frac{1}{\varepsilon}$ and a regular term. Since we are interested in the limit $\varepsilon \to 0$, we find up to order $\mathcal{O}(1)$

$$I(\varepsilon) = \int_0^1 \mathrm{d}x\, x^{-1-\varepsilon} f(x) = \int_0^1 \mathrm{d}x \left[\left(\frac{1}{x}\right)_+ - \frac{1}{\varepsilon}\delta(x) \right] f(x). \tag{E.6}$$

if $f(x)$ has no poles in ε. In the following we give properties of plus distributions and how they can be modified.

E.1. Removing Non-Singular Parts from the Plus Distribution

We assume that we have an integral

$$\int_a^b \mathrm{d}x\, \left(f(x)s(x)\right)_+ t(x), \tag{E.7}$$

where $t(x)$ and $f(x)$ are test functions and $s(x)$ is a function which leads to a singularity at $x = a$. When we use the definition of the plus distribution and add a 0, we obtain

$$\int_a^b \mathrm{d}x\, s(x)f(x)t(x) - t(a)\int_a^b \mathrm{d}x\, f(x)s(x) + \underbrace{\left[f(a)t(a) - f(a)t(a)\right]\int_a^b \mathrm{d}x\, s(x)}_{=0}. \tag{E.8}$$

Combining the terms to plus distributions leads to

$$\int_a^b \mathrm{d}x\, \left(s(x)\right)_+ f(x)t(x) - t(a)\int_a^b \mathrm{d}x\, \left(s(x)\right)_+ f(x). \tag{E.9}$$

The integration in the second term is independent of the test function $t(x)$. Therefore, we can perform this integration and define

$$I = \int_a^b \mathrm{d}x\, \left(s(x)\right)_+ f(x). \tag{E.10}$$

If we reintroduce the $\mathrm{d}x$ integration in the second term, we obtain

$$\int_a^b \mathrm{d}x\, \left(f(x)s(x)\right)_+ t(x) = \int_a^b \mathrm{d}x\, \left(s(x)\right)_+ f(x)t(x) - I\int_a^b \mathrm{d}x\, \delta(x-a)t(x) \tag{E.11}$$

E.2. Plus Distributions with Theta Functions

If we perform the variable transformation $x' = (1-\xi)x$ in the first integral of

$$I = \int_0^1 \mathrm{d}x \int_0^1 \mathrm{d}\xi \left(\frac{1}{\xi}\right)_+ f(x)g(\xi) = \int_0^1 \mathrm{d}x \int_0^1 \mathrm{d}\xi \frac{1}{\xi} f(x)[g(\xi) - g(0)], \tag{E.12}$$

we obtain

$$I = \int_0^1 \mathrm{d}x' \int_0^{1-x'} \mathrm{d}\xi \frac{1}{\xi} \frac{1}{1-\xi} f\left(\frac{x'}{1-\xi}\right) g(\xi) - \int_0^1 \mathrm{d}x \int_0^1 \mathrm{d}\xi \frac{1}{\xi} f(x)g(0). \tag{E.13}$$

This is equivalent to

$$I = \int_0^1 \mathrm{d}x' \int_0^1 \mathrm{d}\xi \left(\frac{1}{\xi}\right)_+ \theta(1-\xi-x') \frac{1}{1-\xi} f\left(\frac{x'}{1-\xi}\right) g(\xi), \tag{E.14}$$

where the plus distribution acts on the θ function. It is possible to combine the first term with parts of the second term in (E.13), i.e.

$$I = \int_0^1 \mathrm{d}x' \int_0^{1-x'} \mathrm{d}\xi \frac{1}{\xi} \left[\frac{1}{1-\xi} f\left(\frac{x'}{1-\xi}\right) g(\xi) - f(x)g(0)\right] - \int_0^1 \mathrm{d}x \int_0^1 \mathrm{d}\xi \frac{1}{\xi} f(x)g(0). \tag{E.15}$$

The last term can be integrated analytically and yields

$$I = \int_0^1 \mathrm{d}x' \int_0^{1-x'} \mathrm{d}\xi \frac{1}{\xi} \left[\frac{1}{1-\xi} f\left(\frac{x'}{1-\xi}\right) g(\xi) - f(x)g(0)\right] + \int_0^1 \mathrm{d}x' \, g(0) f(x') \log(1-x'). \tag{E.16}$$

Forgetting the last term is a common mistake.

E.3. Distribution Expansion for the Collinear Singularities

The collinear term

$$I = \int_{-1}^1 \mathrm{d}y \, (1-y^2)^{-1-\varepsilon} f(y) \tag{E.17}$$

has singularities at $y = \pm 1$. To expand this term, we have to split the integration in two parts because the plus distribution can only subtract one singularity at a time. We split the integral at 0 because we want to use the fact that the term is even, i.e.

$$I = \int_{-1}^1 \mathrm{d}y \, (1-y^2)^{-1-\varepsilon} f(y) = \int_{-1}^0 \mathrm{d}y \, (1-y^2)^{-1-\varepsilon} f(y) + \int_0^1 \mathrm{d}y \, (1-y^2)^{-1-\varepsilon} f(y). \tag{E.18}$$

Each integral has only one singularity (at $y = +1$ or $y = -1$). We can substract the singularity separately in each integral:

$$I = \int_{-1}^{0} \mathrm{d}y \, (1-y^2)^{-1-\varepsilon} \left[f(y) - f(-1) \right] + \int_{0}^{1} \mathrm{d}y \, (1-y^2)^{-1-\varepsilon} \left[f(y) - f(1) \right] + \\ + f(1) \int_{0}^{1} \mathrm{d}y \, (1-y^2)^{-1-\varepsilon} + f(-1) \int_{-1}^{0} \mathrm{d}y \, (1-y^2)^{-1-\varepsilon}. \quad \text{(E.19)}$$

We rewrite the first line and combine the integrals in the second line because the integrands are even, i.e.

$$\begin{aligned} I = & \int_{-1}^{0} \mathrm{d}y \frac{1}{(1-y)(1+y)} (1-y^2)^{-\varepsilon} \left[f(y) - f(-1) \right] \\ & + \int_{0}^{1} \mathrm{d}y \frac{1}{(1-y)(1+y)} (1-y^2)^{-\varepsilon} \left[f(y) - f(1) \right] \\ & + \frac{1}{2} \left[f(1) + f(-1) \right] \int_{-1}^{1} \mathrm{d}y (1-y^2)^{-1-\varepsilon}. \end{aligned} \quad \text{(E.20)}$$

In the first two lines we use a partial fraction decomposition to obtain terms in $\frac{1}{1-y}$ and $\frac{1}{1+y}$. Afterwards we can combine all terms to obtain integrals from -1 to 1. (Note that we have to use the variable transformation $y = -y$). We can solve the integral in the last line analytically, i.e.

$$\begin{aligned} I = & \frac{1}{2} \int_{-1}^{1} \mathrm{d}y \frac{1}{1-y} (1-y^2)^{-\varepsilon} \left[f(y) - f(1) \right] \\ & + \frac{1}{2} \int_{-1}^{1} \mathrm{d}y \frac{1}{1+y} (1-y^2)^{-\varepsilon} \left[f(y) - f(-1) \right] \\ & - \frac{4^{-\varepsilon}}{2\varepsilon} \frac{\Gamma^2(1-\varepsilon)}{\Gamma(1-2\varepsilon)} \left[f(1) - f(-1) \right]. \end{aligned} \quad \text{(E.21)}$$

We can expand the first two integrals in ε and write the integrals with plus distributions and obtain

$$\begin{aligned} I = \int_{-1}^{1} \mathrm{d}y \Bigg\{ & \sum_{n=0}^{\infty} \frac{(-1)^n}{n!} \varepsilon^n \left(\frac{\log^n(1-y^2)}{1-y} \right)_+ f(y) \\ & + \sum_{n=0}^{\infty} \frac{(-1)^n}{n!} \varepsilon^n \left(\frac{\log^n(1-y^2)}{1+y} \right)_+ f(y) \\ & - \frac{4^{-\varepsilon}}{2\varepsilon} \frac{\Gamma^2(1-\varepsilon)}{\Gamma(1-2\varepsilon)} \left[\delta(1-y) + \delta(1+y) \right] \Bigg\}. \end{aligned} \quad \text{(E.22)}$$

Note that the definition of the plus distribution depends on the singular endpoint. The singular point in the first line is $y = 1$ and the singular point in the second line is $y = -1$.

E.4. Plus Distribution for Mass Regularization

We want to transform the expression

$$I = \int_b^1 \mathrm{d}x\, f\left(\frac{a^2}{x^2}\right) \frac{1}{x} g(x) \tag{E.23}$$

into an expression with a plus distribution $\left(\frac{1}{x}\right)_+$. The quantity a is a regulator (e.g. the photon mass), i.e. we are only interested in terms that are divergent for $a \to 0$. The lower integration bound is an intermediate scale with $a \ll b$. We are only interested in singular terms for this intermediate scale. First, we write f as power series in $\frac{a^2}{x^2}$ and g as power series in x, i.e.

$$\begin{aligned} I &= \sum_{n=0}^{\infty} \sum_{m=0}^{\infty} a_n b_m \int_a^1 \mathrm{d}x \left(\frac{a}{x}\right)^{2n} \frac{1}{x} x^m \\ &= \sum_{n=0}^{\infty} \sum_{m=1}^{\infty} a_n b_m a^{2n} \int_a^1 \mathrm{d}x\, x^{m-1-2n} + \sum_{n=0}^{\infty} a_n b_0 \int_a^1 \mathrm{d}x \left(\frac{a}{x}\right)^{2n} \frac{1}{x}. \end{aligned} \tag{E.24}$$

To evaluate the integral in the first term of the second line, we have to investigate two cases:

1. $m - 2n \neq 0$

$$a^{2n} \int_b^1 \mathrm{d}x\, x^{m-1-2n} = \frac{a^{2n} - b^m}{m - 2n} \tag{E.25}$$

2. $2n = m + 1$

$$a^{m+1} \int_b^1 \mathrm{d}x\, x^{-1} = -a^{m+1} \log(b) \tag{E.26}$$

Neglecting terms in a, b, and $a^2 \log b$, we obtain

$$I = a_0 \sum_{m=1}^{\infty} \frac{b_m}{m} + b_0 \sum_{n=0}^{\infty} a^{2n} \int_b^1 \mathrm{d}x\, x^{-2n-1} + \mathcal{O}(a, b). \tag{E.27}$$

Using the same integrals as above for the second term, we see that we can write

$$I = a_0 \sum_{m=1}^{\infty} \frac{b_m}{m} - a_0 b_0 \log(b) - \frac{1}{2} b_0 \sum_{n=1}^{\infty} \frac{a_n}{n} \left(\frac{a}{b}\right)^{2n} + \mathcal{O}(a, b). \tag{E.28}$$

We can neglect the last term if a goes much faster to zero than b. Next, we express the remnants of the power series in terms of the original functions f and g. We can use

$$a_0 = f\left(\frac{a^2}{x^2} = 0\right), \tag{E.29}$$

$$b_0 = g(0) \tag{E.30}$$

and

$$\sum_{m=1}^{\infty} \frac{b_m}{m} = \int_0^1 \mathrm{d}x \sum_{m=0}^{\infty} b_m x^{m-1} = \int_0^1 \mathrm{d}x \sum_{m=1}^{\infty} \frac{1}{x}\left[b_m x^m - b_0\right] = \int_0^1 \mathrm{d}x \left(\frac{1}{x}\right)_+ g(x) \tag{E.31}$$

Therefore, we find

$$I = f\left(\frac{a^2}{x^2} = 0\right) \int_0^1 \mathrm{d}x \left(\frac{1}{x}\right)_+ g(x) - f\left(\frac{a^2}{x^2} = 0\right) g(0) \log(b) + \mathcal{O}(a, b). \tag{E.32}$$

F. Integrating the Eikonal Factor

F.1. Angular Integration

We want to integrate the eikonal factor of the soft matrix element i over the angles of the radiated parton in d dimensions. We have

$$I_{ij} \equiv \int_0^\pi \mathrm{d}\phi \, (\sin\phi)^{-2\varepsilon} \int_{-1}^1 \mathrm{d}y \, (1-y^2)^{-\varepsilon} \frac{k_i \cdot k_j}{(p \cdot k_i)(p \cdot k_j)}, \tag{F.1}$$

where k_i and k_j are the momenta of the partons emitting the parton with momentum p.

F.1.1. Massless Partons

We parametrize the momenta of the partons such that the parton i defines the z direction of our coordinate system, i.e.

$$k_i = k_i^0 = \begin{pmatrix} 1 \\ \vec{0}_{d-2} \\ 1 \end{pmatrix} \tag{F.2}$$

and parton j is in the $\phi = 0$ plane

$$k_j = k_j^0 \begin{pmatrix} 1 \\ \vec{0}_{d-3} \\ \sin\theta_{ij} \\ \cos\theta_{ij} \end{pmatrix} \tag{F.3}$$

The momentum of the radiated parton in spherical coordinates is given by

$$p = p^0 \begin{pmatrix} 1 \\ \vec{0}_{d-4} \\ \sin\theta\sin\phi \\ \sin\theta\cos\phi \\ \cos\theta \end{pmatrix}. \tag{F.4}$$

The eikonal factor in this parametrization is given by

$$\frac{k_i \cdot k_j}{(p \cdot k_i)(p \cdot k_j)} = \frac{k_i \cdot k_j}{k_i^0 k_j^0 (p^0)^2 (1 - \cos\theta)(1 - \sin\theta_{ij} \sin\theta \cos\phi - \cos\theta_{ij} \cos\theta)}, \tag{F.5}$$

where $y = \cos\theta$. The integration over the angles θ and ϕ yields [155, appendix A]

$$I_{ij} = -\frac{\pi}{\varepsilon} {}_2\mathrm{F}_1 \left(1, 1, 1 - \varepsilon; \cos^2\left(\frac{\theta_{ij}}{2}\right)\right) \frac{1 - \cos\theta_{ij}}{(p^0)^2} \tag{F.6}$$

where we use the standard notation for the hypergeometric function ${}_2\mathrm{F}_1$. We have to expand the hypergeometric function around $\varepsilon = 0$. We use the integral representation

$${}_2\mathrm{F}_1(1, 1, 1 - \varepsilon; x) = \frac{\Gamma(1 - \varepsilon)}{\Gamma(-\varepsilon)} \int_0^1 \mathrm{d}t \, \frac{(1 - t)^{-1-\varepsilon}}{1 - xt}. \tag{F.7}$$

Since the integral is divergent for $t = 1$, we use the plus distribution trick to separate the pole. The hypergeometric function itself has no pole. The pole from the integral cancels with the prefactor. We obtain

$${}_2\mathrm{F}_1(1, 1, 1 - \varepsilon; x) = \frac{1}{1 - x} \left(1 - \varepsilon \log(1 - x) - \varepsilon^2 \, \mathrm{Li}_2\left(\frac{x}{x - 1}\right) + \mathcal{O}(\varepsilon^3)\right). \tag{F.8}$$

We can express $\cos\theta_{ij}$ in terms of the momenta of the partons

$$x_{ij} = \frac{1}{2}(1 + \cos\theta_{ij}) = 1 - \frac{k_i \cdot k_j}{2 k_i^0 k_j^0} \tag{F.9}$$

and we obtain

$$I_{ij} = -2\pi \frac{1}{(p^0)^2} \left(\frac{1}{\varepsilon} - \log(1 - x_{ij}) - \varepsilon \, \mathrm{Li}_2\left(\frac{x_{ij}}{x_{ij} - 1}\right) + \mathcal{O}(\varepsilon^2)\right). \tag{F.10}$$

Using identities for the dilogarithm, we can write

$$\begin{aligned} \mathrm{Li}_2\left(\frac{x_{ij}}{x_{ij} - 1}\right) = -\frac{\pi^2}{6} - \frac{1}{2} \log^2\left(\frac{k_i \cdot k_j}{2 k_i^0 k_j^0}\right) + \mathrm{Li}_2\left(\frac{k_i \cdot k_j}{2 k_i^0 k_j^0}\right) + \\ + \log\left(\frac{k_i \cdot k_j}{2 k_i^0 k_j^0}\right) \log\left(1 - \frac{k_i \cdot k_j}{2 k_i^0 k_j^0}\right). \end{aligned} \tag{F.11}$$

The benefit of the latter form is that the argument of the dilog is between zero and one which makes it possible to use simple expansions for the numerical evaluation of the dilog.

F.1.2. Massive Partons

The eikonal factor for one massless and one massive parton is a bit more complicated. We obtain

$$\frac{k_i \cdot m}{(p \cdot k_i)(p \cdot m)} = \frac{k_i \cdot m}{(p^0)^2 k_i^0 (1 - \cos\theta)(m^0 - |\vec{m}\,| \cos\theta_{im} \cos\theta - |\vec{m}\,| \sin\theta_{im} \sin\theta \cos\phi)} \tag{F.12}$$

The solution to the integral is given in [156] appendix B. The solution for two massive partons is given in [157].

F.1.3. Soft Integral for Mass Regularization

We want to evaluate the integral

$$I_{ij} = \int_{-1}^{1} \mathrm{d}y \int_{0}^{2\pi} \mathrm{d}\phi \, \frac{1}{(k_i \cdot k)(k_j \cdot k)}, \tag{F.13}$$

where k_i and k_j are four-momenta of massive particles. After introducing a Feynman parameter, we have

$$I_{ij} = \int_{0}^{1} \mathrm{d}x \int_{-1}^{1} \mathrm{d}y \int_{0}^{2\pi} \mathrm{d}\phi \, \frac{1}{(p \cdot k)^2}, \tag{F.14}$$

where $p \equiv x k_i + (1 - x) k_j$. We choose a reference frame where

$$p = \begin{pmatrix} p^0 \\ \vec{p} \end{pmatrix} = \begin{pmatrix} p^0 \\ 0 \\ 0 \\ |\vec{p}| \end{pmatrix}. \tag{F.15}$$

Defining the massless four momentum k with spherical coordinates in this frame, we obtain

$$I_{ij} = \int_{0}^{1} \mathrm{d}x \int_{-1}^{1} \mathrm{d}y \int_{0}^{2\pi} \mathrm{d}\phi \, \frac{1}{[k^0(p^0 - |\vec{p}|y)]^2} = \frac{4\pi}{(k^0)^2} \int_{0}^{1} \mathrm{d}x \, \frac{1}{p^2}. \tag{F.16}$$

Only an integration over the Feynman parameter is left. Using the definition of p, we obtain

$$I_{ij} = \frac{4\pi}{(k^0)^2} \int_{0}^{1} \mathrm{d}x \, \frac{1}{\left(m_i^2 + m_j^2 - 2k_i \cdot k_j\right) x^2 + (2k_i \cdot k_j - 2m_j^2) x + m_j^2}. \tag{F.17}$$

The integral which we have to solve has the form

$$I_{ij} = \int_0^1 \mathrm{d}x \, \frac{1}{ax^2 + bx + c} = \frac{1}{\sqrt{b^2 - 4ac}} \int_0^1 \mathrm{d}x \, \left[\frac{1}{x + A_-} - \frac{1}{x + A_+} \right], \tag{F.18}$$

where we used a partial fraction decomposition and we defined

$$A_\pm = \frac{b \pm \sqrt{b^2 - 4ac}}{2a}. \tag{F.19}$$

Performing the Feynman parameter integral we have

$$I_{ij} = \frac{1}{\sqrt{b^2 - 4ac}} \left[\log\left(1 + \frac{2a}{b - \sqrt{b^2 - 4ac}}\right) - \log\left(1 + \frac{2a}{b + \sqrt{b^2 - 4ac}}\right) \right] \tag{F.20}$$

This result can be reduced to

$$\begin{aligned} I_{ij} &= \frac{2\pi}{(k^0)^2 (k_i \cdot k_j) \beta_{ij}} \log \frac{1 - \beta_{ij}}{1 + \beta_{ij}} \\ &= -\frac{2\pi}{(k^0)^2 (k_i \cdot k_j)} \left(\log \frac{m_i^2}{2k_i \cdot k_j} + \frac{m_j^2}{2k_i \cdot k_j} \right) + \mathcal{O}(m_i^2, m_j^2), \end{aligned} \tag{F.21}$$

where $\beta_{ij} = \sqrt{1 - \frac{m_i^2 m_j^2}{(k_i \cdot k_j)^2}}$ and in the last step we expanded the log around small masses.

F.2. Momentum Integral

In this section we calculate the momentum integral of the eikonal factor

$$I_{ij} = \int_{|k| \leq \Delta E} \frac{\mathrm{d}^3 k}{\omega_k} \frac{(p_i \cdot p_j)}{(p_i \cdot k)(p_j \cdot k)}, \tag{F.22}$$

where k is the four momentum of the radiated particle and $\omega_k = \sqrt{|\vec{k}|^2 + \lambda^2}$, and p_i, p_j are massive. This integral was solved in [158, section 7]. The result is given by

$$\begin{aligned} I_{ij} = \frac{4\pi\alpha (p_i \cdot p_j)}{\alpha^2 p_i^2 - p_j^2} \Bigg\{ &\frac{1}{2} \log \frac{\alpha^2 p_i^2}{p_j^2} \log \frac{4\Delta E^2}{\lambda^2} + \\ &+ \left[\frac{1}{4} \log^2 \frac{u^0 - |\vec{u}|}{u^0 + |\vec{u}|} + \mathrm{Li}_2\left(1 - \frac{u^0 + |\vec{u}|}{v}\right) + \mathrm{Li}_2\left(1 - \frac{u^0 - |\vec{u}|}{v}\right) \right]_{u = p_j}^{\alpha p_i} \Bigg\}, \end{aligned} \tag{F.23}$$

where

$$v = \frac{\alpha^2 p_i^2 - p_j^2}{2(\alpha p_i^0 - p_j^0)}. \tag{F.24}$$

The factor α is defined by a quadratic equation

$$\alpha^2 p_i^2 - 2\alpha(p_i \cdot p_j) + p_j^2 = 0, \tag{F.25}$$

where $\frac{\alpha p_i^0}{p_j^0} > 1$. In (4.8) in chapter 4 we need the expansion for small masses. Hence, we expand the integral for $i \neq j$ and small masses m_i and m_j and keep only the logarithmic and constant terms. We start with the expansion of α. After solving the quadratic equation we obtain the two results

$$\alpha_\pm = \frac{|\vec{p}_i||\vec{p}_j|\left[(1-\cos\theta_{ij}) \pm (1-\cos\theta_{ij})\right]}{m_i^2}. \tag{F.26}$$

Only the solution α_+ fulfills the constraint we set on α. Therefore, we have

$$\alpha = \frac{2|\vec{p}_i||\vec{p}_j|(1-\cos\theta_{ij})}{m_i^2} \gg 1. \tag{F.27}$$

Note that $\cos\theta_{ij}$ cannot be equal to one because this would mean that the two born particles are collinear. The overall prefactor for small masses reduces to

$$\frac{\alpha(p_i \cdot p_j)}{\alpha^2 p_i^2 - p_j^2} = \frac{(p_i \cdot p_j)}{\alpha m_i^2} = \frac{1}{2}. \tag{F.28}$$

When we expand the arguments of the logarithms and dilogs, we obtain

$$I_{ij} = 2\pi \left\{ \frac{1}{2} \log \frac{4(p_i \cdot p_j)^2}{m_i^2 m_j^2} \log \frac{4\Delta E^2}{\lambda^2} + \frac{1}{4} \log^2 \frac{m_i^2}{4E_i^2} + \mathrm{Li}_2\left(1 - \frac{4|\vec{p}_i|^2}{m_i^2}\right) + \mathrm{Li}_2(0) + \right.$$
$$\left. - \frac{1}{4} \log^2 \frac{m_j^2}{4E_j^2} - \mathrm{Li}_2\left(1 - \frac{2|\vec{p}_i||\vec{p}_j|}{(p_i \cdot p_j)}\right) - \mathrm{Li}_2(1) \right\}. \tag{F.29}$$

To make the invariance of I_{ij} with respect to an interchange $i \leftrightarrow j$ more obvious we use the identity

$$\mathrm{Li}_2(1-x) = -\frac{1}{2}\log^2 x - \mathrm{Li}_2\left(1 - \frac{1}{x}\right) \tag{F.30}$$

and obtain

$$I_{ij} = 2\pi \left\{ \frac{1}{2} \log \frac{4(p_i \cdot p_j)^2}{m_i^2 m_j^2} \log \frac{4\Delta E^2}{\lambda^2} - \frac{1}{4} \log^2 \frac{m_i^2}{4E_i^2} - \mathrm{Li}_2(1) + \mathrm{Li}_2(0) + \right.$$
$$\left. - \frac{1}{4} \log^2 \frac{m_j^2}{4E_j^2} - \mathrm{Li}_2\left(1 - \frac{2|\vec{p}_i||\vec{p}_j|}{(p_i \cdot p_j)}\right) - \mathrm{Li}_2(1) \right\}. \tag{F.31}$$

We can use the identity

$$\mathrm{Li}_2\left(1-\frac{2|\vec{p}_i||\vec{p}_j|}{(p_i\cdot p_j)}\right)=\mathrm{Li}_2\left(\frac{p_i\cdot p_j}{2|\vec{p}_i||\vec{p}_j|}\right)+ \\ +\log\left(\frac{p_i\cdot p_j}{2|\vec{p}_i||\vec{p}_j|}\right)\log\left(1-\frac{p_i\cdot p_j}{2|\vec{p}_i||\vec{p}_j|}\right)-\frac{1}{2}\log^2\left(\frac{p_i\cdot p_j}{2|\vec{p}_i||\vec{p}_j|}\right)-\frac{\pi^2}{6} \quad \text{(F.32)}$$

to obtain an argument of the dilog in $[0,1]$. When we also remove the constant factor from the argument of the mass logarithms, we obtain

$$I_{ij}=2\pi\left\{\frac{1}{2}\log\frac{4(p_i\cdot p_j)^2}{m_i^2m_j^2}\log\frac{\Delta E^2}{\lambda^2}-\frac{1}{4}\log^2\frac{m_i^2}{E_i^2}-\frac{1}{4}\log^2\frac{m_j^2}{E_j^2}+2\log 2\log\frac{p_i\cdot p_j}{2E_iE_j}\right. \\ -\mathrm{Li}_2\left(\frac{p_i\cdot p_j}{2E_iE_j}\right)-\log\left(\frac{p_i\cdot p_j}{2E_iE_j}\right)\log\left(1-\frac{p_i\cdot p_j}{2E_iE_j}\right)+\frac{1}{2}\log^2\left(\frac{p_i\cdot p_j}{2E_iE_j}\right) \\ \left.+2\log^2 2-\frac{\pi^2}{6}\right\}, \quad \text{(F.33)}$$

where we used $|\vec{p}_i|=E_i$ in the massless limit.

G. Scalar Integrals

When we calculate the virtual corrections, we always need basic scalar integrals which are defined in [158]. We give some of these scalar integrals in certain limits in this section.

G.1. Scalar One Point Function

The scalar one point function is defined as

$$A_0(m) = \frac{(2\pi\mu)^{4-d}}{i\pi^2} \int \mathrm{d}^d k \frac{1}{k^2 - m^2}. \tag{G.1}$$

We can use a Wick rotation and integrate over euclidean d dimensional polar coordinates to obtain

$$A_0(m) = -m^2 \left(\frac{m^2}{4\pi\mu^2}\right)^{\frac{d-4}{2}} \Gamma\left(\frac{2-d}{2}\right) = m^2 \left[\frac{1}{\varepsilon} - \gamma_E + \log 4\pi - \log\frac{m^2}{\mu^2} + 1\right] + \mathcal{O}(\varepsilon). \tag{G.2}$$

G.2. Scalar Two Point Function

The scalar two point function is defined as

$$B_0(p, m_0^2, m_1^2) = \frac{(2\pi\mu)^{4-d}}{i\pi^2} \int \mathrm{d}^d k \frac{1}{(k^2 - m_0^2)\left[(k+p)^2 - m_1^2\right]}. \tag{G.3}$$

We introduce Feynman parameters to reduce B_0 to an one dimensional integral

$$B_0(q, \lambda, m) = \frac{(2\pi\mu)^{4-d}}{i\pi^2} \int_0^1 \mathrm{d}x \int_0^1 \mathrm{d}y\, \delta(x+y-1) \int \mathrm{d}^d l \frac{1}{\left(l^2 - \Delta\right)^2}, \tag{G.4}$$

where $l = k + yq$ and $\Delta = x^2 q^2 - x(q^2 - m^2 + \lambda^2) + \lambda^2$. We use

$$\int \mathrm{d}^d l \frac{1}{\left(l^2 - \Delta\right)^2} = i\pi^{\frac{d}{2}} \Gamma\left(2 - \frac{d}{2}\right) \left(\frac{1}{\Delta}\right)^{2-\frac{d}{2}} \tag{G.5}$$

to obtain

$$B_0(q,\lambda,m) = (4\pi\mu^2)^\varepsilon \Gamma(\varepsilon) \int_0^1 \mathrm{d}x\, \Delta^{-\varepsilon} = \frac{1}{\varepsilon} - \gamma_E + \log 4\pi - \int_0^1 \mathrm{d}x\, \log\frac{\Delta}{\mu^2} + \mathcal{O}(\varepsilon) \tag{G.6}$$

small photon mass Neglecting λ^2 we have

$$\log\Delta = \log x + \log\left(xq^2 - q^2 + m^2\right) \tag{G.7}$$

$$\int_0^1 \mathrm{d}x\, \log\frac{\Delta}{\mu^2} = -2 - \frac{m^2-q^2}{q^2}\log\frac{m^2-q^2}{q^2} + \log\frac{m^2}{\mu^2} \tag{G.8}$$

$$B_0(q,\lambda,m) = \frac{1}{\varepsilon} - \gamma_E + \log 4\pi + 2 + \frac{m^2-q^2}{q^2}\log\frac{m^2-q^2}{q^2} - \log\frac{m^2}{\mu^2} \tag{G.9}$$

small masses

$$\log\Delta = \log x + \log k_1^2 + \log(-1) + \log(1-x) \tag{G.10}$$

$$B_0(q,0,0) = \frac{1}{\varepsilon} - \gamma_E + \log 4\pi + 2 - \log\frac{q^2}{\mu^2} + i\pi \tag{G.11}$$

derivative for small photon mass The derivative of the scalar 2 point function is given by

$$\frac{\partial}{\partial q^2} B_0(q^2,\lambda,m^2) = -\int_0^1 \mathrm{d}x\, \frac{\partial}{\partial q^2}\log\Delta = -\int_0^1 \mathrm{d}x\, \frac{x^2-x}{-x(p^2-m^2)+\lambda^2+p^2x^2}, \tag{G.12}$$

where we used that $\lambda^2 \ll m^2$. When we evaluate this for $q^2 = m^2$, we obtain

$$\left.\frac{\partial}{\partial q^2} B_0(q^2,\lambda,m^2)\right|_{q^2=m^2} = -\frac{1}{m^2}\left[\int_0^1 \mathrm{d}x\, \frac{x^2}{x^2+\frac{\lambda^2}{m^2}} - \int_0^1 \mathrm{d}x\, \frac{x}{x^2+\frac{\lambda^2}{m^2}}\right]. \tag{G.13}$$

We can expand the first integral around $\frac{\lambda^2}{m^2} = 0$ because the remaining integral is finite. The second integral is easy to solve because the numerator is proportional to the derivative of the denominator. We obtain

$$\left.\frac{\partial}{\partial q^2} B_0(q^2,\lambda,m^2)\right|_{q^2=m^2} = -\frac{1}{m^2}\left(\log\frac{\lambda}{m} + 1\right) + \mathcal{O}\left(\frac{\lambda}{m}\right) \tag{G.14}$$

after expanding in $\frac{\lambda^2}{m^2} = 0$. We can use $p^2 = \not{p}^2$ to arrive at

$$\left.\frac{\partial}{\partial \not{q}} B_0(q^2,\lambda,m)\right|_{\not{q}=m} = \left.\frac{\partial}{\partial q^2} B_0(q^2,\lambda,m^2)\right|_{q^2=m^2} \left.\frac{\mathrm{d}q^2}{\mathrm{d}\not{q}}\right|_{\not{q}=m} = -\frac{2}{m}\left(\log\frac{\lambda}{m} + 1\right) + \mathcal{O}\left(\frac{\lambda}{m}\right) \tag{G.15}$$

G.3. Vectorlike Two Point Function

The vectorlike two point function is defined by

$$B^\mu(q,m_1,m_2) \equiv \frac{(2\pi\mu)^{4-d}}{i\pi^2}\int \mathrm{d}^d k \frac{k^\mu}{(k^2-m_2^2)\left[(q+k)^2-m_1^2\right]}. \tag{G.16}$$

The integral B^μ has one Lorentz index and can therefore only depend on q^μ. Therefore, it has the form $B^\mu = \bar{B}q^\mu$. When we contract B^μ with q^μ, we find

$$q_\mu B^\mu(q,m_1,m_2) = \frac{1}{2}\left[A_0(m_2) - A_0(m_1) + (m_2^2-m_1^2-q^2)B_0(q,m_2,m_1)\right] = \bar{B}q^2. \tag{G.17}$$

Hence, we obtain

$$B^\mu(q,m_1,m_2) = \frac{1}{2q^2}\left[A_0(m_2) - A_0(m_1) + (m_2^2-m_1^2-q^2)B_0(q,m_2,m_1)\right] q^\mu \tag{G.18}$$

derivative We now calculate the derivative of the vectorlike two point function, i.e.

$$\begin{aligned}\frac{\partial}{\partial \not{p}}\gamma^\mu B_\mu(p,m,\lambda) = \frac{1}{2}\Bigg[&\frac{1}{\not{p}^2}(A_0(m)-A_0(\lambda)) - \frac{\lambda^2-m^2+\not{p}^2}{\not{p}^2}B_0(p,m_1,m_2) \\ &+ \frac{\lambda^2-m^2-\not{p}^2}{\not{p}}\frac{\partial}{\partial \not{p}}B_0(p,m,\lambda)\Bigg]\end{aligned} \tag{G.19}$$

When we evaluate this function at $\not{p} = m$, we arrive at

$$\frac{\partial}{\partial \not{p}}\gamma^\mu B_\mu(p,m,\lambda)\bigg|_{\not{p}=m} = \frac{1}{2}\left[-\frac{1}{m^2}A_0(m) - 2m\,\frac{\partial}{\partial \not{p}}B_0(p,m,\lambda)\bigg|_{\not{p}=m}\right] + \mathcal{O}\left(\frac{\lambda}{m}\right). \tag{G.20}$$

We can use (G.2) and (G.15) to obtain

$$\frac{\partial}{\partial \not{p}}\gamma^\mu B_\mu(p,m,\lambda)\bigg|_{\not{p}=m} = \frac{1}{2}\left[-\frac{1}{\varepsilon} + \gamma_E - \log 4\pi + \log\frac{m^2}{\mu^2} + 4\log\frac{\lambda}{m} + 3\right]. \tag{G.21}$$

G.4. Three Point Function

The scalar three point function is defined by

$$C_0(p_1,p_2,m_0^2,m_1^2,m_1^2) = \frac{(2\pi\mu)^{4-d}}{i\pi^2}\int \mathrm{d}^d k \frac{1}{(k^2-m_0^2)\left[(k+p_1)^2-m_1^2\right]\left[(k+p_2)^2-m_2^2\right]}. \tag{G.22}$$

The three point function is in the limit $m_1^2, m_2^2 \ll s$ is given by [159, appendix C]

$$\operatorname{Re} C_0 = \frac{1}{s}\left\{\frac{1}{2}\left(\log\frac{m_1^2}{s} + \log\frac{m_2^2}{s}\right)\log\frac{\lambda^2}{s} - \frac{1}{4}\log^2\frac{m_1^2}{s} - \frac{1}{4}\log^2\frac{m_2^2}{s} - \frac{2}{3}\pi^2\right\}. \quad \text{(G.23)}$$

H. Soft and Collinear Limits

In this chapter we investigate the soft and collinear limits of real emission matrix elements. We find explicit results for the limits of the born matrix element and a factor that depends on the splitting process. The limits are crucial ingredients of NLO calculations.

H.1. Soft Limit

We start with the radiation of a soft gluon from an initial-state quark (Figure H.1). The matrix element reads

$$\mathcal{M} = \mathcal{M}_0 \frac{\not{k}_1 - \not{k}_2 + m_1}{(k_1 - k_2)^2 - m_1^2} \gamma^\mu g_s t^a u(k_1) \varepsilon_\mu^*(k_2). \tag{H.1}$$

We can use the *eikonal approximation* for a soft gluon ($\not{k}_2 \ll \not{k}_1$) to see that the real matrix element factorizes into the born matrix element and a process independent factor. When we use Dirac equation $(\not{k} - m)u(k) = 0$ and $\{\gamma^\mu, \gamma^\nu\} = 2g^{\mu\nu}$, we find

$$\mathcal{M} \approx -\frac{k_1 \cdot \varepsilon^*(k_2)}{k_1 \cdot k_2} g_s t^a \mathcal{M}_{\text{born}}, \tag{H.2}$$

where $\mathcal{M}_{\text{born}} = \mathcal{M}_0 u(k_1)$. For an initial-state antiquark, we obtain with a similar calculation

$$\mathcal{M} = g_s t^a \frac{k_1 \cdot \varepsilon^*(k_2)}{k_1 \cdot k_2} \mathcal{M}_{\text{born}}. \tag{H.3}$$

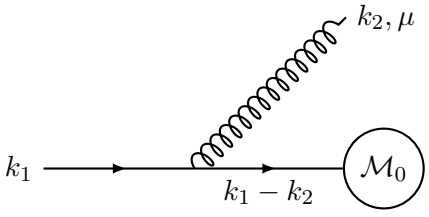

Figure H.1.: Feynman diagram for soft gluon radiation from an initial-state quark

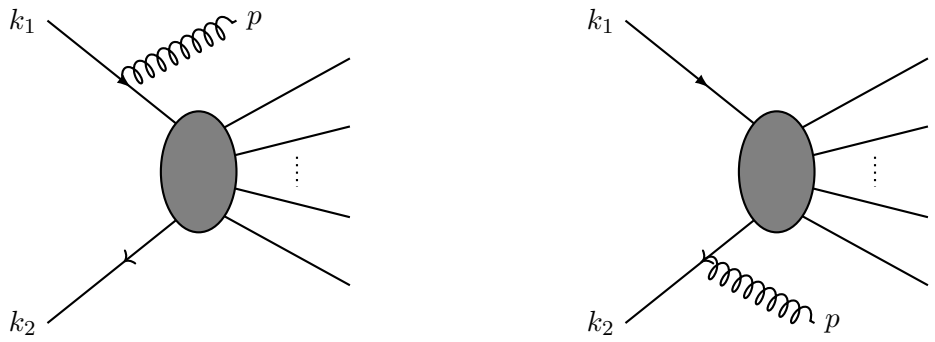

Figure H.2.: Feynman diagrams for initial-state gluon radiation in $q\bar{q} \to X$

Obviously, we can us the same tricks for final-state radiation. With these equations we can evaluate the soft squared matrix element for the Drell-Yan like process $q\bar{q} \to X$ where X is not charged under QCD (Figure H.2). When we neglect the color matrices, we find

$$|\mathcal{M}_{\text{soft}}|^2 = \sum_{\text{pol}} g_s^2 \varepsilon_\mu^*(p)\varepsilon_\nu(p) \left(-\frac{k_1^\mu}{k_1 \cdot p} + \frac{k_2^\mu}{k_2 \cdot p}\right)\left(-\frac{k_1^\nu}{k_1 \cdot p} + \frac{k_2^\nu}{k_2 \cdot p}\right) |\mathcal{M}_{\text{born}}|^2. \tag{H.4}$$

The evalutation of the color matrices is postponed to section H.1.1. After using the polarization sum in an axial gauge

$$\sum_{\text{pol}} \varepsilon_\mu^*(k)\varepsilon_\nu(k) = -g_{\mu\nu} + \frac{k_\mu n_\nu + n_\mu k_\nu}{n \cdot k} \tag{H.5}$$

where $n^2 = 0$, we obtain

$$|\mathcal{M}_{\text{soft}}|^2 = g_s^2 \left[\frac{2k_1 \cdot k_2}{(k_1 \cdot p)(k_2 \cdot p)} - \frac{m_1^2}{(k_1 \cdot p)^2} - \frac{m_2^2}{(k_2 \cdot p)^2}\right] |\mathcal{M}_{\text{born}}|^2. \tag{H.6}$$

The structure of the matrix element with gluon radiation from a gluon is more complicated. From the Feynman diagram in Figure H.3 we obtain

$$\mathcal{M} = \mathcal{M}_0^\alpha \frac{g_{\alpha\mu}}{p^2} g_s \left[g^{\mu\nu}(g+p)^\lambda + g^{\nu\lambda}(k-g)^\mu + g^{\lambda\mu}(-k-p)^\nu\right] \varepsilon_\lambda^*(k)\varepsilon_\nu^*(g), \tag{H.7}$$

where $p = g + k$ and color is again neglected. When we neglect the soft momentum k in the numerator and use $g \cdot \varepsilon(g) = 0$, we find

$$\mathcal{M} = g_s \frac{g \cdot \varepsilon^*(k)}{g \cdot k} \mathcal{M}_{\text{born}}. \tag{H.8}$$

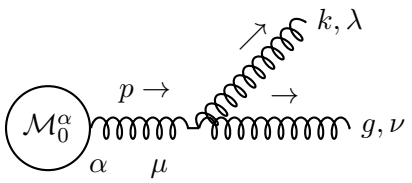

Figure H.3.: Feynman diagram for the radiation of a gluon from a gluon

The structure of the matrix element is the same as for the radiation from quarks because the wave length of the soft gluon is so large that it cannot distinguish between different spins and the result is spin independent. The general form of the real matrix element with soft gluon radiation reads

$$|\mathcal{M}_{\text{soft}}|^2 = 4\pi\alpha_s \sum_{i \neq j} \frac{k_i \cdot k_j}{(k_i \cdot k)(k_j \cdot k)} |\mathcal{M}_{\text{born}}|^2 \tag{H.9}$$

where k_i and k_j are massless born momenta and k is the gluon momentum. Note that we have neglected color factors. We will calculate them later. Next, we investigate is the radiation of a soft quark. When a quark with momentum k is emitted, we have

$$\mathcal{M} = \bar{u}(k)\mathcal{M}', \tag{H.10}$$

where $\mathcal{M}'$ denotes the rest of the matrix element. The squared matrix element for massless quarks reads

$$\mathcal{M}_1^\dagger u(k)\bar{u}(k)\mathcal{M}_2 = \mathcal{M}_1^\dagger \not{k} \mathcal{M}_2. \tag{H.11}$$

Since $k^\mu \propto E$, there is an additional power of energy in the numerator compared to the gluon emission. Hence, there is no soft divergence, since the usual factor $\frac{1}{E}$ is canceled.

H.1.1. Color Factor

The color factor is not an overall factor if there is a more complex color structure in the process. In this section we look at the color structure of a general process. The born color part is shown in Figure H.4a and written as

$$\mathcal{M}_{\text{col}}^{a_1 a_2 \ldots a_n} C_{a_1} C_{a_2} \ldots C_{a_n}, \tag{H.12}$$

where C are the color states of the external particles, a_i are the corresponding color indices and $\mathcal{M}_{\text{col}}$ is the color structure of the diagram obtained with the usual Feynman

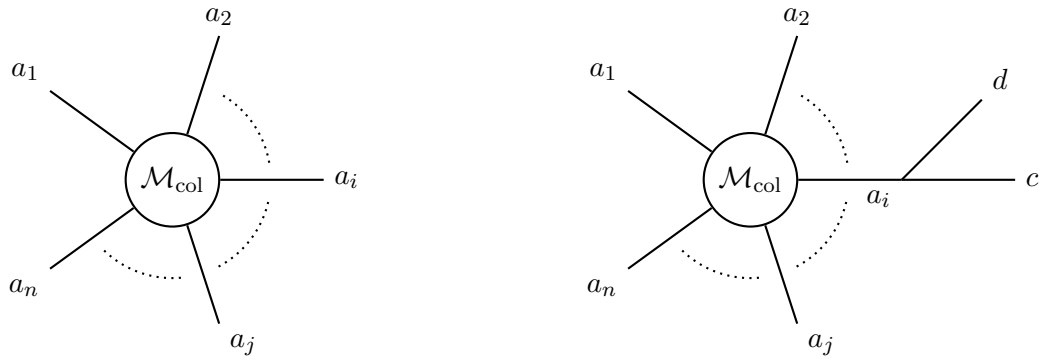

(a) born level color structure of external particles

(b) color structure of external particles with radiation from parton i

Figure H.4.: color structure of amplitudes. $a_1 \dots a_n$ are the color indices of the external particles and $\mathcal{M}_{\text{col}}$ is the color structure of the diagram which we can obtain with the normal Feynman rules.

rules. The color states are defined as

$$C_a = \begin{cases} c_a & \text{incoming quark/outgoing antiquark} \\ c_a^\dagger & \text{outgoing quark/incoming antiquark} \\ \chi_a & \text{incoming gluon} \\ \chi_a^* & \text{outgoing gluon} \end{cases} \tag{H.13}$$

where $a = 1 \dots N_C$ for (anti)quarks and $a = 1 \dots (N_C^2 - 1)$ for gluons. We study the splitting of parton a_i. The corresponding diagram is shown in Figure H.4b. We write the matrix element as

$$\mathcal{M}_{\text{col}}^{a_1 a_2 \dots a_i \dots a_n} T^d_{a_i c} C_{a_1} C_{a_2} \dots C_c \dots C_{a_n} C_d, \tag{H.14}$$

where T is the color matrix of the vertex of the radiation, i.e.

$$T^d_{a_i c} = \begin{cases} t^d_{c a_i} & a_i = \text{quark} \\ t^d_{a_i c} & a_i = \text{antiquark} \\ i f_{a_i d c} & a_i = \text{gluon} \end{cases} \tag{H.15}$$

Next, we can calculate the interference term for radiation from partons $i \neq j$. We obtain

$$\begin{aligned}|\mathcal{M}_{\text{col}}^{ij}|^2 &= \left[\mathcal{M}_{\text{col}}^{a_1 a_2 \dots a_i \dots a_j \dots a_n} T_{a_i c}^d C_{a_1} C_{a_2} \dots C_c \dots C_{a_j} \dots C_{a_n} C_d\right] \\ &\quad \times \left[\mathcal{M}_{\text{col}}^{\alpha_1 \alpha_2 \dots \alpha_i \dots \alpha_j \dots \alpha_n} T_{\alpha_j \gamma}^{\delta} C_{\alpha_1} C_{\alpha_2} \dots C_{\alpha_i} \dots C_\gamma \dots C_{a_n} C_\delta\right]^* \\ &= \mathcal{M}_{\text{col}}^{a_1 a_2 \dots a_i \dots a_j \dots a_n} \left[\mathcal{M}_{\text{col}}^{a_1 a_2 \dots \alpha_i \dots \alpha_j \dots a_n}\right]^* T_{a_i \alpha_i}^d T_{\alpha_j a_j}^{d*},\end{aligned} \tag{H.16}$$

where we used that $C_a C_\alpha^* = \delta_{a\alpha}$ if a and α label the same particle. For the term where $i = j$, we obtain

$$\begin{aligned}|\mathcal{M}_{\text{col}}^{i}|^2 &= \mathcal{M}_{\text{col}}^{a_1 a_2 \dots a_i \dots a_n} \left[\mathcal{M}_{\text{col}}^{a_1 a_2 \dots \alpha_i \dots a_n}\right]^* T_{a_i c}^d T_{\alpha_i c}^{d*} \\ &= \mathcal{M}_{\text{col}}^{a_1 a_2 \dots a_i \dots a_n} \left[\mathcal{M}_{\text{col}}^{a_1 a_2 \dots a_i \dots a_n}\right]^* \begin{cases} C_F & \text{for } i = \text{quark/antiquark} \\ C_A & \text{for } i = \text{gluon} \end{cases}\end{aligned} \tag{H.17}$$

We can use color conservation [160] to obtain

$$0 = \sum_{ij} |\mathcal{M}_{\text{col}}^{ij}|^2 = \sum_j \left[\sum_{\substack{i \\ i \neq j}} |\mathcal{M}_{\text{col}}^{ij}|^2 + C_{f_j} \mathcal{M}_{\text{col}}^{a_1 a_2 \dots a_j \dots a_n} \left[\mathcal{M}_{\text{col}}^{a_1 a_2 \dots a_j \dots a_n}\right]^*\right]. \tag{H.18}$$

Therefore, we can write

$$\sum_{\substack{i,j \\ i \neq j}} |\mathcal{M}_{\text{col}}^{ij}|^2 = -\sum_j C_{f_j} \mathcal{M}_{\text{col}}^{a_1 a_2 \dots a_j \dots a_n} \left[\mathcal{M}_{\text{col}}^{a_1 a_2 \dots a_j \dots a_n}\right]^*, \tag{H.19}$$

where $C_{f_j} = C_F$ for $j = q, \bar{q}$ and $C_{f_j} = C_A$ for $j = g$.

The soft matrix element including the color factor reads

$$|\mathcal{M}_{\text{soft}}|^2 = 4\pi\alpha \sum_{\substack{ij \\ i \neq j}} \frac{k_i \cdot k_j}{(k_i \cdot k)(k_j \cdot k)} B_{ij}, \tag{H.20}$$

where we defined the *color correlated born amplitude* B_{ij} as

$$B_{ij} = \mathcal{M}_{\{a_k\}} \mathcal{M}_{\{a_k^*\}}^* T_{a_i \alpha_i}^d T_{\alpha_j a_j}^d. \tag{H.21}$$

The born amplitude is denoted by $\mathcal{M}_{\{a_k\}}$, where $\{a_k\}$ stands for all color indices of external partons, i.e. $\{a_k\} = a_1 \dots a_i \dots a_j \dots a_n$ and $\{a_k^*\} = a_1 \dots \alpha_i \dots \alpha_j \dots a_n$. In practice, we can calculate the color correlated born matrix element for simple processes by dividing the born matrix element by its color factor and multiplying it by the real

color factor of the interference terms. When we average over initial-state spins we have to take the spins $s_\pm$ from the real process. Also symmetry factors N_{sym} of the real process have to be taken into account. We define

$$\mathcal{B}_{ij} = \frac{1}{N_{\text{sym}}} \frac{1}{(2s_+ + 1)(2s_- + 1)d_+ d_-} B_{ij}, \tag{H.22}$$

where $d_\pm$ is the dimension of the color representation of incoming partons, i.e. $d_\pm = N_C$ for an incoming quark and $d = (N_C^2 - 1)$ for a gluon.

H.2. Collinear Limit

The discussion of the collinear limit is based on [161] and references therein. We consider first the case of a collinear splitting of a final-state gluon p into p_i and p_j. We can use a Sudakov decomposition for the final-state momenta, i.e.

$$p_i^\mu = zp^\mu + k_\perp^\mu - \frac{k_\perp^2}{z} \frac{n^\mu}{2(p \cdot n)}, \tag{H.23}$$

$$p_j^\mu = (1-z)p^\mu - k_\perp^\mu - \frac{k_\perp^2}{1-z} \frac{n^\mu}{2(p \cdot n)}. \tag{H.24}$$

The collinear direction is given by p^μ and n^μ is an auxiliary light-like vector. The vector $k_\perp$ gives the transverse direction w.r.t. p and n ($k_\perp^2 < 0, k_\perp \cdot p = k_\perp \cdot n = 0$). The collinear limit is approached if $k_\perp^2 \to 0$. The factor z corresponds to the energy fraction of p_i in the collinear limit. The collinear limit of the squared matrix element reads

$$|\mathcal{M}_{n+1}^{\text{coll}}|^2 = \frac{8\pi\alpha_s}{p^2} \mathcal{M}^{\mu\nu} P_{\mu\nu}(z, k_\perp), \tag{H.25}$$

where $\mathcal{M}_{\mu\nu}$ is the *spin-correlated born matrix element* and $P_{\mu\nu}$ is a splitting function. The *spin correlated born matrix element* is the born matrix element with open polarization vectors ε^μ for the external gluon, i.e. the squared born matrix element reads

$$|\mathcal{M}|^2 = \mathcal{M}^\mu \varepsilon_\mu \varepsilon_\nu^* \mathcal{M}^{\nu *} \quad \text{and} \quad \mathcal{M}^{\mu\nu} \equiv \mathcal{M}^\mu \mathcal{M}^{\nu *}, \tag{H.26}$$

where $\mathcal{M}^\mu$ is the born matrix element without the gluon polarization vector. We can use the completeness relation of the polarization vectors to write

$$\mathcal{M}^{\mu\nu} = \sum_{s,s'} \mathcal{M}_s \mathcal{M}_{s'}^* \varepsilon_s^{\mu *} \varepsilon_{s'}^\nu, \tag{H.27}$$

where $\mathcal{M}_s$ is the born matrix element with gluon polarization s. Explicit polarization vectors are given in [162]. The splitting function for a gluon splitting into two gluons reads [64, 67]

$$P_{gg}^{\mu\nu}(z, k_\perp) = 2C_A \left\{ -2 \left[\frac{z}{1-z} + \frac{1-z}{z} \right] g^{\mu\nu} + 4z(1-z)\hat{k}_\perp^\mu \hat{k}_\perp^\nu \right\}, \tag{H.28}$$

where $\hat{k}_\perp = k_\perp/|k_\perp|$. The $g^{\mu\nu}$ part of the splitting function leads to a term proportional to the squared born matrix element because $g^{\mu\nu} M_{\mu\nu} = -|\mathcal{M}|^2$. We also find

$$\mathcal{M}^{\mu\nu} \hat{k}_\perp^\mu \hat{k}_\perp^\nu = \sum_{ss'} \mathcal{M}_s \varepsilon_{\alpha,s} \frac{p_i^\alpha p_j^\nu}{2z(1-z)(p_i \cdot p_j)} \varepsilon^*_{\nu,s'} \mathcal{M}^*_{s'}, \tag{H.29}$$

where we used (H.23), (H.24) and

$$p_i \cdot \varepsilon = \quad k_\perp \cdot \varepsilon(p) + \mathcal{O}(k_\perp^2), \tag{H.30}$$

$$p \cdot \varepsilon(p) = \quad 0, \tag{H.31}$$

$$k_\perp^2 = \quad -2z(1-z) p_i \cdot p_j. \tag{H.32}$$

We can also calculate an explicit form for $\hat{k}_\perp$. We rotate p_i to a system where it points in z direction. All momenta in this frame are written with a prime, i.e. p_i', $k_\perp'$ etc. We can choose $n'^\mu = (1, 0, 0, -1)$ and we find

$$k_\perp' = \begin{pmatrix} 0 \\ p_x' \\ p_y' \\ 0 \end{pmatrix}, \tag{H.33}$$

where p' is the born momentum. After normalization and a rotation back to the original system, we have an explicit form of $\hat{k}_\perp$. For a final-state gluon splitting, the splitting functions are given by [64, 67]

$$P_{gg}^{\mu\nu}(z, k_\perp) = 2C_A \left\{ - \left[\frac{z}{1-z} + \frac{1-z}{z} \right] g^{\mu\nu} - 2(1-\varepsilon)z(1-z)\hat{k}_\perp^\mu \hat{k}_\perp^\nu \right\}, \tag{H.34}$$

$$P_{gq}^{\mu\nu}(z, k_\perp) = T_F \left[-g^{\mu\nu} + 4z(1-z)\hat{k}_\perp^\mu \hat{k}_\perp^\nu \right]. \tag{H.35}$$

When we integrate (H.25) over the radiation phase-space [163]

$$\mathrm{d}\Phi_{\mathrm{rad}} = \frac{\mathrm{d}k_\perp^2 \, \mathrm{d}z \, \mathrm{d}\phi}{4(2\pi)^3} \frac{1}{z(1-z)}, \tag{H.36}$$

we obtain

$$I = -\,\mathrm{d}\Phi_{\mathrm{rad}} \frac{8\pi\alpha}{4(2\pi)^3} \mathcal{M}^{\mu\nu} I_{\mu\nu}. \tag{H.37}$$

The solution has the following form

$$I^{\mu\nu} = X g^{\mu\nu} + Y p^\mu p^\nu + Z n^\mu n^\nu + U p^\mu n^\nu + V p^\nu n^\mu. \tag{H.38}$$

When we contract $I^{\mu\nu}$ with all combinations of $g^{\mu\nu}$, p^μ, n^μ and write

$$P_{\mu\nu} = A g_{\mu\nu} + B \hat{k}_\perp^\mu \hat{k}_\perp^\nu, \tag{H.39}$$

we obtain

$$X = \int \mathrm{d}z \int \mathrm{d}k_\perp^2 \int \mathrm{d}\phi \frac{1}{k_\perp^2} \left(A + \frac{1}{d-2} B \right). \tag{H.40}$$

Using this in (H.37) leads to

$$I = -\,\mathrm{d}\Phi_{\mathrm{rad}} \frac{8\pi\alpha}{4(2\pi)^3} \mathcal{M}^{\mu\nu} \left(X g_{\mu\nu} + Z n_\mu n_\nu \right) \tag{H.41}$$

because all other contributions are zero due to $\varepsilon \cdot p = 0$. We obtain

$$I = \frac{8\pi\alpha}{4(2\pi)^3} |\mathcal{M}|^2 X = -\,\mathrm{d}\Phi_{\mathrm{rad}} |\mathcal{M}|^2 \frac{8\pi\alpha_s}{p^2} \left(A + \frac{1}{d-2} B \right) \tag{H.42}$$

if we we use $n = (1, 0, 0, -1)$ and, hence, $n \cdot \varepsilon = 0$. We can rewrite I in terms of the Altarelli-Parisi splitting functions (3.23) and (3.24), i.e.

$$I = \mathrm{d}\Phi_{\mathrm{rad}} |\mathcal{M}|^2 \frac{8\pi\alpha_s}{p^2} P_{gi}(z). \tag{H.43}$$

For ISR, one finds in 4 dimensions [164]

$$P_{gg}^{\mu\nu}(z, k_\perp) = 2C_A \left[-2 g^{\mu\nu} \left(\frac{z}{1-z} + z(1-z) \right) + \frac{4(1-z)}{z} \hat{k}_\perp^\mu \hat{k}_\perp^\nu \right], \tag{H.44}$$

$$P_{qg}^{\mu\nu}(z, k_\perp) = C_F \left[-z g^{\mu\nu} + \frac{4(1-z)}{z} \hat{k}_\perp^\mu \hat{k}_\perp^\nu \right] \tag{H.45}$$

and (H.43) also holds.

When we consider a quark that splits into a quark and a gluon, we have to define a spin correlated born matrix element $\mathcal{M}_{ss'}$ with open spinor indices s, s' of the quark, for example

$$|\mathcal{M}|^2 = \mathcal{M}_s u_s(p) \bar{u}_{s'}(p) \mathcal{M}_{s'}^* \quad \Rightarrow \quad \mathcal{M}_{ss'} = \mathcal{M}_s \mathcal{M}_{s'}^*. \tag{H.46}$$

In analogy to (H.25), the collinear limit reads

$$|\mathcal{M}_{n+1}^{\text{coll}}|^2 = \frac{8\pi\alpha_s}{-p^2}\mathcal{M}_{ss'}P_{ss'}(z). \tag{H.47}$$

The splitting functions $P_{ss'}$ are independent of $k_\perp$ and proportional to $\delta_{ss'}$ [55, 64]. Therefore, we can use the spin averaged splittings functions to calculate the limit, i.e.

$$|\mathcal{M}_{n+1}^{\text{coll}}|^2 = \frac{8\pi\alpha_s}{-p^2}\hat{P}_{qq}(z)|\mathcal{M}_n|^2. \tag{H.48}$$

I. Implementation

In this chapter, we show how a Drell-Yan born process and its QCD radiation is added to the event generator. The user has to subclass the class

UserProcess::Data

which stores all informations about the process. In particular, the user has to implement the abstract functions

```
class Data {
// ...
protected:
virtual int ProcessInit(Config::File &) = 0;
virtual void ProcessPrint() const = 0;
// ...
};
```

In ProcessInit, the user has to set the following member variables:

- `MatrixElement` to an implementation of the `UserProcess::IMatrixElement` interface,
- `Params` to an implementation of the standard model parameters `FKS::Param`,
- `cuts` to an implementation of the `UserProcess::ICuts` interface,
- `hists` to an implementation of the `UserProcess::Histograms` interface,
- `Scales` to an implementation of the `UserProcess::IScales` interface.

Furthermore, all subprocesses have to be added to the `Process` member variable which is a list of `FKS::FlavourConfig`. In the following section we show how to add a Drell-Yan like process.

I.1. Adding a Process

In this section we add the processes $\bar{u}u \to \mu^+\mu^-$ and $\bar{c}c \to \mu^+\mu^-$ with QCD corrections. First, we have to define the born flavour configuration

```
std::vector<FKS::PDGList> born = {{-2,2,-13,13},{-4,4,-13,13}};
```

We use the standard PDG codes to identify the particles. We also have to define the color configuration for the LHE file

```
FKS::ColorFlow color1 = {0, 501, 0, 0};
FKS::ColorFlow color2 = {501, 0, 0, 0};
```

The user has to implement the interface `UserProcess::IMatrixElement` which calculates all matrix elements, i.e. born, real, and virtual matrix elements of all processes. Each available born and virtual matrix element is identified by an integer number. Here, we assume that the matrix element for $\bar{u}u \to \mu^+\mu^-$ is identified by 0. Hence, we have

```
int me_born = 0;
```

Next, we can define the actual flavour configuration, i.e.

```
FKS::FlavourConfig fl(me_born, 0, color1, color2);
```

where the second argument is not used. At NLO QCD, this process has only ISR singularities. Since every real Drell-Yan process has a unique underlying born process, we can use one singular region, i.e.

```
FKS::RegionList rlist;
rlist.push_back(FKS::Region(4, 0));
```

As for the born and virtual matrix element, the real matrix elements are also identified by integer numbers. We assume that the NLO matrix elements are identified by

```
int me_real0 = 0; // u~ u -> mu+ mu- g
int me_real1 = 1; // u~ g -> mu+ mu- u~
int me_real2 = 2; // g u -> mu+ mu- u
```

The flavour configuration is given by

```
std::vector<FKS::PDGList> real0 =
        {{-2, 2, -13, 13, 21},{-4, 4, -13, 13, 21}};
std::vector<FKS::PDGList> real1 =
        {{-2, 21, -13, 13, -2},{-4, 21, -13, 13, -4}};
std::vector<FKS::PDGList> real2 =
        {{21, 2, -13, 13, 2},{21, 4, -13, 13, 4}};
```

Next, we can add the NLO corrections to the process `fl`

```
fl.AddReal(me_real0, FKS::Type_t::QCD, real0, rlist, rlist);
fl.AddReal(me_real1, FKS::Type_t::QCD, real1, rlist, rlist);
fl.AddReal(me_real2, FKS::Type_t::QCD, real2, rlist, rlist);
```

Note, that the second `rlist` argument specifies all singular regions of a real process. The first `rlist` argument contains all singular regions that are connected to the underlying born process. For Drell-Yan, the underlying born is unique and, therefore, there is no difference between both arguments. For more complicated processes, the first `rlist` could be a subset of the second singular region list (s. $W + \text{jet}$).

The specification of the subprocess is now complete and the flavour configuration `fl` can be added to the list in `UserProcess::Data::Process`.

Acknowledgments

First, I want to thank Alexander Mück for his support and supervision during this work and all the discussions about football and all the rest. I would also like to thank my colleagues at the *Institute for Theoretical Particle Physics and Cosmology* who made my time as a member of the institute enjoyable. In particular, I want to thank Leila Ali Cavasonza, Mathieu Pellen, Frederic "Fredo" Poncza, and Jory Sonneveld for all the coffee breaks, discussions about cheese cake and all the fun I had with them.

Bibliography

[1] **CMS** Collaboration, S. Chatrchyan *et al.*, "Observation of a new boson at a mass of 125 GeV with the CMS experiment at the LHC," *Phys. Lett.* **B716** (2012) 30–61, arXiv:1207.7235 [hep-ex].

[2] **ATLAS** Collaboration, G. Aad *et al.*, "Observation of a new particle in the search for the Standard Model Higgs boson with the ATLAS detector at the LHC," *Phys. Lett.* **B716** (2012) 1–29, arXiv:1207.7214 [hep-ex].

[3] S. L. Glashow, "Partial Symmetries of Weak Interactions," *Nucl. Phys.* **22** (1961) 579–588.

[4] S. Weinberg, "A Model of Leptons," *Phys. Rev. Lett.* **19** (1967) 1264–1266.

[5] A. Salam, "Weak and Electromagnetic Interactions," *Conf. Proc.* **C680519** (1968) 367–377.

[6] P. W. Higgs, "Broken Symmetries and the Masses of Gauge Bosons," *Phys. Rev. Lett.* **13** (1964) 508–509.

[7] P. W. Higgs, "Broken symmetries, massless particles and gauge fields," *Phys. Lett.* **12** (1964) 132–133.

[8] G. S. Guralnik, C. R. Hagen, and T. W. B. Kibble, "Global Conservation Laws and Massless Particles," *Phys. Rev. Lett.* **13** (1964) 585–587.

[9] F. Englert and R. Brout, "Broken Symmetry and the Mass of Gauge Vector Mesons," *Phys. Rev. Lett.* **13** (1964) 321–323.

[10] S. D. Drell and T.-M. Yan, "Massive Lepton Pair Production in Hadron-Hadron Collisions at High-Energies," *Phys. Rev. Lett.* **25** (1970) 316–320. [Erratum: Phys. Rev. Lett.25,902(1970)].

[11] **CMS** Collaboration, S. Chatrchyan *et al.*, "Measurement of the weak mixing angle with the Drell-Yan process in proton-proton collisions at the LHC," *Phys. Rev.* **D84** (2011) 112002, arXiv:1110.2682 [hep-ex].

[12] **ATLAS** Collaboration, G. Aad *et al.*, "Measurement of the forward-backward asymmetry of electron and muon pair-production in pp collisions at $\sqrt{s} = 7$ TeV with the ATLAS detector," *JHEP* **09** (2015) 049, arXiv:1503.03709 [hep-ex].

[13] **ATLAS** Collaboration, M. Aaboud *et al.*, "Measurement of the W-boson mass in pp collisions at $\sqrt{s} = 7$ TeV with the ATLAS detector," arXiv:1701.07240 [hep-ex].

[14] S. Forte and G. Watt, "Progress in the Determination of the Partonic Structure of the Proton," *Ann. Rev. Nucl. Part. Sci.* **63** (2013) 291–328, arXiv:1301.6754 [hep-ph].

[15] M. Baak *et al.*, "Working Group Report: Precision Study of Electroweak Interactions," in *Proceedings, Community Summer Study 2013: Snowmass on the Mississippi (CSS2013): Minneapolis, MN, USA, July 29-August 6, 2013*. 2013. arXiv:1310.6708 [hep-ph]. http://www.slac.stanford.edu/econf/C1307292/docs/EnergyFrontier/Electroweak-19.pdf.

[16] M. L. Mangano, "Production of electroweak bosons at hadron colliders: theoretical aspects," *Adv. Ser. Direct. High Energy Phys.* **26** (2016) 231–253, arXiv:1512.00220 [hep-ph].

[17] G. Altarelli, R. K. Ellis, and G. Martinelli, "Large Perturbative Corrections to the Drell-Yan Process in QCD," *Nucl.Phys.* **B157** (1979) 461.

[18] R. Hamberg, W. L. van Neerven, and T. Matsuura, "A Complete calculation of the order α_s^2 correction to the Drell-Yan K factor," *Nucl. Phys.* **B359** (1991) 343–405. [Erratum: Nucl. Phys.B644,403(2002)].

[19] R. V. Harlander and W. B. Kilgore, "Next-to-next-to-leading order Higgs production at hadron colliders," *Phys. Rev. Lett.* **88** (2002) 201801, arXiv:hep-ph/0201206 [hep-ph].

[20] C. Anastasiou, L. J. Dixon, K. Melnikov, and F. Petriello, "High precision QCD at hadron colliders: Electroweak gauge boson rapidity distributions at NNLO," *Phys. Rev.* **D69** (2004) 094008, arXiv:hep-ph/0312266 [hep-ph].

[21] S. Catani, L. Cieri, G. Ferrera, D. de Florian, and M. Grazzini, "Vector boson production at hadron colliders: a fully exclusive QCD calculation at NNLO," *Phys. Rev. Lett.* **103** (2009) 082001, arXiv:0903.2120 [hep-ph].

[22] K. Melnikov and F. Petriello, "The W boson production cross section at the LHC through $O(\alpha_s^2)$," *Phys. Rev. Lett.* **96** (2006) 231803, arXiv:hep-ph/0603182 [hep-ph].

[23] K. Melnikov and F. Petriello, "Electroweak gauge boson production at hadron colliders through $\mathcal{O}(\alpha_s^2)$," *Phys. Rev.* **D74** (2006) 114017, arXiv:hep-ph/0609070 [hep-ph].

[24] R. Gavin, Y. Li, F. Petriello, and S. Quackenbush, "FEWZ 2.0: A code for hadronic Z production at next-to-next-to-leading order," *Comput. Phys. Commun.* **182** (2011) 2388–2403, arXiv:1011.3540 [hep-ph].

[25] R. Gavin, Y. Li, F. Petriello, and S. Quackenbush, "W Physics at the LHC with FEWZ 2.1," *Comput. Phys. Commun.* **184** (2013) 208–214, arXiv:1201.5896 [hep-ph].

[26] R. Boughezal, J. M. Campbell, R. K. Ellis, C. Focke, W. Giele, X. Liu, F. Petriello, and C. Williams, "Color Singlet Production at NNLO in MCFM," *Submitted to: JHEP* (2016) , arXiv:1605.08011 [hep-ph].

[27] S. Dittmaier and M. Krämer, "Electroweak radiative corrections to W boson production at hadron colliders," *Phys. Rev.* **D65** (2002) 073007, arXiv:hep-ph/0109062 [hep-ph].

[28] U. Baur, O. Brein, W. Hollik, C. Schappacher, and D. Wackeroth, "Electroweak radiative corrections to neutral current Drell-Yan processes at hadron colliders," *Phys. Rev.* **D65** (2002) 033007, arXiv:hep-ph/0108274 [hep-ph].

[29] U. Baur and D. Wackeroth, "Electroweak radiative corrections to $p\bar{p} \to W^{\pm} \to \ell^{\pm}\nu$ beyond the pole approximation," *Phys. Rev.* **D70** (2004) 073015, arXiv:hep-ph/0405191 [hep-ph].

[30] S. Dittmaier and M. Huber, "Radiative corrections to the neutral-current Drell-Yan process in the Standard Model and its minimal supersymmetric extension," *JHEP* **01** (2010) 060, arXiv:0911.2329 [hep-ph].

[31] G. Balossini, G. Montagna, C. M. Carloni Calame, M. Moretti, O. Nicrosini, F. Piccinini, M. Treccani, and A. Vicini, "Combination of electroweak and QCD corrections to single W production at the Fermilab Tevatron and the CERN LHC," *JHEP* **01** (2010) 013, arXiv:0907.0276 [hep-ph].

[32] C. M. Carloni Calame, G. Montagna, O. Nicrosini, and A. Vicini, "Precision electroweak calculation of the charged current Drell-Yan process," *JHEP* **12** (2006) 016, arXiv:hep-ph/0609170 [hep-ph].

[33] C. M. Carloni Calame, G. Montagna, O. Nicrosini, and A. Vicini, "Precision electroweak calculation of the production of a high transverse-momentum lepton pair at hadron colliders," *JHEP* **10** (2007) 109, arXiv:0710.1722 [hep-ph].

[34] U. Baur, S. Keller, and W. K. Sakumoto, "QED radiative corrections to Z boson production and the forward backward asymmetry at hadron colliders," *Phys. Rev.* **D57** (1998) 199–215, arXiv:hep-ph/9707301 [hep-ph].

[35] U. Baur, S. Keller, and D. Wackeroth, "Electroweak radiative corrections to W boson production in hadronic collisions," *Phys. Rev.* **D59** (1999) 013002, arXiv:hep-ph/9807417 [hep-ph].

[36] W. Płaczek, S. Jadach, and M. W. Krasny, "Drell-Yan processes with WINHAC," *Acta Phys. Polon.* **B44** no. 11, (2013) 2171–2178, arXiv:1310.5994 [hep-ph].

[37] A. Arbuzov, D. Bardin, S. Bondarenko, P. Christova, L. Kalinovskaya, G. Nanava, and R. Sadykov, "One-loop corrections to the Drell-Yan process in SANC. I. The Charged current case," *Eur. Phys. J.* **C46** (2006) 407–412, arXiv:hep-ph/0506110 [hep-ph]. [Erratum: Eur. Phys. J.C50,505(2007)].

[38] A. Arbuzov, D. Bardin, S. Bondarenko, P. Christova, L. Kalinovskaya, G. Nanava, and R. Sadykov, "One-loop corrections to the Drell–Yan process in SANC. (II). The Neutral current case," *Eur. Phys. J.* **C54** (2008) 451–460, arXiv:0711.0625 [hep-ph].

[39] A. Andonov, A. Arbuzov, D. Bardin, S. Bondarenko, P. Christova, L. Kalinovskaya, V. Kolesnikov, and R. Sadykov, "Standard SANC Modules," *Comput. Phys. Commun.* **181** (2010) 305–312, arXiv:0812.4207 [physics.comp-ph].

[40] D. Bardin, S. Bondarenko, P. Christova, L. Kalinovskaya, L. Rumyantsev, A. Sapronov, and W. von Schlippe, "SANC integrator in the progress: QCD and EW contributions," *JETP Lett.* **96** (2012) 285–289, arXiv:1207.4400 [hep-ph].

[41] S. G. Bondarenko and A. A. Sapronov, "NLO EW and QCD proton-proton cross section calculations with mcsanc-v1.01," *Comput. Phys. Commun.* **184** (2013) 2343–2350, arXiv:1301.3687 [hep-ph].

[42] Y. Li and F. Petriello, "Combining QCD and electroweak corrections to dilepton production in FEWZ," *Phys. Rev.* **D86** (2012) 094034, arXiv:1208.5967 [hep-ph].

[43] S. Dittmaier, A. Huss, and C. Schwinn, "Mixed QCD-electroweak $O(\alpha_s\alpha)$ corrections to Drell-Yan processes in the resonance region: pole approximation and non-factorizable corrections," *Nucl. Phys.* **B885** (2014) 318–372, arXiv:1403.3216 [hep-ph].

[44] S. Dittmaier, A. Huss, and C. Schwinn, "Dominant mixed QCD-electroweak $O(\alpha_s\alpha)$ corrections to Drell–Yan processes in the resonance region," *Nucl. Phys.* **B904** (2016) 216–252, arXiv:1511.08016 [hep-ph].

[45] S. Catani, D. de Florian, G. Ferrera, and M. Grazzini, "Vector boson production at hadron colliders: transverse-momentum resummation and leptonic decay," *JHEP* **12** (2015) 047, arXiv:1507.06937 [hep-ph].

[46] S. Frixione and B. R. Webber, "Matching NLO QCD computations and parton shower simulations," *JHEP* **06** (2002) 029, arXiv:hep-ph/0204244 [hep-ph].

[47] S. Frixione, P. Nason, and C. Oleari, "Matching NLO QCD computations with Parton Shower simulations: the POWHEG method," *JHEP* **0711** (2007) 070, arXiv:0709.2092 [hep-ph].

[48] S. Alioli, P. Nason, C. Oleari, and E. Re, "NLO vector-boson production matched with shower in POWHEG," *JHEP* **07** (2008) 060, arXiv:0805.4802 [hep-ph].

[49] C. Bernaciak and D. Wackeroth, "Combining NLO QCD and Electroweak Radiative Corrections to W boson Production at Hadron Colliders in the POWHEG Framework," *Phys. Rev.* **D85** (2012) 093003, arXiv:1201.4804 [hep-ph].

[50] L. Barze, G. Montagna, P. Nason, O. Nicrosini, and F. Piccinini, "Implementation of electroweak corrections in the POWHEG BOX: single W production," *JHEP* **04** (2012) 037, arXiv:1202.0465 [hep-ph].

[51] L. Barze, G. Montagna, P. Nason, O. Nicrosini, F. Piccinini, and A. Vicini, "Neutral current Drell-Yan with combined QCD and electroweak corrections in the POWHEG BOX," *Eur. Phys. J.* **C73** no. 6, (2013) 2474, arXiv:1302.4606 [hep-ph].

[52] S. Höche, Y. Li, and S. Prestel, "Drell-Yan lepton pair production at NNLO QCD with parton showers," *Phys. Rev.* **D91** no. 7, (2015) 074015, arXiv:1405.3607 [hep-ph].

[53] A. Karlberg, E. Re, and G. Zanderighi, "NNLOPS accurate Drell-Yan production," *JHEP* **09** (2014) 134, arXiv:1407.2940 [hep-ph].

[54] S. Alioli, C. W. Bauer, C. Berggren, F. J. Tackmann, and J. R. Walsh, "Drell-Yan production at NNLL'+NNLO matched to parton showers," *Phys. Rev.* **D92** no. 9, (2015) 094020, arXiv:1508.01475 [hep-ph].

[55] S. Catani and M. H. Seymour, "A General algorithm for calculating jet cross-sections in NLO QCD," *Nucl. Phys.* **B485** (1997) 291–419, arXiv:hep-ph/9605323 [hep-ph]. [Erratum: Nucl. Phys.B510,503(1998)].

[56] S. Frixione, Z. Kunszt, and A. Signer, "Three jet cross-sections to next-to-leading order," *Nucl. Phys.* **B467** (1996) 399–442, arXiv:hep-ph/9512328 [hep-ph].

[57] A. Mück and L. Oymanns, "Resonance-improved parton-shower matching for the Drell-Yan process including electroweak corrections," arXiv:1612.04292 [hep-ph].

[58] T. Ježo and P. Nason, "On the Treatment of Resonances in Next-to-Leading Order Calculations Matched to a Parton Shower," *JHEP* **12** (2015) 065, arXiv:1509.09071 [hep-ph].

[59] G. 't Hooft and M. J. G. Veltman, "Regularization and Renormalization of Gauge Fields," *Nucl. Phys.* **B44** (1972) 189–213.

[60] T. Kinoshita, "Mass singularities of Feynman amplitudes," *J. Math. Phys.* **3** (1962) 650–677.

[61] T. D. Lee and M. Nauenberg, "Degenerate Systems and Mass Singularities," *Phys. Rev.* **133** (1964) B1549–B1562. [,25(1964)].

[62] Y. L. Dokshitzer, "Calculation of the Structure Functions for Deep Inelastic Scattering and e+ e- Annihilation by Perturbation Theory in Quantum Chromodynamics.," *Sov. Phys. JETP* **46** (1977) 641–653. [Zh. Eksp. Teor. Fiz.73,1216(1977)].

[63] V. N. Gribov and L. N. Lipatov, "Deep inelastic e p scattering in perturbation theory," *Sov. J. Nucl. Phys.* **15** (1972) 438–450. [Yad. Fiz.15,781(1972)].

[64] G. Altarelli and G. Parisi, "Asymptotic Freedom in Parton Language," *Nucl. Phys.* **B126** (1977) 298–318.

[65] G. Dissertori, I. G. Knowles, and M. Schmelling, *Quantum Chromodynamics: High Energy Experiments and Theory*. International series of monographs on physics. Clarendon Press, 2005.

[66] S. Frixione, E. Laenen, P. Motylinski, and B. R. Webber, "Single-top production in MC@NLO," *JHEP* **0603** (2006) 092, arXiv:hep-ph/0512250 [hep-ph].

[67] S. Alioli, P. Nason, C. Oleari, and E. Re, "A general framework for implementing NLO calculations in shower Monte Carlo programs: the POWHEG BOX," *JHEP* **1006** (2010) 043, arXiv:1002.2581 [hep-ph].

[68] S. Dittmaier, "A General approach to photon radiation off fermions," *Nucl.Phys.* **B565** (2000) 69–122, arXiv:hep-ph/9904440 [hep-ph].

[69] K. P. O. Diener, S. Dittmaier, and W. Hollik, "Electroweak higher-order effects and theoretical uncertainties in deep-inelastic neutrino scattering," *Phys. Rev.* **D72** (2005) 093002, arXiv:hep-ph/0509084 [hep-ph].

[70] S. Dittmaier, "A General approach to photon radiation off fermions," *Nucl.Phys.* **B565** (2000) 69–122, arXiv:hep-ph/9904440 [hep-ph].

[71] L. Basso, S. Dittmaier, A. Huss, and L. Oggero, "Techniques for the treatment of IR divergences in decay processes at NLO and application to the top-quark decay," *Eur. Phys. J.* **C76** no. 2, (2016) 56, arXiv:1507.04676 [hep-ph].

[72] T. Sjostrand, S. Mrenna, and P. Z. Skands, "PYTHIA 6.4 Physics and Manual," *JHEP* **0605** (2006) 026, arXiv:hep-ph/0603175 [hep-ph].

[73] T. Sjostrand, S. Mrenna, and P. Z. Skands, "A Brief Introduction to PYTHIA 8.1," *Comput. Phys. Commun.* **178** (2008) 852–867, arXiv:0710.3820 [hep-ph].

[74] M. Bahr *et al.*, "Herwig++ Physics and Manual," *Eur. Phys. J.* **C58** (2008) 639–707, arXiv:0803.0883 [hep-ph].

[75] J. Bellm *et al.*, "Herwig 7.0/Herwig++ 3.0 release note," *Eur. Phys. J.* **C76** no. 4, (2016) 196, arXiv:1512.01178 [hep-ph].

[76] T. Gleisberg, S. Hoeche, F. Krauss, M. Schonherr, S. Schumann, F. Siegert, and J. Winter, "Event generation with SHERPA 1.1," *JHEP* **02** (2009) 007, arXiv:0811.4622 [hep-ph].

[77] P. Nason and B. Webber, "Next-to-Leading-Order Event Generators," *Ann. Rev. Nucl. Part. Sci.* **62** (2012) 187–213, arXiv:1202.1251 [hep-ph].

[78] P. Nason, "A New method for combining NLO QCD with shower Monte Carlo algorithms," *JHEP* **11** (2004) 040, arXiv:hep-ph/0409146 [hep-ph].

[79] S. Catani, B. R. Webber, and G. Marchesini, "QCD coherent branching and semiinclusive processes at large x," *Nucl. Phys.* **B349** (1991) 635–654.

[80] P. Nason, "MINT: A Computer program for adaptive Monte Carlo integration and generation of unweighted distributions," arXiv:0709.2085 [hep-ph].

[81] S. Weinzierl, "Introduction to Monte Carlo methods," arXiv:hep-ph/0006269 [hep-ph].

[82] P. Nason and G. Ridolfi, "A Positive-weight next-to-leading-order Monte Carlo for Z pair hadroproduction," *JHEP* **0608** (2006) 077, arXiv:hep-ph/0606275 [hep-ph].

[83] E. Boos *et al.*, "Generic user process interface for event generators," in *Physics at TeV colliders. Proceedings, Euro Summer School, Les Houches, France, May 21-June 1, 2001*. 2001. arXiv:hep-ph/0109068 [hep-ph]. http://lss.fnal.gov/archive/preprint/fermilab-conf-01-496-t.shtml.

[84] J. Alwall *et al.*, "A Standard format for Les Houches event files," *Comput. Phys. Commun.* **176** (2007) 300–304, arXiv:hep-ph/0609017 [hep-ph].

[85] T. Ježo, J. M. Lindert, P. Nason, C. Oleari, and S. Pozzorini, "An NLO+PS generator for $t\bar{t}$ and Wt production and decay including non-resonant and interference effects," *Eur. Phys. J.* **C76** no. 12, (2016) 691, arXiv:1607.04538 [hep-ph].

[86] "Powheg merging." https://web.archive.org/web/20170120102438/http://home.thep.lu.se/~torbjorn/pythia82html/POWHEGMerging.html. Accessed: 2017-01-20.

[87] J. Alwall, R. Frederix, S. Frixione, V. Hirschi, F. Maltoni, O. Mattelaer, H. S. Shao, T. Stelzer, P. Torrielli, and M. Zaro, "The automated computation of tree-level and next-to-leading order differential cross sections, and their matching to parton shower simulations," *JHEP* **07** (2014) 079, arXiv:1405.0301 [hep-ph].

[88] P. de Aquino, W. Link, F. Maltoni, O. Mattelaer, and T. Stelzer, "ALOHA: Automatic Libraries Of Helicity Amplitudes for Feynman Diagram Computations," *Comput. Phys. Commun.* **183** (2012) 2254–2263, arXiv:1108.2041 [hep-ph].

[89] S. Dittmaier and M. Huber, "Radiative corrections to the neutral-current Drell-Yan process in the Standard Model and its minimal supersymmetric extension," *JHEP* **01** (2010) 060, arXiv:0911.2329 [hep-ph].

[90] Private communication with Alexander Mück. Matrix elements checked against reference [89].

[91] M. Peskin and D. Schroeder, *An Introduction To Quantum Field Theory.* Westview Press, 1995.

[92] E. N. Argyres, W. Beenakker, G. J. van Oldenborgh, A. Denner, S. Dittmaier, J. Hoogland, R. Kleiss, C. G. Papadopoulos, and G. Passarino, "Stable calculations for unstable particles: Restoring gauge invariance," *Phys. Lett.* **B358** (1995) 339–346, arXiv:hep-ph/9507216 [hep-ph].

[93] Y. Kurihara, D. Perret-Gallix, and Y. Shimizu, "e+ e- —> e- anti-electron-neutrino u anti-d from LEP to linear collider energies," *Phys. Lett.* **B349** (1995) 367–374, arXiv:hep-ph/9412215 [hep-ph].

[94] A. Denner, S. Dittmaier, M. Roth, and D. Wackeroth, "Predictions for all processes $e^+e^- \to 4$ fermions + gamma," *Nucl. Phys.* **B560** (1999) 33–65, arXiv:hep-ph/9904472 [hep-ph].

[95] A. Denner, S. Dittmaier, M. Roth, and L. H. Wieders, "Electroweak corrections to charged-current $e^+e^- \to 4$ fermion processes: Technical details and further results," *Nucl. Phys.* **B724** (2005) 247–294, arXiv:hep-ph/0505042 [hep-ph]. [Erratum: Nucl. Phys.B854,504(2012)].

[96] A. Denner and S. Dittmaier, "The Complex-mass scheme for perturbative calculations with unstable particles," *Nucl. Phys. Proc. Suppl.* **160** (2006) 22–26, arXiv:hep-ph/0605312 [hep-ph].

[97] S. Dittmaier, A. Kabelschacht, and T. Kasprzik, "Polarized QED splittings of massive fermions and dipole subtraction for non-collinear-safe observables," *Nucl. Phys.* **B800** (2008) 146–189, arXiv:0802.1405 [hep-ph].

[98] **Particle Data Group** Collaboration, K. A. Olive *et al.*, "Review of Particle Physics," *Chin. Phys.* **C38** (2014) 090001.

[99] A. Denner, "Techniques for calculation of electroweak radiative corrections at the one loop level and results for W physics at LEP-200," *Fortsch. Phys.* **41** (1993) 307–420, arXiv:0709.1075 [hep-ph].

[100] A. Sirlin, "Radiative Corrections in the $SU(2)_L \times U(1)$ Theory: A Simple Renormalization Framework," *Phys. Rev.* **D22** (1980) 971–981.

[101] **NNPDF** Collaboration, R. D. Ball, V. Bertone, S. Carrazza, L. Del Debbio, S. Forte, A. Guffanti, N. P. Hartland, and J. Rojo, "Parton distributions with QED corrections," *Nucl. Phys.* **B877** (2013) 290–320, arXiv:1308.0598 [hep-ph].

[102] **NNPDF** Collaboration, S. Carrazza, "Towards the determination of the photon parton distribution function constrained by LHC data," *PoS* **DIS2013** (2013) 279, arXiv:1307.1131 [hep-ph].

[103] **NNPDF** Collaboration, S. Carrazza, "Towards an unbiased determination of parton distributions with QED corrections," in *Proceedings, 48th Rencontres de Moriond on QCD and High Energy Interactions*, pp. 357–360. 2013. arXiv:1305.4179 [hep-ph]. https://inspirehep.net/record/1234242/files/arXiv:1305.4179.pdf.

[104] A. Buckley, J. Ferrando, S. Lloyd, K. Nordström, B. Page, M. Rüfenacht, M. Schönherr, and G. Watt, "LHAPDF6: parton density access in the LHC precision era," *Eur. Phys. J.* **C75** (2015) 132, arXiv:1412.7420 [hep-ph].

[105] A. Buckley, J. Butterworth, L. Lonnblad, D. Grellscheid, H. Hoeth, J. Monk, H. Schulz, and F. Siegert, "Rivet user manual," *Comput. Phys. Commun.* **184** (2013) 2803–2819, arXiv:1003.0694 [hep-ph].

[106] C. M. Carloni Calame, M. Chiesa, H. Martinez, G. Montagna, O. Nicrosini, F. Piccinini, and A. Vicini, "Precision Measurement of the W-Boson Mass: Theoretical Contributions and Uncertainties," arXiv:1612.02841 [hep-ph].

[107] V. Buge, C. Jung, G. Quast, A. Ghezzi, M. Malberti, and T. Tabarelli de Fatis, "Prospects for the precision measurement of the W mass with the CMS detector at the LHC," *J. Phys.* **G34** (2007) N193–N220.

[108] **ATLAS** Collaboration, N. Besson, M. Boonekamp, E. Klinkby, S. Mehlhase, and T. Petersen, "Re-evaluation of the LHC potential for the measurement of Mw," *Eur. Phys. J.* **C57** (2008) 627–651, arXiv:0805.2093 [hep-ex].

[109] **ATLAS Collaboration** Collaboration, "Measurement of the W Boson Mass in Proton-Proton Collisions at s = 7 TeV with the ATLAS Detector," Tech. Rep. ATLAS-CONF-2016-113, CERN, Geneva, Dec, 2016. https://cds.cern.ch/record/2238954.

[110] M. Baak, M. Goebel, J. Haller, A. Hoecker, D. Kennedy, R. Kogler, K. Moenig, M. Schott, and J. Stelzer, "The Electroweak Fit of the Standard Model after the Discovery of a New Boson at the LHC," *Eur. Phys. J.* **C72** (2012) 2205, arXiv:1209.2716 [hep-ph].

[111] **Gfitter Group** Collaboration, M. Baak, J. Cúth, J. Haller, A. Hoecker, R. Kogler, K. Mönig, M. Schott, and J. Stelzer, "The global electroweak fit at NNLO and prospects for the LHC and ILC," *Eur. Phys. J.* **C74** (2014) 3046, arXiv:1407.3792 [hep-ph].

[112] A. D. Martin, R. G. Roberts, W. J. Stirling, and R. S. Thorne, "Parton distributions and the LHC: W and Z production," *Eur. Phys. J.* **C14** (2000) 133–145, arXiv:hep-ph/9907231 [hep-ph].

[113] M. Dittmar, F. Pauss, and D. Zurcher, "Towards a precise parton luminosity determination at the CERN LHC," *Phys. Rev.* **D56** (1997) 7284–7290, arXiv:hep-ex/9705004 [hep-ex].

[114] S. Brensing, S. Dittmaier, M. Krämer, and A. Mück, "Radiative corrections to W^- boson hadroproduction: Higher-order electroweak and supersymmetric effects," *Phys. Rev.* **D77** (2008) 073006, arXiv:0710.3309 [hep-ph].

[115] S. Alioli *et al.*, "Precision Studies of Observables in $pp \to W \to \ell\nu$ and $pp \to \gamma, Z \to \ell^+\ell^-$ processes at the LHC," *Submitted to: Working Group Report* (2016) , arXiv:1606.02330 [hep-ph].

[116] N. Davidson, T. Przedzinski, and Z. Was, "PHOTOS Interface in C++: Technical and Physics Documentation," *Comput. Phys. Commun.* **199** (2016) 86–101, arXiv:1011.0937 [hep-ph].

[117] **ATLAS** Collaboration, G. Aad *et al.*, "Measurements of the W production cross sections in association with jets with the ATLAS detector," *Eur. Phys. J.* **C75** no. 2, (2015) 82, arXiv:1409.8639 [hep-ex].

[118] **CMS Collaboration** Collaboration, "Differential cross section measurements of W bosons produced in association with jets in proton-proton collisions at

$\sqrt{s} = 8$ TeV," Tech. Rep. CMS-PAS-SMP-14-023, CERN, Geneva, 2016. https://cds.cern.ch/record/2147989.

[119] **CMS** Collaboration, V. Khachatryan *et al.*, "Differential cross section measurements for the production of a W boson in association with jets in proton–proton collisions at $\sqrt{s} = 7$ TeV," *Phys. Lett.* **B741** (2015) 12–37, arXiv:1406.7533 [hep-ex].

[120] **CMS Collaboration** Collaboration, "Measurement of the differential cross section for the production of a W (rightarrow munu) boson in association with jets at sqrt(s) = 13 TeV," Tech. Rep. CMS-PAS-SMP-16-005, CERN, Geneva, 2016. https://cds.cern.ch/record/2204927.

[121] W. T. Giele, E. W. N. Glover, and D. A. Kosower, "Higher order corrections to jet cross-sections in hadron colliders," *Nucl. Phys.* **B403** (1993) 633–670, arXiv:hep-ph/9302225 [hep-ph].

[122] J. M. Campbell, R. K. Ellis, and D. L. Rainwater, "Next-to-leading order QCD predictions for $W + 2$ jet and $Z + 2$ jet production at the CERN LHC," *Phys. Rev.* **D68** (2003) 094021, arXiv:hep-ph/0308195 [hep-ph].

[123] R. J. Gonsalves, J. Pawlowski, and C.-F. Wai, "QCD Radiative Corrections to Electroweak Boson Production at Large Transverse Momentum in Hadron Collisions," *Phys. Rev.* **D40** (1989) 2245.

[124] R. K. Ellis, G. Martinelli, and R. Petronzio, "Lepton Pair Production at Large Transverse Momentum in Second Order QCD," *Nucl. Phys.* **B211** (1983) 106–138.

[125] R. Boughezal, C. Focke, X. Liu, and F. Petriello, "W-boson production in association with a jet at next-to-next-to-leading order in perturbative QCD," *Phys. Rev. Lett.* **115** no. 6, (2015) 062002, arXiv:1504.02131 [hep-ph].

[126] R. Boughezal, X. Liu, and F. Petriello, "A comparison of NNLO QCD predictions with 7 TeV ATLAS and CMS data for V+jet processes," *Phys. Lett.* **B760** (2016) 6–13, arXiv:1602.05612 [hep-ph].

[127] J. H. Kühn, A. Kulesza, S. Pozzorini, and M. Schulze, "Electroweak corrections to large transverse momentum production of W bosons at the LHC," *Phys. Lett.* **B651** (2007) 160–165, arXiv:hep-ph/0703283 [HEP-PH].

[128] J. H. Kühn, A. Kulesza, S. Pozzorini, and M. Schulze, "Electroweak corrections to hadronic production of W bosons at large transverse momenta," *Nucl. Phys.* **B797** (2008) 27–77, arXiv:0708.0476 [hep-ph].

[129] W. Hollik, T. Kasprzik, and B. A. Kniehl, "Electroweak corrections to W-boson hadroproduction at finite transverse momentum," *Nucl. Phys.* **B790** (2008) 138–159, arXiv:0707.2553 [hep-ph].

[130] A. Denner, S. Dittmaier, T. Kasprzik, and A. Mück, "Electroweak corrections to W + jet hadroproduction including leptonic W-boson decays," *JHEP* **08** (2009) 075, arXiv:0906.1656 [hep-ph].

[131] S. Kallweit, J. M. Lindert, P. Maierhofer, S. Pozzorini, and M. Schönherr, "NLO QCD+EW predictions for V + jets including off-shell vector-boson decays and multijet merging," *JHEP* **04** (2016) 021, arXiv:1511.08692 [hep-ph].

[132] S. Hoeche, F. Krauss, M. Schonherr, and F. Siegert, "QCD matrix elements + parton showers: The NLO case," *JHEP* **04** (2013) 027, arXiv:1207.5030 [hep-ph].

[133] T. Gehrmann, S. Hoche, F. Krauss, M. Schonherr, and F. Siegert, "NLO QCD matrix elements + parton showers in $e^+e^- \to$ hadrons," *JHEP* **01** (2013) 144, arXiv:1207.5031 [hep-ph].

[134] L. Lönnblad and S. Prestel, "Merging Multi-leg NLO Matrix Elements with Parton Showers," *JHEP* **03** (2013) 166, arXiv:1211.7278 [hep-ph].

[135] R. Frederix and S. Frixione, "Merging meets matching in MC@NLO," *JHEP* **12** (2012) 061, arXiv:1209.6215 [hep-ph].

[136] J. H. Kühn, A. Kulesza, S. Pozzorini, and M. Schulze, "One-loop weak corrections to hadronic production of Z bosons at large transverse momenta," *Nucl. Phys.* **B727** (2005) 368–394, arXiv:hep-ph/0507178 [hep-ph].

[137] A. Denner, S. Dittmaier, T. Kasprzik, and A. Mück, "Electroweak corrections to dilepton + jet production at hadron colliders," *JHEP* **06** (2011) 069, arXiv:1103.0914 [hep-ph].

[138] A. Denner, S. Dittmaier, T. Kasprzik, and A. Mück, "Electroweak corrections to monojet production at the LHC," *Eur. Phys. J.* **C73** no. 2, (2013) 2297, arXiv:1211.5078 [hep-ph].

[139] A. Gehrmann-De Ridder, T. Gehrmann, E. W. N. Glover, A. Huss, and T. A. Morgan, "Precise QCD predictions for the production of a Z boson in association with a hadronic jet," *Phys. Rev. Lett.* **117** no. 2, (2016) 022001, arXiv:1507.02850 [hep-ph].

[140] R. Boughezal, J. M. Campbell, R. K. Ellis, C. Focke, W. T. Giele, X. Liu, and F. Petriello, "Z-boson production in association with a jet at next-to-next-to-leading order in perturbative QCD," *Phys. Rev. Lett.* **116** no. 15, (2016) 152001, arXiv:1512.01291 [hep-ph].

[141] S. Alioli, P. Nason, C. Oleari, and E. Re, "Vector boson plus one jet production in POWHEG," *JHEP* **01** (2011) 095, arXiv:1009.5594 [hep-ph].

[142] M. Cacciari, G. P. Salam, and G. Soyez, "The Anti-k(t) jet clustering algorithm," *JHEP* **04** (2008) 063, arXiv:0802.1189 [hep-ph].

[143] E. W. N. Glover and A. G. Morgan, "Measuring the photon fragmentation function at LEP," *Z. Phys.* **C62** (1994) 311–322.

[144] A. Gehrmann-De Ridder, T. Gehrmann, and E. W. N. Glover, "Radiative corrections to the photon + 1 jet rate at LEP," *Phys. Lett.* **B414** (1997) 354–361, arXiv:hep-ph/9705305 [hep-ph].

[145] A. Gehrmann-De Ridder and E. W. N. Glover, "Final state photon production at LEP," *Eur. Phys. J.* **C7** (1999) 29–48, arXiv:hep-ph/9806316 [hep-ph].

[146] S. Kallweit, J. M. Lindert, P. Maierhöfer, S. Pozzorini, and M. Schönherr, "NLO electroweak automation and precise predictions for W+multijet production at the LHC," *JHEP* **04** (2015) 012, arXiv:1412.5157 [hep-ph].

[147] M. Rubin, G. P. Salam, and S. Sapeta, "Giant QCD K-factors beyond NLO," *JHEP* **09** (2010) 084, arXiv:1006.2144 [hep-ph].

[148] A. Denner and S. Pozzorini, "One loop leading logarithms in electroweak radiative corrections. 1. Results," *Eur. Phys. J.* **C18** (2001) 461–480, arXiv:hep-ph/0010201 [hep-ph].

[149] G. Passarino and M. J. G. Veltman, "One Loop Corrections for e+ e- Annihilation Into mu+ mu- in the Weinberg Model," *Nucl. Phys.* **B160** (1979) 151–207.

[150] G. P. Lepage, "A New Algorithm for Adaptive Multidimensional Integration," *J.Comput.Phys.* **27** (1978) 192.

[151] G. P. Lepage, "VEGAS: AN ADAPTIVE MULTIDIMENSIONAL INTEGRATION PROGRAM,".

[152] W. Gropp, *The MPI-2 extensions*. MIT Press, Cambridge, Mass. u.a, 1998.

[153] "Message Passing Interface standard.". `http://mpi-forum.org/`.

[154] M. H. Seymour, "Matrix element corrections to parton shower algorithms," *Comput.Phys.Commun.* **90** (1995) 95–101, `arXiv:hep-ph/9410414 [hep-ph]`.

[155] W. van Neerven, "Dimensional Regularization of Mass and Infrared Singularities in Two Loop On-shell Vertex Functions," *Nucl.Phys.* **B268** (1986) 453.

[156] J. Smith, D. Thomas, and W. van Neerven, "QCD Corrections to the Reaction $p\bar{p} \to W\gamma$ X," *Z.Phys.* **C44** (1989) 267.

[157] G. Rodrigo, A. Santamaria, and M. S. Bilenky, "Dimensionally regularized box and phase space integrals involving gluons and massive quarks," *J.Phys.* **G25** (1999) 1593–1606, `arXiv:hep-ph/9703360 [hep-ph]`.

[158] G. 't Hooft and M. Veltman, "Scalar One Loop Integrals," *Nucl.Phys.* **B153** (1979) 365–401.

[159] W. Beenakker and A. Denner, "Infrared Divergent Scalar Box Integrals With Applications in the Electroweak Standard Model," *Nucl.Phys.* **B338** (1990) 349–370.

[160] S. Frixione, P. Nason, and C. Oleari, "Matching NLO QCD computations with Parton Shower simulations: the POWHEG method," *JHEP* **0711** (2007) 070, `arXiv:0709.2092 [hep-ph]`.

[161] S. Catani and M. Grazzini, "Collinear factorization and splitting functions for next-to-next-to-leading order QCD calculations," *Phys. Lett.* **B446** (1999) 143–152, `arXiv:hep-ph/9810389 [hep-ph]`.

[162] K. Hagiwara and D. Zeppenfeld, "Amplitudes for Multiparton Processes Involving a Current at e^+e^-, $e^\pm p$, and Hadron Colliders," *Nucl. Phys.* **B313** (1989) 560–594.

[163] T. Plehn, "Lectures on LHC Physics," *Lect. Notes Phys.* **844** (2012) 1–193, `arXiv:0910.4182 [hep-ph]`.

[164] S. Alioli, P. Nason, C. Oleari, and E. Re, "A general framework for implementing NLO calculations in shower Monte Carlo programs: the POWHEG BOX," *JHEP* **1006** (2010) 043, `arXiv:1002.2581 [hep-ph]`.